THE ELECTRONIC SPECTROSCOPY OF TRANSITION METAL DIATOMIC MOLECULES MODELED WITH SEMIEMPIRICAL QUANTUM CHEMISTRY

By

TED A O'BRIEN

A DISSERTATION PRESENTED TO THE GRADUATE SCHOOL
OF THE UNIVERSITY OF FLORIDA IN PARTIAL FULFILLMENT
OF THE REQUIREMENTS FOR THE DEGREE OF
DOCTOR OF PHILOSOPHY

UNIVERSITY OF FLORIDA

2000

Dedicated to the Memory of Professor Michael Charles Zerner
1940 – 2000
Friend and Mentor

Sorrow, who to this house scarce knew the way:
Is, oh, heir of it, our all is his prey.
This strange chance claims strange wonder, and to us
Nothing can be so strange, as to weep thus.
'Tis well his life's loud speaking works deserve,
And give praise too, our cold tongues could not serve:
'Tis well, he kept tears from our eyes before,
That to fit this deep ill, we might have store.
Oh, if a sweet briar climb up by a tree,
If to a paradise that transplanted be,
Or felled, and burnt for holy sacrifice,
Yet, that must wither, which by it did rise,
As we for him dead: though no family
E'er rigged a soul for heaven's discovery
With whom more venturers more boldly dare
Venture their states, with him in joy to share.
We lose what all friends loved, him; he gains now
But life by death, which worst foes would allow,
If he could have foes, in whose practice grew
All virtues, whose names subtle schoolmen knew;
What ease, can hope that we shall see him, beget,
When we must die first, and cannot die yet?
His children are his pictures, oh they be
Pictures of him dead, senseless, cold as he,
Here needs no marble tomb, since he is gone,
He, and about him, his, are turned to stone.
— John Donne, *Elegy on the L. C.*

ACKNOWLEDGMENTS

The road I have traveled these last six years has had some rather unusual twists and turns that nobody expected at the beginning. I could not have made it without help and support from a large number of people. First and foremost I acknowledge my wonderful wife, Julie, without whose continuous love, support and devotion I might not have survived the last years, let alone finished a dissertation. I can't thank her enough for her courage and loyalty. She's been with me through the best and worst times of my life so far, and wouldn't let me quit when I thought I had to. I also received immense support and encouragement from my family, my parents Jim and Barbara O'Brien, my brother Michael, my grandmother Louise Wiley and my late grandfather, Dean Wiley. Without their shaping, I wouldn't have had the strength of character to accomplish what I've accomplished in the face of what have at times been great obstacles. I thank my Dad, Jim O'Brien, for staying with me during the last month of writing, and my brother Mike for keeping me company via e-mail during the long nights of writing.

I owe a debt of gratitude of another sort to my friends. Thanks go to Krista Lewis, my best friend. I cannot imagine a better friend than Krista. She's been by turns supportive, loyal, and tough. In times of trouble I know I can count on her. Heather Weimer also deserves my thanks. She always seemed to be there at the worst moments to pull me through. Her advice on how to stay sane while writing a thesis has been invaluable. Thanks go also to Katrin Albert, for her encouragement, not to mention a lot of help with coding, Greg Pearl, who helped me with everything from compiling fast executables to assembling furniture, Marshall Cory, who provided judicious tutelage and occasional car repairs, and Gail Fanucci, for a lot of help at the library and for inspiring me by her example of uncompromising excellence. Quim Da Motta, Dan Dekee, Thomas Herz and his wife Uschi, Ed Webster, Ya-wen Hsiao, Ajith Perera, and Remigio Cabrera-Trujillo also deserve acknowledgment and appreciation. I couldn't have made it without the efforts of my physician in Gainesville, Dr. Mark Barrow, who supplied faith as well as healing (though not faith-healing). Similarly, I thank the team at the Muscular Dystrophy Association Clinic in St. Louis, Julaine Florence, Jeanine Schierbecker, Dr. Alan Pestronk, and, earlier, Dr. Michael Brooke. They if anybody completely understand the struggle I've had, and what it means to me to have prevailed.

From a professional standpoint, I thank my committee members Professors Jack Sabin, Yngve Öhrn, Rod Bartlett, William Weltner, Jr., and Dan Talham, and the members, visitors, and collaborators of the Zerner group, past and present: Katrin Albert, Rajiv Bendale, Arianna Beste, Hozefa Botee, Sylvio Canuto, , Cristian Cardenas-Lailhacar, Marshall Cory, Kaline Coutinho, Joaquim da Motta, Jonas Danielsson, Dan Dekee, Professor Janet Del Bene, Mari DeMarco, Guillermina Estiú, Thomas Herz, Tom Higgins, Professor Paul Holloway, Ya-wen Hsiao, Professor Geo Klopman, Mike Lee, Jay Lewis, Chuck Martin, Lane Newsom, Greg Pearl, Philip Rack, Professor Notker Rösch, Josh Schrier, Krassimir Stavrev, Hege Strömsne, Toomas Tamm, DeCarlos Taylor, Sergio Urahata, Ed Webster, Xuehe Zheng, and Igor Zilberberg. I acknowledge Jim O'Brien for enlightening discussions of transition metal catalysis. The staff of the Quantum Theory Project, Judy Parker, Coralu Clements, Sandy Weakland, and Cindy

LePrell, have provided a lot of help in navigating/circumventing the bureaucracy of the University. Erik Deumens has my thanks for all of his help with computing over the years, and for holding Gloria at bay at dire moments.

The hardest part of these acknowledgments is to thank my mentor, Professor Michael C. Zerner. Hs impact on my life has been amazing, and all for the better. It is hard to comprehend the vastness of the knowledge he imparted to me in a scientific sense, and he was and will remain my example of courage in the face of great adversity. His integrity, his enthusiasm and *joie de vivre*, his generosity and inner fire, his determination, were unrivaled. Z gave them hell for a lot longer than most people expected after his initial diagnosis, and did it with class and an unfailing sense of humor to the very end. The world has been diminished by his loss. I miss him, but can glean some satisfaction from the fact that his teaching and his example will be with me always. His spirit lives on in all of us whose lives he helped to shape.

TABLE OF CONTENTS

page

DEDICATION ii

ACKNOWLEDGMENTS iii

ABSTRACT viii

CHAPTERS

1 INTRODUCTION 1

- Relevance: Why Study Metal Clusters? 1
- The Smallest Metal Clusters: Transition Metal Diatomics 5
- The Quantum Chemistry of Transition Metal Diatomics 18
- Semiempirical Methods: Potential Tools of Study for Small and Medium-sized Clusters 28
- Summary and Purpose 35

2 METHODS OF CALCULATION 37

- Fundamental Considerations 37
- Electron Correlation 64
- Bridge Between Ab Initio and Semiempirical Methods 72
- The INDO/S Model 77

3 OPTIMIZATION OF THE INDO/S SOCI PROGRAM 114

- Optimization of Memory Allocation for SOCI Calculations 114
- Implementation of Schmidt Orthogonalization Code 116
- Optimization of Spin-Orbit Output Format 124
- Determination of Spin Character of Spin-Orbit Eigenvectors 125

4 THE ELECTRONIC STRUCTURE AND SPECTROSCOPY OF DIVANADIUM 128

- Summary and Purpose 128
- Background and Motivation 129

Methodological Considerations 146
Results and Discussion 147
Self-Consistent Field Ground State 147
Configuration Interaction 151
Conclusions 167

5 GROUND STATE ISOCONFIGURATIONAL MIXING IN V_2, VNb, AND Nb_2 169

Summary and Purpose 169
Background and Motivation 171
Methodological Considerations and Empirical Models 176
INDO/S Calculations 176
Empirical Models 177
Results and Discussion 184
Self-Consistent Field Ground States 184
Configuration Interaction Calculations 188
Analysis of Empirical Two State Models 203
Correlation Effects in the INDO/S Model 207
Conclusions 209

6 CONCLUSIONS AND FUTURE PLANS 211

Conclusions 211
Future Plans 214

REFERENCES 219

BIOGRAPHICAL SKETCH 233

Abstract of Dissertation Presented to the Graduate School
of the University of Florida in Partial Fulfillment of the
Requirements for the Degree of Doctor of Philosophy

THE ELECTRONIC SPECTROSCOPY OF TRANSITION METAL DIATOMIC MOLECULES MODELED WITH SEMIEMPIRICAL QUANTUM CHEMISTRY

By

Ted A O'Brien

December 2000

Chair: N. Yngve Öhrn
Major Department: Chemistry

Transition metal cluster research has attracted interest because of to the importance of clusters and surfaces in catalysis. Basic research on small clusters is vital because interactions between metal atoms in clusters are not completely understood. Theory and experiment both contribute, with theory helping to interpret and understand experimental data. Theoretical methods that model electronic spectroscopy are crucial, as the data on small clusters are largely spectroscopic. Spectral interpretation is often difficult, so methods that predict state symmetries, transition energies and intensities, and spin-orbit effects play a key role. Unfortunately there are no methods for treating the spectroscopy of medium-sized clusters, as even diatomics pose difficulties for quantum chemistry. There is a need for methods applicable to larger clusters.

The primary difficulty in applying quantum chemistry to metal clusters is electron correlation, or the effect the motions electrons undergo to avoid each other has on energies and wavefunctions. Correlation has a major impact on the electronic structure of metal clusters, so diatomics are studied with highly-correlated ab initio methods, which are limited because of computational cost. Inexpensive semiempirical methods offer an alternative, but have historically assumed a low level of correlation. There are arguments supporting the application of semiempirical methods to clusters, however. The INDO/S model is a candidate because it effectively models the spectroscopy of metal complexes, including spin-orbit effects, and has shown promise with clusters of up to fifty atoms. The role of correlation in semiempirical methods is not well-understood, however, and must be elucidated if methods applicable to larger clusters are to be developed.

This dissertation describes correlated INDO/S calculations on V_2, VNb, and Nb_2. Results obtained for the electronic spectroscopy of V_2 and VNb serve as a proof of concept and illustrate the role of correlation in the calculations. An examination of ground state spin-orbit effects in the three molecules provides additional insight. The results obtained agree well with experiment. Basic questions left by the spectroscopy have been investigated as well, including identities of unassigned transitions and orbital symmetries of observed transitions. This work demonstrates that semiempirical methods can in principle be successfully applied to metal clusters.

CHAPTER 1
INTRODUCTION

Relevance: Why Study Metal Clusters?

In the present day United States of America chemical manufacturing is very important economically and socially. Its impact ranges from the availability of life-saving pharmaceuticals to the myriad of consumer products that contribute to the high standard of living. Many of these applications begin with base chemicals that are produced in quantities of billions of kilograms per year. The industrial processes used to produce chemicals such as ethylene, urea, and acetic acid all rely on catalysis, the use of chemical reagents not consumed in a reaction to increase the rate of reaction. The economic value of catalysis is obvious, as a higher rate for a process generating billions of kilograms of reagent per year will lower production costs, a savings that manifests itself through the entire spectrum of products made from the base chemicals. In addition, homogeneous catalysis often enhances selectivity, allowing one product to be obtained in very high yield. Catalysis thus has a role to play in environmental issues because of selectivity and the milder reaction conditions catalysis makes possible. The motivation for studying existing catalysts and developing more effective ones is clear.

Of the ten base organic chemicals produced in largest quantities in the United States in 1999, seven are manufactured with processes involving metal catalysts (table 1-1). Transition metal elements are seen to be particularly represented. Most of these

Table 1-1: Organic compounds produced in largest quantity in the United States, 1999, and metal catalysts used in production.

Organic Compound	**Production, 10^9 kg, 1999**[a]	**Metal catalysts used**[b]
Ethylene	23.4	—
Propylene	13.2	$TiCl_3$ or $TiCl_4 + AlR_3$
Ethylene Dichloride	10.4	$FeCl_3$, $AlCl_3$
Urea	8.5	—
Ethylbenzene	6.0	$AlCl_3$
Styrene	5.4	ZnO, Cr_2O_3
Xylenes	4.5	Pt + Re
Ethylene Oxide	4.0	Ag
Cumene	3.2	—
1,3-Butadiene	1.9	Fe_2O_3

[a] Source: reference [1]
[b] Source: reference [2]

processes are heterogeneous, meaning that reactions taking place in solution are catalyzed by solid-state metal species. The underlying processes are not well-understood in many cases, but likely involve the solid surface in some way. Hence there has been ongoing interest in studying and modeling the interactions of molecules and atoms with metal surfaces. Several recent papers discuss modeling efforts [3-8]. An important part of this effort has involved studies of metal clusters of discrete size, which can serve as models of surfaces or of some heterogeneous catalysts (those composed of porous oxides supporting metal clusters of finite dimension). Here the term "metal cluster" is taken to indicate a conglomerate of two or more metal atoms in the absence of nonmetallic ligands. The clusters themselves also have novel properties, and are being explored for potential applications in materials engineering.

Metal clusters can generally be divided into size regimes of small, medium, and large [9]. Small clusters are considered to be composed of 10 atoms or fewer, and are studied with matrix isolation and high-resolution molecular beam spectroscopy, electron spin resonance, and molecular quantum chemical theoretical methods. Medium-sized clusters are larger than the small clusters but can still be interrogated by molecular spectroscopic techniques with acceptable resolution, and contain 10-100 atoms. Methods brought to bear on these systems include the aforementioned spectroscopic techniques as well as classical simulations of structure, experimental methods also useful for determining bulk properties such as ionization potentials, and mass spectrometry. Large clusters then include anything in size beyond the medium regime. Such clusters are studied with methods for determining bulk properties, photodepletion spectroscopy, negative ion photoelectron spectroscopy, and solid state theoretical methods (band theory).

Clusters of all three sizes are worthy of scientific study. Large clusters have potential for immediate applications as catalysts. Clusters of medium size are of potential interest for applications in materials engineering, and for more fundamental reasons as states of matter intermediate between discrete molecules and bulk materials. Basic research on small clusters is vital as well for a number of reasons, even though short-term applications are unlikely. First and foremost, studies of small clusters can potentially provide an understanding of the fundamental aspects of the bonding between metal atoms, which should prove useful in studying properties of larger clusters and surfaces.

Second, they can be studied in great detail spectroscopically in the gas phase at very high resolution, allowing examination of the electronic structure of the ground and excited states. Third, the most accurate quantum chemical techniques can be applied (though still often with only modest success, as discussed later), providing crucial information on geometries and working hand-in-hand with experiment to further understanding of the electronic structure and spectroscopy. Theory is especially important in this last capacity since metal clusters are difficult to prepare and characterize, so spectroscopic coverage of excited states is incidental rather than exhaustive. Theoretical methods for treating electronic spectroscopy thus play a key role by confirming state assignments, for example. Finally, small clusters can provide a benchmark for methods that might eventually be applied to larger clusters.

An important aspect of cluster size is the evolution of properties such as ionization potential from values found for discrete small clusters to those known for the bulk [10-12]. Trends with cluster size are often not monotonic, displaying intriguing variations. Examples include magnetic moments and mass spectra, which often display “magic numbers,” or masses that are far more abundant than other masses [9,10]. Another example pertinent to surface chemistry is rate constants for dissociation of H_2 from clusters of varying size [13,14]. In addition to being intrinsically interesting, these phenomena are important to understand so that models of surface processes can be developed that satisfactorily reflect the answer (as yet unknown) to the question: when is a cluster a reasonable approximation of a surface? Theoretical studies have been reported that model a surface with a single metal atom (see, for example, Duarte and Salahub [15]), which is likely not a reasonable approximation. Other studies represent the surface with a cluster of finite size augmented by potentials meant to approximate bulk effects, which quite possibly are valid representations of a surface. Only a concerted effort involving experimental and theoretical studies of clusters of intermediate size can give a definitive answer.

Unfortunately clusters of medium size are very difficult to study theoretically, since they are too large to be treated with highly correlated ab initio quantum chemical methods, and too small to be treated with periodic methods. Recently classical methods have been applied to clusters in this size range [16-19], but these studies are solely concerned with structure. There are no effective methods that can provide information on the electronic structure and electronic spectroscopy of clusters of medium size. It is therefore of great interest to explore more efficient quantum chemical methods that might be applied to clusters in this size range. The logical starting point of such an analysis are the smaller clusters that can be treated with the accurate but expensive methods as a basis for comparison. Diatomic clusters are the first candidates, because of the wealth of spectroscopic data on diatomics and because highly correlated ab initio methods are difficult to apply beyond this size. There are also basic research issues for the diatomics, as described in the next section. The purpose of this dissertation is to contribute to basic research on transition metal diatomics while also investigating a theoretical method of modeling electronic spectroscopy that could be applied (after future development) to the electronic spectroscopy of medium-sized clusters.

The Smallest Metal Clusters: Transition Metal Diatomics

Even the simplest of metal clusters, the diatomics, are important to study because the electronic structure of these molecules and the chemical bonding that occurs between

---

individual transition metal atoms is not completely understood. They provide the most fundamental examples of bonds between two transition metal atoms, and have thus been the subject of intensive study. An early review article by Morse on transition metal dimers [20] has garnered more than 575 citations,[1] with many of the papers reporting more recent investigations of diatomics and larger small clusters. Clearly, the chemical physics community considers the study of these molecules to be significant. Matrix isolation spectroscopy has been applied to transition metal diatomics for quite some time and has provided a wealth of valuable information (see the review article by Weltner and Van Zee [21]), but high-resolution gas phase laser spectroscopy has been applied to these molecules only over the last twenty years. These efforts were made possible by the pioneering development of Smalley and coworkers [22] of the laser vaporization supersonic expansion technique, which allows small clusters to be interrogated spectroscopically at low rotational temperatures.

Over this time period there has been a concomitant development of theoretical methods in tandem with vast improvements in computing technology, but for transition metal diatomics this development has lagged behind the advances in spectroscopic characterization. Molecules containing transition elements have traditionally been considered among the most difficult to treat with theoretical methods, particularly those with two or more transition metal atoms [23-25]. The dichromium molecule has been notorious as an extremely difficult case [26-29], for example, and only very recently has a treatment that can be considered even partially successful been presented [28,30-32]. Even the most prohibitively expensive methods often yield only qualitative accuracy in estimating the ground state bond length and vibrational stretching frequency of dichromium [33] and other transition metal diatomics.

---

[1] Source: The Web of Science Citation Databases, copyright © 2000 Institute for Scientific Information.

In considering the troublesome nature of transition metal diatomics for theoretical methods, the three rows of transition elements must be considered separately, as there are different requirements needed for successful treatment of each. The 5d metals (i.e., La, Hf, Ta, etc.) represent some of the heaviest elements in the periodic table, so relativistic effects are of primary importance. Their large numbers of orbitals and electrons make it difficult to treat these elements with the most accurate theoretical methods, which often cannot be applied as rigorously as needed even to 3d metal diatomics. There is thus very little experience with computational applications to 5d metals [23]. The work described herein is concerned exclusively with the 3d and 4d metals, so further discussion is limited to these elements.

An important difference between transition and main group elements is that several electron configurations are of low energy for the transition elements, $(n-1)d^m ns^2$, $(n-1)d^{m+1} ns^1$, and $(n-1)d^{m+2} ns^0$. Main group elements like carbon, in contrast, typically have one electron configuration of low energy. A second difference is that the (n-1)d and ns orbitals, though both properly considered valence orbitals, are in different shells and hence very different in size. Again this contrasts with the situation for main group elements, in which the valence orbitals fall in the same shell and are comparable in size. Both factors (table 1-2) affect the bonding in the diatomics, as well as impacting their theoretical study. The radial expectation values $\langle r_{ns} \rangle$ and $\langle r_{(n-1)d} \rangle$ given in the table are a measure of orbital size [34].

Table 1-2: Energies of low-lying electron configurations and comparison of (n-1)d and ns orbital sizes[a].

Element	$\frac{\langle r_{ns} \rangle}{\langle r_{(n-1)d} \rangle}$	Relative energy, $ns^2(n-1)d^m$ (eV)	Relative energy, $ns^1(n-1)d^{m+1}$ (eV)	Relative energy, $(n-1)d^{m+2}$ (eV)
Sc	2.03	0.00	1.43	4.19
Ti	2.32	0.00	0.81	3.35
V	2.51	0.00	0.25	2.47
Cr	2.69	1.00	0.00	4.40
Mn	2.81	0.00	2.14	5.59
Fe	2.95	0.00	0.87	4.07
Co	3.08	0.00	0.42	3.36
Ni	3.22	0.03	0.00	1.74
Cu	3.36	1.49	0.00	--
Y	1.61	0.00	1.36	3.63
Zr	1.79	0.00	0.59	2.66
Nb	1.92	0.18	0.00	1.32
Mo	2.05	1.47	0.00	3.18
Tc	2.16	0.00	0.41	--
Ru	2.29	0.87	0.00	1.09
Rh	2.42	1.63	0.00	0.34
Pd	2.54	3.38	0.95	0.00
Ag	2.67	3.97	0.00	--

[a] Source: reference [35].

The data in table 1-2 show that the ns orbitals are considerably larger than the (n-1)d orbitals for all 3d and 4d metals, with the disparity being generally larger for the 3d metals and increasing across each period. Though both ns and (n-1)d orbitals contract as atomic number increases across a given row, the decrease in size is more rapid for d orbitals, leading to the monotonic increase in ratio. The disparity in rate of contraction comes about because the (n-1)d orbitals penetrate closer to the nucleus (on average) than the ns orbitals, being in a lower shell and having fewer radial nodes. Electrons in the (n-1)d orbitals are thus shielded from the nuclear charge much less effectively than the ns electrons, so the d orbitals contract more rapidly as nuclear charge increases.

An important effect of the disparity in orbital sizes is that the (n-1)d–(n-1)d bonds are partially localized even for those diatomics with short bond lengths. This occurs because the overlap of the (n-1)d orbitals on the two atoms is very small. The bonding molecular orbitals that are formed by this overlap therefore have partial atomic or local character, rather than being delocalized over the entire molecule, and are only weakly bonding. This is known as the orbital localization effect. It is analogous to the well-known "dissociation problem" for main group molecules like H_2 (discussed in detail in chapter two), but occurs even at the equilibrium bond distance for the (n-1)d–(n-1)d interaction due to small overlap. As discussed below, weak interactions of this kind are known to be difficult to treat with theoretical methods

An additional problem is that the weak (n-1)d–(n-1)d bonds coupled with the large number of d orbitals and electrons give rise to very high densities of electronic states of low energy. This is the so-called near-degeneracy effect, which poses problems for theoretical as well as spectroscopic studies. In the former case, the theoretical representation of the ground state of the molecule is often multiconfigurational, or composed of many electron configurations that mix strongly. It can also be difficult to obtain the correct ground state since there are other states of very similar energy. The near-degeneracy phenomenon makes interpretation of spectroscopic data difficult, as spectra can be congested and because it is not easy to correlate observed transitions with specific states when there are many states with similar energies. Both near-degeneracy and orbital localization problems are worse for the 3d metals than for the 4d metals, because of the larger ratios of orbital sizes encountered in the former.

The disparity in sizes of ns and (n-1)d orbitals also has a strong effect on the ground states of the diatomics because the ns orbitals begin to interact before the (n-1)d orbitals do as two transition metals come together to bond. If both atoms have$(n-1)d^m ns^2$ electron configurations, the long-range interaction between the filled ns orbitals on the two metals is repulsive, and only a weak van der Waals complex with a long bond length results. If, however, the two metals have $(n-1)d^{m+1}ns^1$ electron configurations, the ns-ns interaction is attractive at long range, and becomes repulsive only well inside the optimum distance for ns-ns interaction. This allows (n-1)d–(n-1)d interactions to come into play [35], resulting in a short bond distance, often much shorter than the interatomic separation in the bulk metal. In many cases, metals that have atomic ground states with $(n-1)d^m ns^2$ electron configurations but $(n-1)d^{m+1}ns^1$ configurations of low energy will form short bonds with d orbital participation by utilizing the low-lying excited configuration. Though the bonds are slightly weaker than would be the case if the ground state configuration were involved, the interaction made possible by opening the filled ns orbitals more than makes up for the cost of the promotion to the excited configuration.

Finally, in cases where the energy of the $(n-1)d^{m+1}ns^1$ configuration is not quite low enough to allow both metals to adopt this configuration, the metals come together with one having the $(n-1)d^mns^2$ configuration and the other having the $(n-1)d^{m+1}ns^1$ configuration. This is known even in cases where the metal atoms are the same element. This asymmetry in a homonuclear diatomic seems counterintuitive, but it should be recalled that the discussion is focused on the formation of the dimer, which occurs in a plasma in the molecular beam experiment. There can thus be atoms with both $(n-1)d^mns^2$ and $(n-1)d^{m+1}ns^1$ configurations present, and the ns^1-ns^2 interaction is attractive at intermediate distances, allowing two atoms with different configurations to begin to interact. Once that happens, a molecular ground state is formed by interaction of the atomic orbitals on the two atoms. The so-called "separated atom limit," or the electron configurations the metal atoms adopt as they begin to interact in forming a diatomic, has a large influence on whether or not the molecule will form, but only a secondary effect on the molecular ground state by means of this influence. The ns^1-ns^2 interaction, for example, becomes repulsive more quickly than the ns^1-ns^1 interaction, leading to intermediate bond distances in diatomics with the ns^1-ns^2 separated atom limit [35].

Exactly which form of bonding occurs in a transition metal diatomic depends on the relative energies of the atomic electron configurations involved (table 1-2). The trends in configurational energies are explained satisfactorily on the basis of greater penetration by the d electrons and the number of d-d exchange integrals [35]. Scandium and yttrium both have $(n-1)d^mns^2$ electron configurations. As atomic number increases across each period, electrons in the smaller d orbitals are increasingly stabilized relative to those in the larger s orbitals since on average they penetrate closer to the nucleus. This increasingly favors the $(n-1)d^{m+1}ns^1$ configuration, a trend seen for both periods, but with discontinuities between the fourth and fifth elements of each row. The discontinuities arise because of the number of d-d exchange integrals, which are generally large and lower the energy of an electron configuration. When the d shell is less than half full, adding additional electrons in proceeding across the period increases the number of exchange interactions between electrons in d orbitals, and the increase is more rapid for the $(n-1)d^{m+1}ns^1$ configuration. This increasingly favors the $(n-1)d^{m+1}ns^1$ configuration for scandium through chromium and yttrium through molybdenum. When the d shell is more than half full, however, increasing the number of d electrons decreases the number of exchange integrals. For manganese through nickel and technetium through palladium the $(n-1)d^mns^2$ configuration is therefore favored, with this bias decreasing across the rest of the period. Thus the $(n-1)d^{m+1}ns^1$ configuration is most strongly favored by the number of d-d exchange integrals for chromium and molybdenum, while the $(n-1)d^mns^2$ configuration is most strongly favored for manganese and technetium. This explains the discontinuities between Cr and Mn and between Mo and Tc in the energies listed in table 1-2.

Another distinctive feature of the ground states of certain metal diatomics is high spin multiplicity. Small differences in energies of molecular orbitals formed from the weakly interacting (n-1)d orbitals coupled with the large d-d exchange integrals can lead to open-shell electron configurations that violate the Aufbau principle (i.e., that lower energy orbitals fill before higher energy orbitals are occupied). The interaction energy of bonding molecular orbitals that are singly-occupied decreases linearly with the overlap, while that for doubly-occupied bonding molecular orbitals decreases with the square of the overlap [35]. If the bond distance is long, then, single occupation of the molecular orbitals formed from atomic d orbitals is encouraged. Prior to the advent of molecular beam spectroscopy it was thought that early transition metal diatomics might have very high spin ground states, with all or most of the d electrons unpaired [36]. This has not proven to be the case [20], but ground states are often not diamagnetic. Though theoretical methods for dealing with open shell ground states are well-developed, their presence in transition metal diatomics is an additional complication.

The ground state properties of the 3d homonuclear diatomics provide a good example of the interplay between the factors just described (table 1-3). In the following discussion theoretical methods are referred to without being described in order to preserve clarity of discussion. Chapter two provides definitions and technical details. The ground state of the scandium dimer has been assigned as ${}^5\Sigma_u^-$ by Weltner and coworkers based on matrix isolated ESR work [37]. The atomic ground state has configuration $3d^1 4s^2$. The $3d^2 4s^1$ configuration is not low enough in energy to be readily utilized in forming the ground state, but is low enough in energy that one atom adopts this configuration as the two atoms approach and begin to bond. The bond distance has not been determined experimentally, but has been predicted to be 2.72 Å by complete active space self-consistent field calculations [38] and 2.60 Å by density functional calculations using the B3LYP functional [39]. This bond distance is seen to be of intermediate length (table 1-3), as expected for a diatomic with separated atom limit $3d^{m+1}4s^1 + 3d^m 4s^2$. The linear dependence of the interaction strength of single-electron

Table 1-3: Comparison of properties of homonuclear diatomic molecules composed of the 3d transition metals. Results in parentheses are theoretical predictions, all others determined experimentally.

Molecule	**Bond distance (Å)**	**Stretching frequency (wavenumbers)**	**Ground state**	**Separated atom limit**
Sc_2	(2.60)[a] (2.72)[b]	239.9[c]	$^{5}\Sigma_{u}^{-}$ [d]	$3d^24s^1 + 3d^14s^2$
Ti_2	1.94[e]	408.9[f]	$^{3}\Delta_{g}$ [e]	$3d^34s^1 + 3d^34s^1$
V_2	1.77[g]	537.5[f]	$^{3}\Sigma_{g}^{-}$ [g]	$3d^44s^1 + 3d^44s^1$
Cr_2	1.68[h]	480.6[i]	$^{1}\Sigma_{g}^{+}$ [j]	$3d^54s^1 + 3d^54s^1$
Mn_2	3.40[k]	68.1[l]	$^{1}\Sigma_{g}^{+}$ [k]	$3d^54s^2 + 3d^54s^2$
Fe_2	2.02[m]	299.7[n]	$(^{7}\Delta_{u})$ [a]	$3d^74s^1 + 3d^74s^1$
Co_2	(2.44)[a]	296.8[o]	$(^{5}\Sigma_{g}^{+})$ [a,p]	$3d^84s^1 + 3d^84s^1$
Ni_2	2.15[q]	259.2[r]	$(^{3}\Sigma_{g}^{-} + {}^{1}\Sigma_{g}^{+})$ [s,q,t] $(^{3}\Sigma_{u}^{+} + {}^{1}\Sigma_{u}^{-})$ [s,q,,t]	$3d^94s^1 + 3d^94s^1$
Cu_2	2.22[u]	266.5[u]	$^{1}\Sigma_{g}^{+}$ [u]	$3d^{10}4s^1 +$ $3d^{10}4s^1$

[a] Source: reference [39].
[b] Source: reference [38].
[c] Source: reference [42].
[d] Source: reference [37].
[e] Source: reference [45].
[f] Source: reference [47].
[g] Source: reference [49].
[h] Source: reference [50].
[i] Source: reference [52].
[j] Source: reference [54].
[k] Source: reference [55].
[l] Source: reference [56].
[m] Source: reference [40]
[n] Source: reference [41].
[o] Source: reference [43].
[p] Source: reference [44].
[q] Source: reference [46].
[r] Source: reference [48].
[s] See text for details.
[t] Source: reference [51].
[u] Source: reference [53].

bonds on the overlap (as opposed to dependence on the square of the overlap, as for two-electron bonds) causes the three 3d electrons to be unpaired, leading to the high ground state spin multiplicity.

The next three molecules, Ti_2, V_2, and Cr_2, provide sharp contrasts to what is known about Sc_2. In the first two cases the atomic ground state has the $3d^m4s^2$ configuration, but with the $3d^{m+1}4s^1$ configuration readily available, and in the case of chromium the $3d^{m+1}4s^1$configuration is the ground state configuration. In all three cases, then, the separated atom limit is $3d^{m+1}4s^1 + 3d^{m+1}4s^1$, resulting in short bond lengths particularly for Cr_2 and V_2, and extensive participation of the d orbitals in the bonding. At the very short bond distances of Cr_2 and V_2 two-electron bonds are strongly favored, leading to the low spin multiplicities.

The ground state of dititanium is quite interesting. It has been assigned as $^3\Delta_g$ based on resonant two-photon ionization molecular beam spectroscopy [45]. The molecular electron configuration is thought to be $(3d\pi_u)^4(4s\sigma_g)^2(3d\sigma_g)^1(3d\delta_g)^1$ [57], in which a single electron occupies the degenerate $3d\delta_g$ shell, leaving a single electron in the lower-energy $3d\sigma_g$ orbital. This arises for the reasons already described, the general weakness of (n-1)d-(n-1)d interactions and large d-d exchange integrals. This broken occupation of a degenerate orbital cannot be described by a single reference configuration. This example illustrates the complexity of the bonding in transition metal diatomics, and it is no surprise that theoretical methods (and concepts!) that work well for simpler molecules composed of main group atoms are not as successful for transition metal clusters.

In the case of dimanganese, the $3d^{m+1}4s^1$ configuration is too high in energy to be available for bonding. As expected for a diatomic with separated atom limit $3d^54s^2$ + $3d^54s^2$ only a weakly bound complex with a very long bond distance has been observed in matrix isolation work [58]. Dimanganese has not been observed in the gas phase. An interesting aspect of the $^1\Sigma_g^+$ ground state of this molecule is that at the extremely long bond distance the 3d orbitals on each atom are completely localized atomic orbitals, each retaining the unpaired electron populating the orbital in the atomic ground state. The five electrons on each atom are antiferromagnetically coupled with the electrons on the other atom, resulting in a singlet ground state despite the presence of ten unpaired electrons [55,58-60]. Mn_2 is very difficult to treat computationally because of the very weak bonding and antiferromagnetic coupling.

Moving from manganese to iron, it is seen that the $3d^74s^1$ configuration is low enough in energy to be utilized for bonding, though it is not the atomic ground state. The resulting bond length is 2.02 Å, as determined by extended x-ray absorption fine structure spectroscopy [40]. This distance is short, though relatively much longer than the distances in Ti_2, Cr_2, and V_2 since the atomic orbitals contract across the period. The ground state has not been assigned on the basis of experimental spectroscopy, but DFT calculations using a variety of different functionals and calculations with several correlated ab initio methods all agree that the ground state symmetry is $^7\Delta_u$ [39,61]. The electron configuration predicted by all of the theoretical calculations, $(3d\sigma_g)^2(3d\pi_u)^4(3d\delta_g)^3(3d\delta_u)^2(4s\sigma_g)^2(3d\pi_g)^2(3d\sigma_u)^1$, shows broken occupancy of degenerate orbitals, similar to what is seen for Ti_2. In the case of Fe_2, however, the 3d orbitals have become so compact compared to the 4s orbitals that their interaction is much weaker than in Ti_2. This allows population of the antibonding orbitals with unpaired electrons and hence the high spin multiplicity. The broken occupation of the $3d\delta_g$ shell can be attributed to a delicate interplay of the Coulomb repulsion energy of electrons in these orbitals, the large size of d-d atomic exchange integrals, and the relative strengths of one-electron and two-electron bonds with the very small overlaps of the d orbitals at the bond distance of Fe_2. It should be noted that the ground state symmetry and electron configuration of Fe_2 must be considered somewhat conjectural, since the success of even the best theoretical methods is not routine for the 3d metal diatomics.

Available data on dicobalt are sparse, as the molecule has not been observed in the gas phase. Matrix isolation resonance Raman spectroscopy has yielded the vibrational frequency of Co_2 [43], but the bond distance and ground state symmetry have not been determined. Both correlated ab initio calculations [44] and DFT calculations [39] indicate that the ground state is ${}^5\Sigma_g^+$. The electron configuration of the dimer is not certain, as different methods give different predictions, but all possibilities are derived from the separated atom limit $3d^84s^1 + 3d^84s^1$ due to the low energy of the $3d^84s^1$ configuration relative to the ground state $3d^74s^2$ configuration.

The last two dimers described in table 1-3, Ni_2 and Cu_2, are similar. In both cases the primary interaction responsible for the bonding is from the $4s^1$–$4s^1$ interaction. The d orbitals are so compact that they remain local, and do not contribute to the bonding in either molecule. The d orbitals are filled in the case of Cu_2 and have two holes in the $3d\delta$ shell in the case of Ni_2 [46,51], though it is unclear whether the unpaired electrons reside in the gerade or ungerade combinations [46]. In the former case, spin-orbit coupling is expected to thoroughly mix the ${}^3\Sigma_g^-$ and ${}^1\Sigma_g^+$ states, while in the latter case the

${}^3\Sigma_u^+$ and ${}^1\Sigma_u^-$ states are mixed [46,51]. Theory predicts that the true ground state is the $\Omega'' = 0$ spin-orbit component of the ${}^3\Sigma_g^- + {}^1\Sigma_g^+$ mixture, but with the same component of the ${}^3\Sigma_u^+ + {}^1\Sigma_u^-$ mixture only 12 cm^{-1} higher in energy. Experiment has not yet been able to distinguish between the two possibilities [46]. Both molecules have bond distances of intermediate length.

The Quantum Chemistry of Transition Metal Diatomics

The phenomena of near-degeneracy and orbital localization, the possibility of high-spin ground states, the large numbers of electrons occupying the compact (n-1)d orbitals, and the large variation in bond lengths just described for the 3d transition metal dimers make these molecules rather challenging for the methods of quantum chemistry. The primary difficulty in applying quantum chemical methods to molecules containing transition metals is adequately accounting for electron correlation, which refers to the fact that the motions of electrons in molecules are instantaneously correlated with the motions of other electrons due to the Coulombic repulsion between them. The correlation energy as originally defined by Löwdin [62] refers to the difference between the exact energy of the molecule (assuming a certain Hamiltonian, in the present case the nonrelativistic, time-independent, Born-Oppenheimer molecular Hamiltonian) and the energy obtained for that Hamiltonian at the Hartree-Fock (HF) level. A formal discussion of electron correlation and the correlation energy is given in chapter two. For purposes of the present discussion, the important point is that the single determinant Hartree-Fock (HF) level is assumed to be uncorrelated.

Practical calculations that seek to incorporate correlation effects beyond the Hartree-Fock level must use some approximation to the correlation energy, since the true correlation energy can be obtained only at the full configuration interaction (CI) level in a complete basis set, clearly an impossible task. Nevertheless methods that include an approximation to the correlation energy are referred to as "correlated," as are wavefunctions obtained from such methods. The term "correlation effects" then refers to effects that arise from inclusion of an approximation to the correlation energy in a method, and will be applied rather loosely to energies and wavefunctions in the following discussion.

Correlation effects are extremely important in calculations on transition metal clusters. They can be divided into two types, essential and dynamic. The former involves breakdown of the single determinant description, and refers to strong mixing of one or more excited determinants with the Hartree-Fock reference determinant. This happens when a single determinant is not a qualitatively correct wavefunction. It is crucial to include essential correlation for cases where there are configurations with energies similar to the energy of the reference configuration, as is the case for weakly bound molecules and excited states. Dynamic correlation effects correct the treatment of the interelectronic repulsion at the Hartree-Fock level, which overestimates the energy of repulsion since the electrons are treated as independent particles at that level . Dynamic correlation specifically refers to contributions to the wavefunction that do not affect the qualitative nature of the wavefunction [63]. Dynamic correlation is increasingly important as the number of electrons in a given volume becomes larger.

Near-degeneracy and orbital localization effects lead to severe essential correlation problems. In the former case, the small energy differences between the (n-1)$d^m ns^2$, (n-1)$d^{m+1} ns^1$, and (n-1)d^{m+2} configurations often requires a multireference treatment even for ground states of molecules with one transition metal atom. A classic example of this is provided by NiCO, in which the bonding involves an equal admixture of the $3d^9 4s^1$ and $3d^{10}$ configurations [64,65]. In clusters the problem is compounded by the presence of additional metal atoms, leading to a high density of states at low energy, and hence extensive multireference character of ground and excited states. This is the near-degeneracy problem as seen from a theoretical standpoint, which leads to severe essential correlation effects. Orbital localization contributes as well, since localization is realized by mixing of configurations in which bonding molecular orbitals are occupied with configurations in which the corresponding antibonding orbitals are occupied (a detailed discussion of this is given in chapter two). This again leads to mixing of the reference determinant with excited determinants. Both problems are worse for the 3d metals than for the 4d metals [35] due to the larger discrepancies in the sizes of 3d and 4s orbitals. The 4d metals are, in fact, generally considered to be easier to treat computationally than the 3d metals because of the severity of the near-degeneracy and orbital localization problem for the latter [23].

Dynamic correlation is also very important in calculations on metal clusters, because the d orbitals are compact and occupied by potentially large numbers of electrons [23,28]. This is true even for diatomics composed of elements early in the transition series. Divanadium and dichromium, for example, formally have pentuple and sextuple bonds, respectively. There are thus roughly ten or twelve electrons in the volume between nuclei, which are separated by distances of 1.77 Å or 1.68 Å. This can be compared with ethane, which has a comparable bond distance of 1.54 Å but only two electrons representing the carbon-carbon single bond. Dynamic correlation effects are important for clusters of both 3d and 4d metals, though perhaps slightly worse in the former case as the 3d orbitals are smaller.

Before illustrating the computational difficulties described above for dichromium, relativistic effects deserve mention for the 3d and 4d metals. These effects can be divided into two general types. The first, scalar relativistic effects, have to do with expansion and contraction of orbitals due to relativistic mass increases of electrons in heavy elements, which are moving at an appreciable fraction of the speed of light due to the high nuclear charge [66]. Scalar relativity is insignificant for the 3d metals, and of very minor importance for the 4d metals, so is not considered further. The other type is spin-orbit coupling, which is the coupling of the spin and orbital angular momenta of electrons, thought of as a relativistic effect because of the relativistic nature of electron spin [67]. This too becomes increasingly important for heavier elements, as it can be shown that the magnitude of energy splitting caused by spin-orbit coupling is proportional to the fourth power of the nuclear charge [68]. Spin-orbit effects are generally small in 3d and 4d metal clusters, providing additional structure to spectroscopic levels but not greatly impacting their energies. They are, however, often vital to state assignments and can provide indirect information on states that are not directly observable. It is thus useful but not crucial for a theoretical method to include spin-orbit coupling.

The chromium dimer, Cr_2, provides a vivid illustration of the problems that beset theoretical calculations on metal clusters. As discussed above, dichromium has a formal bond order of six, but the overlap of the 3d orbitals is very small even at the short bond distance, so the bond order is reduced by orbital localization [28]. The dissociation energy D_0, for example, is 35.3 kcal/mol [69], smaller than D_0 of the singly-bonded dicopper molecule (47.9 kcal/mol [70]). Casey and Leopold have determined the potential energy curve for dissociation of Cr_2 with negative ion photoelectron spectroscopy [52]. The potential has a minimum at the experimental bond distance, and a distinct shelf between about 2.25 Å and 3.00 Å. The explanation for this behavior that has been developed is that in the shelf region there is interaction between the 4s orbitals of the two atoms (which have the ground state configuration $3d^5 4s^1$), with the 3d electrons on each atom coupled antiferromagnetically, as is the case with the 3d electrons in Mn_2. The inner well arises because of 3d–3d bonding.

Obtaining a potential energy curve for Cr_2 in reasonable agreement with experiment has proved to be an elusive goal for theory until recently. Early generalized valence bond structure calculations had indicated that there might be a minimum in the potential curve at roughly 3.00 Å, but with a potential energy barrier between this minimum and a deeper minimum in the vicinity of the equilibrium bond distance (r_e) [71]. More modern calculations also failed to provide a potential surface in qualitative agreement with experiment [27,29,33,35,72]. Calculations at the coupled cluster level including single and double excitations and connected triple excitations (CCSD(T)) using a spin-restricted wavefunction gave a bond distance shorter than r_e but a minimum energy above the energy of two isolated chromium atoms [27]. This represents the sextuple bond involving the ten 3d electrons and the two 4s electrons. The restricted wavefunction does not dissociate properly, however, and cannot describe the antiferromagnetic coupling expected for the 3d electrons at longer distances. CCSD(T) calculations with an unrestricted wavefunction, on the other hand, gave the minimum of the potential curve in the vicinity of the shelf, and no minimum near r_e [27]. This wavefunction represents long-range 4s–4s bonding and antiferromagnetically coupled 3d electrons.

The consensus that has emerged based on both experimental and theoretical investigations is that the ground state of Cr_2 is somewhere between the sextuply-bonded description and the antiferromagnetic picture [20,24,26-33,35,52,71-73]. In the vicinity of the equilibrium bond distance the 3d orbitals participate in the bonding but are partially dissociated, requiring mixing with configurations with occupied antibonding orbitals. The closed-shell restricted sextuply-bonded configuration and the unrestricted antiferromagnetic configuration are thus coupled through off-diagonal Hamiltonian matrix elements. An extremely large configurational space would be required to properly describe this coupling. Langhoff and Bauschlicher have estimated that on the order of ten billion configurations would be necessary in the large basis set required for quantitative accuracy [74], a calculation that is far from tractable at the present time. Clearly a less expensive approach is necessary, and has been provided by multiconfigurational perturbation theory [28,30-32,73].

A widely-used approach to treating wavefunctions with strong multireference character is the complete active space self-consistent field (CASSCF) method [75], in which all possible configurations for a specified number of electrons in a specified number of orbitals are considered. These "active orbitals" are chosen to (hopefully) yield all of the important configurations. State wavefunctions are taken as linear combinations of the configurations, with expansion coefficients and orbitals optimized simultaneously so that the energy of a given state reaches a stationary value. Further details are beyond the scope of this discussion. CASSCF is an expensive computational method, and is difficult to apply (at present) to clusters larger than diatomics due to practical limitations of computing technology (in principle the CASSCF formalism could be applied to any number of orbitals and electrons). Indeed, limitations in computing power can pose a problem even for CASSCF calculations on dimers. Cr_2 is again a good example, as the CASSCF wavefunction for Cr_2 has a shoulder near r_e rather than a minimum, with the predicted minimum in the vicinity of the shelf seen in the experimental potential energy curve [30]. Clearly dynamic correlation effects from outside the active space that are neglected in the calculation have an important role to play.[2]

One approach to improving CASSCF wavefunctions is multireference configuration interaction (MRCI) using the CASSCF orbitals, with excitations involving the inactive electrons and/or virtual orbitals. This sort of treatment was the one envisioned by Langhoff and Bauschlicher [74] with ten billion configurations. Dachsel, Harrison, and Dixon have recently reported CASSCF/MRCI calculations on Cr_2 that included over one billion configurations [33]. These calculations were extremely expensive and gave what can generously be called semiquantitative accuracy for spectroscopic constants. Values obtained were 1.72 Å for r_e, 25.1 kcal/mol for D_e, and

---

[2] These contributions are assumed to be dynamic because the active space is supposed to capture the essential correlation.

339 cm^{-1} for the fundamental vibrational energy ω_e, compared to the experimental values of 1.6788 Å [50], 35.3 kcal/mol [69], and 480.6 cm^{-1} [52].

An alternative to CASSCF/MRCI is the CASPT2 method [76], which uses second order multireference perturbation theory to incorporate correlation effects from outside the active space. The present implementation of CASPT2 is limited to 12-14 orbitals due to technological limits in computing power [30], so again can realistically be applied only to diatomics of the 3d metals. A major problem with the method involves intruder states, or states that involve orbitals outside the active space but have energies close to the energy of the reference state. If this is the case, the second-order energy diverges. This problem is severe for 3d transition metal diatomics because the unoccupied valence 4p orbitals are only slightly higher in energy than the 4s and 3d orbitals. The most obvious solution to this problem would be to include the 4p orbitals in the active space, but the orbital space would then be intractably large, with eighteen orbitals. In the case of Cr_2 Roos and Andersson were able to circumvent the intruder state problem by modifying the zeroth-order Hamiltonian so that the first-order interacting space is shifted up in energy [31]. This removes the intruder states from the active space, allowing the perturbation expansion to converge. A correction is then applied to the second order energy to approximate the unshifted energy. A reasonable approximation of the Cr_2 potential surface was generated using this method [31]. Results for the spectroscopic constants of the ground state were $r_e = 1.686$ Å, $D_0 = 35.5$ kcal/mol, and $\omega_e = 550$ cm^{-1} which compare favorably with the experimental values of 1.6788 Å [50], 35.3 kcal/mol [69], and 480.6 cm^{-1} [52].

An advantage of CASPT2 is that it can be applied to excited states without a considerable increase in computational effort [73]. Potential surfaces for a number of excited states have been obtained for Cr_2 [32], but again severe intruder state problems required level shifting, raising questions about the validity of the results. The strong presence of intruder states involving the 4p orbitals indicate that they should be in the active space, and the possibility exists that these orbitals play a role in the electronic spectrum of Cr_2.

In summary, for Cr_2 a CASSCF calculation using the 3d and 4s orbitals as active space does not have a minimum in the vicinity of the experimentally-determined bond distance, indicating that there are important correlation effects involving the inactive orbitals. CASPT2 gives a qualitatively reasonable potential energy surface and good estimates of spectroscopic constants, if a level shift is used to alleviate the intruder state problem. That, together with sensitivity of the results to the form of the zeroth-order Hamiltonian, leaves the success of the CASPT2 treatment of Cr_2 unsatisfactory [29]. The method has not been applied to other transition metal diatomics. Computational limitations have been seen to come into play already for dichromium as well, so CASPT2 is not a method that can be applied to clusters larger than diatomics. The CASPT2 results do, however, indicate that a successful method will need to account for essential and dynamic correlation effects within the 4s and 3d orbital space, and for dynamic correlation effects from outside this orbital space.

In assessing the general situation of theoretical methodologies and their application to metal clusters it is important to note that dichromium is known to be a pathological case. The problems of near-degeneracy and orbital localization described previously are complicated in the case of Cr_2 by the stability of the $3d^5 4s^1$ configuration relative to the $3d^4 4s^2$ configuration. This allows the long-range 4s–4s interaction to couple strongly with the short-range 3d–3d bonding. An additional complication is that the formal bond order is higher for Cr_2 than for any of the other 3d homonuclear diatomics. Dimolybdenum might be expected to behave similarly, but the near-degeneracy and orbital localization are less severe for the 4d diatomics due to the more similar sizes of the 5s and 4d orbitals, which allows stronger d–d bonding. This is exemplified by the early CASSCF results of Walch and Bauschlicher on Mo_2 [35], which gave ground state spectroscopic constants in qualitative agreement with experimental values. The same is not true of analogous calculations on Cr_2. Though other transition metal diatomics are not as difficult to treat as dichromium, accurate highly-correlated ab initio calculations are not tractable when applied to clusters larger than diatomics. Recourse to more efficient methods is necessary if medium-sized clusters are to be treated.

A computational approach with great promise for describing transition metal diatomics and larger clusters is density functional theory. DFT has met with considerable success for transition metal complexes [23,77], and application of DFT methods to the 3d homonuclear diatomics has been examined recently [39,61]. The results show that ground state spin multiplicities and symmetries are correctly predicted in most cases. For ground state spectroscopic constants, errors are on the order of five percent in r_e depending on the details of the functionals used, but twenty-five to forty percent in ω_e, and dissociation energies are severely overestimated [39]. In connection with the previous discussion, calculations on Cr_2 with the BLYP functional give a potential curve with some indication of the shelf, but underestimate r_e and badly overestimate the binding energy; with other functionals, only a shallow minimum in the vicinity of the shelf is obtained [27]. Clearly, DFT is not yet greatly successful for these molecules. The major advantage of DFT is that it is inexpensive compared to the highly correlated ab initio models, and has been applied to clusters larger than diatomics. See, for example, the recent calculations on clusters of iron, cobalt, and nickel of up to five atoms of Castro, Jamorski, and Salahub [78].

Another problem with DFT is that it is not generally applicable to excited states and electronic spectroscopy, though progress is being made in that direction (see, for example, the recent paper by Rösch and coworkers [79]). Additionally, results of DFT calculations are not very interpretable, since they do not yield a formal wavefunction [25].[3] Properties that are readily calculated by taking the expectation value of an appropriate operator with standard wavefunctions can therefore be difficult to describe with DFT. Finally, DFT struggles with intermediate spin states, or cases where the spin multiplicity is not equal to one greater than the number of unpaired electrons. An example is the antiferromagnetically coupled ${}^1\Sigma_g^+$ ground state of Mn_2 [39]. The conclusion is that DFT is not yet a viable tool for the study of transition metal clusters, but is promising.

Semiempirical Methods: Potential Tools of Study for Small and Medium-sized Clusters

In main group chemistry there has been a complementary use of highly-correlated ab initio theory, DFT, and semiempirical methods to treat problems of various sizes. Ab initio calculations are used for small molecules and semiempirical models for large molecules, with DFT playing a growingly prominent role for molecules of intermediate size. The same has not been true for metal clusters for several reasons, some of which were described in the previous sections. Even the most accurate, expensive ab initio calculations often struggle with small clusters, and so the less accurate semiempirical methods have not been considered as potential alternatives. If the best methods do not necessarily work, why expect that methods that are generally considered to be less accurate would be applicable? In fact there are several arguments that can be made to support the potential for application of semiempirical methods to metal clusters.

---

[3] DFT orbitals give an accurate electron density, and can be interpreted as if they give an accurate density matrix, but do not represent a wavefunction in the traditional sense.

As the discussion of the electronic structure of transition metal diatomics revealed, electron correlation must be included in any model that will be applied to metal clusters. In considering correlation in semiempirical methods it is important to observe the distinction between the terms "model" and "level." Model is meant to indicate the form of the molecular Hamiltonian, including the various approximations made in obtaining a soluble Schrödinger equation. From the standpoint of second quantization [80], this includes specification of the salient one electron and two electron integrals, and any approximation invoked in that specification. The various forms of the zero differential overlap approximation [81-85], for example, are therefore considered to be models. Level, on the other hand, describes the treatment of electron correlation with reference to the Hartree-Fock (variational independent particle) approximation. Thus, a semiempirical model can in principle be applied at any level of correlation. Traditionally that level has been low, often the Hartree-Fock level, because the intended purpose of semiempirical methods has been to treat molecules that are so large (these days on the

---

order of thousands of atoms) that every aspect of the calculation must be as cheap as possible. This choice of level does not follow from any requirement, however, and a correlated semiempirical method (MNDOC of Thiel and coworkers) has been proposed [86]. MNDOC was found to perform well for certain cases where correlation is necessary, including excited states [87] and transition states [88-90]. The example of MNDOC shows that a semiempirical method can be successfully applied at a correlated level.

One of the major goals of this work is to investigate the possibility of using a semiempirical method to study the electronic spectroscopy of transition metal dimers and clusters. The intermediate neglect of differential overlap model parameterized for electronic spectroscopy (INDO/S) of Zerner [91,92] is a natural choice for this purpose, as its usefulness for molecules containing transition metals is well-established [24,93]. Experience with INDO/S provides additional support for applying such a model to metal clusters. The model was originally parameterized for the transition metals at the level of configuration interaction truncated to single excitations (CIS) [91,92], which is not sufficient for calculations on clusters. However, calculations on complexes of the form $M(H_2O)_6^{q+}$ at the level of full CI in the metal 3d and 4s orbitals [94] showed that the model could be successfully applied at this level, but with modification of certain parameters. In fact, at this level INDO/S has been shown to be as accurate as large-scale correlated ab initio CASSCF calculations for predicting gas-phase transition energies and intensities for transition metal complexes [95,96].

Calculations have also been carried out with INDO/S on nickel clusters of up to fifty-one atoms [97-99]. These calculations highlight the potential value of a semiempirical method that could be applied to clusters, as fifty atoms is far beyond the size of cluster that can be treated with ab initio models. It is unclear if these calculations are successful, however, due to a lack of experimental corroboration of predictions made for the larger clusters, and unscientific changes made in the semiempirical parameters. For Ni_2, for example, the resonance integrals (defined in chapter two) for the nickel 3d orbitals were increased greatly to obtain an accurate description of the electronic spectroscopy [97], but the resulting bond order is unrealistically high due to consequent exaggeration of the strength of the 3d-3d interaction. As discussed above, in the case of Ni_2 the 3d orbitals are completely local and hence do not contribute to the bond order.

The previous results obtained with INDO/S for nickel clusters are a clear indication that the model has great promise for describing the electronic structure of metal dimers and clusters, but with the caveat that the model in its present form has not been applied using the high level of electron correlation needed for describing metal clusters. There are fundamental questions regarding the role of electron correlation in semiempirical methods that must eventually be addressed if a systematic application to clusters is to be possible. A brief summary is given in the next paragraph, with more technical details presented in chapter two.

Semiempirical methods are implemented at a certain level of theory, which is typically applied within an orbital space limited to the valence orbitals, but are parameterized to reproduce experimental data on a range of test cases. By this it is meant that certain numerical parameters used as simplifications to an ab initio theory are adjusted until the best possible agreement is obtained between theory and experiment for the test cases. Whatever the specific details of a model (semiempirical or other) might be, the experimentally determined value of a quantity being computed represents truth, within the confines of the accuracy and precision of the experiment. This implies an inherent representation of the exact electron correlation, which must be encompassed by the method if it yields the experimental result. Therefore it is thought that correlation effects are being incorporated into the parameters of semiempirical methods [24,100-104]. This inclusion is unsystematic since the parameterization procedure yields the best possible fit between theory and experiment but an exact fit is never in practice obtained, and only approximate transferability of the parameters to molecules not in the set of test cases can be assumed.

The theoretical foundation of the assertion that correlation effects are implicitly included in a semiempirical parameterization rests on the partitioning of the Hamiltonian matrix into a valence space and a correlating space. The valence space contains all electron configurations that can be obtained by distributing the valence electrons in the valence orbitals. The correlating space includes all configurations in which electrons in core orbitals have been promoted, unoccupied orbitals above the valence shell have been occupied, or both. The partitioning procedure formally leads to an effective Hamiltonian for the valence space that yields the correct wavefunctions and energies for all states within the valence space, as first demonstrated by Löwdin [105]. This effective Hamiltonian implicitly includes contributions from outside the valence space (details are given in chapter two), and it has been demonstrated through analysis of the ab initio effective valence shell Hamiltonian method that semiempirical models approximate these contributions through the parameterization procedure [100]. It is believed that dynamic correlation can be accounted for in this way since it does not qualitatively alter the wavefunction, but essential correlation cannot be since it does [93].

An important question that has been raised involves "overcounting" of the dynamic correlation when applying a semiempirical method at a correlated level. If this correlation is implicitly present in the model and also treated explicitly, it has been included twice, which can lead to poor results [104]. Based on the effective valence shell Hamiltonian approach, the semiempirical method is envisioned as being applied at the full CI level in the valence space, with dynamic correlation from outside the valence space entering via the parameters. This is roughly analogous to the CASPT2 procedure, where full CI is performed in the active space and dynamic correlation from outside the active space is estimated with second order multireference perturbation theory. However, the widely-used semiempirical methods were not parameterized at the full CI level. Thus some dynamic correlation within the valence space might be assumed to be present in these models as well.[4] If so, the overcounting problem might be present if a semiempirical method was applied at the full CI level in the valence space, or at any level higher than the level at which it was parameterized.

Clearly these questions must be investigated if a systematic approach to including electron correlation in semiempirical methods is to be developed. The work with the ab initio effective valence shell Hamiltonian on semiempirical methods, while valuable, is open to the same criticisms given earlier regarding the CASPT2 formalism, including sensitivity of results to the choice of zeroth-order (uncorrelated) Hamiltonian and truncation of the multireference perturbation theory at second order. Furthermore, the ab initio effective valence shell Hamiltonian calculations do not give parameters similar to those used in the popular semiempirical methods, though they do support certain approximations such as the zero differential overlap approximation and transferability of parameters between different molecules [101]. It would therefore be valuable to test the assertions regarding electron correlation described above in a widely-used semiempirical method, as well as the implications of applying the method at a correlated level less than the full CI level in the valence space. Transition metal dimers are good test cases for such study, since correlation effects are so important in their electronic structure.

---

[4] Some authors consider dynamic correlation to specifically indicate correlation effects from outside a defined active space [106], while others give the more general definition used here [63].

The diatomic molecules V_2, VNb, and Nb_2 and have been chosen as examples for several reasons. First, V_2 is in many ways similar to Cr_2, with a very short bond length (table 1-3), a low ground state spin multiplicity, and a high formal bond order but a relatively small fundamental stretching frequency. There should thus be distinct correlation effects in the electronic structure of V_2 and the related molecules. However, V_2 is expected to be easier to treat than Cr_2 [35,72] In support of the suggestion that V_2 is a less difficult problem, it is pointed out that CASSCF [72] and DFT [107] calculations on V_2 give a reasonable description of the ground state, which is not the case with Cr_2. Secondly, V_2, VNb, and Nb_2 are known spectroscopically, but very little modern computational work on excited states has been reported. Although much has been learned from the spectroscopic studies, a number of questions remain and there is at least one ongoing controversy over state assignments (later chapters give a full account). There is thus a need for theoretical calculations on the electronic spectroscopy and electronic structure of the molecules from a basic research standpoint. This is a major focus of the present work. One specific aspect of this focus is interesting spin-orbit effects that have been observed for V_2, VNb, and Nb_2. These phenomena can be investigated with the spin-orbit capability of the INDO/S implementation in the ZINDO program package [108].

The spin-orbit effects are also related to the previously-mentioned goal of investigating electron correlation in the INDO/S model, since the ground state spin-orbit phenomena allow a separation of dynamic and essential correlation (details are given later). This allows an investigation of the conceptual predictions of the ab initio effective valence shell Hamiltonian work within the framework of a widely-used and successful semiempirical method. Using V_2, VNb and Nb_2 for this purpose provides examples involving metals from both the 3d and 4d transition series, and of homonuclear and heteronuclear diatomics.

Summary and Purpose

In summary, the purposes of this thesis are three-fold. First, to demonstrate the ability of a semiempirical method to successfully account for the electronic structure and spectroscopy of transition metal dimers. Second, to provide an in-depth examination of the spectroscopy and spin-orbit effects in neutral and positive V_2, VNb, and Nb_2 as a complement to the experimental spectroscopy, examining state assignments, investigating unassigned transitions, and so forth. Third, to investigate correlation effects in the INDO/S model. In this last case, the work reported here represents only a small initial step which future work can build on, along with the ongoing work on the fundamental basis of semiempirical methods [100,101]. The eventual goal is the design of a semiempirical method of general use for larger clusters.

The remainder of the dissertation is organized as follows: chapter two presents the fundamental theory behind the methods used and the details of their implementation. Chapter three describes improvements made by the author and collaborators to the ZINDO program [108] to make possible the calculations reported in later chapters. Chapters four and five describe various calculations on the molecules V_2, VNb, and Nb_2, and their interpretation. All of the calculations and interpretations described in chapters four and five are original work done by the author. Chapter six provides a summary and conclusions

CHAPTER 2
METHODS OF CALCULATION

Fundamental Considerations

The basis of the semiempirical and ab initio molecular electronic structure methods considered here is the nonrelativistic time independent Schrödinger wave equation [109],

$$\hat{H}\Psi_i = E_i \Psi_i \quad i = 1,2,... \tag{2-1}$$

where the $\{\Psi_i\}$ are wavefunctions representing the states of the system, each with a particular state energy E_i. The methods to be described are thus concerned with determining the energies of stationary electronic states of molecules and wavefunctions for those states. The latter can be used to determine stationary properties and, within the framework of a time-independent theory, estimates for intensities of spectroscopic transitions between stationary states. No provision is made for dynamical properties or processes, which would require recourse to the more general time-dependent theory. Two fundamental postulates of quantum mechanics [34] are that the wavefunction contains all information that can be learned about a given state of the molecule, and that the probability distribution of the particles comprising the molecule is given by the square of the wavefunction (the Copenhagen or Born interpretation, after Max Born). $\hat{H}$, the Hamiltonian operator, is a differential operator containing terms representing the various interactions between the particles comprising the molecule. Once an appropriate form has been chosen for the wavefunctions, equation (2-1) could in principle be solved for the wavefunctions $\{\Psi_i\}$ and the energies $\{E_i\}$. In practice, however, the Schrödinger equation can be solved analytically only for a very small number of specific cases, and a number of approximations are necessary in the case of molecules.

The fundamental interactions between particles comprising a molecule in the nonrelativistic, time-independent model include kinetic energies of the nuclei and electrons, attraction between electrons and nuclei, repulsion between electrons, and repulsion between nuclei. The Hamiltonian operator in atomic units corresponding to these interactions is, in the same order,

$$\hat{H} = -\frac{1}{2}\sum_{A=1}^{N}\frac{1}{M_A}\nabla_A^2 - \frac{1}{2}\sum_{i=1}^{n}\nabla_i^2 - \sum_i\sum_A\frac{Z_A}{r_{iA}} + \sum_i\sum_{j>i}\frac{1}{r_{ij}} + \sum_A\sum_{B>A}\frac{Z_A Z_B}{r_{AB}} \qquad (2\text{-}2)$$

where there are N nuclei labeled A, B, ... and n electrons labeled i, j, ..., the $\{M_A\}$ are masses of the nuclei, the $\{Z_A\}$ are nuclear charges, the $\{r_{iA}\}$ are distances between electrons and nuclei, the $\{r_{ij}\}$ are distances between electrons, and the $\{R_{AB}\}$ are distances between nuclei. ∇_α^2 is the square of the Laplacian operator, containing a sum of second derivatives of the spatial coordinates of particle α. Certain other interactions which are excluded from equation (2-2), such as relativistic effects, can be added later. For example, spin-orbit coupling effects play a role in the electronic spectroscopy of metal clusters. A method for incorporating the spin-orbit effect into the nonrelativistic theory described here is presented later. It is important to note that the wavefunctions $\{\Psi_i\}$ must be functions of (at the least) the 3N spatial coordinates of the nuclei and the 3n spatial coordinates of the electrons, given the form of the Hamiltonian operator. It is seen immediately from equation (2-2) that the differential equation (2-1) is not exactly soluble because of the terms coupling the spatial coordinates of the particles through the $r_{\alpha\beta}^{-1}$ terms.

A major simplification results from the Born-Oppenheimer approximation [110], which is that electronic motions can be separated from nuclear motions, including translation, rotations, and vibrations. The validity of this approximation rests on the fact that the kinetic energies of nuclei are very small compared to kinetic energies of electrons. This is apparent when comparing the first two terms of equation (2-2). The first term, representing kinetic energies of the nuclei, contains the inverse of the nuclear mass, which has a value of roughly 1840 atomic units for even the lightest element, hydrogen. The separation of nuclear and electronic motions implies that the wavefunctions $\{\Psi_i\}$ can be factored into two separate functions, one depending on the electron coordinates $\{r_i\}$ and one depending on the nuclear coordinates $\{R_A\}$,

$$\Psi_j = \Phi(\{r_i\})\chi(\{R_A\}) \tag{2-3}$$

The most restrictive realization of the Born-Oppenheimer approximation is the "clamped nuclei" model, in which it is assumed that the nuclei are fixed with respect to the movement of electrons. In this approximation momentum couplings of the form of $\nabla_A\Phi(\{r_i\})$ and $\nabla_A^2\Phi(\{r_i\})$ are set exactly to zero, and the Schrödinger equation can be separated into an electronic and a nuclear part as

$$\hat{H}^{elec}\Phi_i^{elec} = \left(-\tfrac{1}{2}\sum_i \nabla_i^2 - \sum_{i,A}\frac{Z_A}{r_{iA}} + \sum_{i<j}\frac{1}{r_{ij}}\right)\Phi_i^{elec} = E_i^{elec}\Phi_i^{elec} \tag{2-4}$$

$$\hat{H}^{nuc}\chi_i^{nuc} = \left(-\tfrac{1}{2}\sum_A \frac{1}{M_A}\nabla_A^2 + E_i^{elec} + \sum_{A<B}\frac{Z_A Z_B}{R_{AB}}\right)\chi_i^{nuc} = E_i^{nuc}\chi_i^{nuc} \tag{2-5}$$

The clamped nuclei restriction can be relaxed by treating the neglected terms with perturbation theory, resulting in the addition of energetic terms arising from the coupling of nuclear and electronic motions [111].

From equation (2-5) it can be seen that the term $E_i^{total} = E_i^{elec} + \sum \frac{Z_A Z_B}{R_{AB}}$ represents the potential energy surface for nuclear motion (i.e. vibrations, rotations, translations) in a particular electronic state, and the equilibrium structure of a molecule in that state can be found by finding the nuclear configuration for which this quantity is at a minimum. Methods for accomplishing this are beyond the scope of the discussion. The primary goal here is to determine electronic state energies E_i^{total} and wavefunctions Φ_i^{elec} by finding approximate solutions to equation (2-4) within the clamped nuclei approximation.

The electronic wavefunctions of equation (2-4) form an orthonormal set for each fixed molecular geometry, defined by $\left\langle \Phi_i^{elec} \middle| \Phi_j^{elec} \right\rangle = \delta_{ij}$, where the bracket notation indicates integration of the product of the complex conjugate of the function (formally the adjoint of the function) enclosed in the bracket to the left times the function enclosed in the rightmost bracket over all coordinates of the electrons. δ_{ij} is defined as 1 if $i = j$ and 0 otherwise. Left multiplication of equation (2-4) by $(\Phi_i^{elec})^*$ and integration over the electronic coordinates yields the energy of the ith state:

$$\left\langle \Phi_i^{elec} \middle| \hat{H}^{elec} \middle| \Phi_i^{elec} \right\rangle = E_i^{elec} \qquad (2\text{-}6)$$

Since it is assumed that the nuclei are fixed, the term $\sum \frac{Z_A Z_B}{R_{AB}}$ is a constant, and can be added to the electronic Hamiltonian without changing the electronic wavefunction or the electronic energy E_i^{elec}, yielding

$$\left\langle \Phi_i^{elec} \middle| -\frac{1}{2}\sum_i \nabla_i^2 - \sum_{i,A}\frac{Z_A}{r_{iA}} + \sum_{i<j}\frac{1}{r_{ij}} + \sum_{A<B}\frac{Z_A Z_B}{R_{AB}} \middle| \Phi_i^{elec} \right\rangle = E_i^{total} \qquad (2\text{-}7)$$

As the rest of the chapter describes approximate solutions to the problem of equation (2-7), it is convenient to drop the cumbersome notation specifying the wavefunction as the electronic wavefunction, leaving

$$\left\langle \Phi_i \middle| \hat{H} \middle| \Phi_i \right\rangle = E_i \qquad (2\text{-}8)$$

Although the Born-Oppenheimer approximation affords considerable simplification by reducing the problem of equation (2-1) to an electronic problem, it is apparent that equation (2-7) cannot be solved analytically due to the coupling of the electronic coordinates in the $\{ r_{ij}^{-1} \}$ terms. An approximate form for the electronic wavefunctions $\{\Phi_i\}$ is thus required. According to the orbital approximation, the electronic wavefunction Φ_i, which is a function of the coordinates of all electrons, is represented by a product of orthonormal functions that each depend on the coordinates of a single electron,

$$\Phi_i(\alpha_1\beta_1\gamma_1\alpha_2\beta_2\gamma_2\cdots\alpha_n\beta_n\gamma_n) = \psi_1(\alpha_1\beta_1\gamma_1)\psi_2(\alpha_2\beta_2\gamma_2)\cdots\psi_n(\alpha_n\beta_n\gamma_n) \qquad (2\text{-}9)$$

where here α_i, β_i, and γ_i are the spatial coordinates of the particle with label i. These could be Cartesian coordinates x_i, y_i, z_i, spherical polar coordinates r_i, θ_i, ϕ_i, or some other choice. Equation (2-9) amounts to approximating the effect of the interelectronic repulsion since this part of the electronic Hamiltonian operator couples the electron coordinates and prevents an analytic separation of variables. The orbital approximation can be quite severe in certain cases, and can be moderated by application of a variety of systematic techniques, some of which are discussed subsequently.

Before adopting the final form to be used for the electronic wavefunctions two additional properties of electrons must be considered. First, electrons are known to possess an intrinsic angular momentum, or "spin." This additional degree of freedom was known to be present quite early based on the results of atomic spectroscopy, and a number of empirical "ersatzmodells" were proposed to fit the observations [112]. Uhlenbeck and Goudsmit first hit upon the idea that the electron was spinning [113,114], and though the electron cannot in fact be spinning in the macroscopic sense, the electron "spin" behaves exactly as if it were an angular momentum. This equivalence was formally demonstrated by Dirac in his relativistic treatment of the electron [67]. Although the electronic Hamiltonian operator of equation (2-4) does not explicitly include spin, and hence the electronic energy does not directly depend on it, it is crucial to include spin because it confers certain symmetry requirements on the wavefunctions (see below). Each electron is then assigned a spin coordinate, ξ, and the two possible spin functions, labeled $|\alpha\rangle$ and $|\beta\rangle$, are assumed to form an orthonormal set. An orbital will thus be represented by

$$\psi_i(\alpha_i,\beta_i,\gamma_i,\xi_i) = \psi_i(\alpha_i,\beta_i,\gamma_i)|\alpha\,(\mathrm{or}\,\beta)\rangle \equiv \psi_i(\mathrm{i}) \qquad (2\text{-}10)$$

It is understood that the three spatial and one spin coordinates of the electron are represented by the electron label in parentheses on the right side of equation (2-10). Orbitals of the form of equation (2-10) comprised of a spatial part times a spin part are referred to as spin orbitals.

A fundamental postulate of quantum mechanics is that the wavefunction for a system of fermions (e.g., electrons) must be antisymmetric with respect to interchange of any two of the particles, or in other words must change sign when two particles are exchanged [34]. A qualitative explanation of this is that the probability distribution for electron density is related to the square of the wavefunction, and this distribution cannot be changed by interchanging two indistinguishable particles such as electrons. Since it is the square of the wavefunction that does not change, the wavefunction itself may either remain the same, or change sign. Wavefunctions for particles collectively known as bosons (e.g., photons) are known to retain the same sign upon particle exchange, while wavefunctions for fermions, including electrons, change sign. Therefore this antisymmetry must be built into electronic wavefunctions.

The antisymmetry property is satisfied by replacing the simple product wavefunction of equation (2-9) (called a Hartree product) with a Slater determinant [115], equation (2-11).

$$\Phi(1,2,\ldots,n) = \left|\psi_1(1)\psi_2(2)\cdots\psi_n(n)\right\rangle$$

$$= \frac{1}{\sqrt{n!}} \begin{vmatrix} \psi_1(1) & \psi_2(1) & \cdots & \psi_n(1) \\ \psi_1(2) & \psi_2(2) & \cdots & \psi_n(2) \\ \vdots & \vdots & \ddots & \vdots \\ \psi_1(n) & \psi_2(n) & \cdots & \psi_n(n) \end{vmatrix} \qquad (2\text{-}11)$$

The factor $(n!)^{-\frac{1}{2}}$ is a normalization factor appropriate for orthonormal spin-orbitals. It is clear that exchanging the coordinates of two electrons will change the sign of the wavefunction, since exchanging any two rows of a determinant changes the sign of the determinant. The Slater determinant is the antisymmetric generalization of the Hartree product [116], as originally suggested by Fock [117].

The best form of the spin orbitals $\{\psi_i\}$ in a variational sense is obtained by solution of the Hartee-Fock equations [118]. In the Hartree-Fock procedure, equation (2-7) is written for the ground state of the molecule (i = 0) using the determinantal wavefunction of equation (2-11), and the resulting ground state energy,

$$E_0 = \sum_i \langle \psi_i | -\tfrac{1}{2}\nabla_i^2 - \sum_A \frac{Z_A}{r_{iA}} | \psi_i \rangle + \sum_{i<j} \left[\langle \psi_i \psi_j | \frac{1}{r_{ij}} | \psi_i \psi_j \rangle - \langle \psi_i \psi_j | \frac{1}{r_{ij}} | \psi_j \psi_i \rangle \right] \tag{2-12}$$

is made stationary by applying functional variation to the set of spin orbitals. This stationary point corresponds to a minimum since the electronic energy is bounded from below according to the variational theorem. In equation (2-12) the integrals in the first summation are referred to as core orbitals and are denoted h_{ii}, integrals just after the second summation symbol are referred to as Coulomb integrals and denoted J_{ij}, and integrals of the third sort are referred to as exchange integrals and denoted K_{ij}. Connection with equation (2-4) is apparent in equation (2-12), as the terms contain the kinetic energies of the electrons, electron-nuclear attractions, and interelectronic repulsions r_{ij}^{-1}. The exchange integrals arise because of the determinantal form of the wavefunction.

The functional variation procedure ensures that the best possible (i.e. lowest energy) approximation to the interelectronic repulsion is obtained within the orbital model, under the constraint that the spin orbitals remain orthonormal. An effective one-electron "Fock operator" is yielded by the variation procedure for each occupied spin orbital. In canonical form, these operators define eigenvalue equations for the energies $\{\varepsilon_i\}$ of the spin orbitals, which are compactly expressed in matrix form as

$$\hat{f}\,\psi = \hat{f}\,[\psi_1 \quad \psi_2 \quad \cdots \quad \psi_n] = [\varepsilon_1\psi_1 \quad \varepsilon_2\psi_2 \quad \cdots \quad \varepsilon_n\psi_n] = \psi\mathbf{E} \qquad (2\text{-}13)$$

where **E** is a diagonal square matrix containing the $\{\varepsilon_i\}$. The Fock operator $\hat{f}$ is defined as

$$\hat{f}(i) = h(i) + \sum_{j=1}^{n} J_j(i) - K_j(i) \qquad (2\text{-}14)$$

where the one-electron, Coulomb, and exchange operators are defined as

$$h(i) = -\tfrac{1}{2}\nabla_i^2 - \sum_A \frac{Z_A}{r_{iA}} \qquad (2\text{-}15)$$

$$J_j(i) = \left\langle \psi_j(j) \middle| \frac{1}{r_{ij}} \middle| \psi_j(j) \right\rangle \qquad (2\text{-}16)$$

$$K_j(i)\psi_i(i) = \left\langle \psi_j(j) \middle| \frac{1}{r_{ij}} \middle| \psi_i(j) \right\rangle \psi_j(i) \qquad (2\text{-}17)$$

respectively. It is seen that the Fock operators themselves depend on the spin orbitals, which also are yielded as solutions to the eigenvalue equations (equation (2-13)). The Hartree-Fock equations are thus nonlinear and must be solved with an iterative procedure.

Hartree-Fock theory was originally formulated as a perturbative rather than a variational theory, and utilized as the perturbation the difference between the actual potential $\sum_{i<j} r_{ij}^{-1}$ and the Hartree-Fock potential defined in terms of the Coulomb and exchange operators. This was necessary because $\sum_{i<j} r_{ij}^{-1}$ itself as a perturbation is large enough to cause convergence problems in the perturbation expansion of the

wavefunction. Later it was shown that the variational approach described above is formally equivalent to the earlier perturbative development through first order.

The Hartree-Fock potential represents interactions between statistical distributions of electrons in orbitals. This is intuitively clear in equation (2-16) for the Coulomb operator for the *i*th electron, which contains the probability density $\psi_j^*(j)\psi_j(j)$. A Coulomb integral $J_{ij} = \langle \psi_i \psi_j | r_{ij}^{-1} | \psi_i \psi_j \rangle$ thus represents the classical Coulomb repulsion between the charge distributions $\psi_i^*(i)\psi_i(i)$ and $\psi_j^*(j)\psi_j(j)$. Exchange integrals arise because of the antisymmetric form of the wavefunction, and have no convenient classical interpretation. In the case of i = j, the exchange integral K_{ii} is identical to the Coulomb integral J_{ii}, and corrects for the nonphysical interaction of the ith electron with itself, since $J_{ii} - K_{ii}$ therefore equals zero in equation (2-12). Both Coulomb and exchange integrals are positive in sign.

To this point electron spin has not been considered other than in the form of the spin orbitals, equation (2-10), but the importance of spin can be seen in the Coulomb and exchange integrals in equation (2-12). Coulomb integrals of the form $\langle \psi_i \psi_j | r_{ij}^{-1} | \psi_i \psi_j \rangle$ can be nonzero regardless of the spin of the electrons in ψ_i and ψ_j, since the spin will integrate to one in any case. Exchange integrals of the form $\langle \psi_i \psi_j | r_{ij}^{-1} | \psi_j \psi_i \rangle$, on the other hand, are exactly zero due to spin integration unless the spin of the electrons in ψ_i and ψ_j is the same. This illustrates how electron spin, which is not included in the Hamiltonian operator, can influence the ground state energy of equation (2-12) by eliminating certain integrals due to spin integration.

It is now useful to introduce a choice regarding the form of the spin orbitals in order to develop approaches for explicit solution of the Hartree Fock equations. One choice is to allow spatial orbitals to be occupied by two electrons of opposite spin, i.e., constrain two electrons, one of alpha spin and one of beta spin, to occupy an identical spatial orbital. Wavefunctions of this form are known as closed shell restricted Hartree-Fock (RHF) wavefunctions [80]. An obvious limitation of the RHF approach is that open shell ground states (including those of many transition metal diatomics) cannot be treated. More general approaches that relax this restriction can be adopted, and will be discussed in detail subsequently. For purposes of the present discussion, however, the RHF approach offers the most straightforward example of the additional details of modern molecular Hartree-Fock calculations.

Under the closed shell RHF formalism, it is assumed that there is an even number of electrons, and these electrons are paired in the spatial orbitals. The ground state wavefunction is taken as

$$\Phi_0 = \left|\psi_1\overline{\psi}_1\psi_2\overline{\psi}_2\cdots\psi_{n/2}\overline{\psi}_{n/2}\right\rangle \tag{2-18}$$

where bars over a spatial orbital indicate beta spin, and there are now $n/2$ spatial orbitals. Substitution of this spin-restricted determinant into equations (2-12) and (2-14) yields the RHF expressions for the ground state energy and the Fock operators,

$$E_0^{RHF} = 2\sum_{i=1}^{n/2} h_{ii} + \sum_{i=1}^{n/2}\sum_{j=1}^{n/2}\left[2J_{ij} - K_{ij}\right] \tag{2-19}$$

$$\hat{f}(i) = h(i) + \sum_{j=1}^{n/2}\left[2J_j(i) - K_j(i)\right] \tag{2-20}$$

The RHF equations are analogous to equation (2-13), with $\frac{n}{2}$ rather than n orbitals and eigenenergies.

Numerical solutions of the RHF equations are typically employed for atoms, but solving the equations numerically for molecular orbitals becomes exceedingly difficult except for very simple cases. Fortunately the set of coupled differential equations of equation (2-13) can be transformed to a matrix equation, which is amenable to solution using high speed computers, as demonstrated by Roothaan [119] and Hall [120]. To accomplish this transformation, each molecular orbital is expanded in a basis set of normalized but nonorthogonal (overlapping) atomic orbitals $\{\chi_\mu\}$ according to

$$\psi_i = \sum_{\mu=1}^{m} \chi_\mu C_{\mu i} \tag{2-21}$$

This LCAO (linear combination of atomic orbitals) was originally suggested by Mulliken [121,122]. The expansion is formally exact only in the limit of a complete (infinite) basis set, but in practice must be limited to some finite number of basis functions. According to the variational principle the approximation to the energy E_0 becomes lower as the number of basis functions becomes more complete, with the lower limit referred to as the Hartree-Fock limit.

The expansions for a set of m molecular orbitals ψ_i according to equation (2-21) can be collected as the matrix equation

$$\psi = \mathbf{XC} = \begin{bmatrix} \chi_1 & \chi_2 & \cdots & \chi_m \end{bmatrix} \cdot \begin{bmatrix} C_{11} & C_{12} & \cdots & C_{1m} \\ C_{21} & C_{22} & \cdots & C_{2m} \\ \vdots & \vdots & \ddots & \vdots \\ C_{m1} & C_{m2} & \cdots & C_{mm} \end{bmatrix} \tag{2-22}$$

Substitution of this linear expansion for the molecular orbitals into the Hartree-Fock equations, equation (2-13), left-multiplication of the result by the adjoint of **X**, $\mathbf{X}^{\dagger}$, defined by $X^{\dagger}_{ij} = X^{*}_{ji}$, and integration over the electronic coordinates yields

$$\langle \mathbf{X} | \hat{f} | \mathbf{X} \rangle \mathbf{C} = \langle \mathbf{X} | \mathbf{X} \rangle \mathbf{C}\mathbf{E} \qquad (2\text{-}23)$$

or

$$\mathbf{F}\mathbf{C} = \mathbf{S}\mathbf{C}\mathbf{E} \qquad (2\text{-}24)$$

where

$$\mathbf{F} = \begin{bmatrix} \langle \chi_1 | \\ \langle \chi_2 | \\ \vdots \\ \langle \chi_m | \end{bmatrix} \hat{f} \begin{bmatrix} |\chi_1\rangle & |\chi_2\rangle & \cdots & |\chi_m\rangle \end{bmatrix} \qquad (2\text{-}25)$$

is the Fock matrix, an $m \times m$ square matrix with elements $F_{\mu\nu} = \left\langle \chi_\mu \middle| \hat{f} \middle| \chi_\nu \right\rangle$, and

$$\mathbf{S} = \begin{bmatrix} \langle \chi_1 | \\ \langle \chi_2 | \\ \vdots \\ \langle \chi_m | \end{bmatrix} \cdot \begin{bmatrix} |\chi_1\rangle & |\chi_2\rangle & \cdots & |\chi_m\rangle \end{bmatrix} \qquad (2\text{-}26)$$

is the overlap matrix, an $m \times m$ square matrix with elements $S_{\mu\nu} = \left\langle \chi_\mu \middle| \chi_\nu \right\rangle$. **E** is a square matrix with the molecular orbital eigenenergies on the diagonal. It is important to note that according to this prescription there are now *m* molecular orbitals, where m is the size of the basis set, typically larger than the number of occupied orbitals. There will thus be a number of unoccupied or virtual orbitals obtained as solutions to equation (2-24). The ground state wavefunction, however, is still a Slater determinant that includes

---

only the occupied molecular orbitals. Equation (2-24) is referred to as the Roothaan-Hall matrix equation [80].

Once the integrals $F_{\mu\nu}$ and $S_{\mu\nu}$ are computed, the matrix equation **FC** = **SCE** can be solved by standard linear algebra techniques appropriate for solution on a computer to yield the coefficient matrix **C** and the orbital energies as the elements of the diagonal matrix **E**. A specific formula in terms of the basis functions for elements of the Fock matrix $F_{\mu\nu} = \left\langle \chi_\mu \middle| \hat{f} \middle| \chi_\nu \right\rangle$ is obtained by substituting the linear expansion for the molecular orbitals into the Fock operators, equation (2-20). The result is

$$F_{\mu\nu} = H_{\mu\nu} + \sum_{\lambda,\sigma=1}^{m} P_{\lambda\sigma}\left[(\mu\nu \mid \sigma\lambda) - \tfrac{1}{2}(\mu\lambda \mid \sigma\nu)\right] \tag{2-27}$$

where **H** is the core-Hamiltonian matrix with elements

$$H_{\mu\nu} = \left\langle \chi_\mu \middle| h(1) \middle| \chi_\nu \right\rangle = \left\langle \chi_\mu \middle| -\tfrac{1}{2}\nabla^2 - \sum_A \frac{Z_A}{r_{1A}} \middle| \chi_\nu \right\rangle, \tag{2-28}$$

P is the first-order Fock-Dirac density matrix, with elements

$$P_{\mu\nu} = \sum_{i=1}^{n/2} 2C_{\mu i}C_{\nu i} \tag{2-29}$$

and $(\mu\nu|\sigma\lambda)$ is a two-electron integral of the form

$$(\mu\nu|\lambda\sigma) = \left\langle \chi_\mu \chi_\lambda \middle| \frac{1}{r_{12}} \middle| \chi_\nu \chi_\sigma \right\rangle \tag{2-30}$$

The summation containing two-electron integrals in equation (2-28) is denoted as $G_{\mu\nu}$,

$$G_{\mu\nu} = \sum_{\lambda,\sigma=1}^{m} P_{\lambda\sigma}\left[(\mu\nu \mid \sigma\lambda) - \tfrac{1}{2}(\mu\lambda \mid \sigma\nu)\right] \tag{2-31}$$

This definition will prove useful in describing semiempirical methods.

Elements of the Fock matrix depend on the molecular orbital expansion coefficients $\{C_{\mu i}\}$ through the density matrix elements present in the matrix elements of **G**, so equation (2-24) is nonlinear in the coefficient matrix **C**. Equation (2-24) must therefore be solved in an iterative fashion, by assuming a set of coefficients as a starting guess, constructing the Fock matrix according to equations (2-27) through (2-31), and solving equation (2-24) via a diagonalization procedure to obtain **E** and an updated **C** matrix. This new **C** matrix is used to construct a new Fock matrix, which is again solved for **E** and an additional **C** matrix, which is then used to construct a new Fock matrix, and so on. The various integrals involved, $H_{\mu\nu}$ and the two-electron integrals $(\mu\nu|\sigma\lambda)$, depend only on the nuclear positions and the basis set, and need to be computed only once during the SCF iterations (though in calculations with large basis sets it is often more efficient to compute the integrals each time they are needed rather than storing and retrieving them). The process continues until the density matrix is stable with respect to further iterations, within some specified criterion. At this point the calculation is considered to be converged, and the potential or "field" experienced by a given electron due to repulsion by the other electrons is said to be self-consistent. For this reason, Hartree-Fock calculations as described above are often referred to as self-consistent field (SCF) calculations. The SCF approach was originally proposed by Hartree [116] in slightly different form, as Hartree's work predated the LCAO approach for molecular calculations.

The major limitation of the RHF formalism is that only molecules with closed shell ground states can be treated. Many transition metal diatomics have open shell ground states, including V_2, VNb, and Nb_2, so techniques that are more general than the

---

RHF method are needed. The most general method in wide use that can treat open-shell ground states is the unrestricted Hartree-Fock (UHF) method [80], in which the restriction that each spatial orbital is occupied by two spin-paired electrons is removed. In the UHF formalism a different set of spin-orbitals is assumed for electrons of different spin, and there can be unequal numbers of electrons of each spin. This leads to a set of coupled equations of the form of equation (2-13) for electrons of each spin. Fock operators for each spin are:

$$\hat{f}^{\alpha}(i) = h(i) + \sum_{j=1}^{n(\alpha)} [J_j^{\alpha}(i) - K_j^{\alpha}(i)] + \sum_{j=1}^{n(\beta)} J_j^{\beta}(i) \tag{2-32}$$

$$\hat{f}^{\beta}(i) = h(i) + \sum_{j=1}^{n(\beta)} [J_j^{\beta}(i) - K_j^{\beta}(i)] + \sum_{j=1}^{n(\alpha)} J_j^{\alpha}(i) \tag{2-33}$$

where $n(\alpha)$ and $n(\beta)$ are the number of alpha and beta electrons, respectively, and $J_j^{\alpha,\beta}$ and $K_j^{\alpha,\beta}$ are Coulomb and exchange operators as defined in equations (2-16) and (2-17) for the spin-orbitals for alpha spin electrons or for beta spin electrons. The qualitative sense of equations (2-32) and (2-33) is that only electrons of the same spin can have exchange interactions, while electrons of both spins have Coulomb interactions, as discussed previously.

In analogy to the RHF method, the molecular orbitals of both spins are represented as expansions in a basis set of known atomic functions, with separate sets of expansion coefficients:

$$\psi_i^{\alpha} = \sum_{\mu=1}^{m} \chi_{\mu} C_{\mu i}^{\alpha} \tag{2-34}$$

$$\psi_i^\beta = \sum_{\mu=1}^{m} \chi_\mu C_{\mu i}^\beta \tag{2-35}$$

Use of these linear expansions in the unrestricted Hartree-Fock equations leads to a set of two coupled matrix equations of the form of equation (2-24),

$$\mathbf{F}^\alpha \mathbf{C}^\alpha = \mathbf{S}\mathbf{C}^\alpha \mathbf{E}^\alpha \tag{2-36}$$

$$\mathbf{F}^\beta \mathbf{C}^\beta = \mathbf{S}\mathbf{C}^\beta \mathbf{E}^\beta \tag{2-37}$$

Relevant expressions for the elements of the Fock matrices are

$$F_{\mu\nu}^\alpha = H_{\mu\nu} + \sum_{\lambda,\sigma=1}^{m} P_{\lambda\sigma}^\alpha \left[(\mu\nu\,|\,\sigma\lambda) - \tfrac{1}{2}(\mu\lambda\,|\,\sigma\nu)\right] + \sum_{\lambda,\sigma=1}^{m} P_{\lambda\sigma}^\beta (\mu\nu\,|\,\sigma\lambda) \tag{2-38}$$

$$F_{\mu\nu}^\beta = H_{\mu\nu} + \sum_{\lambda,\sigma=1}^{m} P_{\lambda\sigma}^\beta \left[(\mu\nu\,|\,\sigma\lambda) - \tfrac{1}{2}(\mu\lambda\,|\,\sigma\nu)\right] + \sum_{\lambda,\sigma=1}^{m} P_{\lambda\sigma}^\alpha (\mu\nu\,|\,\sigma\lambda) \tag{2-39}$$

where $\mathbf{P}^\alpha$ is the density matrix analogous to equation (2-29) defined over the $\{C_{\mu i}^\alpha\}$. Equations (2-36) and (2-37) are solved together using an iterative procedure akin to that described for RHF calculations.

While the UHF method is straightforward to implement, one major drawback of UHF wavefunctions for the purpose of treating electronic spectroscopy is that UHF wavefunctions are not eigenfunctions of total spin. It can be shown that a UHF wavefunction for a given spin multiplicity is contaminated by contributions from higher spin multiplicities [85]. This is especially true for states of multiplicity lower than the highest possible multiplicity for a given number of unpaired electrons. There are several methods available for alleviating this problem, but such methods are typically designed for the ground state only. An additional complication is that improvement of UHF wavefunctions by means of configuration interaction (CI) is problematic, and CI is typically used for treating spectroscopy [123].

An alternative to the UHF method that yields wavefunctions that do not suffer from spin contamination is the restricted open shell Hartree-Fock (ROHF) method [124]. ROHF wavefunctions are also amenable to CI methods. Under the ROHF formalism a number of electrons are considered to be spin-paired in identical spatial orbitals, as in the RHF method, while some additional number of unpaired electrons are in open shell orbitals. The ground state wavefunction is taken to be a linear combination of a small number of Slater determinants with expansion coefficients fixed so that the wavefunction is a proper spin eigenfunction. The method is thus versatile with regard to total spin, since equally valid wavefunctions are used, for example, for both the triplet and singlet states possible for two open shell electrons, whereas the UHF description of the singlet state typically suffers from substantial spin contamination. In addition it is possible to utilize averages over several configurations within the framework of the ROHF formalism, which can be useful in certain difficult-to-converge cases. This idea is pursued later.

The price to be paid for the flexibility of ROHF methods is that they are not in general automated like RHF and UHF methods, requiring in some cases input from the user, and the algebra is much more complicated than the straightforward algebra of RHF and UHF calculations presented above. The method uses separate Fock operators $\hat{f}^{\mu}$ for the molecular orbitals comprising the closed shell, and one or more "open shells" consisting of groups of orbitals with identical open-shell operators. Here the right superscript indicates the shell for which the operator is defined. The condition

$$\langle \psi_i | \hat{f}^{\mu} - \hat{f}^{\nu} | \psi_j \rangle = 0 \qquad (2\text{-}40)$$

must be imposed as a constraint to guarantee that the wavefunction obtained corresponds to a formal minimum in the functional variation procedure. In the previous methods, where there is only a single operator, equation (2-40) is automatically fulfilled. Further complication arises because orbitals in different shells are not in general orthogonal. This desirable condition is met by specifying the closed shell operator first and solving for the set of closed-shell orbitals, then projecting the orbitals for each open shell operator into the orthogonal complement of the operators for preceding shells. The details of the algebra involved are beyond the scope of the present discussion and will not be presented.

Another feature of the ROHF method is that the ROHF energy expression, analogous to the closed shell expression of equation (2-19), depends on the specific spin state desired for the wavefunction. This can easily be understood by considering triplet and open-shell singlet states of a two-electron system. In the former case, the electrons have the same spin and thus an exchange interaction, while in the latter case the electrons are of different spin and thus have no exchange interaction. It is not therefore possible to write a general expression of the form of equation (2-19) for all cases. Within the framework of the ROHF Hamiltonian of Edwards and Zerner [123] the SCF energy is expressed as

$$E_{\mathrm{ROHF}} = 2\sum_i h_i + \sum_{i<j}(2J_{ij} - K_{ij}) + \tfrac{1}{2}\sum_{i,m} n_m (2J_{im} - K_{im}) + \sum_m n_m h_m$$

$$+ \tfrac{1}{4}\sum_{\mu}\sum_{\nu}\sum_{m\in\mu}\sum_{p\in\nu} n_m n_p (2a^{\mu\nu} J_{mp} - b^{\mu\nu} K_{mp}) \qquad (2\text{-}41)$$

where i, j, etc. represent closed shell orbitals; μ, ν, etc. represent open shells (i.e. separate groups of open shell orbitals); m, p, etc. represent open-shell orbitals, n_m is the number of electrons in orbital m, h_α, $J_{\alpha\beta}$, and $K_{\alpha\beta}$ are the usual one-electron, Coulomb, and exchange integrals, respectively; and $a^{\mu\nu}$ and $b^{\mu\nu}$ are "vector coupling coefficients" that define interactions between the open shell electrons. The choice of vector coupling coefficients fixes the configuration or average over configurations used in the calculation.

As an example of determining vector coupling coefficients, consider again the triplet formed from two electrons in two separate open-shell orbitals, $|\psi_1\alpha\psi_2\alpha\rangle$. By inspection the open shell two-electron energy contribution for this configuration is $E^{ee} = J_{12} - K_{12}$. The vector coupling coefficients must be chosen so that the summation in equation (2-41) that contains the coefficients gives E^{ee}. In this case there is a single open shell, so there are no sums over μ and ν, and each orbital has occupancy $n_m = 1$. The diagonal terms of the summation (i.e. those with m = p) are $\frac{1}{4}(2a - b)J_{11}$ and $\frac{1}{4}(2a - b)J_{22}$ since in general $K_{ii} = J_{ii}$. It is clear that the coefficient $\frac{1}{4}(2a - b)$ must be zero, since E^{ee} does not contain J_{11} or J_{22}. Therefore 2a = b. The off-diagonal terms give $\left(aJ_{12} - \frac{1}{2}bK_{12}\right)$ using the fact that $J_{ij} = J_{ji}$ and $K_{ij} = K_{ji}$. By comparison to $E^{ee} = J_{12} - K_{12}$, it is clear that a = 1 and b = 2. These values satisfy the condition 2a = b derived above.

In the context of equation (2-41), separate open shells correspond to groups of orbitals in which each orbital has the same values of $a^{\mu\mu}$ and $b^{\mu\mu}$. Different open shells are coupled by coefficients $a^{\mu\nu}$ and $b^{\mu\nu}$. Consider a high-spin d^4 transition metal such as aqueous Cr^{+2} as an example in which two open-shell operators are required. The first shell consists of the three degenerate orbitals of t_{2g} symmetry, each occupied by a single electron. The second shell consists of the two degenerate orbitals of e_g symmetry, and contains a total of one electron. There are thus two configurations to be considered, as shown in figure 2-1, and the vector coupling coefficients are chosen so that the energy expression represents the average energy of the two configurations. Since the t_{2g} orbitals have the same occupancy in both configurations, no average is necessary, and the appropriate energy is $E^{ee} = J_{12} + J_{13} + J_{23} - K_{12} - K_{13} - K_{23}$. This case is identical to the situation described above for two electrons in two orbitals, except that there are more terms in the rightmost summation in equation (2-41) to go along with the larger number of Coulomb and exchange integrals in E^{ee}. In both cases there is a single Coulomb and a single exchange integral for all unique pairs of separate orbitals, and a corresponding term $\left(a^{11}J_{mp} - \frac{1}{2}b^{11}K_{mp}\right)$. There is also the condition $(2a^{11} - b^{11}) = 0$ since there are no doubly-occupied orbitals under consideration. The coefficients found above, $a^{11} = 1$, $b^{11} = 2$, apply here as well.

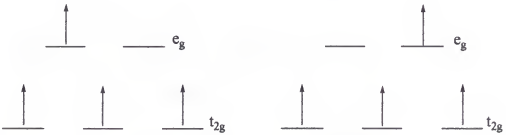

Figure 2-1: Two possible configurations of electrons in the d orbitals of a high-spin octahedral d^4 transition metal ion.

For the second open shell, consisting of the two e_g orbitals and with a total occupancy of one electron, there are no Coulomb and exchange integrals as there is only one electron. The occupancy of the orbitals n_1 and n_2 is one-half. Comparison between the two-electron energy expression for this shell, $E^{ee} = 0$, and the rightmost summation in equation (2-41) yields

$$\frac{1}{4}\cdot\frac{1}{2}\cdot\frac{1}{2}\cdot\left[\left(2a^{22}-b^{22}\right)J_{11}+\left(2a^{22}-b^{22}\right)J_{22}+4a^{22}J_{12}-2b^{22}K_{12}\right]=0 \quad (2\text{-}42)$$

The only possible solution is $a^{22} = b^{22} = 0$.

An average over the open shell two-electron energies for the two configurations shown in figure (2-1) must be considered to determine the off-diagonal vector coupling coefficients a^{12} and b^{12} between the two shells. Denoting the orbitals in the second shell as *c* and *d* to avoid confusion with the orbitals of the first shell (denoted 1, 2, 3), the appropriate energy expression is

$$E^{ee}=\frac{1}{2}\left[J_{1c}+J_{2c}+J_{3c}+J_{1d}+J_{2d}+J_{3d}-K_{1c}-K_{2c}-K_{3c}-K_{1d}-K_{2d}-K_{3d}\right] \quad (2\text{-}43)$$

Terms such as

$$\frac{1}{2}\cdot 1\cdot\frac{1}{2}\left[2a^{12}J_{1c}-b^{12}K_{1c}\right] \qquad (2\text{-}44)$$

are yielded by equation (2-41), where the orbital occupancies are one in the first shell and one-half in the second shell, and assuming the facts that $a^{12} = a^{21}$, $b^{12} = b^{21}$, $J_{1c} = J_{c1}$, $K_{1c} = K_{c1}$, etc. Values of a^{12} and b^{12} satisfied by equations (2-43) and (2-44) are 1 and 2, respectively. The values obtained for all vector coupling coefficients in this example can be expressed as 2×2 matrices:

$$\mathbf{a}=\begin{bmatrix}1 & 1\\ 1 & 0\end{bmatrix} \qquad \mathbf{b}=\begin{bmatrix}2 & 2\\ 2 & 0\end{bmatrix} \qquad (2\text{-}45)$$

Definition of two separate open shells is necessary in this case because the coupling in the second shell cannot be described by the same vector coupling coefficients that describe the coupling in the first shell and between shells.

One potential drawback of ROHF methods is that the open shell orbital energies do not necessarily follow Koopman's approximation (that the negative of the orbital energy equals the ionization energy of an electron in that orbital). This problem is easily overcome by adding certain two electron integrals to the orbital energies to obtain orbital ionization potentials if these quantities are of interest [123]. Details of the procedure depend on the definition of the vector coupling coefficients and the numbers of open shell orbitals and electrons.

The three SCF methods described above, RHF, UHF, and ROHF, are the three "standard" SCF procedures, and are in wide use [80]. For many molecules the methods are stable and proceed regularly to convergence without modification. There are also a number of convergence acceleration techniques that can be used in difficult or slow-to-converge cases, typically involving techniques that "damp" changes between iterations by considering a weighted average of densities of the current step and one or more previous steps as input for the next step in the iterations. A widely used example is the direct inversion in iterative subspace (DIIS) method of Pulay [125]. Often these methods are useful for cases that converge regularly to a given point, then oscillate.

Transition metal diatomics are notorious as difficult-to-converge cases [24]. Convergence behavior is often so pathological that acceleration methods such as DIIS are not useful. The near degeneracy phenomenon discussed in the previous chapter is largely responsible for this behavior, as several configurations lie very close in energy to the ground state configuration. The electron configuration frequently changes from one to another of these low-lying configurations between SCF iterations, precluding efficient convergence with conventional techniques. The method used in the calculations reported here to counter this problem is the configuration-averaged Hartree-Fock (CAHF) procedure [126], which has been found to be effective in obtaining well-converged ground states for transition metal clusters [24]. The CAHF method utilizes the average energy of a number of electron configurations in constructing the Fock matrix. Changes in the electron configuration between iterations then no longer occur since the low-energy configurations are included in the average.

The CAHF approach is similar to several other methodologies that have been proposed, including the hyper-Hartree-Fock approach of Slater [127] and the grand canonical Hartree-Fock method [128,129], and is an extension of the ROHF method. As is the case there, a number of electrons can be assumed to occupy closed-shell orbitals, with the remainder occupying a fixed number of open-shell orbitals. Standard ROHF calculations are designed to represent an average over configurations to obtain a wavefunction that is a spin eigenstate. The CAHF method takes advantage of this capacity of the ROHF technique to incorporate all possible configurations that can be obtained from a given number of electrons in a specified number of open-shell orbitals in the average. The method uses a judicious choice of vector coupling coefficients to construct the average, and proceeds as a standard ROHF calculation once those coefficients are fixed. The development is given following reference [126].

Consider a set of m orbitals occupied by n electrons, where in general $n < 2m$. Each orbital then has an occupancy, on average, of n/m. Again the open shell two-electron summation of equation (2-41) must be used along with the proper expression for this contribution to the energy to obtain the appropriate values for the vector coupling coefficients. In the examples given above in the discussion of the ROHF method, this was accomplished by determining the number of times each integral J_{ij} or K_{ij} appeared in the energy expression for each configuration, dividing this number by the total number of configurations (recall the case of the coupling between open shells in the example of a high-spin d^4 transition metal atom), comparing the result with the coefficient of the integral given by equation (2-41), and solving for the vector coupling coefficient. The same procedure will be used here, but is more complicated.

First consider that a particular orbital is doubly occupied. In that case there are (n-2) electrons remaining. Since the interest is in an average over all possible configurations, the integral J_{ii} will occur once for each possible way of arranging the n-2 electrons in the remaining (2m – 2) spin orbitals. The number of possibilities is given by the binomial coefficient

$$\binom{2m-2}{n-2} = \frac{(2m-2)!}{(n-2)!\cdot(2m-n)!} \tag{2-46}$$

where it is understood that the binomial coefficient is taken as zero if n – 2 or (2m – n) is less than zero. The total number of configurations is

$$\binom{2m}{n} = \frac{(2m)!}{n!\cdot(2m-n)!} \tag{2-47}$$

Each J_{ii} integral is therefore weighted by the coefficient

$$\frac{\binom{2m-2}{n-2}}{\binom{2m}{n}} = \frac{n(n-1)}{2m(2m-1)} \tag{2-48}$$

in the average energy expression (referred to as E^{ee} above). From equation (2-41), the coefficient for integrals J_{ii} is

$$\frac{1}{4}\cdot n_i \cdot n_i \cdot (2a-b) = \frac{1}{4}\cdot\frac{n}{m}\cdot\frac{n}{m}(2a-b) \tag{2-49}$$

Comparing the right sides of equations (2-48) and (2-49) gives a condition on the values of a and b,

$$(2a-b) = \frac{2m(n-1)}{n(2m-1)} \tag{2-50}$$

Values for a and b must be found, as in the above examples, by considering off-diagonal Coulomb and exchange integrals.

Configurations in which two orbitals i and j are each singly-occupied are now considered (all configurations in which either i or j is doubly occupied were considered in the previous paragraph). In this case the other n – 2 electrons can again be arranged in the remaining 2m – 2 spin orbitals, with number of possibilities given in equation (2-46), but now there are four possibilities for arranging the two electrons in orbitals i and j, since their spins can be αα, αβ, βα, or ββ. Therefore the number of times an integral J_{ij} appears is $4\binom{2m-2}{n-2}$. It is immediately clear that the number of times an exchange integral K_{ij} occurs is half of this, since exchange integrals will arise for only αα and ββ spin configurations of the electrons in orbitals i and j. To determine the vector coupling coefficients, the average number of occurrences of each sort of integral is compared to the coefficient given by equation (2-41). For the Coulomb integrals, this gives the equation

$$\frac{1}{4}\cdot\frac{n^2}{m^2}\cdot 4a = \frac{4\binom{2m-2}{n-2}}{\binom{2m}{n}} \tag{2-51}$$

which solves to give

$$a = \frac{2m(n-1)}{n(2m-1)} \tag{2-52}$$

Comparing the right side of equation (2-52) with the right side of equation (2-50) gives $(2a - b) = a$, or $b = a$. This value of b can also be obtained following a development analogous to that just described. Vector coupling coefficients for the CAHF model are therefore given by

$$a = b = \frac{2m(n-1)}{n(2m-1)} \tag{2-53}$$

The method can be extended in a straightforward fashion to cases that include an average over all configurations possible for two separate sets of open-shell orbitals [126], and a similar methodology where an average over all states of a particular spin multiplicity is used have been proposed [130].

SCF orbitals obtained using the CAHF method can be used as a refined starting point for standard ROHF calculations or additional CAHF calculations, or used immediately in a correlation treatment (see below for discussion of electron correlation). For typical cases where convergence of an ROHF calculation is poor, often one or more stable closed-shell orbitals can be identified based on the density matrix at each iteration of the nonconvergent calculation. In such cases a CAHF calculation in which those orbitals are assumed to be doubly occupied and the remaining electrons are distributed in a large number of orbitals is often a good starting-point. The resulting orbitals are then used as the initial guess for a subsequent CAHF calculation in which a smaller number of orbitals is included in the open shell. This in turn provides starting orbitals for a calculation with an again smaller number of open-shell orbitals, and so on until a standard ROHF calculation that successfully converges is possible. A well-defined set of SCF orbitals appropriate for use in a correlation treatment can be obtained for many difficult cases in this way.

Electron Correlation

The four SCF methodologies presented thus far (RHF, UHF, ROHF, CAHF) are different methods for approximating solutions to the Hartree-Fock equations, which define the lowest-energy form of the molecular orbitals within the orbital approximation. In a mathematical sense the orbital approximation amounts to a separation of variables (the electronic coordinates) that is not formally possible due to the presence of the operators $\{r_{ij}^{-1}\}$ in the Hamiltonian. The orbital approximation is therefore often referred to as the “independent particle” model [117,118] since the coupling of the electronic motions is neglected, i.e., it is assumed that the electrons move independently of each other. Electronic motions are in fact correlated due to the instantaneous repulsion between electrons. For many problems the independent particle approximation is adequate, but for particularly problems that include transition metals, it is necessary to incorporate at some level the effect of electron correlation.

Löwdin defined the correlation energy for a particular energy state of a specified Hamiltonian as the difference between the exact eigenvalue of the Hamiltonian (equation (2-4) for the electronic Hamiltonian) and its expectation value in the Hartree-Fock approximation (equation (2-12)) [62]. In the strictest sense of this definition, the Hartree-

Fock energy must be taken as the energy at the Hartree-Fock limit, which requires a complete (infinite) basis set, and compared to the energy of equation (2-4), which cannot be obtained for molecular systems with more than a single electron. Therefore in practice some approximation to the correlation energy must be used. In a less rigorously defined sense wavefunctions are often referred to as "correlated" as well, when obtained from a method that approximates the correlation energy.

In the Hartree-Fock methods discussed previously, the ground state wavefunction is assumed to be a single Slater determinant (or in the ROHF formulation, perhaps a linear combination of a small number of determinants fixed to represent a spin eigenstate). The exact electronic wavefunction of equation (2-4) could in principle be represented without approximation by a linear expansion in a complete basis of n-electron Slater determinants, if such a basis could be found. If a complete basis set of atomic orbitals could be used in equation (2-21), an infinite number of molecular orbitals would be obtained by solution of the Roothaan matrix equation (equation (2-24)). A complete set of n-electron Slater determinants could then be obtained by writing determinantal wavefunctions for all possible arrangements, or configurations, of the electrons in the set of molecular orbitals.

The exact ground state wavefunction (or in fact the wavefunction for any state of the system) is then represented by

$$\Psi_0 = C_0\left|\Phi_0\right\rangle + \sum_{i,a} C_i^a \left|\Phi_i^a\right\rangle + \sum_{\substack{i<j\\ a<b}} C_{ij}^{ab}\left|\Phi_{ij}^{ab}\right\rangle + \sum_{\substack{i<j<k\\ a<b<c}} C_{ijk}^{abc}\left|\Phi_{ijk}^{abc}\right\rangle + \cdots \qquad (2\text{-}54)$$

where Φ_0 is the Hartree-Fock ground state determinant and the additional determinants are denoted by promotions, or excitations, of electrons from the molecular orbitals occupied in the HF determinant to virtual orbitals. Here $i, j, k, \ldots$ represent orbitals occupied in the HF ground state, $a, b, c, \ldots$ represent virtual orbitals, and $\left|\Phi_{ij\ldots}^{ab\ldots}\right\rangle$ represents the determinant for the configuration in which an electron in orbital i has been promoted to orbital a, an electron in orbital j has been promoted to orbital b, etc. The expansion coefficients are denoted in the same way for convenience. Clearly it is never possible to obtain a complete set of Slater determinants due to practical limitations, and finite basis sets of both atomic orbitals and determinants must be used.

The configuration interaction (CI) method [80] is based on the idea of equation (2-54). CI calculations utilize a finite basis set of atomic orbitals, and construct a set of Slater determinants by considering excitations from the HF ground state configuration. All possible configurations are considered in full CI calculations. For basis sets of even modest size the number of configurations can be very large, and so often a truncated set of configurations are included. For example, the HF ground state configuration and all possible double excitations might be included. Such a calculation is referred to as a CID calculation. CISD indicates all single and double excitations, CISDT all singles, doubles, and triples, etc. Only in the limit of full CI and an infinite atomic orbital basis set can the exact state energy and wavefunction be obtained.

Once the basis set and set of excitations to be included is fixed, CI methods seek to determine wavefunctions and eigenenergies that are solutions to

$$\hat{H}\left|\Psi_i^{CI}\right\rangle = E_i^{CI}\left|\Psi_i^{CI}\right\rangle, \; i = 1,2,\ldots,k \qquad (2\text{-}55)$$

where *k* is equal to the number of configurations included. Each CI wavefunction is taken as a linear expansion similar to equation (2-54), except that the number of terms included is limited. Left multiplication of both sides of equation (2-55) by $\left\langle \Psi_j^{CI} \right|$, substitution of the linear expansion (2-54) for the CI wavefunctions, and integration over the electronic coordinates yields a matrix equation,

$$\begin{bmatrix} \langle \Phi_1|\hat{H}|\Phi_1\rangle & \langle \Phi_1|\hat{H}|\Phi_2\rangle & \cdots & \langle \Phi_1|\hat{H}|\Phi_k\rangle \\ \langle \Phi_2|\hat{H}|\Phi_1\rangle & \langle \Phi_2|\hat{H}|\Phi_2\rangle & \cdots & \langle \Phi_2|\hat{H}|\Phi_k\rangle \\ \vdots & \vdots & \ddots & \vdots \\ \langle \Phi_k|\hat{H}|\Phi_1\rangle & \langle \Phi_k|\hat{H}|\Phi_2\rangle & \cdots & \langle \Phi_k|\hat{H}|\Phi_k\rangle \end{bmatrix} \begin{bmatrix} C_{11} & C_{12} & \cdots & C_{1k} \\ C_{21} & C_{22} & \cdots & C_{2k} \\ \vdots & \vdots & \ddots & \vdots \\ C_{k1} & C_{k2} & \cdots & C_{kk} \end{bmatrix}$$

$$= \begin{bmatrix} C_{11} & C_{12} & \cdots & C_{1k} \\ C_{21} & C_{22} & \cdots & C_{2k} \\ \vdots & \vdots & \ddots & \vdots \\ C_{k1} & C_{k2} & \cdots & C_{kk} \end{bmatrix} \begin{bmatrix} E_1 & 0 & \cdots & 0 \\ 0 & E_2 & \cdots & 0 \\ \vdots & \vdots & \ddots & \vdots \\ 0 & 0 & \cdots & E_k \end{bmatrix} \qquad (2\text{-}56)$$

or **HC** = **CE**, where the configurations and expansion coefficients are enumerated 1,2,... for convenience. Here it is assumed that the configurational functions are orthonormal, as is the case with a basis of n-electron Slater determinants. Diagonalization of the **H** matrix to yield **C** and **E** provides wavefunctions and energies for k states of the system.

For purposes where it is useful for the CI states to be eigenfunctions of spin, for example when spectroscopy (i.e., transitions between different CI states) is of interest, the configurations $\{\Phi_i\}$ are replaced with linear combinations of Slater determinants chosen to be spin eigenfunctions, much as is done in the ROHF method. A number of methods for obtaining the exact forms of the linear combinations have been developed [131], one of which is discussed later. The linear combinations are referred to as configuration state functions. Once the forms of the CSFs are fixed, the calculation proceeds as outlined above, with the CSFs replacing the configurations in equation (2-56). CSFs produced by certain methods are nonorthogonal, in which case equation (2-56) becomes

---

$$\mathbf{HC} = \mathbf{SCE} \tag{2-57}$$

where here **S** is the overlap matrix in the basis of CSFs, $S_{ij} = \left\langle \Phi_i^{CSF} \middle| \Phi_j^{CSF} \right\rangle$. In such cases it is necessary to orthogonalize the basis of CSFs before **H** can be diagonalized, which greatly increases the computational effort required for a calculation.

An important point to be considered is that according to Brillouin's Theorem [132] the ground state of a CIS (single excitations only) calculation is not correlated in a basis of Slater determinants. It can be shown that matrix elements between different determinants related by a single excitation are equal to off-diagonal elements of the Fock matrix between the two orbitals involved in the excitation, and in the canonical representation these matrix elements are zero by definition [80]. Therefore the ground state configuration will not mix with excited configurations (though configurations can mix in excited states), and CIS ground state wavefunction are uncorrelated. If, however, the CI basis set consists of CSFs constructed based on an open-shell ROHF ground state, there can be mixing between the reference configuration and excited configurations [24]. This is a result of the presence of CSFs related to the ROHF ground state by the promotion of a single electron, but with a reversal of two electron spins relative to the ground state.

CI is not the only approach available for incorporating electron correlation. It was mentioned earlier that the Hartree-Fock wavefunction is correct through first order taking the difference between the Hartree-Fock potential and the true potential $\sum_{i<j} r_{ij}^{-1}$ as the perturbation. The perturbative expansion can be extended to higher orders, leading to what is referred to as many-body perturbation theory [80]. This approach has advantages

---

and disadvantages compared to CI, with CI being more generally appropriate for predicting electronic spectroscopy.

Another ansatz that has many advantages is the coupled-cluster theory, first examined for molecules by Cizek and Paldus [133], in which the wavefunction is taken as

$$\left|\Psi^{CC}\right\rangle = e^{T}\left|\Psi_0\right\rangle \qquad (2\text{-}58)$$

where T is an operator that generates all possible excitations when applied to $\left|\Psi_0\right\rangle$. The T operator is a summation of operators that generate single excitations, double excitations, etc.:

$$T = T_1 + T_2 + T_3 + \ldots \qquad (2\text{-}59)$$

The summation is truncated at some level of excitation, giving rise to methods such as CCD (coupled-cluster approximation using only double excitations), CCSD, etc. The series expansion for the exponential operator, $e^x = 1 + x + \frac{1}{2}x^2 + \cdots$, is used to obtain a wavefunction similar to the CI wavefunction, equation (2-54), only with certain conditions relating coefficients weighting higher-order excitations to coefficients of lower-order excitations. For example, in the CCD method, T is limited to T_2, and the series expansion includes the term $\frac{1}{2}T_2^2$. When applied to $\left|\Psi_0\right\rangle$ this operator will generate quadruple excitations, but each weighted by a product of two doubles coefficients, $C_{ij}^{ab}C_{kl}^{cd}$. One attractive feature of coupled-cluster theory is size-consistency, meaning that results will scale properly with size [134]. Coupled-cluster methods are computationally intensive and are difficult to apply to excited states. The calculations used in the present work are CI calculations, as spectroscopy is of primary interest.

Correlation contributions to a wavefunction are generally categorized as dynamic correlation contributions or essential correlation contributions. Essential correlation refers to contributions to the ground (or other) state from excited configurations that significantly alter the form of the state wavefunction. These excited configurations thus have large coefficients in the expansion over configurations representing the state. The best-known example of essential correlation is correction of the improper dissociation of the RHF wavefunction for H_2 [80]. The RHF ground state places both electrons in the $1s\sigma_g$ orbital, which is a bonding combination of the 1s orbitals on each hydrogen atom, given by

$$\psi_{1s\sigma_g} = \frac{1}{\sqrt{2}\sqrt{1+S}}\left(1s^A + 1s^B\right) \qquad (2\text{-}60)$$

where S is the overlap of the 1s orbitals on the two atoms, the two atoms are denoted A and B, and $1s^A$ is the 1s atomic orbital function on atom A. This molecular orbital is delocalized over the two atoms, and cannot properly describe the dissociated limit of two hydrogen atoms, each with an electron in a local atomic orbital. The RHF solution is adequate at the equilibrium bond length of H_2, but as the bond is stretched, the quality of the RHF wavefunction decreases, until at the separated atom limit it is completely unrealistic.

This “dissociation problem” of the H_2 wavefunction is solved in a simple CI treatment by inclusion of the doubly-excited $1s\sigma_u^2$ configuration. The $1s\sigma_u$ orbital is the antibonding combination of the 1s orbitals, given by

$$\psi_{1s\sigma_u} = \frac{1}{\sqrt{2}\sqrt{1-S}}\left(1s^A - 1s^B\right) \tag{2-61}$$

The CI wavefunction for the ground state is then

$$\left|\Psi_0^{CI}\right\rangle = C_1\left|\psi_{1s\sigma_g}\alpha\psi_{1s\sigma_g}\beta\right\rangle + C_2\left|\psi_{1s\sigma_u}\alpha\psi_{1s\sigma_u}\beta\right\rangle \tag{2-62}$$

or, in terms of the atomic orbitals (dropping the unwieldy normalization constants involving S for convenience),

$$\left|\Psi_0^{CI}\right\rangle = \left[(C_1 + C_2)\left(1s^A 1s^A + 1s^B 1s^B\right) + (C_1 - C_2)\left(1s^A 1s^B + 1s^B 1s^A\right)\right](\alpha\beta - \beta\alpha) \tag{2-63}$$

At the dissociation limit the overlap is zero and $C_1 = \frac{1}{\sqrt{2}}$ and $C_2 = -\frac{1}{\sqrt{2}}$, leading to

$$\left|\Psi_0^{CI}\right\rangle = \frac{1}{\sqrt{2}}\left(\left|1s^A\alpha 1s^B\beta\right\rangle + \left|1s^B\alpha 1s^A\beta\right\rangle\right) \tag{2-64}$$

when care is taken with the normalization constants. This is the correct dissociated atom limit, represented by a proper quantum mechanical average of determinants consisting of localized atomic orbitals. The CI expansion of equation (2-62) can therefore be said to localize the ground state wavefunction of H_2 at long bond distances. This is, in fact, a simple example of the orbital localization problem discussed in chapter one. The situation is much more complicated for metal clusters because the dissociation problem exists even at equilibrium bond distances and the number of orbitals and electrons is larger in number. At the dissociated atom limit, the $1s\sigma_u^2$ configuration makes an essential correlation contribution, with its coefficient in the CI wavefunction equal in magnitude to the coefficient of the RHF reference configuration.

Dynamic correlation, on the other hand, refers to the effect of a large number of configurations, each making a very small contribution that does not fundamentally alter the form of the wavefunction. These configurations thus have expansion coefficients that are very small, and each makes only a small difference in the ground state energy, but their cumulative effect can be large. Dynamic correlation corrects for overestimation of the interelectronic repulsion at the Hartree-Fock level. Inclusion of both essential and dynamic correlation is vital to obtaining accurate wavefunctions for transition metal dimers, as demonstrated by the few successful treatments of the chromium dimer [28,30-33].

Bridge Between Ab Initio and Semiempirical Methods

The preceding discussion has assumed that all integrals necessary for the various methods are calculated over the basis set, and that all electrons are treated. This is the most rigorous way to proceed, and the state-of-the-art, for small molecules at least, are ab initio calculations utilizing large basis sets and a high level of electron correlation. Such calculations quickly become intractable as the size of the molecule under consideration gets larger, however. The various semiempirical methods circumvent this bottle-neck by obtaining many of the necessary integrals empirically, and neglecting classes of other integrals whose values are generally small. These methods thus sacrifice the very high level of accuracy possible with ab initio methods in return for a wider range of applicability. Both approaches are designed to construct electronic wavefunctions for the electronic states of molecules, so must be related in a fundamental way. The purpose of this section is to describe the bridge between ab initio and semiempirical methods.

Semiempirical methods are generally assumed to use an effective or model Hamiltonian in place of the full time-independent nonrelativistic Born-Oppenheimer electronic Hamiltonian of equations (2-6) and (2-7). Ab initio methods can also be said to be models, albeit models that are more accurate than their semiempirical counterparts.

This is most clearly displayed by casting the electronic Hamiltonian into the form of a second-quantized operator [80],

$$\hat{H} = \sum_{i,j} h_{ij} \hat{a}_i^\dagger \hat{a}_j + \frac{1}{2} \sum_{i,j,k,l} (ik \mid jl) \hat{a}_i^\dagger \hat{a}_j^\dagger \hat{a}_l \hat{a}_k \tag{2-65}$$

where the $\{h_{ij}\}$ and the $(ij|kl)$ are, respectively, one-electron and two-electron integrals as defined previously, and $\hat{a}_i^\dagger$ and $\hat{a}_j$ are the standard creation and annihilation operators for spin-orbitals ψ_i and ψ_j, respectively. The Hamiltonian in this form can be used at any level of electron correlation: the Hartree-Fock approach can be developed by taking the expectation value of this Hamiltonian for the ground state, matrix elements of this Hamiltonian in a basis of the ground and excited states lead to the CI matrix equation, etc. The word model is used here to indicate the range of spin-orbitals included (i.e., orbitals for all electrons, valence orbitals only, etc.), and the method used to obtain the integrals h_{ij} and $(ij|kl)$. This method could be computation of all integrals over a set of basis functions, or a semiempirical ansatz for fixing values of certain integrals and neglecting other integrals. It is made clear by this discussion that semiempirical models can be explicitly applied at any level of electron correlation. Caution is necessary, however, because semiempirical model Hamiltonians are known to incorporate electron correlation in an ad hoc manner into the parameters used to represent integrals.

Connection with the previous discussion in terms of configuration interaction can be made by partitioning the CI matrix into a valence space and an excited or correlating space, and considering coupling between these spaces. The valence space contains all configurations with filled core orbitals and valence electrons distributed in the valence orbitals. The excited space contains all configurations in which electrons have been promoted from the core orbitals to the valence orbitals, from the core orbitals to the excited orbitals, or from the valence orbitals to the excited orbitals. In an exact formulation the excited space must be of infinite dimension. In this representation the CI matrix equation **HC** = **CE** becomes, for a particular state i,

$$\begin{bmatrix} \mathbf{H}_{PP} & \mathbf{H}_{PQ} \\ \mathbf{H}_{QP} & \mathbf{H}_{QQ} \end{bmatrix} \begin{bmatrix} \mathbf{C}_{Pi} \\ \mathbf{C}_{Qi} \end{bmatrix} = \mathrm{E}_i \begin{bmatrix} \mathbf{C}_{Pi} \\ \mathbf{C}_{Qi} \end{bmatrix} \tag{2-66}$$

where $\mathbf{H}_{PP}$ is a matrix with matrix elements of the Hamiltonian taken between valence space configurations, $\mathbf{H}_{QQ}$ is a matrix similarly defined in the excited space, $\mathbf{H}_{PQ}$ and $\mathbf{H}_{QP}$ contain matrix elements between configurations in the two spaces, and $\mathbf{C}_{Pi}$ and $\mathbf{C}_{Qi}$ are column vectors containing coefficients weighting the valence space and excited space configurations for state i, respectively. A derivation of this partitioning was given by Löwdin [105].

Expanding equation (2-66) by multiplying the matrices yields two coupled matrix equations,

$$\mathbf{H}_{PP}\mathbf{C}_P + \mathbf{H}_{PQ}\mathbf{C}_Q = \mathrm{E}\mathbf{C}_P \tag{2-67}$$

$$\mathbf{H}_{QP}\mathbf{C}_P + \mathbf{H}_{QQ}\mathbf{C}_Q = \mathrm{E}\mathbf{C}_Q \tag{2-68}$$

where the state index i has been dropped for convenience. Solving equation (2-68) for $\mathbf{C}_Q$ yields

$$\mathbf{C}_Q = \left(\mathrm{E}\cdot\mathbf{1} - \mathbf{H}_{QQ}\right)^{-1}\mathbf{H}_{QP}\mathbf{C}_P \tag{2-69}$$

where **1** is a unit matrix of the dimension of the excited space. Substitution of equation (2-69) into equation (2-67) yields

$$\left[\mathbf{H}_{PP} + \mathbf{H}_{PQ}\left(\mathrm{E}\cdot\mathbf{1} - \mathbf{H}_{QQ}\right)^{-1}\mathbf{H}_{QP}\right]\mathbf{C}_P = \mathrm{E}\mathbf{C}_p \tag{2-70}$$

Defining the quantity in brackets as the effective valence shell Hamiltonian matrix $\mathbf{H}^V$,

$$\mathbf{H}^{\mathbf{V}} = \mathbf{H}_{\mathbf{PP}} + \mathbf{H}_{\mathbf{PQ}}\left(\mathrm{E}\cdot\mathbf{1} - \mathbf{H}_{\mathbf{QQ}}\right)^{-1}\mathbf{H}_{\mathbf{QP}} \qquad (2\text{-}71)$$

and reinserting the state index gives

$$\mathbf{H}^{\mathbf{V}}\mathbf{C}_{\mathbf{P}i} = \mathrm{E}_i\mathbf{C}_{\mathbf{P}i} \qquad (2\text{-}72)$$

This equation shows that in principle it is possible to solve for the exact state energy E_i in the valence space, but with correlation corrections entering through interaction with the remainder of the complete space through the second term on the right side of equation (2-71). The functional form of effective valence shell Hamiltonians analogous to those implicitly assumed by semiempirical methods can be explored with an in-depth analysis of the partitioning of the Hamiltonian matrix [100,101,135].

Historically the original semiempirical methods were designed as cheaper alternatives to uncorrelated Hartree-Fock calculations, which at that time were beyond the capabilities of the available computing technology for even simple molecules with a few atoms. As such, these methods were concerned only with the ground state, and in terms of the formal development of the previous paragraph, made the further approximation of truncating the valence space to include only the ground state configuration. The partitioning described above is formally exact, as long as a complete basis is assumed, for any choice of valence space, though clearly the effective valence shell Hamiltonian is different for different choices. Modern semiempirical methods still employ restricted valence spaces consisting of the ground state only, or perhaps including single excitations in the manifold of valence orbitals. The effect of the additional approximation of truncation of the valence space remains to be examined in terms of the ab initio effective valence shell Hamiltonian [100].

The earliest incarnations of all-electron semiempirical methods were parameterized to reproduce the results of uncorrelated valence orbital-only basis ab initio Hartree-Fock calculations. Modern methods have adopted the procedure of parameterizing directly on the results of experiment, meaning the parameters used in the method are fitted so that calculated quantities (i.e., dipole moments, heats of formation, electronic spectroscopy, geometry, etc.) agree well with experimental data.. Since experimental results must include the effects of electron correlation, the parameterization is attempting to incorporate in an average way correlation corrections due to interaction with the Q space. It is generally thought that dynamic correlation can be implicitly incorporated into a set of parameters [24,102-104,136], in much the same way that density functional theory is thought to [137], but essential correlation cannot be [93]. This can be understood qualitatively based on the definitions of essential and dynamic correlation given above: dynamic correlation does not significantly alter the form of the wavefunction, while essential correlation contributions do. The model must provide a qualitatively correct wavefunction, i.e., essential correlation contributions must be explicitly incorporated, while the effect of dynamic correlation can be subsumed into the parameters.

Another interesting feature of electron correlation in semiempirical methods that follows from the above discussion is that the parameterization is carried out based on a comparison of experimental data with the results of calculations performed at a certain level of theory. The parameterization then incorporates dynamic correlation in roughly the right amount to reproduce the experimental results. If later calculations are then performed at a higher level of theory that also explicitly includes, in some amount, the

---

dynamic correlation that was already included in the parameters, then this correlation is said to have been "overcounted" [104]. Similar considerations apply if later calculations are performed at a lower level of theory. In either case, the results of the calculation are assumed to be deleteriously affected, and experience has shown that semiempirical methods designed at one level of theory are not as useful when applied at a different level.

The bridge between semiempirical and ab initio methods is still an open field of research [100,101]. The issues described in the preceding paragraphs have been explored both by ab initio computations utilizing effective valence shell Hamiltonians [100], and through experience with the semiempirical methods themselves [24,93,138], but many questions remain. If a semiempirical method is to be successfully applied to transition metal clusters, the question of essential versus dynamic correlation in the model is of primary importance, since both forms of correlation make large contributions to ground and excited state wavefunctions. One purpose of the present work is to investigate the hypothesis that dynamic correlation is incorporated into semiempirical models through their parameters, while essential correlation is not.

The INDO/S Model

Modern semiempirical methods rely on the zero differential overlap (ZDO) approximation [85], in which the "differential overlap" $\chi_\mu^*(1)\chi_\nu(1)$ is neglected in forming **F** unless χ_μ and χ_ν are identical. It should be noted that this is a more stringent requirement than orthogonality of the basis set, which would require that the integral of $\chi_\mu^*(1)\chi_\nu(1)d\tau_1$ be zero. The complete neglect of differential overlap (CNDO) method

[81,82] rigorously applies ZDO to all two-electron integrals. Only those of the Coulomb type, $(\mu\mu|\nu\nu)$, are thus included. A second, more rigorous approach is the neglect of diatomic differential overlap (NDDO) method [81], in which $\chi_\mu^*\chi_\nu$ is neglected only if χ_μ and χ_ν are on different atoms. All integrals of the form $(\mu^A\nu^A|\lambda^B\sigma^B)$ are thus included.

Intermediate between CNDO and NDDO is INDO [84], in which all one-center integrals $(\mu^A\nu^A|\lambda^A\sigma^A)$ are retained in addition to two-center integrals $(\mu^A\mu^A|\nu^B\nu^B)$ of the CNDO type. INDO is the appropriate choice for large systems because it includes terms necessary for proper description of atomic multiplet structure (for example the ^3P, ^1D, and ^1S states arising from the $(2s)^2(2p)^2$ configuration of the carbon atom, which are degenerate under CNDO) while not sacrificing the computational efficiency of CNDO [93].

The original CNDO and INDO methods referred to above were parameterized to reproduce the results of minimal basis ab initio calculations [81,82,84]. These methods were generalizations of the earlier Pariser-Parr-Pople method [139-142], which was a π electron-only theory designed to reproduce the electronic spectra of unsaturated hydrocarbons. The CNDO and INDO methods were designed to include both σ and π electrons, and departed from the philosophy of the earlier theory of parameterizing on experimental results. Both methods were applied to ground state properties including geometry and dipole moments.

More recent semiempirical methods following the school of Dewar should be considered derivatives of the original CNDO and INDO methods, sharing their emphasis on ground state properties, though parameters have been fitted based on experimental data. These methods include MINDO/3 [143,144]of Dewar, an INDO model, and the NDDO models MNDO of Dewar and Thiel [138,145], AM1 of Dewar and Stewart [146], and PM3 of Stewart [147,148]. There is also the SINDO1 method of Jug [149,150], an INDO method designed for ground state properties. No attempt is made to review these methods.

The original CNDO method was also modified for the purpose of predicting electronic spectroscopy by Del Bene and Jaffé [151,152]. This method, called CNDO/S, returned to the procedure of fitting parameters against experimental results, and utilized experience learned with the PPP model to provide predictions of spectroscopy for nonplanar molecules involving both π and σ electrons. The model is therefore properly considered a derivative of the original PPP theory. Though implemented within the framework of the CNDO models of Pople [81,82], CNDO/S incorporated important modifications for the purpose of predicting spectroscopy, and was parameterized at the CIS level.

Zerner and Ridley later introduced an INDO model based on CNDO/S, appropriately named INDO/S [91]. In its present incarnation, INDO/S has been extended to cover all of the first and second rows of the periodic table [91,92,153], the 3d [92,153] and 4d transition metals [154,155], and the lanthanides [156,157] and actinides [158]. As with CNDO/S, the parameterization of INDO/S was carried out based on comparison of calculated results with experimental spectroscopic data. CNDO/S was parameterized to reproduce band origins of electronic transitions, while INDO/S was optimized to reproduce band maxima. An additional important difference between the semiempirical

---

methods of the Dewar school and INDO/S is that the latter includes only one empirical parameter for each element (the resonance integral, see below), with all others being taken from experimental data such as atomic ionization potentials and atomic spectroscopy. By contrast, methods of the Dewar school were optimized by empirically fitting most of the parameters, and incorporating additional nonphysical parameters not present in the original CNDO and INDO methods. This approach sacrifices a strict adherence to atomic physics in return for greater flexibility in fitting results to experimental data for a large set of test cases. The philosophy behind INDO/S, on the other hand, is that a semiempirical parameter set should reflect the underlying physics, with little reliance on parameter fitting. Although higher accuracy might be achieved otherwise, retention of the basic attributes of the elements ensures adequate behavior even in cases that are quite different than those represented in the set of molecules used in the parameterization. For example, the resonance integrals of carbon and hydrogen used in INDO/S were fit for benzene alone [91], and it stands to the credit of the underlying physics that such a model works well for a variety of carbon- and hydrogen-containing compounds.

The INDO/S model is a valence orbital-only model, and prescribes a parameterization scheme that fixes the various integrals rather than computing integrals over a basis set of atomic orbital functions. Many of the parameters are semiempirical, meaning they are taken from experimental data, while one, the resonance integral, is fit at the CIS level to give good agreement between calculated and experimental electronic spectra. It is useful in discussing the exact forms adopted for the integrals to denote matrix elements and integrals by both orbital indices and indices that specify the nucleus

---

the atomic orbitals are centered on. Hence $H_{\mu\nu}^{AB}$ indicates the matrix element $\langle \chi_\mu | h(1) | \chi_\nu \rangle$ where the atomic orbital χ_μ is centered on nucleus A and the orbital χ_ν is centered on nucleus B.

The form of the matrix elements of the Fock operator is presented below assuming the RHF case, equation (2-27). Matrix elements for the UHF and ROHF cases are not as simple but no loss of generality in discussing the integral approximations and parameters is suffered by framing the discussion in terms of the RHF model. The approximations used can be understood in a natural way by starting with the ab initio expression for Fock matrix elements, equation (2-27), and invoking the ZDO approximation, but with the caveat that INDO retains certain terms (e.g., all one center two-electron integrals) that would be neglected in the CNDO model.

Starting with elements of the two-electron matrix **G**, the ab initio expression for matrix elements in the RHF model is $G_{\mu\nu} = \sum_{\lambda,\sigma=1}^{m} P_{\lambda\sigma}\left[(\mu\nu \mid \sigma\lambda) - \frac{1}{2}(\mu\lambda \mid \sigma\nu)\right]$. Starting with the diagonal terms, $G_{\mu\mu}^{AA}$, all terms in the summation over λ and σ where orbitals χ_λ and χ_σ are also centered on atom A are kept, and only two-center Coulomb integrals are kept otherwise, giving

$$G_{\mu\mu} = \sum_{\sigma,\lambda}^{A} P_{\sigma\lambda}\left[(\mu\mu \mid \sigma\lambda) - \frac{1}{2}(\mu\lambda \mid \sigma\mu)\right] + \sum_{\sigma}^{B \neq A} P_{\sigma\sigma}(\mu\mu \mid \sigma\sigma) \tag{2-73}$$

In equation (2-73) the notation $\Sigma_{\sigma,\lambda}^{A}$ indicates that the summation runs over all orbitals λ and σ that are centered on atom A. For off-diagonal matrix elements between orbitals on the same atom, only one-center terms are retained because two-center Coulomb integrals are not possible when it is assumed that the orbitals χ_μ and χ_ν are different orbitals on the same atom, leaving

$$G_{\mu\nu}^{AA} = \sum_{\sigma,\lambda}^{A} P_{\sigma\lambda}\left[(\mu\nu \mid \sigma\lambda) - \tfrac{1}{2}(\mu\sigma \mid \nu\lambda)\right] \tag{2-74}$$

For terms involving orbitals on different atoms, $G_{\mu\nu}^{AB}$, only terms from the rightmost integral summation in equation (2-27) can be of the two-center Coulomb type, leaving

$$G_{\mu\nu}^{AB} = -\tfrac{1}{2}P_{\mu\nu}(\mu\mu \mid \nu\nu) \tag{2-75}$$

The various integrals in equations (2-73) through (2-75) are replaced with semiempirical parameters, subject to an additional constraint involving transformation properties of the integrals. This important aspect of the model is considered next.

Care must be taken with the form of the Coulomb integrals $(\mu^A\mu^A|\nu^B\nu^B)$ to ensure that the method has the property of rotational invariance, meaning that any unitary transformation of the basis set should not affect results for any calculated property [81]. A transformation of the atomic orbital basis set according to

$$\chi'_\mu = \sum_{\nu} \chi_\nu U_{\nu\mu} \tag{2-76}$$

is unitary if $\mathbf{U}^\dagger\mathbf{U} = \mathbf{U}\mathbf{U}^\dagger = \mathbf{1}$, where $\mathbf{1}$ is the unit matrix. If this is true, the transformed single determinant wavefunction $|\Psi'_0\rangle$ differs from $|\Psi_0\rangle$ by only a phase factor, which for real transformation matrices is ± 1 [80]. Since expectation values depend on the square of the wavefunction, unitary transformation will therefore not affect expectation values, including the state energy. Following Pople et al. [81] basis set transformations can be divided into three classes. The first class includes transformations that mix orbitals of the same angular momentum on the same atoms. Invariance under this class of transformation is essential because rotation of molecular coordinates falls under this category. The second class includes transformations mixing all orbitals on the same atom, which includes transformations to a basis set of hybrid orbitals, for example. The third class includes nonlocal transformations that mix basis functions on different atoms. This class is excluded from consideration, as such transformations are not employed with the model. Therefore only transformations that mix orbitals on the same atom are considered.

As an example of how rotational invariance impacts a semiempirical integral approximation, consider transformation of a two electron integral according to equation (2-76). Denoting the orbitals in the transformed basis as m, n, etc. the transformation is given by

$$(m^A n^B \mid l^C s^D) = \sum_{\mu}^{A} \sum_{\nu}^{B} \sum_{\lambda}^{C} \sum_{\sigma}^{D} U^{\dagger}_{m\mu} U_{\nu n} U^{\dagger}_{l\lambda} U_{\sigma s} (\mu^A \nu^B \mid \lambda^C \sigma^D) \qquad (2\text{-}77)$$

where as stated above it has been assumed that only orbitals on the same atom are mixed by the transformation. Rotational invariance is an intrinsic feature of ab initio methods, because all integrals $(\mu\nu|\lambda\sigma)$ are present and equation (2-77) is therefore satisfied. In a semiempirical method, however, certain integrals have been neglected. Caution is necessary to be sure that any approximation applied in one basis set applies in a transformed basis set. In the CNDO model, for example, the two-electron integrals follow the rule

$$(\mu\nu|\lambda\sigma) = \delta_{\mu\nu}\delta_{\lambda\sigma}(\mu\mu|\sigma\sigma) \qquad (2\text{–}78)$$

Inserting this approximation into equation (2-77) gives

$$(m^A n^B \,|\, l^C s^D) = \sum_{\mu}^{A}\sum_{\nu}^{B}\sum_{\lambda}^{C}\sum_{\sigma}^{D} U^{\dagger}_{m\mu} U_{\nu n} U^{\dagger}_{l\lambda} U_{\sigma s}\left[\delta_{\mu\nu}\delta_{\lambda\sigma}(\mu^A \mu^A \,|\, \sigma^C \sigma^C)\right]$$

$$= \sum_{\mu}^{A}\sum_{\sigma}^{C} U^{\dagger}_{m\mu} U_{\mu n} U^{\dagger}_{l\sigma} U_{\sigma s}(\mu^A \mu^A \,|\, \sigma^C \sigma^C) \qquad (2\text{-}79)$$

Now if the Coulomb integrals in the summation in equation (2-79) did not depend on the orbital, but only on the atom, i.e., the ZDO approximation is replaced with the more stringent requirement

$$(\mu^A \nu^B \,|\, \lambda^C \sigma^D) = \delta_{\mu\nu}\delta_{\lambda\sigma}(\mu^A \mu^A \,|\, \sigma^C \sigma^C) = \delta_{\mu\nu}\delta_{\lambda\sigma}\gamma_{AC} \qquad (2\text{-}80)$$

then the quantity γ_{AC} can be factored out of equation (2-79), giving

$$(m^A n^B \,|\, l^C s^D) = \gamma_{AC}\left(\sum_{\mu}^{A} U^{\dagger}_{m\mu} U_{\mu n}\right)\left(\sum_{\sigma}^{C} U^{\dagger}_{l\sigma} U_{\sigma s}\right) \qquad (2\text{-}81)$$

Since the basis set transformations being considered are limited to transformations mixing only orbitals on the same atom, the summations in brackets reduce to the matrix elements $(\mathbf{U}^{\dagger}\mathbf{U})_{mn}$ and $(\mathbf{U}^{\dagger}\mathbf{U})_{ls}$. But since $\mathbf{U}^{\dagger}\mathbf{U} = \mathbf{U}\mathbf{U}^{\dagger} = \mathbf{1}$, the elements of the matrix product $\mathbf{U}^{\dagger}\mathbf{U}$ are given by the Kronecker delta function, and equation (2-81) becomes

$$(m^A n^B \,|\, l^C s^D) = \delta_{mn}\delta_{ls}\gamma_{AC} \qquad (2\text{-}82)$$

which is the same approximation applied in the original basis set. This is true only if two-center Coulomb integrals are made to depend on atoms but not on the specific orbital. Similar considerations are necessary for an INDO model.

A crucial factor in the design of a semiempirical parameter set is the availability of experimental data upon which the parameters are built. As an example, consider the ionization energy of an atom, which is of vital importance for constructing semiempirical parameters. The ionization process involves removing an electron from the ground electronic state, which might be one of several microstates arising from the ground configuration. In the carbon atom, for example, the ground state configuration is $1s^22s^22p^2$, which gives rise to the microstates ^3P, ^1D, and ^1S. The ground state is ^3P, and the three states are split by a total of over 20,000 cm^{-1} [159]. Semiempirical methods use configurational ionization energies (referred to as VSIP's, for valence shell ionization potentials), constructed by taking appropriate averages of the energies of the various microstates involved in the neutral and cation ground states. This is only possible, of course, if these various states have been observed experimentally. The quality of semiempirical parameters thus depends to some extent on the availability of experimental data on the elements. In the case of the first transition series, most of the pertinent states have been characterized [159] and parameters may be developed using a straightforward procedure, as described below. In the case of the second transition series, on the other hand, the experimental picture is much less complete, leading to the need for additional approximations. The parameterizations for the two series are therefore somewhat different, and will be developed in parallel.

For the 3d metals, two-center Coulomb integrals γ_{AB} can be evaluated theoretically when ground state properties are of interest [153], but for the purpose of calculating spectroscopy a great deal of experience has shown that semiempirical integrals are a better choice [91,160]. INDO/S uses the Mataga-Nishimoto form [161],

$$\gamma_{AB} = \frac{1.2}{2.4(\gamma_{AA} + \gamma_{BB})^{-1} + R_{AB}} \tag{2-83}$$

where R_{AB} is the distance between atoms *A* and *B*. This functional form for γ_{AB} is designed to properly scale as 1/R at large internuclear separation, and scale appropriately to a finite value as R_{AB} approaches zero. The one-center Coulomb integrals γ_{AA} used here and in equations (2-73) and (2-74) are obtained from the difference between the ionization potential and electron affinity, IP – EA, for the appropriate orbital, as originally suggested by Pariser [139].

A problem is encountered with this approximation for the transition metals, because although IP – EA is similar for *s* and *p* electrons, IP – EA for the *d* orbitals is significantly different. Therefore it is necessary to adopt different values for $\gamma_{ss}^{AA} = \gamma_{sp}^{AA} = \gamma_{pp}^{AA}$ and γ_{dd}^{AA} if the method is to have any hope of successfully describing the electronic structure of molecules that include transition metals. Doing so sacrifices rotational invariance with respect to hybridization between shells, but is necessary to achieve accurate results, and retains the essential property of invariance with respect to transformations of the molecular coordinates. Further complications arise because the electron configurations $4s^2 3d^{n-2}$ and $4s^1 3d^{n-1}$ lie very close in energy. There are thus two possible ionization processes, depending on which configuration is the ground state configuration, and the ionization potentials are competitive in energy for the two configurations. Therefore γ_{ss}^{AA} and γ_{dd}^{AA} are taken as averages of IP – EA for s and d electrons for the two low-energy electron configurations. The resulting values for the 3d elements are smoothed by fitting quadratically against the core charge to obtain the final parameters.

One center Coulomb integrals involving *s* (or *p*) and *d* electrons, γ_{sd}^{AA}, are needed as well, and are obtained by considering ionization potentials for the $4s^2 3d^{n-2}$ and $4s^1 3d^{n-1}$ configurations. The average energy of an electron configuration $s^l p^m d^n$ is given by [162]

$$E(s^l p^m d^n) = lU_{ss} + mU_{pp} + nU_{dd} + \frac{1}{2}l(l-1)\bar{J}_{ss} + \frac{1}{2}m(m-1)\bar{J}_{pp} + \frac{1}{2}n(n-1)\bar{J}_{dd}$$

$$+ lm\bar{J}_{sp} + ln\bar{J}_{sd} + mn\bar{J}_{pd} - \frac{1}{5}m(m-1)\bar{K}_{pp} - \frac{2}{9}n(n-1)\bar{K}_{dd}$$

$$-\frac{1}{2}lm\bar{K}_{sp} - \frac{1}{2}ln\bar{K}_{sd} - \frac{1}{2}mn\bar{K}_{pd} \qquad (2\text{-}84)$$

where the bars over the Coulomb and exchange integrals indicate averages over the integrals appropriate for each microstate arising from the electron configuration. The integrals $U_{\mu\mu}$ are atomic one electron integrals, as described below; they play no part in the present development. This general expression can be used to determine ionization potentials for *s* electrons and *d* electrons assuming each of the low-energy electron configurations $4s^2 3d^{n-2}$ and $4s^1 3d^{n-1}$. Neglecting the small exchange integrals, the difference in the ionization energies for *s* electrons is given by

$$I_s(ns^2(n\text{-}1)d^{m-2}) - I_s(ns^1(n\text{-}1)d^{m-1}) = \bar{J}_{sd} - \bar{J}_{ss} = \gamma_{sd} - \gamma_{ss} \qquad (2\text{-}85)$$

Similarly, the difference in ionization energies for *d* electrons is

$$I_d(ns^2(n\text{-}1)d^{m-2}) - I_d(ns^1(n\text{-}1)d^{m-1}) = \gamma_{dd} - \gamma_{sd} \qquad (2\text{-}86)$$

Given the values for γ_{ss} and γ_{dd} derived as detailed above, two values for γ_{sd} are obtained from equations (2-85) and (2-86). Substitution of the average of the two values back into equations (2-85) and (2-86) gives new values of γ_{ss} and γ_{dd}. An iterative process is used to obtain the final values of all three parameters, which are again smoothed for the 3d series using a quadratic fit against the core charges.

The INDO approximation includes all one-center two electron integrals $(\mu^A\nu^A|\lambda^A\sigma^A)$. These integrals are related to the F^k and G^k Slater-Condon factors [163] as shown in table 2-1 for an s, p, d orbital basis. Note that one-center Coulomb integrals $\gamma_{\mu\mu}$ are equivalent to the Slater-Condon factors $F^0(\mu\mu)$. There are 45 unique nonzero

Table 2-1. Relationship between one-center two electron integrals and Slater-Condon F^k and G^k factors. Integrals related by symmetry to those shown omitted. Orbital indices are 1 = s, 2 = p_x, 3 = p_y, 4 = p_z, 5 = $d(z^2)$, 6 = $d(x^2\text{-}y^2)$, 7 = d(xy), 8 = d(xz), 9 = d(yz). Taken from reference 153.

$(11|11) = F^0(ss)$

$(12|12) = \frac{1}{3}G^1(sp)$

$(15|15) = \frac{1}{5}G^2(sd)$

$(11|22) = F^0(sp)$

$(23|23) = \frac{3}{25}F^2(pp)$

$(28|46) = \frac{3}{49}G^3(pd)$

$(39|46) = -\frac{3}{49}G^3(pd)$

$(11|55) = F^0(sd)$

$(56|22) = -\frac{2\sqrt{3}}{35}F^2(pd)$

$(56|33) = \frac{2\sqrt{3}}{35}F^2(pd)$

$(68|24) = \frac{3}{35}F^2(pd)$

$(67|67) = \frac{35}{441}F^4(dd)$

$(22|22) = F^0(pp) + \frac{4}{25}F^2(pp)$

$(25|25) = \frac{1}{15}G^1(pd) + \frac{18}{245}G^3(pd)$

$(25|26) = -\frac{1}{5\sqrt{3}}G^1(pd) - \frac{3\sqrt{3}}{245}G^3(pd)$

$(26|26) = \frac{1}{5}G^1(pd) + \frac{24}{245}G^3(pd)$

$(27|36) = -\frac{1}{5}G^1(pd) + \frac{21}{245}G^3(pd)$

$(28|45) = \frac{2}{5\sqrt{3}}G^1(pd) - \frac{9\sqrt{3}}{245}G^3(pd)$

$(36|35) = \frac{1}{5\sqrt{3}}G^1(pd) + \frac{3\sqrt{3}}{245}G^3(pd)$

$(37|26) = \frac{1}{5}G^1(pd) - \frac{21}{245}G^3(pd)$

$(39|28) = \frac{1}{5}G^1(pd) - \frac{6}{245}G^3(pd)$

$(45|45) = \frac{4}{15}G^1(pd) + \frac{27}{245}G^3(pd)$

$(48|25) = -\frac{1}{5\sqrt{3}}G^1(pd) + \frac{12\sqrt{3}}{245}G^3(pd)$

$(49|36) = -\frac{1}{5}G^1(pd) + \frac{6}{245}G^3(pd)$

$(22|33) = F^0(pp) - \frac{2}{25}F^2(pp)$

$(55|22) = F^0(pd) - \frac{2}{35}F^2(pd)$

$(55|44) = F^0(pd) + \frac{4}{35}F^2(pd)$

$(66|22) = F^0(pd) + \frac{2}{35}F^2(pd)$

$(66|44) = F^0(pd) - \frac{4}{35}F^2(pd)$

$(56|56) = \frac{4}{49}F^2(dd) + \frac{15}{441}F^4(dd)$

$(58|58) = \frac{1}{49}F^2(dd) + \frac{30}{441}F^4(dd)$

$(58|68) = \frac{\sqrt{3}}{49}F^2(dd) - \frac{5\sqrt{3}}{441}F^4(dd)$

$(68|68) = \frac{3}{49}F^2(dd) + \frac{20}{441}F^4(dd)$

$(69|59) = -\frac{\sqrt{3}}{49}F^2(dd) + \frac{5\sqrt{3}}{441}F^4(dd)$

$(69|78) = -\frac{3}{49}F^2(dd) + \frac{15}{441}F^4(dd)$

$(68|79) = \frac{3}{49}F^2(dd) - \frac{15}{441}F^4(dd)$

$(88|56) = -\frac{2\sqrt{3}}{49}F^2(dd) + \frac{10\sqrt{3}}{441}F^4(dd)$

$(99|56) = \frac{2\sqrt{3}}{49}F^2(dd) - \frac{10\sqrt{3}}{441}F^4(dd)$

$(55|66) = F^0(dd) - \frac{4}{49}F^2(dd) + \frac{6}{441}F^4(dd)$

$(58|24) = \frac{\sqrt{3}}{35}F^2(pd)$

$(66|77) = F^0(dd) + \frac{4}{49}F^2(dd) - \frac{34}{441}F^4(dd)$

$(69|34) = -\frac{3}{35}F^2(pd)$

$(55|88) = F^0(dd) + \frac{2}{49}F^2(dd) - \frac{24}{441}F^4(dd)$

$(66|88) = F^0(dd) + \frac{2}{49}F^2(dd) - \frac{24}{441}F^4(dd)$

$(55|55) = F^0(dd) + \frac{4}{49}F^2(dd) + \frac{36}{441}F^4(dd)$

integrals that must be considered, all of which are included in the INDO/S model. Other nonzero integrals derived from the R^k Slater-Condon factors, such as $(sd_{z^2} \mid ss)$, are not included, since they do not contribute to rotational invariance and are small in magnitude [153]. For the 3d metals semiempirical values of the F^k and G^k ($k > 0$) obtained from atomic energy levels of the ground state electron configuration of the metal [164] are used.

In the case of the 4d metals, the dearth of experimental state energies precludes use of the procedure outlined above for obtaining two-center Coulomb integrals and the various one-center Slater Condon factors. For these elements, both one-center Coulomb integrals γ_{AA} and two-center integrals γ_{AB} are calculated over a basis set of atomic orbitals, and the higher Slater-Condon factors F^k and G^k are calculated over the basis set and scaled by a factor of 0.6 [155]. The magnitude of this scaling was assumed [155] based on comparing calculated Slater-Condon factors with values obtained from atomic spectroscopy for those elements where a majority of the necessary microstates have been characterized. Coulomb integrals obtained by calculation over the basis set are referred to a theoretical parameters, while Coulomb integrals obtained empirically from atomic spectroscopy as described above are referred to as spectroscopic parameters.

A valence orbital-only basis set of Slater-type orbitals is employed for the 4d metals. Single-zeta functions for the 5s orbitals (the 5p orbitals are assumed to have the same radial extent) and 4d orbitals are given orbital exponents chosen [155] to give good agreement with $F^0(ss)$ and $F^0(dd)$ computed with the multiple-zeta orbitals of Clementi and Roetti that were obtained from atomic calculations near the Hartree-Fock limit [165]. The resulting single-zeta functions are used to calculate all needed two electron integrals.

One electron matrix elements within the INDO model are fixed in analogy to the procedure used above to determine the form of the two electron integrals, by considering the ab initio expressions for the matrix elements and applying the ZDO approximation. For diagonal terms the ab initio expression is

$$H_{\mu\mu} = (\chi_\mu^A | -\tfrac{1}{2}\nabla^2 - \frac{Z_A}{r_{iA}} | \chi_\mu^A) - (\chi_\mu^A | \sum_{B \neq A} \frac{Z_B}{r_{iB}} | \chi_\mu^A) \tag{2-87}$$

In the INDO/S model this becomes

$$H_{\mu\mu} = U_{\mu\mu} - \sum_{B \neq A} Z_B \gamma_{AB} \tag{2-88}$$

Here $U_{\mu\mu}$ is an atomic quantity that can be extracted from atomic ionization potentials, as described below. In equation (2-88) the replacement

$$\left(\chi_\mu^A \middle| \frac{1}{r_{iB}} \middle| \chi_\mu^A \right) \leftarrow \gamma_{AB} \tag{2-89}$$

is made to compensate for the error introduced by not explicitly considering the core orbitals [83,166]. As discussed above in reference to the two electron parameters, γ_{AB} has different values $\gamma_{ss}^{AB} = \gamma_{sp}^{AB} = \gamma_{pp}^{AB}$, $\gamma_{sd}^{AB} = \gamma_{pd}^{AB}$, and γ_{dd}^{AB} for transition metal elements, which must be taken into account by expressing equation (2-88) as

$$H_{\mu\mu} = U_{\mu\mu} - \sum_{B \neq A} \left[(n_s^B + n_p^B)\gamma_{\mu s} + n_d^B \gamma_{\mu d} \right] \tag{2-90}$$

where n_s^B is the number of *s* electrons in the ground state configuration of atom B, etc.

For off-diagonal matrix elements between orbitals on the same atom, the ab initio expression is

$$H_{\mu\nu}^{AA} = (\chi_\mu^A | -\tfrac{1}{2}\nabla^2 + \frac{Z_A}{r_{iA}} | \chi_\nu^A) + (\chi_\mu^A | \sum_{B \neq A} \frac{Z_B}{r_{iB}} | \chi_\nu^A) \tag{2-91}$$

In this case the first term is a hydrogen-like off-diagonal matrix element $U_{\mu\nu}$ that is equal to zero as long as a basis set of s, p, d, etc. atomic orbitals is used. The second term is set to zero as well, due to neglect of the differential overlap $\chi_{\mu}^{*}(1)\chi_{\nu}(1)$. Therefore in the INDO/S model, off-diagonal one-center one electron matrix elements are set to zero:

$$H_{\mu\nu}^{AA} = 0 \tag{2-92}$$

The atomic core integrals $U_{\mu\mu}$ are extracted from atomic ionization potentials. In a valence orbital-only model, these parameters are meant to make the following replacement:

$$U_{\mu\mu} = (\chi_{\mu} \,|\, -\tfrac{1}{2}\nabla^{2} - \frac{Z_{A}}{r_{iA}} + V^{core} \,|\, \chi_{\mu}) \tag{2-93}$$

where V^{core} is a potential representing repulsion between the valence orbitals and neglected core orbitals [167]. If the matrix elements $U_{\mu\mu}$ are taken from atomic spectroscopy, V^{core} does not need to be accounted for explicitly. The method used for determining values of the core integrals utilizes the average energies of atomic electron configurations, equation (2-84). The average Coulomb and exchange integrals of equation (2-84) are related to the Slater-Condon factors [163] F^{k} and G^{k} as

$$\bar{J}_{ss} = F^{0}(ss); \quad \bar{J}_{pp} = F^{0}(pp) - \tfrac{4}{125}F^{2}(pp); \quad \bar{K}_{pp} = \tfrac{3}{25}F^{2}(pp);$$

$$\bar{J}_{dd} = F^{0}(dd) - \tfrac{4}{441}\left(F^{2}(dd) + F^{4}(dd)\right); \quad \bar{K}_{dd} = \tfrac{5}{98}\left(F^{2}(dd) + F^{4}(dd)\right);$$

$$\bar{J}_{sp} = F^{0}(sp); \quad \bar{K}_{sp} = \tfrac{1}{3}G^{1}(sp); \quad \bar{J}_{sd} = F^{0}(sd); \quad \bar{K}_{sd} = \tfrac{1}{5}G^{1}(sd);$$

$$\bar{J}_{pd} = F^{0}(pd); \quad \bar{K}_{pd} = \tfrac{2}{15}G^{1}(pd) + \tfrac{3}{35}G^{3}(pd) \tag{2-94}$$

These equalities can be obtained from table 2-1. The core integrals $U_{\mu\mu}$ are determined based on atomic ionization potentials using equation (2-84) for the neutral and cation ground state electron configurations, and substituting in the Slater-Condon factors which may be obtained empirically from atomic energy levels (3d metals) or computed over a basis set and scaled by 0.6 (4d metals) as discussed above in reference to one-center two electron integrals. The relevant expressions are shown in equations (2-95):

$$
\begin{aligned}
U_{ss} &= -I_s - (l-1)F^0(ss) - m\left(F^0(sp) - \tfrac{1}{6}G^1(sp)\right) - n\left(F^0(sd) - \tfrac{1}{10}G^2(sd)\right) \\
U_{pp} &= -I_p - (m-1)\left(F^0(pp) - \tfrac{2}{25}F^2(pp)\right) - l\left(F^0(sp) - \tfrac{1}{6}G^1(sp)\right) \\
&\quad - n\left(F^0(pd) - \tfrac{1}{15}G^1(pd) - \tfrac{3}{70}G^3(pd)\right) \\
U_{dd} &= -I_d - (n-1)\left(F^0(dd) - \tfrac{2}{63}F^2(dd) + F^4(dd)\right) - l\left(F^0(sd) - \tfrac{1}{10}G^2(sd)\right) \\
&\quad - m\left(F^0(pd) - \tfrac{1}{15}G^1(pd) - \tfrac{3}{70}G^3(pd)\right) \qquad (2\text{-}95)
\end{aligned}
$$

Extraction of the atomic core integrals from ionization potentials was used in the original CNDO method of Pople and coworkers [81,82], but a later modification referred to as CNDO/2 [83] and the original INDO model [84] used the average of ionization potentials and electron affinities. The reasoning behind this choice is that an atom in a molecule is as likely to gain electron density as it is to lose electron density. Choice of these parameters from ionization potentials alone is supported by several arguments. First, electron affinities have not been accurately determined for the valence states of many atoms, particularly transition metals. Second, ab initio calculations on diatomics that are transformed to closely resemble semiempirical calculations give results that are more consistent with results obtained from INDO calculations using core integrals derived from ionization potentials only [168]. Third, predictions of spectroscopy obtained from INDO/S calculations are more accurate using core integrals derived from ionization potentials only [91].

An important complication that arises in computing the core integrals for transition metals according to the procedure just outlined is that the $4s^2 3d^{n-2}$ and $4s^1 3d^{n-1}$ electron configurations are competitive in energy, as described above. There are thus two ionization processes that might be considered in determining core integrals from equation (2-95). Initial experience with the model indicated that taking parameters based on one or the other of the two possible configurations does not provide accurate descriptions of the ground states of transition metal complexes [92]. The procedure adopted for incorporating both configurations assumes that the two configurations become mixed slightly due to perturbation by the molecular environment. Denoting this perturbation as V^m and the energies of the $4s^2 3d^{n-2}$ and $4s^1 3d^{n-1}$ configurations as H_{11} and H_{22}, respectively, this mixing in the atomic ground state can be represented by the matrix equation

$$\begin{bmatrix} H_{11} & V^m \\ V^m & H_{22} \end{bmatrix} \begin{bmatrix} C_1 \\ C_2 \end{bmatrix} = E \begin{bmatrix} C_1 \\ C_2 \end{bmatrix} \tag{2-96}$$

Assuming a nonzero value for V^m, equation (2-96) can be manipulated to yield

$$\chi = \frac{C_1}{C_2} = \frac{H_{11} - H_{22}}{2V^m} + \sqrt{\left(\frac{H_{11} - H_{22}}{2V^m}\right)^2 + 1} \tag{2-97}$$

and, assuming that wavefunctions representing the two configurations are orthogonal,

$$C_1^2 = \frac{\chi^2}{1 + \chi^2} \tag{2-98}$$

An empirical value of $V^m = -0.02$ atomic units was adopted based on experience [92], and values of C_1^2 were determined based on atomic energy levels [159]. Weighted averages of ionization potentials for the two configurations are used in equation (2-95) according to the values of C_1^2 to obtain the core integrals. The electron populations n_s, n_p, and n_d used in equation (2-90) are also changed according to the weighting determined as above.

For the 4d metals [155], the configuration $5s^0 4d^n$ must be considered in addition to the $5s^2 4d^{n-2}$ and $5s^1 4d^{n-1}$ configurations, since this configuration is low in energy for several of the elements. An additional problem is that the configurational ionization energies themselves that are needed in equation (2-95) are not completely determined for many of the elements since a number of the needed microstates have not been characterized experimentally. The ionization energies were therefore fit versus the core charge, weighting those determined for each element by a factor accounting for the proportion of microstates with known energies (i.e., 5 for 100% of states needed to determine the VSIP, 4 for 80%, etc.). Then, as with the 3d metals, a mixing of configurations induced by complex (or cluster) formation is assumed. The matrix equation in this case is

$$\begin{bmatrix} H_{11} & V^m & V^m \\ V^m & H_{22} & V^m \\ V^m & V^m & H_{33} \end{bmatrix} \begin{bmatrix} C_1 \\ C_2 \\ C_3 \end{bmatrix} = E \begin{bmatrix} C_1 \\ C_2 \\ C_3 \end{bmatrix} \tag{2-99}$$

with again $V^m = -0.02$ a.u. Squares of the coefficients obtained from equation (2-99) are used to weight ionization potentials for each of the three low-lying configurations.

For two-center one electron matrix elements $H_{\mu\nu}^{AB}$, the ab initio expression is written as

$$H_{\mu\nu}^{AB} = (\chi_\mu^A \mid -\tfrac{1}{2}\nabla^2 - \frac{Z_A}{r_{iA}} - \frac{Z_B}{r_{iB}} \mid \chi_\nu^B) - (\chi_\mu^A \mid \sum_{C \neq A,B} \frac{Z_C}{r_{iC}} \mid \chi_\nu^B) \qquad (2\text{-}100)$$

The second term on the right of equation (2-100) is neglected since it is three-center. The first term is referred to as the resonance integral, and represents the lowering of energy that occurs due to an electron being in the field of two nuclei simultaneously [81]. The strength of covalent interaction between bonding orbitals is directly related to the magnitude of the resonance integral.

Resonance integrals are replaced with empirical parameters in all modern semiempirical methods. In the INDO/S method, this is the only term entering into the elements of the Fock matrix that is entirely empirical in nature. Based on the first integral on the right side of equation (2-100), it is clear that the functional form to be adopted for these terms should scale with distance in some way, and also have the symmetry of the molecule. Based on these considerations the overlap between the atomic functions χ_μ and χ_ν is included in the functional form. It is important to understand that this inclusion does not mean that the model now formally contains orbital overlap. The overlap is used to impart a certain symmetry and distance dependence to the two center one-electron integrals, but is not incorporated in the Roothaan-Hall equations, as in the ab initio expression **FC** = **SCE**. The ZDO approximation demands that overlap integrals be neglected. Semiempirical methods consider the matrix elements to be taken in a basis of Löwdin-orthogonalized basis functions (though the exact form of these functions need not be specified, since integrals are replaced with parameters). This assumption has at least partial theoretical justification [169].

INDO/S uses a sum form for the two-center one electron matrix elements,

$$H_{\mu\nu}^{AB} = \frac{1}{2}\left(\beta_{\mu}^{A} + \beta_{\nu}^{B}\right)\Delta_{\mu\nu} \qquad (2\text{-}101)$$

based on the original suggestion of Wolfsberg and Helmholtz [170]. Here Δ is a matrix related to the overlap matrix S, as described below. β_{μ} is an empirical parameter. In the original formulation of INDO [84] β was taken as depending only on the atoms involved, to preserve rotational invariance with respect to hybridization between shells. As with the one-center Coulomb integrals discussed above, this approximation is retained for main group elements, but with the transition metals appropriate values for d orbitals on the one hand and s or p orbitals on the other hand are quite different, and separate values are used in the INDO/S model. This sacrifices invariance with respect to hybridization transformations, but retains the essential property of invariance with respect to rotations of the molecular framework. Values of β_{μ}^{A} were chosen to reproduce spectra of model compounds. No extensive systematic parameterization of the $\{\beta_{\mu}^{A}\}$ has been carried out, but experience with the method indicates that the $d - d^{*}$ electronic spectroscopy of complexes of the 3d metals is accurately represented [93].

In equation (2-101) the Δ matrix was taken as the overlap matrix in the original formulation of INDO [84], but Del Bene and Jaffé [151] found that π and σ molecular orbital energies of benzene were not predicted accurately, with the π orbitals interacting too strongly. A simple scaling factor was adopted for pπ-pπ resonance integrals, as suggested earlier by Mulliken [171]. The factor was set at 0.585 based on spectroscopic predictions for benzene, pyridine, and the diazines. Later it was found that predicted energies of $n \rightarrow \pi^*$ transitions of benzene and pyridine were improved by scaling pσ-pσ resonance integrals by 1.267 [91]. The modern implementation of INDO/S treats $\Delta_{\mu\nu}$ as

$$\Delta_{ss} = S_{ss}$$

$$\Delta_{sp} = S_{sp}$$

$$\Delta_{pp} = g_\sigma f_\sigma S_{p\sigma p\sigma} + g_\pi f_\pi S_{p\pi p\pi} \qquad (2\text{–}102)$$

for s and p orbitals, where g_σ and g_π are factors needed for rotation between the local diatomic coordinates and the molecular coordinates [93], and f_σ and f_π are the factors 1.267 and 0.585, respectively. Similar weighting factors (but not specific values) have been suggested for the resonance integrals for d orbital interactions in situations with orbital interactions between neighboring metal atoms [153], but this idea has not been pursued.

The overlap integrals appearing in equation (2-101) are calculated over a basis set of Slater-type orbitals for both 3d and 4d metals. In the latter case, the single-zeta functions for 5s and 5p orbitals discussed above are used, but overlap integrals between 4d orbitals of Mo and 3s and 3p orbitals of sulfur at representative Mo-S bond lengths were found to be inaccurate [155]. The double-zeta functions of Clementi and Roetti [165] were thus adopted for the purpose of computing the overlap of equation (2-101), after renormalizing to account for excluding core orbitals included in the treatment by Clementi and Roetti. The same approach is used for the 3d metals, with single-zeta functions adopted for s and p orbitals and double-zeta functions adopted for d orbitals, again taken from the tabulation by Clementi and Roetti [165].

Several modifications of the original sum form for the resonance integral have been suggested. One is to use a product form

$$\beta_{\mu\nu} = -\sqrt{\beta_\mu^A \cdot \beta_\nu^B} \tag{2-103}$$

suggested by Lipscomb [172]. This form is identical to the sum form if $\beta_\mu^A = \beta_\nu^B$ but can give quite different results if the values of β_μ^A and β_ν^B are very different. It is generally thought that the product form is better than the sum form for very electronegative atoms like fluorine and oxygen. It has also been suggested [138] that the overlap does not fall off fast enough with distance, and functional forms that scale more sharply with distance have been tested. One example supported by the ab initio form of the integrals [138,173] is

$$\beta_{\mu\nu} = R_{AB}^{m} \cdot e^{\left[-(\alpha_\mu + \alpha_\nu) R_{AB}^2\right]} \cdot \frac{1}{2}\left(\beta_\mu^A + \beta_\nu^B\right)\Delta_{\mu\nu} \tag{2-104}$$

The exponential factor is meant to make the function fall off with distance faster than the overlap does. A modified parameterization of INDO/S for several first row elements using this functional form for β has been proposed [174].

In summary, RHF Fock matrix elements in the INDO/S model are approximated as

$$F_{\mu\mu} = U_{\mu\mu} - \sum_{B\neq A} Z_B \gamma_{AB} + \sum_{\sigma,\lambda}^{A} P_{\sigma\lambda}\left[(\mu\mu|\sigma\lambda) - \frac{1}{2}(\mu\lambda|\sigma\mu)\right] + \sum_{\sigma}^{B\neq A} P_{\sigma\sigma}\gamma_{AB}$$

$$F_{\mu\nu}^{AA} = \sum_{\sigma,\lambda}^{A} P_{\sigma\lambda}\left[(\mu\nu|\sigma\lambda) - \frac{1}{2}(\mu\lambda|\sigma\nu)\right]$$

$$F_{\mu\nu}^{AB} = \frac{1}{2}\left(\beta_\mu^A + \beta_\nu^B\right)\Delta_{\mu\nu} - \frac{1}{2}P_{\mu\nu}\gamma_{AB} \tag{2-105}$$

where the various parameters and their derivations are given in table 2-2. Matrix elements in the UHF and ROHF formulations, though not as simple as equations (2-105), utilize the same parameters and integral approximations. Once the SCF procedure is

Table 2-2. Parameters included in the INDO/S model and their derivation for 3d and 4d metals.

Parameter	Derivation, 3d metals	Derivation, 4d metals
One-center Coulomb integrals γ_{AA}	Diagonal parameters set equal to IP – EA. Off-diagonal parameters extracted from diagonal parameters and orbital ionization energies, equations (2-85) and (2-86).	Calculated over basis set.
Two-center Coulomb integrals γ_{AB}	Mataga-Nishimoto formula, equation (2-83).	Calculated over basis set.
Higher Slater-Condon factors F^k, G^k	From atomic energy levels, reference x.	Calculated over basis set and scaled by 0.6
Atomic core integrals $U_{\mu\mu}$	From orbital ionization energies and higher Slater-Condon factors from above using equations (2-95).	From orbital ionization energies and higher Slater-Condon factors from above using equations (2-95).
Resonance integrals β_{μ}^{A}	Fit to reproduce experimental spectroscopy for model complexes.	Fit to reproduce experimental spectroscopy for model complexes.
Weighted overlap matrix Δ	Overlap matrix over basis set, with empirical factors $f_{p\sigma} = 1.267$ and $f_{p\pi} = 0.585$.	Overlap matrix over basis set, with empirical factors $f_{p\sigma} = 1.267$ and $f_{p\pi} = 0.585$.
Basis set	Single-zeta STOs for 4s, 4p orbitals taken from reference y. Double-zeta STOs for 3d orbitals taken from reference y.	Single-zeta STOs for 5s, 5p, and 4d orbitals used to calculate two electron integrals; from reference y. Double-zeta STOs for 4d orbitals used to compute overlap. Orbitals taken from reference y.

converged to obtain the final form of the density matrix, the ground state molecular orbitals are fixed, and can be used in subsequent CI calculations and CI calculations that include spin-orbit coupling, which are the final topics of this chapter.

CI is intuitively the most obvious method for treating electronic spectroscopy, since it is built upon the concept of excitations of electrons within the ground state orbital manifold. It is important to use spin-adapted configuration state functions in a CI treatment of spectroscopy, so that spin selection rules will be obeyed. Doing so also allows application of spin-dependent operators in the basis of CSFs, such as the spin-orbit operator. Implementation of a spin-orbit capability as part of a spectroscopic CI method provides the ability to obtain spin-orbit splittings in the ground and excited states which can be compared to experimental results. Also, estimates of the intensity of spin-forbidden transitions can be obtained for cases where spin-orbit mixing allows abrogation of the spin selection rule. These features are of primary importance in allowing a definitive analysis of the experimental electronic spectroscopy of the group 5 diatomics and in probing correlation effects in the INDO/S model. The CI method including spin-orbit coupling described below will be referred to as the SOCI method.

The approach used to obtain spin-adapted CSFs is based on the valence bond spin functions of Hietler and Rumer [175] and Slater [176], which are written as

$$\frac{1}{\sqrt{2}}[\alpha(1)\beta(2)-\beta(1)\alpha(2)]\cdots\frac{1}{\sqrt{2}}[\alpha(i)\beta(j)-\beta(i)\alpha(j)]\alpha(k)\alpha(l)\cdots\alpha(n) \qquad (2\text{-}106)$$

It can be shown that such a function is an eigenfunction of spin [131]. So-called valence bonded structures or bonded functions constructed based on spin functions of the form of (2-106) are convenient because matrix elements of the electronic Hamiltonian between two functions can be evaluated readily [177], as can matrix elements of any one-electron spin-dependent operator such as the spin-orbit operator [178]. The work of Rumer [179] and Simonetta [180] led to a diagrammatic technique for determining appropriate spin eigenfunctions for any arbitrary number of electrons and spin quantum number. The technique is illustrated for a simple example, which is then used to demonstrate the basic idea, if not all details, of the SOCI calculations.

As the example, consider three orbitals and three electrons. If each orbital is singly occupied, there is one quartet state and two doublet states. Expressing these spin states as $|\mathrm{SM}\rangle$, where S is the quantum number for total spin and M is the quantum number for the z-component of the spin, the standard orthonormal spin eigenfunctions [181] are

$$\begin{aligned}
\left|\tfrac{3}{2}\tfrac{3}{2}\right\rangle &= \alpha\alpha\alpha \\
\left|\tfrac{3}{2}\tfrac{1}{2}\right\rangle &= \tfrac{1}{\sqrt{3}}[\alpha\alpha\beta+\alpha\beta\alpha+\beta\alpha\alpha] \\
\left|\tfrac{1}{2}\tfrac{1}{2}\right\rangle_1 &= \tfrac{1}{\sqrt{2}}[\alpha\alpha\beta-\alpha\beta\alpha] \\
\left|\tfrac{1}{2}\tfrac{1}{2}\right\rangle_2 &= \tfrac{1}{\sqrt{6}}[2\beta\alpha\alpha-\alpha\alpha\beta-\alpha\beta\alpha]
\end{aligned} \tag{2-107}$$

where the electron labels have been suppressed and are assumed to be in order 1, 2, 3. Spin eigenfunctions for negative values of M are analogous to these.

To obtain spin eigenfunctions by the Rumer diagram technique, numerical indices representing the electrons are placed in a circle or square, along with an additional index called the pole, as shown in figure 2-2. Then $\frac{1}{2}\mathrm{N}-\mathrm{S}$ pairs of indices are connected with arrows in all possible ways, with the remaining indices connected to the pole. For $\mathrm{S}=\frac{3}{2}$, then, no arrows are drawn, as in figure 2-2 (A). For $\mathrm{S}=\frac{1}{2}$ one arrow must be drawn, as

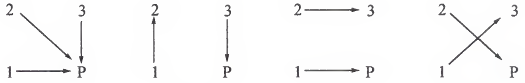

(A) (B) (C) (D)

Figure 2-2: Extended Rumer diagrams representing quartet and doublet states for three electrons in three orbitals.

in figure 2-2 (B)-(D). For cases where N > 2S this procedure will produce a certain number of linearly dependent functions. In figure 2-2, for example, there are three diagrams for $S = \frac{1}{2}$ when in fact there are only two doublet functions (equation (2-107)). It has been shown that a linearly independent set of spin functions is obtained if diagrams with crossed lines such as figure 2-2 (D) are omitted [182].

Considering figure 2-2 (A)-(C), indices connected by arrows are assumed to be spin-paired, giving the function $2^{-1/2}[\alpha(i)\beta(j) - \beta(i)\alpha(j)]$, while indices connected to the pole are assumed to be unpaired. The spin functions obtained from figure 2-2 (A)-(C) are therefore

$$f_A = \alpha\alpha\alpha = \left|\tfrac{3}{2}\tfrac{3}{2}\right\rangle$$

$$f_B = \frac{1}{\sqrt{2}}(\alpha\beta\alpha - \beta\alpha\alpha)$$

$$f_C = \frac{1}{\sqrt{2}}(\alpha\alpha\beta - \alpha\beta\alpha) = \left|\tfrac{1}{2}\tfrac{1}{2}\right\rangle_1 \tag{2-108}$$

A general feature of Rumer spin functions is that they are not orthogonal, as demonstrated by f_B and f_C which have overlap $S_{BC} = -\frac{1}{2}$. It is thus necessary to orthogonalize the basis of Rumer CSFs in some manner so that the CI matrix equations can be transformed from the form of equation (2-57) to the form of equation (2-56). It has been shown that Schmidt orthogonalization yields the standard spin functions as obtained using branching diagrams [180]. For example, taking

$$f'_C = f_C$$

$$f'_B = \frac{f_B - S_{BC} f_C}{\sqrt{1 - S_{BC}^2}} \tag{2-109}$$

yields the following equations for the normalizations of f'_B and f'_C and the overlap $\langle f'_C | f'_B \rangle$:

$$\langle f'_C | f'_C \rangle = 1$$

$$\langle f'_C | f'_B \rangle = \frac{S_{BC} - S_{BC}}{\sqrt{1 - S_{BC}^2}} = 0$$

$$\langle f'_B | f'_B \rangle = \frac{1 - S_{BC}^2}{1 - S_{BC}^2} = 1 \tag{2-110}$$

Substituting f_B, f_C, and S_{BC} into equation (2-109) and assuming the negative normalization constant $-(1 - S^2)^{1/2}$ gives

$$f'_B = \frac{\frac{1}{\sqrt{2}}(\alpha\beta\alpha - \beta\alpha\alpha) + \frac{1}{2}\frac{1}{\sqrt{2}}(\alpha\alpha\beta - \alpha\beta\alpha)}{-\sqrt{1 - \frac{1}{2}^2}} \tag{2-111}$$

which upon rearrangement yields $\left|\frac{1}{2}\frac{1}{2}\right\rangle_2$. Schmidt orthogonalization is not the only method that might be used. Another example is the symmetric or Löwdin transformation [169], in which the CI matrix is transformed according to

$$\mathbf{H}' = \mathbf{S}^{-1/2}\mathbf{H}\mathbf{S}^{-1/2} \tag{2-112}$$

This approach requires diagonalization of the overlap matrix S, which can be quite involved for large CI calculations. More will be said about this important detail in chapter three.

The Rumer diagram technique as developed above provides spin eigenfunctions. Determinantal wavefunctions involving spatial molecular orbitals are then assumed to have the form

$$|\Psi\rangle = \hat{A}\,\overset{\frown}{\psi_1\psi_2}\,\overset{\frown}{\psi_3\psi_4}\cdots\overset{\frown}{\psi_i\psi_j}\,\psi_k\cdots\psi_n \tag{2-113}$$

where orbitals joined by bars are spin-coupled,

$$\overset{\frown}{\psi_i\psi_j} = \psi_i\psi_j 2^{-1/2}[\alpha\beta-\beta\alpha] \tag{2-114}$$

and $\hat{A}$, the antisymmetrizer, is an operator that generates a normalized sum of terms equivalent to that obtained by taking a determinant as in equation (2-11). Appropriate products of spin-coupled and unpaired orbitals are obtained directly from the Rumer diagrams, with orbitals connected by arrows in the diagrams spin-coupled. Functions of the form of equation (2-113) are referred to as bonded functions. For the example considered above, the wavefunctions for the quartet and two doublet states are thus

$$^{\frac{3}{2}}\Psi = |\psi_1\psi_2\psi_3\rangle$$

$$^{\frac{1}{2}}\Psi_B = \frac{1}{\sqrt{2}}\left[|\psi_1\bar{\psi}_2\psi_3\rangle - |\bar{\psi}_1\psi_2\psi_3\rangle\right]$$

$$^{\frac{1}{2}}\Psi_C = \frac{1}{\sqrt{2}}\left[|\psi_1\psi_2\bar{\psi}_3\rangle - |\psi_1\bar{\psi}_2\psi_3\rangle\right] \tag{2-115}$$

In the course of a calculation it is not necessary to specify sums over Slater determinants such as are shown in equations (2-115), as matrix elements between CSFs can be evaluated directly from the diagrams. This is illustrated for the spin-orbit operator in the following discussion.

Manne and Zerner developed general expressions for matrix elements of one electron spin-dependent operators in a basis of bonded functions [178]. Though earlier similar developments were given [183,184], the specific application of the formalism of Manne and Zerner to the spin-orbit operator [185] is presented since the INDO/S SOCI calculations use this approach. The spin-orbit operator is taken as

$$\hat{H}^{\mathrm{S.O.}} = \sum_{i} \xi(r_i)\hat{l}_i \cdot \hat{s}_i \tag{2-116}$$

where the sum is over electrons and $\xi(r_i)$ is the spin-orbit radial operator,

$$\xi(r) = -\frac{1}{2}\frac{Z_A}{r_{iA}^3} \tag{2-117}$$

that integrates to give the spin-orbit coupling constant ζ_μ^A characteristic of a particular atom and orbital,

$$\zeta_\mu^A = \left\langle \chi_\mu^A \middle| \xi(r) \middle| \chi_\mu^A \right\rangle \tag{2-118}$$

with units of energy. $\hat{H}^{\mathrm{S.O.}}$ can be expressed in terms of $\hat{l}_z$, $\hat{s}_z$, and the raising and lowering operators as

$$\hat{H}^{\mathrm{S.O.}} = \sum_{i} \xi(r_i)\left[\hat{l}_{iz}\hat{s}_{iz} + \tfrac{1}{2}\left(\hat{l}_{i+}\hat{s}_{i-} + \hat{l}_{i-}\hat{s}_{i+}\right)\right] \tag{2-119}$$

Nonzero matrix elements can occur between bonded functions of the same spin quantum number or functions with spin quantum numbers that differ by one.

Evaluation of matrix elements of $\hat{H}^{\mathrm{S.O.}}$ between two bonded functions is developed following Kotzian, Rösch, and Zerner [185]. A conjoined diagram is drawn by writing the orbital indices for each function one above the other with bars connecting spin-coupled orbitals as in equation (2-113). The strings of indices must be placed in maximum coincidence, accounting for sign changes for each permutation. Vertical bars are then drawn between indices of the two strings. Consider for example two bonded functions,

$$f_1 = \overgroup{\psi_1\psi_2}\,\psi_3\psi_4\,\overgroup{\psi_5\psi_6}\,\psi_7$$

$$f_2 = \overgroup{\psi_1\psi_2}\,\overgroup{\psi_3\psi_4}\,\psi_5\,\overgroup{\psi_6\psi_7} \qquad (2\text{-}120)$$

The conjoined diagram for these two functions is shown in figure 2-3. Three distinct loop structures are possible, including closed loops (involving indices 1 and 2 in figure 2-3), even chains that start and end with unpaired spins on the same string (indices 3 and 4),

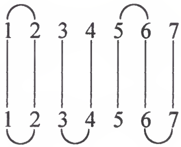

Figure 2-3: Conjoined diagram for two bonded functions.

and odd chains that start on one string and end on the other (indices 5-7). These structures represent interactions between singlet-coupled pairs, between doublet-coupled strings, and between a singlet-coupled and a triplet-coupled string, respectively.

Closed loops make no contribution to matrix elements, odd chains contribute to matrix elements between states of the same spin muiltiplicity, and even chains contribute to matrix elements between states with $\Delta S = \pm 1$. Formulas for the matrix elements are over summations of terms involving indices linked by vertical bars in each distinct chain structure, according to equations (2-121) through (2-126), shown on the next page. These formulas involve a rather complicated and opaque notation, and their use is best understood by example. The notation is as follows: $|SM\rangle_K$ refers to a particular Rumer spin function with characteristic S and M quantum numbers. The summations are over pairs of indices linked by vertical bars in even or odd chains, depending on the spin of the two states. ψ_i represents a molecular orbital in the upper string, and ϕ_i the MO in the lower string that is linked to ψ_i. The factors Q_i^{KL} account for the fact that matrix elements of one electron operators between determinantal wavefunctions are zero if two or more orbitals are different in the two determinants. $Q_i^{KL} = 1$ if the two strings are identical in all orbitals other than ψ_i and ϕ_i and is zero if not. q_i^{KL} is a parity index that alternates $+,-,+,\cdots$ for pairs linked by vertical bars in a particular odd chain, and is zero for pairs linked in even chains or closed loops. Similarly, r_i^{KL} is a parity index defined for pairs linked in even chains, and is zero otherwise. The remaining factors account for normalization and parity. σ and σ' count permutations necessary to bring the orbital strings into maximum coincidence, J is the number of pairs of spin-coupled orbitals with identical indices in one function not matched by a pair of identical indices in the other

---

$$_K\left\langle SM\middle|\xi(r)\hat{I}_z\hat{s}_z\middle|SM\right\rangle_L = \frac{M}{2S}\sqrt{2}^J(-1)^{\sigma+\sigma'}(-2)^{c-b}\sum_i^n Q_i^{KL}q_i^{KL}\left\langle\psi_i\middle|\xi(r)\hat{I}_z\middle|\phi_i\right\rangle \tag{2-121}$$

$$\begin{aligned} _K\left\langle SM-1\middle|\xi(r)\hat{I}_+\hat{s}_-\middle|SM\right\rangle_L &= \frac{\left[S(S+1)-M(M-1)\right]^{1/2}}{2S}\sqrt{2}^J(-1)^{\sigma+\sigma'}(-2)^{c-b} \\ &\quad\times\sum_i^n Q_i^{KL}q_i^{KL}\left\langle\psi_i\middle|\xi(r)\hat{I}_+\middle|\phi_i\right\rangle \end{aligned} \tag{2-122}$$

$$\begin{aligned} _K\left\langle SM-1\middle|\xi(r)\hat{I}_-\hat{s}_+\middle|SM\right\rangle_L &= \frac{\left[S(S+1)-M(M+1)\right]^{1/2}}{2S}\sqrt{2}^J(-1)^{\sigma+\sigma'}(-2)^{c-b} \\ &\quad\times\sum_i^n Q_i^{KL}q_i^{KL}\left\langle\psi_i\middle|\xi(r)\hat{I}_-\middle|\phi_i\right\rangle \end{aligned} \tag{2-123}$$

$$\begin{aligned} _K\left\langle S-1M\middle|\xi(r)\hat{I}_z\hat{s}_z\middle|SM\right\rangle_L &= \frac{1}{2}\left[\frac{(S+M)(S-M)}{S(2S-1)}\right]^{1/2}\sqrt{2}^J(-1)^{\sigma+\sigma'}(-2)^{c-b} \\ &\quad\times\sum_i^n Q_i^{KL}r_i^{KL}\left\langle\psi_i\middle|\xi(r)\hat{I}_z\middle|\phi_i\right\rangle \end{aligned} \tag{2-124}$$

$$\begin{aligned} _K\left\langle S-1M-1\middle|\xi(r)\hat{I}_+\hat{s}_-\middle|SM\right\rangle_L &= -\frac{1}{2}\left[\frac{(S+M)(S+M-1)}{S(2S-1)}\right]^{\frac{1}{2}}\sqrt{2}^J(-1)^{\sigma+\sigma'}(-2)^{c-b} \\ &\quad\times\sum_i^n Q_i^{KL}r_i^{KL}\left\langle\psi_i\middle|\xi(r)\hat{I}_+\middle|\phi_i\right\rangle \end{aligned} \tag{2-125}$$

$$\begin{aligned} _K\left\langle S-1M+1\middle|\xi(r)\hat{I}_-\hat{s}_+\middle|SM\right\rangle_L &= \frac{1}{2}\left[\frac{(S-M)(S-M-1)}{S(2S-1)}\right]^{\frac{1}{2}}\sqrt{2}^J(-1)^{\sigma+\sigma'}(-2)^{c-b} \\ &\quad\times\sum_i^n Q_i^{KL}r_i^{KL}\left\langle\psi_i\middle|\xi(r)\hat{I}_-\middle|\phi_i\right\rangle \end{aligned} \tag{2-126}$$

function. c is the number of closed loops, and b is the number of spin-coupled pairs in the bonded function with greater S (if S $\neq$ S$'$).

As an example of application of equations (2-121) through (2-126), the spin-orbit coupling between the Rumer spin functions for the quartet and doublet states $\left|\frac{3}{2}\frac{1}{2}\right\rangle$ and $\left|\frac{1}{2}\frac{1}{2}\right\rangle_1$, equations (2-107), are considered. A convenient aspect of the method displayed by this example is that the form of components of a state with M < S need never be specified. In the present case, the Rumer diagram for the quartet state corresponds to a bonded function for the M = $\frac{3}{2}$ component of the quartet state, and the matrix element $\left\langle\frac{3}{2}\frac{1}{2}\right|\hat{H}^{S.O.}\left|\frac{1}{2}\frac{1}{2}\right\rangle_1$ can be obtained based on this diagram using equation (2-124). The conjoined Rumer diagram for these functions is shown in figure 2-4. According to equation (2-124) only the even chain involving the second and third orbitals needs to be considered due to the factor r^{KL}. For the other factors in equation (2-124), J, σ, σ', c and b are all zero, and Q^{KL} fixes signs of the matrix elements of $\hat{l}_z$ over the molecular orbitals. The result is equation (2-127),

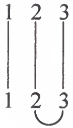

Figure 2-4: Conjoined diagram for ${}^{3/2}\Psi$ and ${}^{1/2}\Psi_1$, equations (2-107).

$$\left\langle \tfrac{3}{2}\tfrac{1}{2} \middle| \hat{H}^{S.O.} \middle| \tfrac{1}{2}\tfrac{1}{2} \right\rangle_1 = \frac{1}{\sqrt{6}}\Big(\langle \psi_2 | \xi(r)\hat{l}_z | \psi_2 \rangle - \langle \psi_3 | \xi(r)\hat{l}_z | \psi_3 \rangle\Big) \qquad (2\text{-}127)$$

Given a set of SCF molecular orbitals, the expansion of each MO over the atomic orbital basis set can be substituted into equations (2-121) through (2-126) to obtain integrals over the atomic basis set.

An important additional simplification is that the spin-orbit operator is limited to one-center terms only [186], which represent the most important contributions since the operator $\xi(r)$ carries r_{iA}^{-3} [181]. With this approximation, matrix elements of the operators $\hat{l}_x$, $\hat{l}_y$, and $\hat{l}_z$ can be evaluated using the real spherical harmonics. It should be noted at this point that the SOCI matrix algebra is complex rather than real due to the presence of the raising and lowering operators. In principle the required radial integrals involving the operator $\xi(r)$ could be evaluated explicitly over the basis set as well, but in the INDO/S model these integrals are replaced with experimental values [181,187,188] of atomic spin-orbit coupling constants ζ_{μ}^{A}.

The INDO/S SOCI procedure is as follows. SCF molecular orbitals are generated with an RHF or ROHF calculation as described above. All integrals are transformed from the atomic orbital basis to the MO basis, and are then used to form the CI matrix for a certain spin multiplicity in a basis of Rumer bonded functions. The INDO/S code is designed to treat any level of excitation from CIS to full CI, and allows flexible definition of the active space. The CI matrix is then orthogonalized by the Löwdin orthogonalization and diagonalized to give state energies and wavefunctions. This procedure is carried out for states with the same spin multiplicity as the ground state and states connected to these by the spin-orbit operator, namely, those with spin multiplicities S + 1 and S – 1. The Hamiltonian matrix including the spin-orbit operator is then formed. Each CI state is taken as a diagonal submatrix of dimension 2S + 1, and spin-orbit matrix elements between the various components of the states are evaluated using equations (2-121) through (2-126). Elements of the CI matrix are added along the diagonal of each (2S + 1)-order submatrix between states of the same spin multiplicity. A schematic example is given in figure 2-5 for two triplet bonded functions and two singlet bonded functions. The orthogonalization transformation matrices for each of the CI matrices are then applied successively to the appropriate blocks of the spin-orbit enhanced Hamiltonian matrix, which is then diagonalized to yield the final spectroscopic levels.

Transition moments are calculated by first constructing a matrix of dipole integrals over the basis of Rumer bonded functions according to

$$\mu_{KL} = -{}_{K}\langle SM|\vec{r}|SM\rangle_{L} = -\sqrt{2}^{J}(-1)^{\sigma+\sigma'}(-2)^{c-b}\sum_{i} Q_{i}^{KL}\langle \psi_i|\vec{r}|\phi_i\rangle \qquad (2\text{-}128)$$

in analogy to equations (2-121) through (2-126). Here matrix elements between states with $S \neq S'$ or $M \neq M'$ are zero since the dipole length operator is spin-independent. Transformation of the μ matrix to the spin-orbit basis yields transition moments,

$$\mu(KL) = \mathbf{C}^{\dagger}(K)\boldsymbol{\mu}\mathbf{C}(L) \qquad (2\text{-}129)$$

where **C**(K) is the column matrix containing the spin-orbit eigenvector coefficients for level *K*. Oscillator strengths are then computed according to

$$f(L \leftarrow K) = 4.7092 \times 10^{-7} |\mu(KL)|^{2} (E_L - E_K) \qquad (2\text{-}130)$$

The unit conversion factor 4.7092×10^{-7} allows $E_L - E_K$ to be in cm^{-1} and μ(KL) to be in

$$
\begin{array}{c|ccc:ccc:c:c}
 & {}^{3}W_{M=1} & {}^{3}W_{0} & {}^{3}W_{-1} & {}^{3}X_{1} & {}^{3}X_{0} & {}^{3}X_{-1} & {}^{1}Y_{0} & {}^{1}Z_{0} \\
\hline
{}^{3}W_{1} & E_{W}^{0}+\hat{H}_{WW}^{SO} & 0 & 0 & \left(\hat{H}+\hat{H}^{SO}\right)_{WX} & \hat{H}_{WX}^{SO} & 0 & \hat{H}_{WY}^{SO} & \hat{H}_{WZ}^{SO} \\
{}^{3}W_{0} & 0 & E_{W}^{0}+\hat{H}_{WW}^{SO} & 0 & \hat{H}_{WX}^{SO} & \left(\hat{H}+\hat{H}^{SO}\right)_{WX} & \hat{H}_{WX}^{SO} & \hat{H}_{WY}^{SO} & \hat{H}_{WZ}^{SO} \\
{}^{3}W_{-1} & 0 & 0 & E_{W}^{0}+\hat{H}_{WW}^{SO} & 0 & \hat{H}_{WX}^{SO} & \left(\hat{H}+\hat{H}^{SO}\right)_{WX} & \hat{H}_{WY}^{SO} & \hat{H}_{WZ}^{SO} \\
\hdashline
{}^{3}X_{1} & \left(\hat{H}+\hat{H}^{SO}\right)_{XW} & \hat{H}_{XW}^{SO} & 0 & E_{X}^{0}+\hat{H}_{XX}^{SO} & 0 & 0 & \hat{H}_{XY}^{SO} & \hat{H}_{XZ}^{SO} \\
{}^{3}X_{0} & \hat{H}_{XW}^{SO} & \left(\hat{H}+\hat{H}^{SO}\right)_{XW} & \hat{H}_{XW}^{SO} & 0 & E_{X}^{0}+\hat{H}_{XX}^{SO} & 0 & \hat{H}_{XY}^{SO} & \hat{H}_{XZ}^{SO} \\
{}^{3}X_{-1} & 0 & \hat{H}_{XW}^{SO} & \left(\hat{H}+\hat{H}^{SO}\right)_{XW} & 0 & 0 & E_{X}^{0}+\hat{H}_{XX}^{SO} & \hat{H}_{XY}^{SO} & \hat{H}_{XZ}^{SO} \\
\hdashline
{}^{1}Y_{0} & \hat{H}_{YW}^{SO} & \hat{H}_{YW}^{SO} & \hat{H}_{YW}^{SO} & \hat{H}_{YX}^{SO} & \hat{H}_{YX}^{SO} & \hat{H}_{YX}^{SO} & E_{Y}^{0} & \hat{H}_{YZ} \\
\hdashline
{}^{1}Z_{0} & \hat{H}_{ZW}^{SO} & \hat{H}_{ZW}^{SO} & \hat{H}_{ZW}^{SO} & \hat{H}_{ZX}^{SO} & \hat{H}_{ZX}^{SO} & \hat{H}_{ZX}^{SO} & \hat{H}_{ZY} & E_{Z}^{0}
\end{array}
$$

Figure 2-5: Schematic of a spin-orbit enhanced Hamiltonian matrix for triplet bonded functions ${}^{3}W$ and ${}^{3}X$ and singlet bonded functions ${}^{1}Y$ and ${}^{1}Z$. E_{X}^{0} represents the diagonal element of the CI matrix for bonded function X (i.e., before the CI matrix is diagonalized). Matrix elements of the spin-orbit operator are evaluated using equations (2-120) through (2-125).

Debye. In practice equation (2-129) is evaluated for transitions originating in only the first few energy levels, and is performed with successive row multiplications.

The Rumer diagram method described above is used for INDO/S SOCI calculations because of the straightforward treatment of spin-orbit coupling within a CI formalism appropriate for electronic spectroscopy. The method is also flexible: any spin multiplicity can be treated, open-shell ground states can be used, and any level of excitation within tailored active spaces is possible. On the other hand, the algebra involved is complex and the method relies on matrix diagonalization, making it slow and limiting the number of spin-orbit levels that can be treated to the order of ten thousand. The inefficiency can be ameliorated somewhat by adopting Schmidt rather than Löwdin orthogonalization, as discussed in the next chapter. Despite these limitations, the advantages of the Rumer diagram SOCI procedure make it a powerful tool for exploring the electronic spectroscopy including spin-orbit effects of small metal clusters.

CHAPTER 3
OPTIMIZATION OF THE INDO/S SOCI PROGRAM

The INDO/S SOCI method as described in the previous chapter was developed and implemented in the ZINDO program package of Zerner [108], as initially reported by Kotzian et al. [185]. Several improvements in the program were necessary before the method could be applied to the spectroscopy of the group five dimers, including optimization of the procedure used to allocate system memory to be used by calculations, implementation of Schmidt orthogonalization of the Hamiltonian matrix in the basis of Rumer diagram-derived CSFs to increase execution speed, and reduction of program output to a tractable form. In addition, code was developed to compute the ratio of contributions of states of different spin multiplicity to each spin-orbit energy level. This capability is useful for studying spin contamination of electronic states via spin-orbit coupling. These improvements are discussed in turn below. All of the work reported in this section was done in collaboration with Dr. Katrin Albert and Dr. Greg Pearl.

Optimization of Memory Allocation for SOCI Calculations

The most expensive part of a semiempirical CI calculation is diagonalization of the CI matrix. Arrays of the dimension of the CI matrix need to be stored in system memory. The ZINDO program [108] uses a dynamic memory allocation scheme to allocate space for the needed arrays, in which the dimensions of many program arrays are computed based on several input parameters at the beginning of a calculation, and memory is requested from the system accordingly. In the original implementation of the Rumer diagram CI method (i.e., before the spin-orbit enhanced CI capability was added), the user input an estimate for the number of CSFs to be generated, which was used to allocate space for arrays needed by the CI subroutines. The minimum amount of memory needed to store arrays was thus obtained, as the user could input the exact number of CSFs. Formulas for obtaining the number of CSFs based on spin multiplicity, number of active electrons and number of active orbitals are available elsewhere [130].

In a SOCI calculation, however, there are generally three CI calculations since states of spin multiplicities $S + 1$ and $S - 1$ are connected via the spin-orbit operator to states of the ground state multiplicity S. In the original implementation of the program the user would input the largest number of CSFs generated by the three CI calculations, and this parameter would be used to estimate the size of the spin-orbit enhanced CI matrix. As can be inferred from figure 2-5, the dimension of this matrix is

$$D = (2S - 1)N_{S-1} + (2S + 1)N_S + (2S + 3)N_{S+1} \tag{3-1}$$

where N_S is the number of CSFs of spin multiplicity S. In general N_{S-1}, N_S, and N_{S+1} are not identical, so an estimate of D based on the largest of the three parameters will always lead to an overestimate of the dimension of the spin-orbit matrix. For example, full CI calculations using six active electrons and eight active orbitals will generate 1176 singlet CSFs, 1512 triplet CSFs, and 420 quintet CSFs. The spin-orbit matrix is therefore of dimension $1176 + 3\times1512 + 5\times420 = 7812$. Assuming $N_{S-1} = N_S = N_{S+1} = 1512$, however, leads to an estimate of $(1 + 3 + 5)\times1512 = 13608$ levels, a considerable overestimate. Since the number of elements of an array depends on the square of the dimension, the overestimate is actually a factor of slightly more than three for this example.

This problem was overcome by adding a switch to the input indicating that a spin-orbit calculation is to be performed, which directs the program to read in a linear array of three values in place of the single dimension of the largest CI matrix used previously. The spin multiplicity was already part of the input, so the proper number of energy levels can be used to dimension the arrays used by the spin-orbit part of the program. Though no systematic testing of memory allocation for calculations of various sizes was carried out, improvement was immediate and obvious. For the example given above, a ZINDO calculation allocated 423 megabytes of random-access memory on a Sun Enterprise 5000 server based on values of 1176, 1512, and 420 CSFs, and 1349 megabytes of RAM based on 1512 CSFs alone. It should be noted that the amount of memory actually used by the two calculations is identical. The only difference is the amount of memory requested by the program. Even so, the improvement is vital for a program that is used to run large calculations on machines that are shared resources, as smaller memory allocation results in smaller usage fees and leaves space free for other users.

Implementation of Schmidt Orthogonalization Code

Another important area in which the program has been improved is in execution speed. As described in the previous section, CSFs generated with the Rumer diagram formalism are not in general orthogonal, leading to the presence of the overlap matrix in equation (2-57), **HC** = **SCE**. The basis of CSFs must be orthogonalized prior to diagonalization of **H** to obtain **C** and **E**. The original version of the program used the symmetric or Löwdin orthogonalization [169] for this purpose, in analogy to modern

Hartree-Fock calculations [80]. In this procedure the matrix product $\mathbf{S}^{-\frac{1}{2}}\mathbf{S}^{\frac{1}{2}}$ (which is equal to the unit matrix) is inserted into equation (2-57) according to

$$\mathbf{H}\mathbf{S}^{-\frac{1}{2}}\mathbf{S}^{\frac{1}{2}}\mathbf{C} = \mathbf{S}\mathbf{S}^{-\frac{1}{2}}\mathbf{S}^{\frac{1}{2}}\mathbf{C}\mathbf{E} \tag{3-2}$$

Left-multiplication by $\mathbf{S}^{-\frac{1}{2}}$ then yields

$$\mathbf{S}^{-\frac{1}{2}}\mathbf{H}\mathbf{S}^{-\frac{1}{2}}\mathbf{S}^{\frac{1}{2}}\mathbf{C} = \mathbf{S}^{-\frac{1}{2}}\mathbf{S}\mathbf{S}^{-\frac{1}{2}}\mathbf{S}^{\frac{1}{2}}\mathbf{C}\mathbf{E} \tag{3-3}$$

or

$$\mathbf{H}'\mathbf{C}' = \mathbf{C}'\mathbf{E} \tag{3-4}$$

where $\mathbf{H}' = \mathbf{S}^{-\frac{1}{2}}\mathbf{H}\mathbf{S}^{-\frac{1}{2}}$ and $\mathbf{C}' = \mathbf{S}^{\frac{1}{2}}\mathbf{C}$. Note that the energy matrix has not been changed by this transformation. Equation (3-4) can be solved by standard linear algebra techniques for $\mathbf{E}$ and $\mathbf{C}'$, and the coefficient matrix in the original basis can be obtained according to $\mathbf{C} = \mathbf{S}^{-\frac{1}{2}}\mathbf{C}'$. The drawback to this approach is that the overlap matrix **S** must be diagonalized in order to obtain $\mathbf{S}^{-\frac{1}{2}}$ [80]. The cost of this single matrix diagonalization is acceptable in an SCF calculation because the Fock matrix must be diagonalized in each iteration. In a CI calculation, on the other hand, the CI matrix is diagonalized exactly once, so an additional diagonalization procedure adds considerably to the total execution time.

In the case of CSFs constructed with Rumer spin functions, only CSFs of the same z-component of spin are nonorthogonal, because otherwise spin integration always yields zero in evaluating the overlap. This can be seen in the CSFs given in chapter two in equations (2-108) for three electrons in three orbitals. By inspection, the quartet spin function $\alpha\alpha\alpha$ has zero overlap with the doublet functions $\frac{1}{\sqrt{2}}(\alpha\beta\alpha - \beta\alpha\alpha)$ and

$\frac{1}{\sqrt{2}}(\alpha\alpha\beta - \alpha\beta\alpha)$, while the doublet functions have overlap of $-\frac{1}{2}$. Thus it is not necessary to invert the entire overlap matrix, and a method of performing the transformation by blocks is actually used. This amounts to replacing diagonalization of a large matrix (the entire overlap matrix) with successive diagonalizations of a number of smaller matrices. Schmidt orthogonalization still represents a more efficient procedure, since each of these diagonalizations is replaced with algebraic manipulations.

In the Schmidt orthogonalization procedure the basis functions are considered in turn, and the projection of a particular basis function onto the space of the previously considered transformed functions is subtracted from that function. In other words, each basis function is made orthogonal to the set of transformed functions already constructed, leading in the end to an orthonormal basis. The orthogonalization transformation matrix required for this transformation is constructed based on an algebraic prescription rather than a matrix diagonalization. Denoting the original basis functions as $|\Psi_\alpha\rangle$ and the transformed basis functions as $|\Psi'_\alpha\rangle$, the transformed functions are taken as

$$|\Psi'_i\rangle = \left(1 - \sum_{\alpha=1}^{i-1} |\Psi'_\alpha\rangle\langle\Psi'_\alpha|\right)|\Psi_i\rangle \times \left[1 - \sum_{\alpha=1}^{i-1} |\langle\Psi_i|\Psi'_\alpha\rangle|^2\right]^{-\frac{1}{2}} \tag{3-5}$$

The second term in equation (3-5) is a normalization factor. $|\Psi'_1\rangle$, $|\Psi'_2\rangle$, and $|\Psi'_3\rangle$ are presented to illustrate the sense of the procedure in equations (3-6), next page. The higher transformed functions $|\Psi'_4\rangle$, $|\Psi'_5\rangle$, etc. can be written in terms of the original basis functions $|\Psi_i\rangle$ rather than the lower transformed functions by substituting in the expansions for the lower transformed functions. For example, it can be shown that $|\Psi'_3\rangle$

$$|\Psi_1'\rangle = |\Psi_1\rangle$$

$$|\Psi_2'\rangle = \frac{|\Psi_2\rangle - |\Psi_1\rangle\langle\Psi_1|\Psi_2\rangle}{\sqrt{1-|\langle\Psi_1|\Psi_2\rangle|^2}} = \frac{|\Psi_2\rangle - |\Psi_1\rangle S_{12}}{\sqrt{1-S_{12}^2}}$$

$$|\Psi_3'\rangle = \frac{|\Psi_3\rangle - |\Psi_1\rangle\langle\Psi_1|\Psi_3\rangle - |\Psi_2'\rangle\langle\Psi_2'|\Psi_3\rangle}{\sqrt{1-|\langle\Psi_3|\Psi_1\rangle|^2 - |\langle\Psi_3|\Psi_2'\rangle|^2}} \qquad (3\text{-}6)$$

is given by equation (3-7). A transformation matrix is then defined by placing the coefficients leading the original basis functions in columns. A schematic of the basis

$$|\Psi_3'\rangle = \left[|\Psi_3\rangle - \frac{S_{13} - S_{12}S_{23}}{1-S_{12}^2}|\Psi_1\rangle - \frac{S_{23} - S_{12}S_{13}}{1-S_{12}^2}|\Psi_2\rangle\right]$$

$$\times\left[1 - \frac{(S_{23} - S_{12}S_{13})^2}{1-S_{12}^2} - S_{13}^2\right]^{-\frac{1}{2}} \qquad (3\text{-}7)$$

set transformation procedure is shown in figure 3-1, where the coefficients from equations (3-6) and (3-7) are replaced with a more compact notation. The procedure can be generalized to any number of basis functions by establishing a recursion relation giving expansions analogous to equation (3-7) for higher transformed basis functions.

The following development demonstrates that the Schmidt-orthogonalized function $|\Psi_k'\rangle$ is orthogonal to all lower functions $|\Psi_{k-1}'\rangle$, $|\Psi_{k-2}'\rangle$, etc. as long as the lower functions form an orthonormal set. The proof is thus inductive, as it can be seen by inspection of equations (3-6) that $|\Psi_2'\rangle$ and $|\Psi_1'\rangle = |\Psi_1\rangle$ are orthogonal. It proves convenient to denote basis functions in the transformed (orthogonal) basis by $|k\rangle$, basis functions in the original (normal but nonorthogonal) basis by $|\Psi_k\rangle$, and normalization

$$\left[|\Psi_1'\rangle \quad |\Psi_2'\rangle \quad |\Psi_3'\rangle\right] = \left[|\Psi_1\rangle \quad |\Psi_2\rangle \quad |\Psi_3\rangle\right] \cdot \begin{bmatrix} 1 & -\frac{S_{12}}{\sqrt{1-S_{12}^2}} & C_1C_N \\ 0 & \frac{1}{\sqrt{1-S_{12}^2}} & C_2C_N \\ 0 & 0 & C_N \end{bmatrix}$$

$$C_N = \left[1 - \frac{(S_{23} - S_{12}S_{13})^2}{1 - S_{12}^2} - S_{13}^2\right]^{-\frac{1}{2}}$$

$$C_2 = -\frac{S_{23} - S_{12}S_{13}}{1 - S_{12}^2}$$

$$C_1 = -\frac{S_{13} - S_{12}S_{23}}{1 - S_{12}^2}$$

Figure 3-1: Schmidt orthogonalization for three overlapping basis functions. C_N is a normalization constant.

constants as N_k. Hence equation (3-5) becomes

$$|k\rangle = N_k\left(1 - \sum_{\alpha=1}^{k-1} |\alpha\rangle\langle\alpha|\right)|\Psi_k\rangle$$

$$N_k = \left(1 - \sum_{\alpha=1}^{k-1} |\langle\Psi_k|\alpha\rangle|^2\right)^{-\frac{1}{2}} \qquad (3\text{-}8)$$

It is important to recall as well that $\langle\Psi_i|\Psi_i\rangle = 1$ and $\langle\Psi_i|\Psi_k\rangle = \langle\Psi_k|\Psi_i\rangle = S_{ik}$.

Since in general for projection operators $P^\dagger = P$, the overlap of two of the transformed functions is given by

$$\langle k|i\rangle = N_k N_i \langle \Psi_k \left| \left(1 - \sum_{\alpha=1}^{k-1} |\alpha\rangle\langle\alpha| \right)\left(1 - \sum_{\beta=1}^{i-1} |\beta\rangle\langle\beta| \right) \right| \Psi_i \rangle \tag{3-9}$$

where it is assumed that *k* is greater than or equal to i. Then equation (3-9) becomes

$$\frac{\langle k|i\rangle}{N_k N_i} = \langle \Psi_k | \Psi_i \rangle - \sum_{\beta=1}^{i-1} \langle \Psi_k | \beta\rangle\langle\beta | \Psi_i \rangle - \sum_{\alpha=1}^{k-1} \langle \Psi_k | \alpha\rangle\langle\alpha | \Psi_i \rangle$$

$$+ \sum_{\alpha=1}^{k-1} \sum_{\beta=1}^{i-1} \langle \Psi_k | \alpha\rangle\langle\alpha | \beta\rangle\langle\beta | \Psi_i \rangle \tag{3-10}$$

Now the transformed functions $|k-1\rangle$, $|k-2\rangle$, …, $|1\rangle$ form an orthonormal set, so $\langle\alpha|\beta\rangle = \delta_{\alpha\beta}$, and the fourth term on the right side of equation (3-10) becomes equal to the second term in magnitude but opposite in sign, and they cancel, leaving

$$\frac{\langle k|i\rangle}{N_k N_i} = \langle \Psi_k | \Psi_i \rangle - \sum_{\alpha=1}^{k-1} \langle \Psi_k | \alpha\rangle\langle\alpha | \Psi_i \rangle \tag{3-11}$$

It is clear from equation (3-11) that if i = k, $\langle k|i\rangle = \langle k|k\rangle = 1$, as

$$\langle k|k\rangle = N_k N_k \left(1 - \sum_{\alpha=1}^{k-1} \langle \Psi_k | \alpha\rangle\langle\alpha | \Psi_k \rangle \right) \tag{3-12}$$

but the term in parentheses on the right side of equation (3-12) is equal to N_k^{-2} according to equation (3-8), leaving $\langle k|k\rangle = 1$.

An identity necessary for proving that off-diagonal overlap matrix elements are zero involves the matrix element $\langle i|\Psi_i\rangle$. Using the adjoint of equation (3-8) for $\langle i|$, $\langle i|\Psi_i\rangle$ is given by

$$\langle i|\Psi_i\rangle = N_i\left(1-\sum_{\alpha=1}^{i-1}\langle\Psi_i|\alpha\rangle\langle\alpha|\Psi_i\rangle\right) \tag{3-13}$$

The term in parentheses on the right side of equation (3-13) is, again, N_i^{-2}, which gives

$$\langle i|\Psi_i\rangle = N_i^{-1} \tag{3-14}$$

Returning to equation (3-11) and bearing in mind that k is greater than i, one proceeds by removing the term for $\alpha = i$ from the summation on the right side of equation (3-11). This gives

$$\frac{\langle k|i\rangle}{N_k N_i} = \langle\Psi_k|\Psi_i\rangle - \langle\Psi_k|i\rangle\langle i|\Psi_i\rangle - \sum_{\alpha=1}^{i-1}\langle\Psi_k|\alpha\rangle\langle\alpha|\Psi_i\rangle - \sum_{\alpha=i+1}^{k-1}\langle\Psi_k|\alpha\rangle\langle\alpha|\Psi_i\rangle \tag{3-15}$$

Concentrating on the second term on the right side of equation (3-15), substitution of equation (3-8) for $|i\rangle$ gives

$$-\langle\Psi_k|i\rangle\langle i|\Psi_i\rangle = -N_i\left(\langle\Psi_k|\Psi_i\rangle - \sum_{\alpha=1}^{i-1}\langle\Psi_k|\alpha\rangle\langle\alpha|\Psi_i\rangle\right)\langle i|\Psi_i\rangle \tag{3-16}$$

Use of equation (3-14) for $\langle i|\Psi_i\rangle$ in equation (3-16), and substitution of the result into equation (3-15) yields

$$\frac{\langle k|i\rangle}{N_k N_i} = \langle\Psi_k|\Psi_i\rangle - \langle\Psi_k|\Psi_i\rangle + \sum_{\alpha=1}^{i-1}\langle\Psi_k|\alpha\rangle\langle\alpha|\Psi_i\rangle$$

$$- \sum_{\alpha=1}^{i-1}\langle\Psi_k|\alpha\rangle\langle\alpha|\Psi_i\rangle - \sum_{\alpha=i+1}^{k-1}\langle\Psi_k|\alpha\rangle\langle\alpha|\Psi_i\rangle \tag{3-17}$$

Canceling terms with opposite sign leaves

$$\frac{\langle k|i\rangle}{N_k N_i} = -\sum_{\alpha=i+1}^{k-1}\langle\Psi_k|\alpha\rangle\langle\alpha|\Psi_i\rangle \tag{3-18}$$

To complete the proof, equation (3-8) is rearranged to give

$$|\Psi_i\rangle = \frac{|i\rangle}{N_i} + \sum_{\beta=1}^{i-1} |\beta\rangle\langle\beta|\Psi_i\rangle \tag{3-19}$$

This equation is substituted into equation (3-18) to give

$$\frac{\langle k|i\rangle}{N_k N_i} = -\sum_{\beta=i+1}^{k-1} \langle\Psi_k|\beta\rangle\langle\beta|i\rangle N_i^{-1} - \sum_{\alpha=i+1}^{k-1}\sum_{\beta=1}^{i-1} \langle\Psi_k|\alpha\rangle\langle\alpha|\beta\rangle\langle\beta|\Psi_i\rangle \tag{3-20}$$

The first term on the right side of equation (3-20) zero since $i < \beta < k$ and the set of transformed functions $|k-1\rangle$, $|k-2\rangle$, …, $|1\rangle$ form an orthonormal set according to the initial conditions of the proof. The second term is also zero since α is always greater than β according to the summation indices. The right side of equation (3-20) is hence equal to zero, leading immediately to $\langle k|i\rangle = 0$ for $i \neq k$. It was previously shown that $\langle k|k\rangle = 1$, so it has been demonstrated that $\langle k|i\rangle = \delta_{ki}$ for $i < k$. Since no conditions were placed on the value of k, it can be inferred that the entire basis of Schmidt-transformed functions forms an orthonormal set.

Much of the code needed to utilize Schmidt rather than symmetric orthogonalization of the Rumer-diagram CSF basis existed in the ZINDO program previously, but was not functional. Implementation was thus largely a matter of correcting the algebra, rather extensive debugging, and testing by comparison of eigenvectors and eigenvalues generated by CI calculations using the two orthogonalization procedures. Table 3-1 lists execute times for calculations of a range of sizes using the previous symmetric orthogonalization and the recently-implemented Schmidt procedure. All calculations were run on a Sun Enterprise 5000 server. The improvement is dramatic, particularly for the larger CI basis sets. To put the result of table 3-1 for the largest calculation in perspective, the calculation took almost seven and

---

Table 3-1. Execute times for CI calculations of various size using Schmidt orthogonalization and Löwdin (symmetric) orthogonalization.

Number of CSFs	**CPU time (seconds), Schmidt orthogonalization**	**CPU time (seconds), Löwdin orthogonalization**	**Ratio**
420	10	23	0.43
1176	353	1331	0.27
1512	828	3391	0.24
2467	4195	16559	0.25
7189	152996	651683	0.23

a half days to run to completion using symmetric orthogonalization of the CI basis, and less than two days using the Schmidt procedure.

Optimization of Spin-Orbit Output Format

Previous versions of ZINDO wrote the entire spin-orbit eigenvector array matrix as output. This procedure is inefficient since the spin-orbit matrix quickly becomes very large as the number of CSFs increases, and the vast majority of elements of the eigenvector array are zero or vanishingly small. The primary shortcoming is in interpretability of results, as it is tedious to search through very lengthy column vectors to locate a few nonzero values. It is interesting to note that the program had incorporated an effective strategy for reducing the output for CI calculations to avoid writing the CI eigenvector array, yet no similar provision had been made for the much larger spin-orbit eigenvector array. The spin-orbit output was troublesome for the generally very small calculations that had been performed prior to the work of this dissertation, but output for the much larger calculations discussed in chapter four was intractable. A more efficient output format was developed to counter this problem.

The original format displayed eigenvectors in groups of five, meaning that five eigenvectors were listed side by side. This feature was retained, as it allows ample room for the real and imaginary parts of the coefficients weighting each basis function to be displayed. Optimization was achieved by retaining only those lines where at least one of the ten coefficients (real and imaginary parts of coefficients for each of five eigenvectors) is larger than a predetermined threshold. A default value of 0.10 was written into the code, but the user has the option of specifying an arbitrary limit. Some coefficients with value zero are still written using this procedure, but output files for large spin-orbit basis sets are considerably smaller, and display largely the interesting coefficients (i.e., those that are nonzero). A final change was a listing of percentage contributions of each spin multiplicity to the spin-orbit eigenvector at the bottom of the list of coefficients. The method used to compute these values is described in the next section.

Determination of Spin Character of Spin-Orbit Eigenvectors

Spin contamination of the energy levels of a state of a certain spin multiplicity by spin-orbit interaction with states of different multiplicity can be important in electronic spectroscopy since it allows relaxation of the usually strict spin selection rule. This phenomenon was suggested as justification for assignment of low-energy transitions in the resonance Raman spectra of V_2 and Nb_2 as $a^1\Sigma_g^+ \leftarrow X^3\Sigma_g^-$ transitions [189,190], as discussed in more detail later. A theoretical examination of assignments such as these should rest not only on computed transition intensities, but also on direct prediction of the extent of the spin contamination. The SOCI method is well-suited for this task, as each spin-orbit level is represented by a linear expansion over components of CSFs of all included spin multiplicities. Taking the above example, triplet contamination of the $^1\Sigma_g^+$ state is revealed by the presence of nonzero coefficients weighting triplet CSFs in the spin-orbit enhanced eigenvector for the $^1\Sigma_g^+$ state. The identity of these triplet CSFs indicates which triplet state (or states) is responsible for the contamination.

For the purpose of calculating the extent of mixing of states of different spin multiplicity in each spin-orbit eigenvector, the obvious approach is to examine the sum of squares of the coefficients weighting components of the CSFs of each multiplicity. Care must be taken, however, since the basis of CSFs is not orthogonal. Consider the spin-orbit enhanced eigenvector for a particular level. The wavefunction of the level is given by the matrix product of a $1 \times n$ row containing the basis functions (in this case the components of each CSF) and a $n \times 1$ column containing the expansion coefficients. The result, a scalar quantity, is the linear expansion over basis functions, as shown in equation (3-21),

$$\Phi_K = \left[|\Psi_1\rangle \quad |\Psi_2\rangle \quad \cdots \quad |\Psi_n\rangle \right] \cdot \begin{bmatrix} C_{1K} \\ C_{2K} \\ \vdots \\ C_{nK} \end{bmatrix} = |\Psi_1\rangle C_{1K} + |\Psi_2\rangle C_{2K} + \cdots + |\Psi_n\rangle C_{nK} \quad (3\text{-}21)$$

where the expansion coefficients are in general complex. Since each spin-orbit level is normalized, the matrix product of $\Phi_K^\dagger$ and Φ_K is equal to one, $\Phi_K^\dagger \Phi_K = 1$. Using equation (3-21) and its adjoint, and labeling matrix products $\langle \Psi_i | \Psi_j \rangle$ in the nonorthogonal basis as S_{ij}, the normalization condition is given by

$$1 = \sum_{i=1}^{n} |C_{iK}|^2 + \sum_{i=1}^{n} \sum_{j \neq i} C_{Ki}^{*} C_{jK} S_{ij} \tag{3-22}$$

Simply taking the modulus squared of each coefficient and summing will therefore not yield a value of one, and the sum of squares of coefficients weighting components of one spin multiplicity will not represent a direct percentage contribution of that multiplicity.

To obtain contributions that do sum to one, the overlap could potentially be included, but this would require considerable computational effort, as each overlap matrix element would have to be accessed in forming the sum of equation (3-22). Fortunately, this is not necessary since only CSFs of the same spin multiplicity are nonorthogonal, as discussed above. Contributions of each spin multiplicity to a particular spin-orbit level can thus be obtained in the basis of Schmidt-orthogonalized Rumer functions, since the Schmidt transformation does not mix states of different multiplicities. By utilizing the orthogonalized basis the summation involving overlap in equation (3-22) is zero, and the percent contribution of each spin multiplicity to an energy level is given by the sum of modulus squared of each coefficient weighting CSFs of that multiplicity. The program was altered to carry out the appropriate summations, and the result is written in the output for each spin-orbit level. This capability will be used later to determine the spin contamination of several excited states of V_2, VNb, and Nb_2.

CHAPTER 4
THE ELECTRONIC STRUCTURE AND SPECTROSCOPY OF DIVINADIUM

Summary and Purpose

There were several motivations for the calculations on divanadium discussed in this chapter. An important initial consideration is to obtain self-consistent field convergence, which is not straightforward for transition metal diatomics. The near-degeneracy of several low-lying electron configurations typically leads to oscillations between them in the course of the SCF iterations, preventing convergence to a stable ground state. The configuration averaged Hartree-Fock method discussed in chapter two overcomes the convergence difficulties encountered for V_2. Once a well-defined set of SCF orbitals has been established, one of the primary questions posed by this dissertation can be addressed: can the INDO/S model accurately describe both the ground and excited states of a metal dimer at an appropriate level of electron correlation? The approach that is found to be successful is roughly analogous to the CASSCF method, using full CI in an active space designed to capture the important essential correlation effects, but without optimization of the orbital themselves for each state. The results obtained for transition energies, oscillator strengths, spin-orbit splittings, and state symmetries for all experimentally-known states of V_2 are in good agreement with experiment, lending confidence to additional predictions and interpretations. Two previously observed but unassigned transitions have been assigned, evidence favoring one side of a dispute involving another state assignment is provided, and questions regarding orbital populations in the excited states are investigated. A full account is given in this chapter.

The text is organized as follows: the existing experimental and theoretical knowledge of the ground and excited states of divanadium is summarized, then specifics of the calculations performed as part of this work are given. Results and discussion are then provided, covering both the SCF and correlated calculations. The chapter ends with a summary of the conclusions reached.

Background and Motivation

The electronic structure and spectroscopy of divanadium is the subject of this chapter. The choice of V_2 as the initial test case has several motivations. First, as a dimer of the early 3d transition series, ground and excited state wavefunctions can be expected to have significant electron correlation effects, and one goal of this work is to investigate the role of correlation in the INDO/S model. At the same time, V_2 is expected to be easier to treat than the notorious Cr_2 owing to the open-shell ground state and longer bond distance [35,72], as discussed in the first chapter. Secondly, the INDO/S model is known to be more successful for 3d rather than 4d metals [93] because the Slater-Condon factors are empirical for the former but calculated and scaled for the latter, as discussed in chapter two. Third, there are interesting spin-orbit effects that have been extensively characterized for the ground and excited states of V_2 (this is not the case with Cr_2), allowing full advantage to be taken of the INDO/S spin-orbit implementation. Finally, there is spectroscopic information available on the ground state and several excited states of V_2 that is much more detailed and in greater abundance than the data on states of VNb and Nb_2. The previous experimental and theoretical investigations of V_2 are described in the following discussion.

Diatomic vanadium was first studied in the gas phase by Langridge-Smith, Morse, Hansen, Smalley, and Merer [49] using resonant two photon ionization spectroscopy of dimers generated by laser vaporization of vanadium metal and cooled by expansion in a molecular beam. They assigned the ground state of V_2 as $X^3\Sigma_g^-$ by analysis of a strong band system observed near 14300 cm^{-1}. The short bond length of 1.77 Å that was found for the ground state was taken to indicate extensive participation of the 3*d* orbitals in the bonding. Based on that and the large second-order spin-orbit splitting of the ground state (75 cm^{-1}), typical of a half-filled π or δ shell, the electron configuration $(d\pi_u)^4(d\sigma_g)^2(s\sigma_g)^2(d\delta_g)^2$ was assumed for the ground state, a prediction that has been supported by CASSCF [35] and density functional calculations [107,191-193].

Spain, Behm, and Morse [189] proposed that the spin-orbit splitting of the $X^3\Sigma_g^-$ ground state of V_2 is caused by interaction with the isoconfigurational $^1\Sigma_g^+$ state due to the nonzero matrix element of the spin-orbit operator between the $M_S = 0$ components of the two states. This is easily demonstrated with the Rumer diagram technique developed in chapter two, using conjoined diagrams and equations (2-120) though (2-126). Only the open shell electrons in the δ_g molecular orbitals need to be considered, since the closed shell electrons do not contribute to spin-orbit effects. This can be seen in a more formal way by considering the conjoined diagram for any two configurations that differ only in the spin and spatial distribution of electrons in the δ_g orbitals. In any such diagram the closed shell electrons will all form closed loops, which do not contribute to the summations in equations (2-120) through (2-126). Following the procedure outlined in chapter two, the $X^3\Sigma_g^-$ state is represented by $\left|\delta_g^+\alpha\delta_g^-\alpha\right\rangle$ and the $^1\Sigma_g^+$ state by $2^{-1/2}\left(\left|\delta_g^+\alpha\delta_g^-\beta\right\rangle - \left|\delta_g^+\beta\delta_g^-\alpha\right\rangle\right)$, where $\left|\delta_g^+\right\rangle$ and $\left|\delta_g^-\right\rangle$ are δ-symmetry molecular orbitals involving the 3d orbitals with $m_l = +2$ and $m_l = -2$, respectively:

$$\left|\delta_g^+\right\rangle = \frac{1}{\sqrt{2}\sqrt{1+S}}\left(\left|2+2\right\rangle^A + \left|2+2\right\rangle^B\right) \tag{4-1}$$

$$\left|\delta_g^-\right\rangle = \frac{1}{\sqrt{2}\sqrt{1+S}}\left(\left|2-2\right\rangle^A + \left|2-2\right\rangle^B\right) \tag{4-2}$$

where S is in this case the delta-symmetry overlap integral and the atomic orbitals are denoted by their angular momentum quantum number *l*, corresponding z-component m_l, and nuclear label γ according to $\left|l\ m_l\right\rangle^\gamma$.

The conjoined diagram for first-order spin-orbit interaction in the ground state is

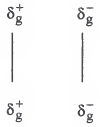

(4-3)

(compare to the diagram shown in figure 2-3). Interactions between the various components of the ground state are evaluated by applying equations (2-120) through (2-123) to diagram (4-3). Taking interaction of the $M_S = 1$ component with itself as an example, equation (2-120) is used. The result is

$$\left\langle\delta_g^+\alpha\delta_g^-\alpha\right|\hat{H}^{SO}\left|\delta_g^+\alpha\delta_g^-\alpha\right\rangle = \tfrac{1}{2}\left(\left\langle\delta_g^+\right|\xi(r)\hat{l}_z\left|\delta_g^+\right\rangle + \left\langle\delta_g^-\right|\xi(r)\hat{l}_z\left|\delta_g^-\right\rangle\right) \tag{4-4}$$

which is equal to zero because the $\hat{l}_z\left|\delta_g^+\right\rangle = 2\left|\delta_g^+\right\rangle$ and $\hat{l}_z\left|\delta_g^-\right\rangle = -2\left|\delta_g^-\right\rangle$ (refer to equations (4-1) and (4-2)), and $\left\langle\delta_g^+\middle|\xi(r)\middle|\delta_g^+\right\rangle$ is equal to $\left\langle\delta_g^-\middle|\xi(r)\middle|\delta_g^-\right\rangle$ since the radial portion is identical for all involved orbitals. It can be shown in a similar fashion that there are no nonzero interactions between any of the components of the $X^3\Sigma_g^-$ state.

The coupling between the two $M_S = 0$ components $X^3\Sigma_g^-(0)$ and ${}^1\Sigma_g^+(0)$ is found with the conjoined diagram

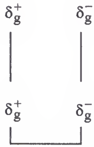

(4-5)

and equation (2-124), which gives

$$\left\langle {}^1\Sigma_g^+ \middle| \hat{H}^{SO} \middle| X^3\Sigma_g^-(0) \right\rangle = \langle 00|\xi(r)\hat{l}_z\hat{s}_z|10\rangle = \frac{1}{2}\left(\left\langle \delta_g^+ \middle|\xi(r)\hat{l}_z\middle|\delta_g^+\right\rangle - \left\langle \delta_g^- \middle|\xi(r)\hat{l}_z\middle|\delta_g^-\right\rangle\right) \tag{4-6}$$

when the various factors in equation (2-124), particularly the parity index r_i^{KL}, are accounted for. This yields

$$\left\langle {}^1\Sigma_g^+ \middle| \hat{H}^{SO} \middle| X^3\Sigma_g^-(0) \right\rangle = \left\langle \delta_g^+ \middle|\xi(r)\middle|\delta_g^+\right\rangle + \left\langle \delta_g^- \middle|\xi(r)\middle|\delta_g^-\right\rangle \tag{4-7}$$

when the $\hat{l}_z$ operator is applied. A final expression for the coupling is obtained by substituting the molecular orbital expansions (4-1) and (4-2) for $\left|\delta_g^+\right\rangle$ and $\left|\delta_g^-\right\rangle$.

Spain et al. [189] and James, Kowalczyk, Langlois, Campbell, Ogawa, and Simard [190] have separately used the approximation that the δ-symmetry overlap can be neglected, in which case the overlap integrals are zero in equations (4-1) and (4-2). The approximation of zero overlap can be justified by the small magnitude of the overlap, and is assumed here to make connection with the previous work of Spain et al. [189] and James et al. [190] The effect of this approximation is explored in chapter five. Substitution of equations (4-1) and (4-2) into equation (4-7) yields

$$\left\langle {}^1\Sigma_g^+ \middle| \hat{H}^{SO} \middle| X^3\Sigma_g^-(0) \right\rangle = 2\zeta_{3d} \qquad (4\text{-}8)$$

under the approximation discussed in chapter two that two-center radial integrals are neglected. ζ_{3d} is the spin-orbit coupling constant of equation (2-117) for the 3d orbitals of vanadium.

The coupling of equation (4-8) is significant because $\zeta_{(n-1)d}$ is on the order of 150 cm^{-1} for vanadium and 500 cm^{-1} for niobium [181]. Since only the $M_S = 0$ component of the $X^3\Sigma_g^-$ state is affected by interaction with the ${}^1\Sigma_g^+$ state, it is depressed below the energy of the $M_S = \pm 1$ components, leading to the observed splitting. Under the assumption that the ground state interacts exclusively with the ${}^1\Sigma_g^+$ state, the latter is increased in energy by the same amount that the $X^3\Sigma_g^-(0)$ component is decreased. This situation is depicted in figure 4-1. Since the splitting of the ground state has been determined experimentally to be 75 cm^{-1} [49] and values for ζ_d are known [181], the energy of the upper state can be estimated. Two approaches to doing so have been presented.

The first is second-order perturbation theory. In this approach the Hamiltonian including spin-orbit coupling is written as

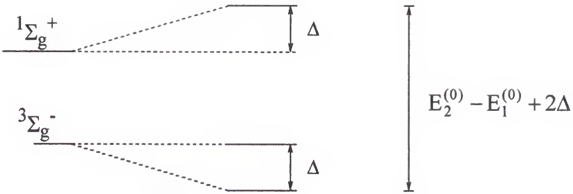

Figure 4-1. Schematic energy level diagram showing perturbation of the $X^3\Sigma_g^-$ ground state of V₂ by spin-orbit interaction with the isoconfigurational $^1\Sigma_g^+$ state.

$$\hat{H} = \hat{H}^{(0)} + \hat{H}^{SO} \tag{4-10}$$

with $\hat{H}^{(0)}$ the time-independent Born-Oppenheimer nonrelativistic Hamiltonian operator, which is assumed to have a complete set of unperturbed orthonormal eigenfunctions according to

$$\hat{H}^{(0)}\left|\psi_i^{(0)}\right\rangle = E_i^{(0)}\left|\psi_i^{(0)}\right\rangle \qquad i = 1,2,\ldots \tag{4-11}$$

The energies and wavefunctions of the perturbed Hamiltonian $\hat{H} = \hat{H}^{(0)} + \hat{H}^{SO}$ are decomposed into zeroth, first, second, etc. orders of correction,

$$\left|\psi_i\right\rangle = \left|\psi_i^{(0)}\right\rangle + \left|\psi_i^{(1)}\right\rangle + \left|\psi_i^{(2)}\right\rangle + \cdots \tag{4-11}$$

$$E_i = E_i^{(0)} + E_i^{(1)} + E_i^{(2)} + \cdots \tag{4-12}$$

which gives the perturbed Schrödinger equation as

$$\left(\hat{H}^{(0)}+\hat{H}^{SO}\right)\left(\left|\psi_1^{(0)}\right\rangle+\left|\psi_1^{(1)}\right\rangle+\left|\psi_1^{(2)}\right\rangle+\cdots\right)=$$

$$\left(E_1^{(0)}+E_1^{(1)}+E_1^{(2)}+\cdots\right)\left(\left|\psi_1^{(0)}\right\rangle+\left|\psi_1^{(1)}\right\rangle+\left|\psi_1^{(2)}\right\rangle+\cdots\right) \qquad (4\text{-}13)$$

where attention is now focused on the ground state. The normalization of the wavefunction $|\psi_1\rangle$ is conveniently chosen so that $\left\langle\psi_1^{(0)}\middle|\psi_1\right\rangle=1$, which implies

$$\left\langle\psi_1^{(0)}\middle|\psi_1^{(i)}\right\rangle=0,\ \ i>0 \qquad (4\text{-}14)$$

Equation (4-13) is now expressed as

$$\hat{H}^{(0)}\left|\psi_1^{(0)}\right\rangle+\hat{H}^{(0)}\left|\psi_1^{(1)}\right\rangle+\hat{H}^{SO}\left|\psi_1^{(0)}\right\rangle+\hat{H}^{(0)}\left|\psi_1^{(2)}\right\rangle+\hat{H}^{SO}\left|\psi_1^{(1)}\right\rangle+\cdots$$

$$=E_1^{(0)}\left|\psi_1^{(0)}\right\rangle+E_1^{(0)}\left|\psi_1^{(1)}\right\rangle+E_1^{(1)}\left|\psi_1^{(0)}\right\rangle+E_1^{(0)}\left|\psi_1^{(2)}\right\rangle+E_1^{(1)}\left|\psi_1^{(1)}\right\rangle+E_1^{(2)}\left|\psi_1^{(0)}\right\rangle+\cdots \qquad (4\text{-}15)$$

Various orders of correction can now be chosen by considering together terms on both sides of equation (4-15) with the same sum of orders, realizing that the spin-orbit Hamiltonian is a first-order correction. Thus at zeroth order the unperturbed problem is recovered,

$$\hat{H}^{(0)}\left|\psi_1^{(0)}\right\rangle=E_1^{(0)}\left|\psi_1^{(0)}\right\rangle \qquad (4\text{-}16)$$

At first order, the appropriate equation is

$$\hat{H}^{(0)}\left|\psi_1^{(1)}\right\rangle+\hat{H}^{SO}\left|\psi_1^{(0)}\right\rangle=E_1^{(0)}\left|\psi_1^{(1)}\right\rangle+E_1^{(1)}\left|\psi_1^{(0)}\right\rangle \qquad (4\text{-}17)$$

Left multiplication of equation (4-17) by $\left\langle\psi_1^{(0)}\right|$ and accounting for equations (4-10) and (4-14) and the orthonormality of the unperturbed wavefunctions yields

$$\left\langle \psi_1^{(0)} \middle| \hat{H}^{SO} \middle| \psi_1^{(0)} \right\rangle = E_1^{(1)} \tag{4-18}$$

The first-order correction to the energy due to spin-orbit coupling is thus zero for the components of the $X^3\Sigma_g^-$ state, since as discussed above the matrix elements of $\hat{H}^{SO}$ between the components of this state are all zero.

Applying the same procedure just used at first order at second order starting with equation (4-15) yields the second order energy correction as

$$\left\langle \psi_1^{(0)} \middle| \hat{H}^{SO} \middle| \psi_1^{(1)} \right\rangle = E_1^{(2)} \tag{4-19}$$

An expression involving $\left| \psi_1^{(1)} \right\rangle$ is therefore needed in order to obtain a convenient expression for $E_1^{(2)}$, and is found by rearranging equation (4-17) to give

$$\left(E_1^{(0)} - \hat{H}^{(0)} \right) \left| \psi_1^{(1)} \right\rangle = \left(\hat{H}^{SO} - \left\langle \psi_1^{(0)} \middle| \hat{H}^{SO} \middle| \psi_1^{(0)} \right\rangle \right) \left| \psi_1^{(0)} \right\rangle \tag{4-20}$$

where equation (4-18) has been used for $E_1^{(1)}$. Requiring that the projection of $\left| \psi_1^{(1)} \right\rangle$ onto the space of the unperturbed wavefunctions $\{ \left| \psi_i^{(0)} \right\rangle \}$ be zero gives

$$\left(1 - \sum_i \left| \psi_i^{(0)} \right\rangle \left\langle \psi_i^{(0)} \right| \right) \left| \psi_1^{(1)} \right\rangle = 0 \tag{4-21}$$

or

$$\left| \psi_1^{(1)} \right\rangle = \sum_{i \neq 1} \left| \psi_i^{(0)} \right\rangle \left\langle \psi_i^{(0)} \middle| \psi_1^{(1)} \right\rangle \tag{4-22}$$

Here it is convenient to limit the summation to not include the ground state unperturbed wavefunction $\left| \psi_1^{(0)} \right\rangle$, which is valid since $\left\langle \psi_1^{(0)} \middle| \psi_1^{(1)} \right\rangle = 0$ (equation (4-14)).

Substitution of equation (4-22) into equation (4-20) yields

$$\sum_{i\neq 1}\left(E_1^{(0)}-\hat{H}^{(0)}\right)\left|\psi_i^{(0)}\right\rangle\left\langle\psi_i^{(0)}\middle|\psi_1^{(1)}\right\rangle=\left(\hat{H}^{SO}-\left\langle\psi_1^{(0)}\middle|\hat{H}^{SO}\middle|\psi_1^{(0)}\right\rangle\right)\left|\psi_1^{(0)}\right\rangle \quad (4\text{-}23)$$

Left-multiplication of this equation by $\left\langle\psi_j^{(0)}\right|$ (with $j \neq 1$) and observing the orthonormality of the unperturbed basis functions gives

$$\left(E_1^{(0)}-E_j^{(0)}\right)\left\langle\psi_j^{(0)}\middle|\psi_1^{(1)}\right\rangle=\left\langle\psi_j^{(0)}\middle|\hat{H}^{SO}\middle|\psi_1^{(0)}\right\rangle \quad (4\text{-}24)$$

or

$$\left\langle\psi_j^{(0)}\middle|\psi_1^{(1)}\right\rangle=\frac{\left\langle\psi_j^{(0)}\middle|\hat{H}^{SO}\middle|\psi_1^{(0)}\right\rangle}{E_1^{(0)}-E_j^{(0)}} \quad (4\text{-}25)$$

With this equality the expression for the second order energy correction can be obtained in terms of the unperturbed basis functions.

Substitution of equation (4-22) into equation (4-19) gives

$$E_1^{(2)}=\sum_{j\neq 1}\left\langle\psi_1^{(0)}\middle|\hat{H}^{SO}\middle|\psi_j^{(0)}\right\rangle\left\langle\psi_j^{(0)}\middle|\psi_1^{(1)}\right\rangle \quad (4\text{-}26)$$

and substitution of equation (4-25) yields

$$E_1^{(2)}=\sum_{j\neq 1}\frac{\left\langle\psi_1^{(0)}\middle|\hat{H}^{SO}\middle|\psi_j^{(0)}\right\rangle\left\langle\psi_j^{(0)}\middle|\hat{H}^{SO}\middle|\psi_1^{(0)}\right\rangle}{E_1^{(0)}-E_j^{(0)}} \quad (4\text{-}27)$$

In the specific case of the $X^3\Sigma_g^-$ and $^1\Sigma_g^+$ states of V_2, if it is again assumed that the former interacts only with the latter, the $X^3\Sigma_g^-$ state is defined as ψ_1 and the $^1\Sigma_g^+$ state as ψ_2. The summation in equation (4-27) is limited to one term ($j = 2$). The change in energy of the $M_S = 0$ component of the $X^3\Sigma_g^-$ state, $E_1^{(2)}$, is then given by

$$\Delta' = \frac{\left|\left\langle {}^1\Sigma_g^+ \middle| \hat{H}^{SO} \middle| X^3\Sigma_g^-(0) \right\rangle\right|^2}{E^{(0)}\left(X^3\Sigma_g^-\right) - E^{(0)}\left({}^1\Sigma_g^+\right)} \tag{4-28}$$

Realizing that Δ' is negative, this can be rewritten as

$$\Delta = \frac{\left|\left\langle {}^1\Sigma_g^+ \middle| \hat{H}^{SO} \middle| X^3\Sigma_g^-(0) \right\rangle\right|^2}{E^{(0)}\left({}^1\Sigma_g^+\right) - E^{(0)}\left(X^3\Sigma_g^-\right)} \tag{4-29}$$

where all quantities are now positive. As shown in figure 4-1 the energy of the ${}^1\Sigma_g^+$ state is given at second order by

$$\begin{aligned} E({}^1\Sigma_g^+) - E({}^3\Sigma_g^-) &= E^{(0)}\left({}^1\Sigma_g^+\right) + E^{(2)}\left({}^1\Sigma_g^+\right) - \left[E^{(0)}\left(X^3\Sigma_g^-\right) + E^{(2)}\left(X^3\Sigma_g^-\right)\right] \\ &= E^{(0)}\left({}^1\Sigma_g^+\right) - E^{(0)}\left(X^3\Sigma_g^-\right) + 2\Delta \end{aligned} \tag{4-30}$$

when it is recalled that $E^{(2)}\left({}^1\Sigma_g^+\right) = -E^{(2)}\left({}^3\Sigma_g^-\right) = \Delta$ (figure 4-1). At second order, then, equation (4-29) is rearranged and manipulated to yield

$$E({}^1\Sigma_g^+) = \frac{V_{12}^2 + 2\Delta^2}{\Delta} \tag{4-31}$$

where $\left\langle {}^1\Sigma_g^+ \middle| \hat{H}^{SO} \middle| X^3\Sigma_g^-(0) \right\rangle$ has been denoted as V_{12}. Equation (4-31) is convenient for extracting $E({}^1\Sigma_g^+)$ based on the known quantities V_{12} (equation (4-8)) and Δ (measured experimentally as 75 cm^{-1}).

A second more exact approach to obtaining an estimate of $E({}^1\Sigma_g^+)$ within the approximation that the $X^3\Sigma_g^-$ state interacts only with the ${}^1\Sigma_g^+$ state is to construct and diagonlize the $\hat{H}^{(0)} + \hat{H}^{SO}$ matrix in the basis of the $M_S = 0$ components of the two states:

$$\begin{bmatrix} C_{11} & C_{12} \\ C_{21} & C_{22} \end{bmatrix}^{\dagger} \begin{bmatrix} E_1^{(0)} & V_{12} \\ V_{12} & E_2^{(0)} \end{bmatrix} \begin{bmatrix} C_{11} & C_{12} \\ C_{21} & C_{22} \end{bmatrix} = \begin{bmatrix} E_1 & 0 \\ 0 & E_2 \end{bmatrix} \qquad (4\text{-}32)$$

The eigenvalues of the $\hat{H}^{(0)} + \hat{H}^{SO}$ matrix are [80]

$$E_1 = E_1^{(0)} - \Delta = \frac{1}{2}\left(E_1^{(0)} + E_2^{(0)} - \left[\left(E_2^{(0)} - E_1^{(0)} \right)^2 + 4V_{12}^2 \right]^{\frac{1}{2}} \right) \qquad (4\text{-}33)$$

$$E_2 = E_2^{(0)} + \Delta = \frac{1}{2}\left(E_1^{(0)} + E_2^{(0)} + \left[\left(E_2^{(0)} - E_1^{(0)} \right)^2 + 4V_{12}^2 \right]^{\frac{1}{2}} \right) \qquad (4\text{-}34)$$

where Δ, the spin-orbit splitting of the ground state, is taken here to be empirical and is not meant as given at second order in equation (4-29). Subtracting equation (4-33) from equation (4-34) gives

$$E_2^{(0)} - E_1^{(0)} + 2\Delta = \left[\left(E_2^{(0)} - E_1^{(0)} \right)^2 + 4V_{12}^2 \right]^{\frac{1}{2}} \qquad (4\text{-}35)$$

or, squaring both sides,

$$\left(E_2^{(0)} - E_1^{(0)} \right)^2 + 4\Delta^2 + 4\Delta\left(E_2^{(0)} - E_1^{(0)} \right) = \left(E_2^{(0)} - E_1^{(0)} \right)^2 + 4V_{12}^2 \qquad (4\text{-}36)$$

Cancellation and rearrangement then yield

$$\frac{V_{12}^2 - \Delta^2}{\Delta} = E_2^{(0)} - E_1^{(0)} \qquad (4\text{-}37)$$

or

$$E(^1\Sigma_g^+) = E_2^{(0)} - E_1^{(0)} + 2\Delta = \frac{V_{12}^2 + \Delta^2}{\Delta} \qquad (4\text{-}38)$$

This expression is correct through infinite order, since within the confines of the two-level model the matrix treatment is equivalent to full configuration interaction. By comparing equations (4-38) and (4-31) it is seen that the difference between the second order and infinite order estimates of $E(^1\Sigma_g^+)$ is equal to Δ, the spin-orbit splitting of the ground state.

Spain et al. [189] used equation (4-31) with $\Delta = 75$ cm^{-1} and $\zeta_{3d} = 177$ cm^{-1} [181] to obtain an estimate of 1821 cm^{-1} for $E(^1\Sigma_g^+)$. Based on this, a state observed at 1860 cm^{-1} in matrix-isolated resonance Raman work [47] was assigned as the $^1\Sigma_g^+$ state. The implied abrogation of the spin selection rule is possible given the singlet-triplet mixing mediated by $\hat{H}^{SO}$. James et al. [190] later pointed out that the value of 177 cm^{-1} used for ζ_{3d} by Spain et al. is appropriate for the ground state of atomic vanadium [181], with valence electron configuration $3d^3 4s^2$, while the separated atom limit of the dimer is $3d^4 4s^1 + 3d^4 4s^1$ (see table 1-3). A value of 145 cm^{-1} is appropriate for the $3d^4 4s^1$ configuration, and yields an estimate of 1196 cm^{-1} for $E(^1\Sigma_g^+)$ using equation (4-38). James et al. disputed the assignment the state observed at 1860 cm^{-1} as the $^1\Sigma_g^+$ state on the basis of their revised estimate. No further evidence, either experimental or theoretical, has been put forth to resolve this dispute. One purpose of the work reported in this chapter is to provide support for one estimate or the other. Furthermore, if the state observed at 1860 cm^{-1} is not the $^1\Sigma_g^+$ state, it is a heretofore unidentified excited state of divanadium. An additional purpose is therefore to find a likely candidate for the identity of this low-lying excited state.

Extensive information on several excited states of V_2 has been obtained by means of molecular beam spectroscopy. The first to be thoroughly characterized was the upper state of the band system observed near 14300 cm^{-1} by Langridge-Smith et al. [49], assigned as $A\,^3\Pi_u$. Spin-orbit splittings of 35 cm^{-1} and 45 cm^{-1} between the $\Omega = 0$ and $\Omega = 1$ and $\Omega = 1$ and $\Omega = 2$ levels,[1] respectively, were observed, and a bond length of 1.70 Å was ascertained for this state. As part of this work a second, weaker band system near 15000 cm^{-1} that is not a subband of the $A\,^3\Pi_u \leftarrow X\,^3\Sigma_g^-$ transition was also observed. Rotational analysis of this band indicated the transition is a $\Omega' = 1 \leftarrow \Omega'' = 1$ transition and that the lower state is the $\Omega'' = 1$ component of the $X\,^3\Sigma_g^-$ state. The intensity indicated a spin-allowed transition.

One or more vibronic band systems of V_2 were observed by Spain et al. [189] in the range 11250 cm^{-1} to 12500 cm^{-1}. The strongest of these was analyzed and unambiguously identified as $A'\,^3\Sigma_u^- \leftarrow X\,^3\Sigma_g^-$, with $\Omega' = 0$ and $\Omega' = 1$ components of the upper state at 11812 cm^{-1} and 11899 cm^{-1}, respectively. The lifetime of the excited state was measured and found to indicate an oscillator strength on the order of 10^{-2}. The bond distance in the excited state was determined to be $r_0 = 1.756$ Å, slightly shorter than the distance of 1.766 Å found for the ground state. Given the ground-state electron configuration of $(d\pi_u)^4(d\sigma_g)^2(s\sigma_g)^2(d\delta_g)^2$ this transition could in principle be the result of a $d\delta_u \leftarrow d\delta_g$, $\pi_g \leftarrow \pi_u$, or $\sigma_u \leftarrow \sigma_g$ promotion. Based on a comparison to the oscillator strengths of *3d*-*3d* transitions in NiCu and Cu_2 and the $s\sigma_u \leftarrow s\sigma_g$ transitions in Cr_2, CrMo, and Mo_2 the transition observed in V_2 was assumed to involve electrons in *3d* orbitals. Of the three possibilities Spain et al. assigned the transition as $d\delta_u \leftarrow d\delta_g$ based on intuitive molecular orbital concepts (that $d\delta_u \leftarrow d\delta_g$ should be at lower energy than $d\pi_g \leftarrow d\pi_u$ or $d\sigma_u \leftarrow d\sigma_g$), the fact that the bond distance changes only slightly, indicating that the electron is not promoted from a strongly-bonding orbital, and the results of Xα calculations [194].

---

[1] Ω is the spin-orbit quantum number for a diatomic molecule, given as the vector sum of Λ and Σ, which are the quantum numbers for orbital and spin angular momentum, respectively. A detailed discussion is found in reference [181].

The symmetry of the orbitals involved in the $A\,^3\Pi_u \leftarrow X^3\Sigma_g^-$ transition reported by Langridge-Smith *et al.* [49] was also reconsidered by Spain et al. [189] based on the results of the Xα calculations [194], which indicated that the transition could involve the $4p\pi_u$ orbitals. Three possibilities were identified, including $4p\pi_u \leftarrow 4s\sigma_g$, $4p\pi_u \leftarrow d\delta_g$, and $d\delta_g \leftarrow d\pi_u$, but no way was found to distinguish between them.

Very few modern theoretical calculations on the vanadium dimer have been reported. Of those, most use density functional theory (DFT) and are concerned exclusively with predicting ground state properties (bond length and vibrational frequency). The results of the linear combination of Gaussian-type orbitals-density functional calculations of James, Kowalczyk, Fournier, and Simard [107] are summarized here. The calculations accurately determined r_e and D_e, while ω_e was qualitatively predicted. Of interest here are the molecular orbital compositions and ionization potentials. The $d\pi_u$ MOs were found to include a small contribution from the 4p orbitals, and the two σ_g orbitals were found to have extensive 4s-3d hybridization, with the lower-lying MO having a slightly larger contribution from the 3dσ orbitals, while the opposite is true for the higher-lying MO. The order of orbitals assumed in the present discussion, with dπ_u lower in energy than the σ_g orbitals, has been firmly established by several DFT studies [107,191-193].

The DFT calculations of James et al. [107] also indicated that the energy of the sσ_u orbital lies between those of the dδ_g and dδ_u orbitals. The sσ_u orbital is thus apparently largely nonbonding. This is at variance with the conceptual molecular orbital picture of transition metal *d-d* bonding, and at first sight is somewhat surprising. Indeed, approximating promotion energies as the difference in orbital energies indicates that the s$\sigma_u \leftarrow$ sσ_g promotion is of energy comparable to that of the d$\delta_u \leftarrow$ dδ_g promotion, raising the possibility that the $A'^3\Sigma_u^- \leftarrow X^3\Sigma_g^-$ transition observed by Spain *et al.* near 11800 cm^{-1} is in fact due to a $\sigma_u \leftarrow \sigma_g$ promotion (though it should be pointed out that in either case the transition energy predicted in this way is in error by 2000-3000 cm^{-1}).

The possibility that the $A'^3\Sigma_u^- \leftarrow X^3\Sigma_g^-$ transition is in fact due to a $\sigma_u \leftarrow \sigma_g$ promotion is bolstered by experimental and theoretical information that has been obtained for V_2^+. Both experiment [190,195] and density functional calculations [196] indicate that ionization of V_2 to form V_2^+ removes an electron from the higher-lying σ_g orbital, giving a $^4\Sigma_g^-$ ground state for the cation. Yang, James, Rayner, and Hackett [195] were able to determine the ground state bond length of the cation as $r_0 = 1.735$ Å, slightly smaller than the bond distance in the ground state of the neutral. Removal of an electron from the bonding 4sσ_g orbital therefore apparently reduces the bond distance.

Taken together with the nonbonding nature of the sσ_u orbital found in the density functional calculations of James et al. [107], this indicates that the reduction in bond length seen in the $A'^3\Sigma_u^- \leftarrow X^3\Sigma_g^-$ transition of V_2 is not necessarily inconsistent with a $\sigma_u \leftarrow \sigma_g$ promotion. A final point involves experimental information on a $^3\Sigma^- \leftarrow X^3\Sigma^-$ transition in VNb observed by James, Kowalczyk, and Simard [197]. These authors concluded that it was unlikely that the transition was a $\delta^* \leftarrow \delta$ promotion due to the changes in bond length and stretching frequency observed to accompany the electronic transition. While it cannot necessarily be assumed that this transition observed for VNb is analogous to the $A'^3\Sigma_u^- \leftarrow X^3\Sigma_g^-$ transition of V_2, the possibility is enough to raise questions regarding the assignment of the transition observed for V_2 as a d$\delta_u \leftarrow$ dδ_g promotion.

Only early calculations of Walch and Bauschlicher [35,72] using the complete active space self-consistent field (CASSCF) approach made any attempt to directly obtain information about excited states. That work was limited to the $^1\Gamma_g$ state arising from the $(d\pi_u)^4(d\sigma_g)^2(s\sigma_g)^2(d\delta_g)^2$ configuration, found to be very low-lying ($T_e = 0.02$ eV), and a $^3\Delta_g$ state arising from a d$\delta_g \leftarrow$ dσ_g promotion, found to have a bond length very similar to that of the ground state and $T_e = 7420\ \mathrm{cm}^{-1}$. Detailed theoretical treatment of higher-lying excited states has not been reported since the Xα calculations of Andrews and Ozin [194].

In summary, although a large body of experimental and theoretical data has been amassed on the vanadium dimer, there are still a number of questions remaining. The electron configuration of the $A^3\Pi_u$ state observed by Langridge-Smith et al. [49] is unknown, a band observed near 15000 cm^{-1} and perhaps one or more in the range 11250-12500 cm^{-1} have not been assigned, an assignment of the state observed at 1860 cm^{-1} as ${}^1\Sigma_g^+$ has come under question, and the DFT results of James et al. [107] indicate that assignment of the $A'^3\Sigma_u^- \leftarrow X^3\Sigma_g^-$ transition as a $d\delta_u \leftarrow d\delta_g$ promotion should be reassessed. Clearly theoretical modeling of the electronic structure of excited states of the vanadium dimer would be useful for addressing these questions.

That completes the summary of the existing knowledge of the electronic structure of V_2. Divanadium is a good test case for the INDO/S model, because enough is known about the ground and excited states that the quality of calculated results can be judged. As will be seen, the results reported in this chapter compare favorably with experiment. As discussed in detail below, the INDO/S calculations yield the correct $X^3\Sigma_g^-$ ground state of V_2 with a spin-orbit splitting in reasonable agreement with the experimentally-determined splitting. The calculated energy of the ${}^1\Sigma_g^+$ state resulting from the ground $(\pi_u)^4(\sigma_g)^2(\sigma_g)^2(\delta_g)^2$ configuration is in good agreement with the prediction of James et al. [190], calling into question the assignment of the state observed at 1860 cm^{-1} as the isoconfigurational ${}^1\Sigma_g^+$. Energies and spin-orbit splittings of the $A'^3\Sigma_u^-$ and $A^3\Pi_u$ states are also reproduced well. The method does seem to be reasonably successful at the restricted active space full CI level used for the calculations, at least for the case of V_2.

The overall quality of agreement between experiment and the INDO/S calculations is good enough that some of the questions that remain regarding the electronic spectroscopy of V_2 can be tentatively answered based on the INDO/S calculations. An allowed transition from the ground state to a second $^3\Sigma_u^-$ state is found close to 15,000 cm^{-1}, and is suggested as a candidate for the unassigned transition observed [49] near this energy. Both $^3\Sigma_u^-$ states are found to result from $\sigma_u \leftarrow \sigma_g$ promotions, and the $A\,^3\Pi_u \leftarrow X^3\Sigma_g^-$ transition is assigned as a $d\delta_g \leftarrow d\pi_u$ promotion. A $^1\Sigma_u^+$ state isoconfigurational with the $A'^3\Sigma_u^-$ state is suggested as a potential candidate for one of the unidentified transitions observed in the range 11500-12500 cm^{-1}.

Methodological Considerations

INDO/S uses a basis set of nine orbitals (the 3*d*, 4*s*, and 4*p* atomic orbitals) for the metals of the first transition series, so a total of eighteen orbitals are included in the calculations on V_2. Fock matrix elements in that basis set are specified following reference [92], as described in chapter two. The ROHF method of Edwards and Zerner [123] is used to insure that the wavefunction is a spin eigenstate, appropriate for prediction of spectroscopy. The SCF procedure fails to converge unless provided with a refined set of MOs as a starting-point, as expected based on the discussion in chapter two. In this work a set of starting orbitals is obtained with the configuration-averaged Hartree-Fock (CAHF) procedure [126], which has been found to be very effective in obtaining stable SCF orbitals in such difficult cases. A detailed description of this was given in chapter two. The resulting manifold of occupied and unoccupied molecular orbitals is used in the subsequent CI calculations, which utilized the Rumer diagram SOCI method described in chapter two. The ZINDO program [108] was used for all calculations, run on either the Sun Enterprise 5000 server or IBM RS/6000 SP server that make up part of the John C. Slater Computing and Visualization Laboratory at the Quantum Theory Project.

Results and Discussion

Self-Consistent Field Ground State

An SCF calculation employing the ROHF formalism of Edwards and Zerner [123] failed to converge. Recourse was then made to the CAHF method to obtain a refined set of starting orbitals. An examination of the unconverged ROHF molecular orbitals revealed that the three lowest-energy closed shell orbitals, the $d\pi_u$ and $d\sigma_g$ orbitals, were energetically stable compared to the rest of the manifold. Oscillations between configurations were thus unlikely to involve these orbitals. Based on this the CAHF calculation was defined so that the $d\pi_u$ and $d\sigma_g$ orbitals were closed shell, and the remaining four electrons were averaged over the other fifteen orbitals. The ground state produced by this calculation had the orbitals in the same order found in the calculations of James et al. [107], and so was used as the starting point for an ROHF calculation with eight electrons occupying the $d\pi_u$, $d\sigma_g$, and $s\sigma_g$ orbitals and two electrons in the $d\delta_g$ orbitals. This calculation converged very quickly to the $X^3\Sigma_g^-$ ground state of V_2 with the electron configuration $(d\pi_u)^4(d\sigma_g)^2(s\sigma_g)^2(d\delta_g)^2$, in accord with the previous experimental [49,189,190,195] and theoretical [35,72,107,191-194] findings.

In the above-described treatment the $d\delta_g$ orbitals are delocalized in nature. The delta-symmetry overlap is very small even at the short bond distance of 1.77 Å, so these orbitals will be localized to some extent. In terms of configuration interaction, localization of the $d\delta_g$ orbitals is realized by mixing the principle configuration of the ground state, $(d\pi_u)^4(d\sigma_g)^2(s\sigma_g)^2(d\delta_g)^2$, with the doubly-excited configuration $(d\pi_u)^4(d\sigma_g)^2(s\sigma_g)^2(d\delta_g)^0(d\delta_u)^2$, in direct analogy to the localization of the ground state wavefunction of H_2 discussed in chapter two. This is indeed observed in the INDO/S CI calculations, as explained in more detail subsequently. That being the case, the delocalized ROHF $d\delta_g$ orbitals may not be the best starting-point for the CI calculations.

To investigate this a second SCF $X^3\Sigma_g^-$ ground state was obtained by first acquiring a starting set of vectors with the CAHF calculation as described above and then using a second CAHF calculation in which eight electrons were placed in the $d\pi_u$, $d\sigma_g$, and $s\sigma_g$ orbitals and the remaining two electrons were averaged over the $d\delta_g$, $s\sigma_u$, and $d\delta_u$ orbitals. The average includes all singlet and triplet states that can be formed by placing two electrons in these five orbitals, anticipating partial occupation of the $d\delta_u$ orbitals that is found later at a correlated level. The SCF ground state obtained in this way is very similar to that obtained with the ROHF formalism. The results are shown in table 4-1 and figure 4-2. All additional calculations used the MOs obtained with the five-orbital CAHF procedure.

The INDO/S MOs are in qualitative agreement with the DFT orbitals, and quantitatively, the orbital ionization potentials computed with INDO/S are much more accurate than those found with DFT. As a check on the INDO/S results the IP obtained for the $s\sigma_g$ orbital, 55004 cm^{-1}, is compared with that determined experimentally by James et al. [190] and Yang et al. [195] for ejection of an electron from this orbital, 51270 cm^{-1}. The DFT calculations of reference [107] are in error by nearly 20000 cm^{-1}

for this orbital IP. The greater accuracy of the molecular orbital calculations in predicting orbital IPs is not surprising, since it is well-known that the functionals used in most DFT calculations do not accurately reproduce orbital ionization energies [137]. The compositions of the MOs also show important deviations from the compositions found with DFT (table 4-1). The lower-lying σ_g orbital found with INDO/S is 95% 3dσ in character, and the higher-lying orbital of this symmetry is 95% 4s in character. In contrast, the DFT σ_g orbitals found by James *et al.* [107] are considerably hybridized. The INDO/S sσ_u orbital resembles that found with DFT more closely, being 95% 4s as compared to the 91% found with DFT. When correlation is added by means of CI, the hybridization of the 3dσ_g and 4sσ_g orbitals is evident, see below, in accord with the DFT

Table 4-1. Compositions and orbital energies of molecular orbitals obtained with INDO/S for the ground state of V_2. DFT results from reference [107] are shown in parentheses. Small contributions from the 4p atomic orbitals are omitted.

Orbital	Composition (%)		Energy (eV)
	4s	3d	
dπ_u	0 (0)	93 (98)	-8.65 (-5.18)
dσ_g	4 (42)	96 (54)	-7.66 (-5.00)
sσ_g	96 (52)	2 (47)	-6.82 (-4.03)
dδ_g	0 (0)	100 (100)	-7.28[a] (-3.89)
sσ_u	96 (91)	0 (0)	-6.84[b] (-2.31)
dδ_u	0 (0)	100 (100)	-5.69[b] (-2.09)
dπ_g	0 (0)	61 (88)	-4.41[b] (-1.19)
dσ_u	0	99	-3.87[b]

[a] The orbital energies of open-shell ROHF orbitals do not correspond to ionization potentials, so cannot be directly compared to the closed-shell orbital energies.

[b] Relative to energy of the open-shell dδ_g orbitals.

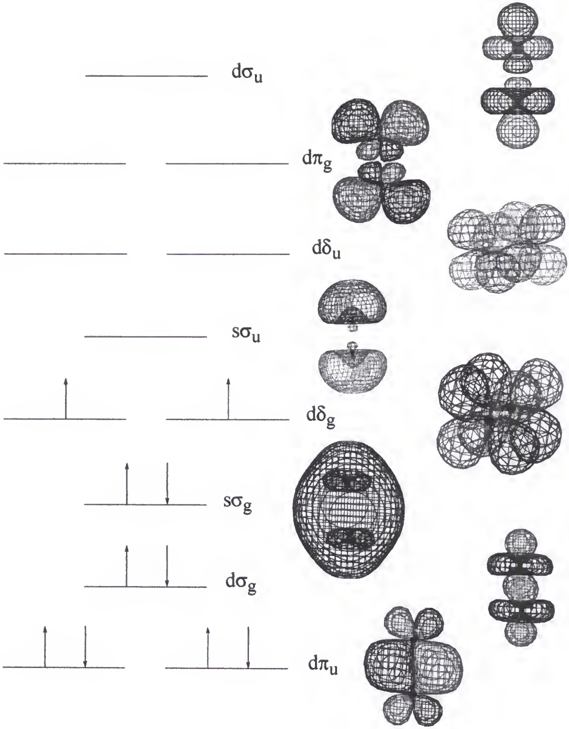

Figure 4-2: INDO/S ground state electron configuration of V_2 and plots of molecular orbitals involving the 3d and 4s orbitals.

results. This is not unexpected since DFT includes electron correlation by means of the exchange-correlation functional [137].

Despite the differences in orbital energies and hybridizations just cited, the INDO/S results are in basic agreement with the DFT results, giving the same order of energies. In both calculations the combinations of 4p orbitals are found to be considerably higher in energy than the 4s- and 3d-based MOs, and will not be explicitly considered. The locations of the $s\sigma_g$ and $s\sigma_u$ MOs require further comment. In both sets of calculations (INDO/S and DFT) the $4s\sigma_g$ MO is only weakly interacting, as shown by the high energy of the $s\sigma_g$ MO and especially the very low energy of the $s\sigma_u$ MO, which is found to be lower than that of the partially localized $d\delta_u$ MOs. This is true despite the large overlap of the 4s orbitals at the relatively short bond distance of V_2. The weak interaction of these orbitals is partially the result of shielding of the 4s orbitals by the much more compact 3d orbitals. This effect is manifested in the $4s\sigma_g$ MO by hybridization of this MO with the $3d\sigma$ atomic orbitals, which have coefficients that lead to cancellation of the $4s\sigma_g$ MO wavefunction between the nuclei. This can be discerned in figure 4-2 in the darker concentrations of density in the regions of the tori of the $3d_{z^2}$ orbitals.

Configuration Interaction

In considering how to go about applying the INDO/S model to the ground and excited states of divanadium, the experience gained with dichromium was valuable. The most successful theoretical treatment of Cr_2 used the CASPT2 method [28,30-32], which shows what is required for a theoretical method to be successful for a metal diatomic:

electron correlation in an appropriate active space must be accounted for, and dynamic correlation from outside that active space must be incorporated as well. The CASPT2 formalism relies on the CASSCF calculation to accomplish the former, and second order multireference perturbation theory to approximate the latter. The discussion of the bridge between semiempirical and ab initio methods given in chapters one and two indicates that the approach that should be used in applying INDO/S to V_2 is directly analogous, with correlation effects within an active space treated with full CI, and dynamic correlation effects from outside the active space provided by the parameterization.

This is not meant to suggest that a semiempirical method is capable of the same accuracy that the CASPT2 method is capable of, as the latter is systematic while the former relies on the assumption that parameters fit based on a limited number of test cases are universal. The very high accuracy of a rigorous but expensive highly-correlated ab initio method is not the goal. Rather, a method with reasonable accuracy in predicting transition energies and intensities, but capable of treating (in principle) tens of transition metal atoms instead of two or three, is the eventual goal of investigations like that undertaken here.

It is also important to note that the INDO/S model was parameterized at the CIS level, and hence some dynamic correlation within the valence space itself is likely incorporated. Full CI within the valence space would then overcount this contribution. This aspect is addressed directly in chapter five. The work in this chapter is meant to show that the INDO/S model applied at a level of correlation beyond the HF (or, equivalently, the CIS[2]) level in the valence space does provide an adequate description of the electronic structure of divanadium.

The most rigorous application of the approach described above to the V_2 problem would be a full CI calculation with the entire 3d and 4s orbital manifold as the active space. Such a calculation would include 283,140 triplet CSFs. Taking into account the three triplet components that must be included in a spin-orbit CI, along with the 169,884 singlet CSFs, a calculation in this active space including spin-orbit coupling would have to include slightly over one million basis functions, and this does not even include contributions from quintets (see below for discussion of exclusion of quintet states from the calculations). The present ZINDO program is limited to approximately twenty thousand CSFs, so clearly this full CI calculation is presently beyond reach and a smaller active space must be adopted. Since the active space is meant to account primarily for essential correlation, it is then crucial to identify the orbitals that need significant essential correlation corrections.

In an early transition metal dimer like V_2 the essential correlation has the effect of restoring some local character to the 3d orbitals in the molecular wavefunction. This is necessary because the 3d orbitals have very small overlap, even at the short bond distances of V_2 and Cr_2. The situation is a pathological example of the well-known problem of the dissociation of the hydrogen molecule, as mentioned previously, for which essential correlation is vital to obtaining a correct description of the potential energy curve as the atoms are separated. The problem is much more difficult for transition metal dimers because the essential correlation is important even at the equilibrium bond distance, there are more electrons to be correlated, and the extent of localization is different for the σ, π, and δ combinations of orbitals. With this in mind the localization of the orbitals was investigated with three separate CI calculations, each with an active space restricted to the MOs of one symmetry.

---

[2] This equivalence is rigorously true only for the ground state.

The extent of orbital localization in each of the σ, π , and δ orbital spaces is most clearly demonstrated by the electron populations of the MOs in the CI ground state for each case (table 4-2). If the orbitals were completely localized there would be an equal distribution of electrons in the bonding and antibonding combinations of each symmetry. Referring again to the example of H_2, the localized wavefunction of equation (2-64) has equal populations of one electron in the $1s\sigma_g$ and $1s\sigma_u$ orbitals. In the case of the $(d\pi_u)^4(d\sigma_g)^2(s\sigma_g)^2(d\delta_g)^2$ ground state of V_2 complete localization would entail one electron in each of the σ_g and σ_u MOs, a total of one electron in the $d\delta_g$ and $d\delta_u$ MOs, and a total of two electrons in the $d\pi_u$ MOs and in the $d\pi_g$ MOs. The extent of localization can thus be judged by the populations of the antibonding $d\pi_g$, σ_u, and $d\delta_u$ MOs found in the CI ground states, conveniently expressed in table 4-2 as the percentage of the total population expected for complete localization. As shown in table 4-2 the effect is most significant in the $d\delta$ space, of lesser importance for the $d\sigma$ MOs, and much smaller for the $d\pi$ orbitals. The extent of localization is, in fact, in the same order as the overlaps of the relevant atomic orbitals.

There is also appreciable population of the $4s\sigma_u$ orbital, indicating that essential correlation is important for describing the interaction of the 4s orbitals as well. In this case the correction is not properly described as localization because the overlap of these orbitals at the short bond distance of V_2 is large. The interaction of the 4s orbitals is weak despite the large overlap because the one-electron matrix elements coupling these

Table 4-2: Populations of the molecular orbitals described in table I from full CI calculations in active spaces restricted to the orbitals of each symmetry.

Orbital	Population	Localization
δ_g	1.61	
δ_u	0.39	0.39
$d\sigma_g$	1.88	
$d\sigma_u$	0.13	0.13
$s\sigma_g$	1.87	
$s\sigma_u$	0.12	0.12
$d\pi_u$	3.91	
$d\pi_g$	0.09	0.05

orbitals are small in magnitude, for reasons described above. The weakness of the 4s-4s interaction leads to the need for essential correlation in obtaining a proper description of the 4s-based MOs.

The orbital populations listed in table 4-2 show that the localization of the dπ MOs is negligible, while the localization of the σ and δ MOs is ten percent or greater. The approximate CI treatment developed based on these considerations is as follows. Essential correlation is accounted for with full CI that has as an active space the orbitals found to be significantly localized, the dσ, sσ, and dδ orbitals. This reduced active space of eight orbitals and six electrons gives rise to a modest number of CSFs, 1512 triplets for example. Dynamic correlation in the INDO/S model is properly obtained using a CIS treatment, since the model was parameterized at this level. Accordingly, all single excitations from the reference configuration $(d\pi_u)^4(d\sigma_g)^2(s\sigma_g)^2(d\delta_g)^2$ in the entire 3d and 4s orbital space are included. All single excitations from the doubly-excited configuration $(\mathrm{d}\pi_u)^4(\mathrm{d}\sigma_g)^2(\mathrm{s}\sigma_g)^2(\mathrm{d}\delta_u)^2$ are also included, since this configuration was found to mix quite strongly with the reference configuration.

Care must be taken in applying a model like that described above to ensure that the correlation of the ground and excited states is balanced. As an example, consider the excited $\mathrm{A}'^3\Sigma_u^-$ state of the vanadium dimer that has been observed experimentally. The transition to this state was tentatively assigned as a $\delta_u \leftarrow \delta_g$ promotion [49], and the results of DFT calculations [107], the SCF orbitals reported in table 4-2, and experimental results on the V_2^+ cation [195] and VNb [197] suggest the possibility that the excited configuration arises from a $\sigma_u \leftarrow \sigma_g$ promotion. In either case, the ground and excited states are correlated in a balanced way since both promotions are within the σ and δ orbital manifold, and that manifold has been correlated with a full CI treatment. In other words, the ground and excited states are both allowed to mix with all other possible configurations of the σ and δ electrons.

The same is not true of the excited $\mathrm{A}\,^3\Pi_u$ state, however, because the only way to obtain Π_u symmetry within the 3d and 4s orbital manifold is to promote an electron from the $\mathrm{d}\pi_u$ MOs. Although electrons are promoted from these orbitals in the CIS treatment described above, the resulting configurations ($(\mathrm{d}\pi_u)^3(\mathrm{d}\sigma_g)^2(\mathrm{s}\sigma_g)^2(\mathrm{d}\delta_g)^3$ for example) are not subjected to the same localization corrections that are applied to the ground configuration (by presence of the $(\mathrm{d}\pi_u)^3(\mathrm{d}\sigma_g)^0(\mathrm{s}\sigma_g)^2(\delta_g)^3(\mathrm{d}\sigma_u)^2$ configuration, for example, that would allow partial localization of the $\mathrm{d}\sigma_g$ MOs). Hence the $\mathrm{A}\,^3\Pi_u$

state would be expected to be artificially high in energy in a CI calculation that includes full CI in the σ and δ orbital manifold and CIS from the reference configurations $(d\pi_u)^4(d\sigma_g)^2(s\sigma_g)^2(d\delta_g)^2$ and $(d\pi_u)^4(d\sigma_g)^2(s\sigma_g)^2(d\delta_u)^2$, and this is what is observed: the energy of the $A'^3\Sigma_u^-$ state is reproduced quite accurately, but the only low-lying $^3\Pi_u$ state, mainly comprised of the configuration $(d\pi_u)^3(d\sigma_g)^2(s\sigma_g)^2(d\delta_g)^3$, is almost three eV (~ 24000 cm^{-1}) above the $X^3\Sigma_g^-$ ground state. Clearly additional configurations are needed to provide an adequate description of the correlation of the $A^3\Pi_u$ state.

The approach adopted to achieve a balance between the correlation of the ground state and the $A^3\Pi_u$ state is to apply all excitations to the $(d\pi_u)^3(d\sigma_g)^2(s\sigma_g)^2(d\delta_g)^3$ configuration that are found to correlate the ground state in the full CI calculation using the σ and δ MOs as the active space. All of the configurations and excitations used in the final calculation are listed in table 4-3. As defined in the table, the calculation includes 1988 triplet and 1520 singlet CSFs, which is small enough to allow application of the INDO/S Rumer diagram spin-orbit treatment. Independent calculations using smaller multireference treatments have suggested that quintet components have a negligible impact on the spin-orbit splittings of the ground and excited states that have been observed for V_2, so only singlets and triplets need to be included in the spin-orbit treatment.

The final results for the ground and excited states of V_2 are shown in tables 4-4 – 4-6. Table 4-4 lists all configurations making contributions to the ground state, table 4-5

Table 4-3. Configurations and excitations included in the configuration interaction model used to describe the ground and excited states of V_2. Orbitals are listed in the order found in table 4-1.

Configuration	**Excitations included**
$(d\pi_u)^4(d\sigma_g)^2(s\sigma_g)^2(\delta_g)^2$	All singles, full CI in σ, δ MOs
$(d\pi_u)^4(d\sigma_g)^2(s\sigma_g)^2(\delta_u)^2$	**All singles**
$(d\pi_u)^3(d\sigma_g)^2(s\sigma_g)^2(\delta_g)^3$	$d\delta_g{}^2\rightarrow d\delta_u{}^2$, $s\sigma_g{}^2\rightarrow s\sigma_u{}^2$, $d\sigma_g{}^2\rightarrow d\sigma_u{}^2$, $s\sigma_g{}^2\rightarrow d\sigma_u{}^2$, $d\sigma_g{}^2\rightarrow s\sigma_u{}^2$, $s\sigma_g{}^2\rightarrow d\delta_u{}^2$, $d\sigma_g{}^2\rightarrow d\delta_u{}^2$, $d\sigma_g{}^1 d\delta_g{}^1\rightarrow s\sigma_u{}^1 d\delta_g{}^1$, $s\sigma_g{}^1 d\delta_g{}^1\rightarrow s\sigma_u{}^1 d\delta_g{}^1$, $s\sigma_g{}^2 d\delta_g{}^2\rightarrow d\delta_u{}^2 s\sigma_u{}^2$, $d\sigma_g{}^2 d\delta_g{}^2\rightarrow d\delta_u{}^2 d\sigma_u{}^2$, $d\sigma_g{}^2 s\sigma_g{}^2\rightarrow s\sigma_u{}^2 d\sigma_g{}^2$, $d\sigma_g{}^2 s\sigma_g{}^2 d\delta_g{}^2\rightarrow s\sigma_u{}^2 d\sigma\delta_g{}^2 d\sigma_g{}^2$.

provides a comparison of the calculated results with experiment for a number of states, and table 4-6 lists populations of the MOs enumerated in table 4-1 for several of the states listed in table 4-5. These results are discussed in detail below.

Ground state

The ground state found with the CI calculations is a singly-degenerate triplet state with the primary contribution from the configuration $(d\pi_u)^4(d\sigma_g)^2(s\sigma_g)^2(d\delta_g)^2$, establishing this state as $X\,^3\Sigma_g^-$ in accord with previous experimental [49,189,190,195] and theoretical [35,72,107,191-194] results. Aside from the leading configuration, the largest contribution is made by the $(d\pi_u)^4(d\sigma_g)^2(s\sigma_g)^2(\delta_u)^2$ configuration (table 4-4), which serves to localize the δ_g MOs, as anticipated previously. Additional significant contributions are made by the $(d\pi_u)^4(d\sigma_g)^2(\delta_g)^2(s\sigma_u)^2$ and $(d\pi_u)^4(s\sigma_g)^2(\delta_g)^2(d\sigma_u)^2$

Table 4-4. Configurations contributing to the $X^3\Sigma_g^-$ ground state of V_2 from the CI calculation described in table 4-3. All configurations with coefficients greater than 0.01 are included.

Configuration	**Coefficient**
$(d\pi_u)^4(d\sigma_g)^2(s\sigma_g)^2(\delta_g)^2$	0.869
$(d\pi_u)^4(d\sigma_g)^2(s\sigma_g)^2(\delta_u)^2$	-0.288
$(d\pi_u)^4(d\sigma_g)^2(\delta_g)^2(s\sigma_u)^2$	-0.172
$(d\pi_u)^4(s\sigma_g)^2(\delta_g)^2(d\sigma_u)^2$	-0.163
$(d\pi_u)^4(s\sigma_g)^2(\delta_u)^2(d\sigma_u)^2$	0.093
$(d\pi_u)^4(d\sigma_g)^2(s\sigma_u)^2(\delta_u)^2$	0.078
$(d\pi_u)^4(d\sigma_g)^1(s\sigma_g)^2(\delta_g)^1(s\sigma_u)^1(\delta_u)^1$	-0.055
$(d\pi_u)^4(s\sigma_g)^2(\delta_g)^2(\delta_u)^2$	-0.050
$(d\pi_u)^4(d\sigma_g)^2(s\sigma_g)^1(\delta_g)^1(s\sigma_u)^1(\delta_u)^1$	0.049
$(d\pi_u)^4(\delta_g)^2(s\sigma_u)^2(d\sigma_u)^2$	0.044
$(d\pi_u)^4(s\sigma_u)^2(\delta_u)^2(d\sigma_u)^2$	0.040

configurations, also as expected. Other configurations making small contributions to the ground state include a number of quadruple excitations and one hextuple excitation. In the latter case, all six electrons in the σ and δ orbitals are promoted, which illustrates the high level of correlation expected for the early dimers of the 3d transition series. The total bond order of V_2 is reduced from its formal value of five to 3.76 by these interactions.

The spin-orbit splitting of the ground state predicted by the calculations, 120 cm^{-1}, is in reasonable agreement with the experimentally-determined splitting of 75 cm^{-1}. The magnitude of this splitting depends on the energy of the $^1\Sigma_g^+$ state isoconfigurational with the ground state, predicted as 873 cm^{-1} in modest agreement with the prediction of 1196 cm^{-1} by James *et al.* [190]. The fact that the ground state splitting is too large shows that the INDO/S calculations are underestimating the energy of the $^1\Sigma_g^+$ state (though the predicted energy is well within the margin of error expected for the INDO/S model). It is possible that overcounting of the dynamic correlation within the active space is contributing to the error of the calculated energy of the upper perturbing state. Some dynamic correlation is present in the state wavefunctions due to the large number of configurations included to achieve a balanced description of the ground and excited states. This hypothesis is explored in the next chapter.

The $^1\Sigma_g^+$ state is found to be contaminated with approximately 6% triplet character by the spin-orbit interaction with the ground state. Spain et al. [189] cited such mixing as partial justification for assigning a state observed at 1860 cm^{-1} in a resonance Raman experiment [47] as the $^1\Sigma_g^+$ state, as the mixing could abrogate the spin selection rule. The intensity of a direct optical transition from the ground state to the $^1\Sigma_g^+$ state is found to be vanishingly small by the INDO/S calculations despite the spin contamination of the upper state. The selection rules for resonance Raman spectroscopy are not the same as those for optical spectroscopy, however. Even so, the much lower energy predicted by both the INDO/S calculations and the approximate treatment of James *et al.* [190] is a strong indication that the state observed at 1860 cm^{-1} is not the $^1\Sigma_g^+$ state, but some other state. The INDO/S results do not include an allowed transition to an excited state in this energy range. The lowest-lying excited states obtained from the calculations are derived from a $\delta_u \leftarrow \delta_g$ promotion, but are roughly have an eV above the ground state. An excited ${}^3\Sigma_u^-$ state derived from the $(d\pi_u)^4(d\sigma_g)^2(s\sigma_g)^2(\delta_g)^1(\delta_u)^1$ configuration thus represents the "best guess" for the identity of the state observed at 1860 cm^{-1}. If there was significant coupling of the $(d\pi_u)^4(d\sigma_g)^2(s\sigma_g)^2(\delta_g)^1(\delta_u)^1$ configuration with other excited configurations involving the dπ electrons in the CI wavefunction of this hypothetical ${}^3\Sigma_u^-$ state, the energy of the state would be artificially high (as found) since the dπ orbitals were not correlated at the same level that the δ orbitals were. Perhaps a full CI calculation correlating all of the 3d- and 4s-derived MOs would shed light on this situation, but such a calculation is intractable with the present ZINDO program. Alternatively, a more rigorous method such as CASPT2 calculation might provide insight regarding the identity of the state observed at 1860 cm^{-1}.

Excited states

The energies and spin-orbit splittings of the excited states predicted by the INDO/S SOCI calculations are in good agreement with the experimental results (table 4-5). Assignments were made on the basis of calculated energies, spin-orbit splittings, transition moments and polarizations, and comparisons of the electron populations of the MOs in the ground and excited states. The $A'^3\Sigma_u^-$ state is described particularly well, with the predicted energy of the $\Omega' = 0 \leftarrow \Omega'' = 0$ band within 100 cm^{-1} of the experimentally-determined energy, and a calculated spin-orbit splitting of 85 cm^{-1}

Table 4-5. Comparison of calculated and experimental results for the ground and excited states of V_2.

Level	INDO/S (cm^{-1})	Experiment (cm^{-1})	Promotion	Oscillator Strength (from ground level)
$X^3\Sigma_g^-,\Omega=0$	0	0^a	–	–
$X^3\Sigma_g^-,\Omega=1$	120	75^a	–	0
$^1\Gamma_g,\Omega=4$	378	$(160)^b$	–	0
$^1\Sigma_g^+,\Omega=0$	873	1196^c 1821^d	–	0
$A'^3\Sigma_u^-,\Omega=0$	11739	11811^d	$\sigma_u \leftarrow \sigma_g$	0.0244 (0.01^e)
$A'^3\Sigma_u^-,\Omega=1$	11824	11899^d		0
$^1\Sigma_u^+,\Omega=0$	12161	11250-12500?^{d}	$\sigma_u \leftarrow \sigma_g$	0
$A^3\Pi_u,\Omega=0$	14808	14303^a	$\delta_g \leftarrow \pi_u$	0
$A^3\Pi_u,\Omega=1$	14862	14338^a		0.0018
$A^3\Pi_u,\Omega=2$	14945	14383^a		0
$B^3\Sigma_u^-,\Omega=0$	14631	–	$\sigma_u \leftarrow \sigma_g$	0.0026
$B^3\Sigma_u^-,\Omega=1$	14655	~ 15000^a		0

[a] Reference [49].
[b] From CASSCF calculations, reference [35].
[c] Reference [190].
[d] Reference [189].

compared to the experimental value of 88 cm^{-1}. The computed oscillator strength of 0.02 also compares favorably with the experimental value of 0.01.

A $^3\Sigma_u^-$ state is found with an energy near 14600 cm^{-1} in the INDO/S results, close to the energy of the unassigned $\Omega' = 1 \leftarrow \Omega'' = 1$ transition observed by Langridge-Smith et al. [49]. The intensity of a transition from the ground state to this state is very similar to that of the $A^3\Pi_u \leftarrow X^3\Sigma_g^-$ transition, also as observed by Langridge-Smith *et al.* Based on both factors the upper state of this transition is assigned as $B^3\Sigma_u^-$. Unfortunately the spin-orbit splitting of this state has not been measured. An experimental determination of the splitting of this state could provide independent corroboration of this assignment.

The energies and spin-orbit splittings of the $A^3\Pi_u$ state obtained here also agree quite well with experiment, though not quite as closely as was found for the $A'^3\Sigma_u^-$ state. The spin-orbit splittings are slightly exaggerated, as was the splitting found for the ground state. Transition energies are reproduced to within 500 cm^{-1} for both the $A^3\Pi_u$ and $B^3\Sigma_u^-$ states. Unfortunately the errors are in opposite directions for the two states, and combine to invert the order of energies found experimentally. Comparison of the MO populations in the $A^3\Pi_u$ excited state and the ground state (table 4-6) allows assignment of the ${}^3\Pi_u \leftarrow {}^3\Sigma_g^-$ transition as a $d\delta_g \leftarrow d\pi_u$ promotion, as anticipated in the discussion regarding the correlation of this state. This is the first firm assignment of the orbital symmetry of this transition.

Both ${}^3\Sigma_u^-$ states are largely composed of configurations involving electron promotion within the sigma-symmetry MOs, $(d\pi_u)^4(d\sigma_g)^2(s\sigma_g)^1(\delta_g)^2(s\sigma_u)^1$ and $(d\pi_u)^4(d\sigma_g)^1(s\sigma_g)^2(\delta_g)^2(s\sigma_u)^1$, see table 4-6. The mixing of these configurations

Table 4-6. Molecular orbital populations in the ground and some excited states of V_2 from the CI calculation described in table 4-3.

Orbital	$X^3\Sigma_g^-$	$A'^3\Sigma_u^-$	$A^3\Pi_u$	$B^3\Sigma_u^-$
$d\pi_u$	4.00	3.98	3.00	3.98
$d\sigma_g$	1.84	1.81	1.87	1.14
$s\sigma_g$	1.88	1.32	1.88	1.90
δ_g	1.73	1.61	2.64	1.62
$s\sigma_u$	0.12	0.70	0.13	0.80
δ_u	0.28	0.43	0.36	0.45
$d\pi_g$	0.00	0.02	0.00	0.02
$d\sigma_u$	0.14	0.12	0.12	0.11

indicates some hybridization of the $4s\sigma_g$ and $3d\sigma_g$ orbitals, in agreement with the results of DFT calculations [107]. Configurations arising from $\delta_u \leftarrow \delta_g$ promotions are present in each state as well but their contribution is small. This is best displayed by the MO occupations for these CI states (table 4-6), where it is clear that the occupations of the $d\sigma_g$ and $s\sigma_g$ orbitals are reduced significantly, and the occupation of $s\sigma_u$ orbital is increased by similar amounts. The INDO/S calculations thus indicate that both transitions are of $\sigma_u \leftarrow \sigma_g$ character, contrary to the assignment made by Spain *et al.* [189].

The assignment of both $^3\Sigma_u^- \leftarrow X^3\Sigma_g^-$ transitions as $\sigma_u \leftarrow \sigma_g$ promotions is supported by the MOs obtained for V_2 with DFT [107], in which the $s\sigma_u$ MO is found to be lower in energy than the δ_u MOs. The computed orbital energies that were found indicate that the $\sigma_u \leftarrow \sigma_g$ and $\delta_u \leftarrow \delta_g$ promotions are comparable in energy. Theoretical

[196] and experimental [190,195] results obtained for V_2^+ have shown that ionization of V_2 removes an electron from the $s\sigma_g$ MO, leading to a small reduction in bond length, which is also observed in the $A'^3\Sigma_u^- \leftarrow X^3\Sigma_g^-$ transition [189]. James et al. [197] have stated that a similar $^3\Sigma^- \leftarrow X^3\Sigma^-$ transition observed for VNb is possibly not a $\delta^* \leftarrow \delta$ transition. The results of the INDO/S calculations reported here, taken together with these indications from DFT calculations and experiments on V_2, V_2^+, and VNb, call for a reassessment of the assignment of the $A'^3\Sigma_u^- \leftarrow X^3\Sigma_g^-$ transition of V_2 as a $\delta_u \leftarrow \delta_g$ promotion.

Finally, Spain et al. observed at least one additional excited state in the energy range 11250-12500 cm^{-1} that has yet to be assigned [189]. The INDO/S results indicate that one of these unidentified excited states is the $^1\Sigma_u^+$ state arising from the same $(d\pi_u)^4(d\sigma_u)^2(s\sigma_g)^1(\delta_g)^2(s\sigma_u)^1$ configuration that gives rise to the observed $A'^3\Sigma_u^-$ state, table 4-5. This $^1\Sigma_u^+$ state causes the spin-orbit splitting of the $A'^3\Sigma_u^-$ state, and is thus contaminated with some triplet character. In the INDO/S wavefunction of this state the contamination is on the order of 17%, explaining the nonzero oscillator strength computed for a transition into this state from the $\Omega'' = 1$ component of the ground state.

Spain et al. did not consider this transition as the possible identity of one of the unassigned states they observed because they predicted the energy of this state to be greater than 13000 cm^{-1} based on their second-order perturbative treatment [189]. They assumed that the $A'^3\Sigma_u^-$ and $^1\Sigma_u^+$ excited states arose from the configuration $(d\pi_u)^4(d\sigma_g)^2(s\sigma_g)^2(\delta_g)^1(\delta_u)^1$, however, which is found to not be the case here, and used the same value for ζ_{3d} that was used in overestimating the energy of the ${}^1\Sigma_g^+$ state that interacts with the $X^3\Sigma_g^-$ ground state. The results in table 4-5 indicate that the energy of the ${}^1\Sigma_u^+$ state is much closer in energy to that of the $A'^3\Sigma_u^-$ state, and lies in the range 11250-12500 cm^{-1}. Further experimental work could potentially help to confirm the suggestion made here that there is an allowed transition to the ${}^1\Sigma_u^+$ state isoconfigurational with the $A'^3\Sigma_u^-$ state in this energy range.

In conclusion, the most surprising aspect of the results presented here is the assignment of the $A'^3\Sigma_u^- \leftarrow X^3\Sigma_g^-$ transition observed near 11800 cm^{-1} as a $\sigma_u \leftarrow \sigma_g$ promotion, given the much higher energy of the $A''^1\Sigma_u^+ \leftarrow X^1\Sigma_g^+$ $\sigma_u \leftarrow \sigma_g$ transition observed near 19350 cm^{-1} [20] in the chromium dimer. The accurate CASPT2 calculations of Andersson on the electronic spectrum of Cr_2 [32] indicate that this transition has a roughly equal admixture of $s\sigma_u \leftarrow d\sigma_g$ and $s\sigma_u \leftarrow s\sigma_g$ character. The CASPT2 results also assign the $a'^3\Sigma_u^+ \leftarrow X^1\Sigma_g^+$ transition, observed at close to 14275 cm^{-1} [52] as predominantly $s\sigma_u \leftarrow s\sigma_g$ in character, in much closer agreement with the INDO/S results for the $A'^3\Sigma_u^- \leftarrow X^3\Sigma_g^-$ $\sigma_u \leftarrow \sigma_g$ promotion in V_2.

The remaining difference can be explained by the essential correlation corrections required for the 4s-4s interaction in the two molecules. CASPT2 calculations on Cr_2 have shown that the occupation of the $4s\sigma_u$ MO in the ground state is of smaller magnitude than the occupations of the 3d-based antibonding MOs [28], while in the INDO/S calculations, occupation of the $4s\sigma_u$ MO is comparable to that of the $3d\sigma_u$ MO.

This can be interpreted as indicating that the 4s orbitals are more strongly interacting in Cr_2 than in V_2, since they require less essential correlation relative to the 3d-based MOs than is observed for V_2. This greater interaction leads to stabilization of the $4s\sigma_g$ MO and destabilization of the $4s\sigma_u$ MO relative to what occurs in V_2, causing the transition between these MOs to occur at higher energy in Cr_2.

Conclusions

Configuration interaction calculations that include spin-orbit effects have been carried out using the INDO/S model, and give results that compare well to experimentally-known state energies and spin-orbit splittings. The $^1\Sigma_g^+$ state isoconfigurational with the $X^3\Sigma_g^-$ ground state is predicted to have an energy that agrees well with the prediction of James et al. [190], bringing into question a previous assignment of a state observed at 1860 cm^{-1} as this $^1\Sigma_g^+$ state. The calculated results do not provide a suggestion for the identity of the state observed at 1860 cm^{-1}, however. The unassigned state might involve a $\delta_u \leftarrow \delta_g$ promotion, but this is no more than a guess. The $A^3\Pi_u \leftarrow X^3\Sigma_g^-$ transition has been assigned as a $d\delta_g \leftarrow d\pi_u$ promotion, providing the first definitive assignment of the orbital symmetry of this transition. A previously unassigned transition observed near 15000 cm^{-1} has been assigned as $B^3\Sigma_u^- \leftarrow X^3\Sigma_g^-$. Both that and the observed $A'^3\Sigma_u^- \leftarrow X^3\Sigma_g^-$ transition are assigned as $\sigma_u \leftarrow \sigma_g$ promotions, which disagrees with the assignment of the nature of the $A'^3\Sigma_u^- \leftarrow X^3\Sigma_g^-$ of Langridge-Smith *et al* [49]. The new assignment is supported by both experimental and theoretical evidence, and an analysis of the similar $\sigma_u \leftarrow \sigma_g$ transition in Cr_2. Finally, the $^1\Sigma_u^+$ state isoconfigurational with $A'^3\Sigma_u^-$ is suggested as a possibility for one of the unassigned states observed in the range 11250-12500 cm^{-1}. The good agreement between theory and experiment for all experimentally known transition energies, oscillator strengths, spin-orbit splittings, and state symmetries indicates that a semiempirical model such as INDO/S can in principle be an effective tool for studying the electronic spectroscopy of transition metal clusters.

CHAPTER 5
GROUND STATE ISOCONFIGURATIONAL MIXING IN V_2, VNb, AND Nb_2

Summary and Purpose

In the previous chapter it was seen that the INDO/S method provided a satisfactory description of the electronic spectroscopy of divanadium by means of full configuration interaction in a defined active space. This outcome follows from the formal bridge between semiempirical and ab initio methods established by partitioning of the full CI matrix to give an effective valence shell Hamiltonian [100,101,135]. A remaining question that has not been directly addressed, however, regards correlation effects within the valence space. It is thought that a semiempirical parameterization incorporates dynamic but not essential correlation effects [93], which are quantitatively defined as contributions to a CI wavefunction with small coefficients [63]. Based on this definition there are dynamic correlation effects within the valence space itself. A model such as INDO/S that was parameterized at the CIS level must incorporate (in a non-systematic way) some part of this correlation in the parameters.

It is thought that "overcounting" dynamic correlation contributions by applying a semiempirical model at a high level of electron correlation adversely affects results [104]. These assertions are based on studies using the effective valence shell Hamiltonian. A major goal of the work reported here is to test the hypotheses just described with a successful, widely-used semiempirical method like INDO/S. The ground state spin-orbit splittings observed for V_2, VNb, and Nb_2 are convenient for this purpose, as described in detail subsequently. The three examples considered here indicate that "overcounting" dynamic correlation in the valence space leads to poorer results.

As in the previous chapter, the results obtained here compare well enough with experiment that several issues not clarified by the experimental results can be addressed. While the spin-orbit splittings in the ground states of V_2 and VNb have been measured experimentally, the magnitude of the splitting of the ground state of Nb_2 is uncertain. The value assumed in the literature [190,198] is attributed to Weltner and coworkers at the University of Florida, but they consider the assignment of their measured value as the ground state spin-orbit splitting in Nb_2 to be tentative.[1] The theoretical results presented here provide corroboration that the measured value is indeed the splitting of the ground state of Nb_2. Predictions of the energy of the isoconfigurational $^1\Sigma^+$ states perturbing the ground states have also been made for the three molecules based on an empirical two-state model [190]. The accuracy of these predictions has been evaluated based on the more rigorous INDO/S SOCI results. As part of this effort, improvements to the two-state models are suggested, and several sources of error are analyzed.

Finally, CI calculations carried out as part of the analysis of correlation effects allow investigation of the Σ-symmetry excited states of the three molecules. Two excited $^3\Sigma_u^-$ states have been observed for V_2 [49,189], but only one excited $^3\Sigma^-$ state has been observed for VNb [197]. Several questions raised by these observations have been investigated, including the orbital symmetry of the $\Sigma \leftarrow \Sigma$ transition observed for VNb, whether or not there is a second $\Sigma \leftarrow \Sigma$ transition in VNb, and if so, why it has not been observed. The chapter concludes with a brief discussion of the electronic spectroscopy of

---

[1] W. Weltner, Jr., personal communication

Nb_2. The observed transitions have not been definitively assigned [107], but the INDO/S results do not provide useful interpretation. It is suggested that this failure occurs because the 4d metal parameters are theoretical rather than spectroscopic.

Background and motivation

This chapter focuses on ground state spin-orbit effects observed for V_2, VNb, and Nb_2 [49,190]. In all three cases the ground state has ${}^3\Sigma^-$ symmetry and electron configuration $(d\pi)^4(d\sigma)^2(s\sigma)^2(d\delta)^2$ [35,49,107,189-193,196-198] The ground state splittings are caused by second-order interaction with the isoconfigurational ${}^1\Sigma^+$ state as described for V_2 in the previous chapter. The interesting aspect of the ground state splittings in these molecules is their large magnitude. In the case of O_2, for example, there is similar second order spin-orbit coupling of the ${}^3\Sigma_g^-$ ground state and isoconfigurational ${}^1\Sigma_g^+$ state arising from the π_g^2 electron configuration. This interaction causes a splitting of only 3.96 cm^{-1} [181] in the ${}^3\Sigma_g^-$ ground state of O_2, while the splitting observed for the ${}^3\Sigma_g^-$ ground state of V_2 is 75 cm^{-1} [49]. This large size of the second order splitting can be attributed to near degeneracy: the energy of the ${}^1\Sigma_g^+$ state is of less than 2000 cm^{-1} above the ground state energy in V_2 [189,190] (see also chapter four), while the analogous ${}^1\Sigma_g^+$ state in O_2 has an energy of approximately 13000 cm^{-1} [181].

Theoretical methods have yet to be applied in detail to the ground state spin-orbit effects in V_2, VNb, and Nb_2, but a considerable body of relevant data has been gathered.

The large size of the ground state splitting in V_2 was first indicated by the abnormal structure of the band system identified as $A\,^3\Pi_u \leftarrow X^3\Sigma_g^-$ [49] that was discussed in the last chapter. The $\Omega' = 1 \leftarrow \Omega'' = 0$ band to the blue of the $\Omega' = 2 \leftarrow \Omega'' = 1$ and $\Omega' = 0 \leftarrow \Omega'' = 1$ bands. Under the usual assumption that first order spin-orbit splitting of the excited state is larger than second-order splitting of the ground state, the energies of these bands should be in order of increasing Ω'. An astute analysis by Langridge-Smith et al. [49] established that the ground state was responsible for the anomalous order, having a spin-orbit splitting almost as large as that of the excited state (75 cm^{-1} versus 80 cm^{-1}). As part of subsequent work on diatomic vanadium, Spain et al. proposed that the ground state spin-orbit splitting was caused by interaction with the isoconfigurational $^1\Sigma_g^+$ state [189], as supported by the results presented in the last chapter. As discussed there, empirical two state models were used to predict the energy of the perturbing state [189,190].

James et al. [190] determined the spin-orbit splitting of the $X\,^3\Sigma^-$ ground state of VNb to be 230 cm^{-1} by measuring the energy of photoionization from the $\Omega'' = 0$ and $\Omega'' = 1$ components of the ground state via a previously-identified [197] $^3\Sigma^-$ excited state. Given this value, the two-state matrix model described in chapter four was again used to predict the energy of the isoconfigurational $^1\Sigma^+$ state presumed to cause the splitting of the ground state. In this case the delta-symmetry MOs were assumed to be 50% V(3d) and 50% Nb(4d), allowing approximation of the coupling matrix element $\left\langle ^1\Sigma^+(0) \middle| \hat{H}_{S.O.} \middle| ^3\Sigma^-(0) \right\rangle$ as twice the average of $\zeta_{(n-1)d}$ for V and Nb. This led to a prediction of 1763.0 cm^{-1} for the energy of the isoconfigurational $^1\Sigma^+$ state. No experimental or theoretical evidence has been presented to corroborate or challenge this prediction.

In the case of Nb_2, James et al. made a prediction of 2375 cm^{-1} [190] for the energy of the isoconfigurational $^1\Sigma_g^+$ state in Nb_2 using the two-state matrix model. In separate work James, Kowalczyk, Fournier, and Simard [107] predicted an energy of 2834 cm^{-1} using second order perturbation theory. An excited state observed near 2450 cm^{-1} for Nb_2 in matrix-isolated resonance Raman work [199] was suggested by James et al. as a candidate for the $^1\Sigma_g^+$ state [190]. In order to make both of the above-mentioned predictions, a value of 410 cm^{-1} was assumed for the ground state spin-orbit splitting, based on matrix-isolated infrared absorption spectroscopy attributed to Li, Van Zee, and Weltner [190]. The assignment of this energy as the ground state spin-orbit splitting of Nb_2 is only tentative, however. Given the lack of any independent experimental corroboration of the value of 410 cm^{-1}, a theoretical prediction of the ground state spin-orbit splitting of Nb_2 would validate or challenge the results of Li et al.

There are thus several issues left open by the previous experimental studies of the ground state spin-orbit effects in the group 5 diatomics. The isoconfigurational mixing also proves to be convenient for analyzing correlation effects within the valence space. A semiempirical model like INDO/S includes some part of the dynamic correlation in the parameters since they are either taken directly from experimental atomic energy levels or fit to give agreement between calculated and experimental results [24,93,102,104,136]. This inclusion can be quite advantageous, but care must be taken to avoid “overcounting” the dynamic correlation by also including it explicitly with a correlation treatment such as configuration interaction [104]. Any essential correlation must be included by such means, however, and obtaining one without the other can be very difficult. In the calculations on V_2, for example, a large number of configurations had to be included to obtain a balanced description of both the ground and excited states. Some amount of dynamic correlation was thus included, and may contribute to the significant overestimation (120 cm^{-1} versus experimental 75 cm^{-1}) of the ground state spin-orbit splitting of V_2.

The isoconfigurational mixing in the group 5 diatomics affords an opportunity to isolate essential correlation. The $^1\Sigma^+$ and $X^3\Sigma^-$ states should experience very similar correlation effects because they are isoconfigurational. Configurations necessary for essential correlation of both states can thus be found by performing a large CI calculation and picking out those configurations that make significant contributions to the ground state wavefunction. A CI calculation using only those configurations will capture the essential correlation of both the $X^3\Sigma^-$ and $^1\Sigma^+$ states while minimizing explicit consideration of dynamic correlation. Since the sizes of the ground state spin-orbit splittings depend directly on the energies of the excited $^1\Sigma^+$ states, the computed size of the splittings can be compared to the experimentally-determined splittings to judge the accuracy of the calculated energies of the $^1\Sigma^+$ states. Furthermore, results obtained for the ground state splittings with full CI calculations and the smaller, "essential correlation only" CI calculations can be compared to evaluate the role of dynamic correlation. The results for the three examples considered here are clear: including only the essential correlations contributions leads to considerably better estimates of the energies of the $^{1}\Sigma^{+}$ states.

The apparent reliability of the energies obtained for the isoconfigurational $^{1}\Sigma^{+}$ states in each molecule allows an analysis of the predictions made by the simple empirical models described in chapter four. This analysis is important because similar empirical models have been used to predict state energies based on observed spin-orbit splittings in other diatomics. For example, Yang et al. [200] recently used a two state model at second order in $\hat{H}^{SO}$ to predict energies of $^{3}\Sigma_{u}^{+}$ and $^{2}\Sigma_{g}^{+}$ states perturbing the $X^{5}\Sigma_{u}^{-}$ and $X^{4}\Sigma_{g}^{-}$ ground states of Y_2 and Y_2^{+}, respectively. It is thus important to test the accuracy of these simple models by comparing results to those obtained at more rigorous levels of theory. An obvious question in this regard is whether or not excited states other than the isoconfigurational $^{1}\Sigma^{+}$ states contribute to the ground state spin-orbit splitting. Based on the highly multireference character of the ground state wavefunction obtained for V_2 in the last chapter, it is likely (and turns out to be the case) that other excited states do contribute to the splitting in each molecule. This has been investigated carefully.

A final issue addressed by the calculations reported in this chapter involves the electronic spectroscopy of VNb and Nb_2. While an in-depth analysis similar to that of chapter four has not been attempted, restricted active space full CI calculations accurately reproduce the energies and intensities of the two $^{3}\Sigma_{u}^{-} \leftarrow X^{3}\Sigma_{g}^{-}$ transitions observed for V_2 [49,189] and the $^{3}\Sigma^{-} \leftarrow X^{3}\Sigma^{-}$ transition observed for VNb [197]. A second

$^3\Sigma^- \leftarrow X^3\Sigma^-$ transition for VNb is predicted by the INDO/S calculations. Suggestions are made regarding the absence of experimental observation of this second transition. INDO/S results for the spectroscopy of Nb_2 bear little resemblance to the experimentally observed spectroscopy. This is disappointing since the experimental work on Nb_2 is much less definitive than the work on V_2 and VNb, without firm state assignments [107]. This failure can be attributed to the Slater-Condon factors, which are spectroscopic for the 3d metals and theoretical for the 4d metals.

Methodological Considerations and Empirical Models

INDO/S Calculations

The calculations on V_2, VNb, and Nb_2 are very similar to those described for V_2 in chapter four. All calculations were performed with the ZINDO software package [108] running on the Sun Enterprise 5000 server or IBM RS/6000 SP server of the Quantum Theory Project. The CI and SOCI calculations use the Rumer diagram method outlined in chapter two. Self-consistent field MOs suitable for use in the correlated calculations were obtained in a basis set consisting of the ns, np, and (n-1)d orbitals for each atom, $n = 4$ for vanadium and $n = 5$ for niobium. The parameters used for vanadium are from reference [92], while those for niobium are from reference [155]. Ground state SCF wavefunctions were obtained using the configuration averaged Hartree Fock (CAHF) formalism of Zerner [126] and the restricted open-shell Hartree Fock approach of Edwards and Zerner [123]. Problems with SCF convergence similar to those found for V_2 in chapter four occur for VNb and Nb_2 as well, but are again easily overcome with the CAHF method.

Empirical Models

The strategy employed in the simple two state empirical models described previously [189,190] is to write an expression for the perturbation of the $\Omega'' = 0$ level of the ground state by means of second order perturbation theory or 2×2 matrix diagonalization. The perturbation is set equal to the experimentally-measured splitting of the ground state in order to extract the energy of the excited state. This also requires an estimation of the perturbation of the excited state, which is equal to the perturbation of the ground state if the model is limited to just two states. It is also necessary to estimate the magnitude of the coupling of the ${}^3\Sigma_g^-(0)$ and ${}^1\Sigma_g^+(0)$ components over the spin-orbit operator. There are thus three important approximations in the two state model: estimation of the coupling term, order at which the perturbation theory is evaluated, and limitation to two states. Each of these approximations is considered in turn.

Evaluation of coupling matrix element with overlap, neutral diatomics

The δ-symmetry MOs of V_2, VNb, and Nb_2 are assumed to be completely localized in the two-state models of Spain et al. [189] and James et al. [190], but the results of chapter four indicate that these are partially delocalized and have nonzero overlap. The coupling matrix element V_{12} was estimated assuming zero overlap to make connection with the previous work [189,190], but this limitation is easily removed. The obvious approach is to simply use expressions (4-1) and (4-2) for the $\left|\delta_g^+\right\rangle$ and $\left|\delta_g^-\right\rangle$ MOs, assuming the overlap integral S is nonzero, in equation (4-7). Doing so leads to the coupling matrix element

$$V_{12} = \frac{2\zeta_{(n-1)d}}{1+S} \qquad (5\text{-}1)$$

This ignores, however, localization of the $\left|\delta_g^+\right\rangle$ MOs by extensive mixing of the $(d\pi_u)^4(d\sigma_g)^2(s\sigma_g)^2(d\delta_g)^2$ and $(d\pi_u)^4(d\sigma_g)^2(s\sigma_g)^2(d\delta_u)^2$ configurations found for V_2. In this section an expression for V_{12} that properly accounts for the partial localization in the δ orbitals is developed.

The first step is to form spin-adapted linear combinations of Slater determinants representing the $\Omega = 0$ singlet and triplet components of Σ symmetry for the two configurations:

$$^3\Phi_0 = \frac{1}{\sqrt{2}}\left(\left|\delta_g^+\alpha\delta_g^-\beta\right| + \left|\delta_g^+\beta\delta_g^-\alpha\right|\right) \tag{5-2}$$

$$^3\Phi_0' = \frac{1}{\sqrt{2}}\left(\left|\delta_u^+\alpha\delta_u^-\beta\right| + \left|\delta_u^+\beta\delta_u^-\alpha\right|\right) \tag{5-3}$$

$$^1\Phi_0 = \frac{1}{\sqrt{2}}\left(\left|\delta_g^+\alpha\delta_g^-\beta\right| - \left|\delta_g^+\beta\delta_g^-\alpha\right|\right) \tag{5-4}$$

$$^1\Phi_0' = \frac{1}{\sqrt{2}}\left(\left|\delta_u^+\alpha\delta_u^-\beta\right| - \left|\delta_u^+\beta\delta_u^-\alpha\right|\right) \tag{5-5}$$

The gerade molecular orbitals in equations (5-2) and (5-4) are given by equations (4-1) and (4-2), and the antibonding ungerade orbitals by

$$\left|\delta_u^+\right\rangle = \frac{1}{\sqrt{2}\sqrt{1-S}}\left(\left|2+2\right\rangle^A - \left|2+2\right\rangle^B\right) \tag{5-6}$$

$$\left|\delta_u^-\right\rangle = \frac{1}{\sqrt{2}\sqrt{1-S}}\left(\left|2-2\right\rangle^A - \left|2-2\right\rangle^B\right) \tag{5-7}$$

The wavefunctions for the $X^3\Sigma^-(0)$ and $^1\Sigma^+(0)$ components are taken as linear combinations of the triplet and singlet configurations, respectively:

$$\Psi\left(X^3\Sigma^-(0)\right) = {}^3C_1\,{}^3\Phi_0 + {}^3C_2\,{}^3\Phi'_0 \tag{5-8}$$

$$\Psi\left({}^1\Sigma^+(0)\right) = {}^1C_1\,{}^1\Phi_0 + {}^1C_2\,{}^1\Phi'_0 \tag{5-9}$$

If the δ orbitals were completely localized (as would be the case if $S = 0$), ${}^3C_1$ would carry the value $\frac{1}{\sqrt{2}}$ and ${}^3C_2$ would be $-\frac{1}{\sqrt{2}}$, for example. If S is not equal to zero, as indeed is the case for V_2, VNb, and Nb_2, $\left|{}^3C_1\right|$ would be larger than $\frac{1}{\sqrt{2}}$ and $\left|{}^3C_2\right|$ would be smaller, with the size of the ratio $\left|{}^3C_1\right|/\left|{}^3C_2\right|$ increasing as S increases. Similar considerations apply to ${}^1C_1$ and ${}^1C_2$.

The coupling of the two states over the spin-orbit operator can now be determined by expanding the Slater determinants in terms of the atomic orbitals that make up the molecular orbitals, and evaluating the resulting matrix elements. Alternatively, the Rumer diagram technique of chapter two can be used. It is again assumed that two-center radial integrals are negligible, as discussed in chapter two. Since the $X^3\Sigma^-$ and ${}^1\Sigma^+$ states are isoconfigurational, it is reasonable to assume that the extent of localization is similar in the two states, and therefore

$${}^3C_1 = {}^1C_1 \equiv C_1 \tag{5-10}$$

$${}^3C_2 = {}^1C_2 \equiv C_2 \tag{5-11}$$

With these two assumptions, the coupling term is given by

$$\left\langle \Psi\left(X^3\Sigma^-(0)\right)\middle|\hat{H}_{S.O.}\middle|\Psi\left({}^1\Sigma^+(0)\right)\right\rangle = 2\zeta_{(n-1)d}\left[\frac{C_1^2}{(1+S)} + \frac{C_2^2}{(1-S)}\right] \tag{17}$$

This equation reduces to the value of $2\zeta(d)$ used by James et al. [190] and Spain et al. [189] when the overlap is zero, since the CI states are orthonormal, but is more general since it is also applicable when S is nonzero.

Order of perturbation expansion

The discussion of order of the perturbation expansion found in the previous chapter is summarized here for completeness. At second order the perturbation of the ground state is

$$\Delta_1 = \sum_{i=2}^{n} \frac{V_{1i}^2}{E_1^{(0)} - E_i^{(0)}} \tag{5-13}$$

(analogous to equation (4-27)) where Δ_1 is the perturbation of the $\Omega'' = 0$ component of the ground state, $E_i^{(0)}$ is the unperturbed energy of the ith level, and V_{1i} is the coupling of the ground level and the ith excited level over the spin-orbit operator. The number of states considered in the model, n in equation (5-13), is limited to two in the treatments of Spain et al. [189] and James et al. [190]. In the following discussion, it is assumed that the i = 2 level is the a $^1\Sigma_g^+(0)$ component. The perturbation of this level is given by

$$\Delta_2 = \sum_{i\neq 2}^{n} \frac{V_{2i}^2}{E_2^{(0)} - E_i^{(0)}} \tag{5-14}$$

If n is limited to two, Δ_1 and Δ_2 are equal in magnitude but opposite in sign:

$$\Delta = -\Delta_1 = \Delta_2 = \frac{V_{12}^2}{E_2^{(0)} - E_1^{(0)}} \tag{5-15}$$

With these definitions, the energy of the excited level is then

$$E_2^{(0)} - E_1^{(0)} + 2\Delta = \frac{V_{12}^2 + 2\Delta^2}{\Delta} \tag{5-16}$$

An expression analogous to equation (5-16) that is correct through infinite order in the spin-orbit perturbation was obtained by diagonalization of a 2×2 matrix, giving

$$E_2^{(0)} - E_1^{(0)} + 2\Delta = \frac{V_{12}^2 + \Delta^2}{\Delta} \tag{5-17}$$

which is smaller than the second-order expression by Δ, the spin-orbit splitting of the ground state. This error ranges from 75 cm^{-1} for V_2 to 410 cm^{-1} for Nb_2.

Extension to four states at second order

The effect of including additional excited levels is illustrated at second order by incorporating two excited levels arising from double excitation of electrons from the 4sσ orbital to the 4sσ^* orbital. For V_2 this configuration is predicted to lie within three eV of the ground state according to the previous INDO/S calculations of chapter four. The two state model as formulated above included the levels $X^3\Sigma_g^-(0)$ and $^1\Sigma_g^+(0)$, both taken as properly spin-adapted CSFs derived from the $(d\pi_u)^4(d\sigma_g)^2(s\sigma_g)^2(\delta_g)^2$ configuration. The new levels are denoted as $C^3\Sigma_g^-(0)$ and $c^1\Sigma_g^+(0)$, and are derived from the configuration $(d\pi_u)^4(d\sigma_g)^2(\delta_g)^2(s\sigma_u)^2$. Zero overlap (and hence no amount of delocalization) is assumed, as in the models of Spain et al. [189] and James et al. [190]. Though a more complicated model could be formulated, overlap is neglected here so that the effects of adding additional states and of including overlap can be evaluated separately.

The four levels included in the model are referred to in the following perturbation expansions as:

$$\Psi_1 = X^3\Sigma_g^-$$

$$\Psi_2 = {}^1\Sigma_g^+$$

$$\Psi_3 = C^3\Sigma_g^-$$

$$\Psi_4 = c^1\Sigma_g^+ \tag{5-18}$$

Through second order the perturbations of the ground and first excited state are given by equations (5-13) and (5-14) as

$$\Delta_1 = -75\,\mathrm{cm}^{-1} = \frac{V_{12}^2}{E_1^{(0)} - E_2^{(0)}} + \frac{V_{13}^2}{E_1^{(0)} - E_3^{(0)}} + \frac{V_{14}^2}{E_1^{(0)} - E_4^{(0)}} \tag{5-19}$$

$$\Delta_2 = \frac{V_{12}^2}{E_2^{(0)} - E_1^{(0)}} + \frac{V_{23}^2}{E_2^{(0)} - E_3^{(0)}} + \frac{V_{24}^2}{E_2^{(0)} - E_4^{(0)}} \tag{5-20}$$

The goal is to extract the energy difference $\Delta E = E_2^{(0)} - E_1^{(0)} + \Delta_2 - \Delta_1$ from equations (5-19) and (5-20).

Estimates of the energies of the $C^3\Sigma_g^-$ and $c^1\Sigma_g^+$ states and the additional coupling terms V_{13}, V_{14}, V_{23}, and V_{24} are required to proceed. To obtain these estimates a simple configuration interaction treatment is considered. INDO/S triplet CI calculations on each molecule limited to the configurations $(d\pi_u)^4(d\sigma_g)^2(s\sigma_g)^2(\delta_g)^2$ and $(d\pi_u)^4(d\sigma_g)^2(\delta_g)^2(s\sigma_u)^2$ are used to obtain the energy of the $C^3\Sigma_g^-$ state, which is represented by $E_3^{(0)}$ in equations (5-19) and (5-20). Other details of these calculations are as described in chapter four. Assuming the INDO approximation, the difference in singlet state energies is equal to the difference in triplet state energies, allowing the following assumptions:

$$E_1^{(0)} = 0 \tag{5-21}$$

$$E_4^{(0)} = E_3^{(0)} + E_2^{(0)} \tag{5-22}$$

The coupling terms are trivial since the CSFs differ only in occupation of doubly occupied orbitals, which do not contribute to spin-orbit effects, and the coupling of the δ_g orbitals was evaluated previously. States of the same multiplicity have no coupling, since these are first order effects (shown to be zero in chapter four). The singlet-triplet couplings reduce to V_{12} as previously evaluated (equation (4-8)). Therefore the coupling terms reduce to

$$V_{12} = V_{14} = V_{23} = 2\zeta_{(n-1)d} \tag{5-23}$$

$$V_{13} = V_{24} = 0 \tag{5-24}$$

Substitution of equations (5-21) through (5-24) into equation (5-19) yields

$$-\Delta_1 = 75\,\text{cm}^{-1} = \frac{V_{12}^2}{E_2^{(0)}} + \frac{V_{12}^2}{E_3^{(0)} + E_2^{(0)}} \tag{5-25}$$

which upon rearrangement yields

$$\left[E_2^{(0)}\right]^2 + \left(E_3^{(0)} + \frac{2V_{12}^2}{\Delta_1}\right)E_2^{(0)} + \frac{V_{12}^2 E_3^{(0)}}{\Delta_1} = 0 \tag{5-26}$$

This quadratic equation in $E_2^{(0)}$ can be solved algebraically to yield two roots. Neglect of the negative root gives an estimate for $E_2^{(0)}$. To obtain the final prediction for ΔE, Δ_2

must be considered. since in this four state model $\Delta_2 \neq \Delta_1$. To obtain a value for Δ_2 equations (5-21) through (5-24) are substituted into equation (5-20), giving

$$\Delta_2 = \frac{V_{12}^2}{E_2^{(0)}} + \frac{V_{12}^2}{E_2^{(0)} - E_3^{(0)}} \tag{5-27}$$

Substitution of the values of V_{12}, $E_2^{(0)}$(from equation (5-26)), and $E_3^{(0)}$ yields a value for Δ_2 that can be combined with $E_2^{(0)}$ and Δ_1 to yield ΔE.

Results and Discussion

Self-Consistent Field Ground States

The SCF ground state for each molecule was obtained by first refining the starting orbitals with CAHF calculations, then using those orbitals as the initial guess for "standard" triplet ROHF calculations with two open-shell orbitals. In all three cases the first step was to allow double occupancy of the three most stable orbitals in the manifold, the dπ orbitals and lowest-lying σ orbital, and use the remaining fifteen orbitals and four electrons in the averaging procedure. The resulting orbitals provided the starting point for the ROHF calculations, in which the dπ, dσ and sσ bonding MOs were doubly occupied, and the δ bonding orbitals were singly-occupied. These ROHF calculations converged very quickly to the $X^3\Sigma^-$ ground state of each diatomic molecule. Triplet ROHF calculations on all three molecules display extremely pathological nonconvergence behavior when attempted without the initial CAHF calculations, which is a demonstration of the utility of an averaging procedure like CAHF for converging difficult ground states. The ROHF orbitals obtained as described above were used in all subsequent CI calculations.

Table 5-1 lists the results of the ROHF calculations for V_2, VNb, and Nb_2, along with the results of DFT calculations on V_2 and Nb_2 [107] for comparison. Additionally, orbital ionization potentials (IPs) determined experimentally for ejection of an electron from the highest-lying σ_g orbital are included, which can be compared to the orbital energies obtained from the two methods according to Koopmans' approximation [80]. The much greater reliability of the INDO/S molecular orbital calculations in estimating the orbital IPs is obvious in the table, especially for V_2. The results for VNb and Nb_2 do not agree as well with experiment, but in the case of Nb_2 are still considerably better than the DFT estimate.

The INDO/S value for the IP of V_2 is in better agreement with experiment than the INDO/S values for VNb and Nb_2 because of the way the two-electron integrals are constructed. For the 3d metals (e.g. vanadium) the Slater-Condon factors were fit to reproduce the atomic energy levels [164], while those for 4d metals (e.g. niobium) are calculated over the INDO/S basis set [155]. The former procedure is much more effective for approximating orbital IPs. The accuracy of the calculated IP of V_2 is somewhat fortuitous, since Koopmans' approximation neglects orbital relaxation effects. The errors in the INDO/S IPs for VNb and Nb_2 can in part be attributed to this neglect, as orbital relaxation can be very large for transition metal dimers. Consider for example the case of Mn_2 and Mn_2^+, which have ${}^1\Sigma_g^+$ and ${}^{12}\Sigma_g^+$ ground states, respectively [58,60]. Both INDO/S and DFT yield closed-shell orbital energies in the order $d\pi_u$, $d\sigma_g$, $s\sigma_g$ for V_2 and VNb, and $d\pi_u$, $s\sigma_g$, $d\sigma_g$ for Nb_2 (table 5-1). The reversal in Nb_2 can be attributed

Table 5-1. Compositions and orbital energies of INDO/S molecular orbitals from the ROHF ground states of V_2, VNb, and Nb_2. DFT results for VNb and Nb_2 (reference 107) shown in parentheses for comparison. Small contributions from p orbitals are omitted.

Molecule	V_2			**VNb**			Nb_2		
Orbital	Composition (%)		**Energy (eV)**	Composition (%)		**Energy (eV)**	Composition (%)		**Energy (eV)**
	3d	4s		d	s		4d	5s	
$d\pi_u$[a]	92 (98)	0 (0)	-8.09 (-5.18)	92	0	-8.81	93 (99)	0 (0)	-8.81 (-5.42)
$d\sigma_g$	96 (54)	3 (42)	-7.13 (-5.00)	55	43	-7.79	90 (74)	8 (25)	-7.25 (-4.27) Exp. –6.37[d]
$s\sigma_g$	3 (47)	97 (52)	-6.36 (-4.03) Exp. –6.36[d]	40	60	-7.55 Exp. –6.39[d]	7 (34)	91 (66)	-8.36 (-5.07)
δ_g[b]	100 (100)	0 (0)	-6.86 (-3.89)	100	0	-7.81			-7.93 (-4.10)
$s\sigma_u$[c]	0 (0)	96 (91)	-1.85 (-2.31)	2	81	-3.09	1 (12)	83 (86)	-3.91 (-2.72)
δ_u[c]	100 (100)	0 (0)	-0.61 (-2.09)	100	0	-2.11	100 (100)	0 (0)	-2.55 (-2.30)
$d\sigma_u$[c]	67	2	+1.64 (--)	94	0	-0.13	94	0	-0.79 (--)
$d\pi_g$[c]	64 (88)	0 (0)	+3.18 (-1.19)	52	0	+1.75	65 (98)	0 (0)	+1.36 (-1.31)

[a] The g and u labels serve only to distinguish the bonding and antibonding combinations in the case of VNb.

[b] Energies of open-shell ROHF orbitals do not correspond to ionization potentials, so should not be compared directly to the closed-shell orbital energies.

[c] Orbital energies relative to the energy of the open-shell δ_g orbitals.

[d] Reference 112.

to stronger bonding character for the $s\sigma_g$ orbital in Nb_2 due to larger coupling of the one-electron matrix elements for the niobium 5s orbitals. In V_2 and VNb the $s\sigma$ bonding interaction is quite weak, despite the large overlap of the s orbitals, leading to a need for extensive correlation of the $s\sigma$ orbitals in V_2 and VNb. This very interesting aspect of the bonding in transition metal dimers is discussed in greater detail below, in connection with the correlated calculations.

There is qualitative similarity between the forms of the INDO/S and DFT orbitals. One distinct difference, however, is that the INDO/S σ_g orbitals of V_2 and Nb_2 are far less hybridized than the DFT orbitals. The INDO/S orbitals for VNb are considerably more hybridized, though the 1σ and 2σ orbitals are still distinctly of $d\sigma$ and $s\sigma$ character, respectively. This difference in hybridization between VNb on one hand and V_2 and Nb_2 on the other likely arises because of differences in s-d sigma overlap. In the latter two cases, the magnitude of the s-d sigma overlap is 0.001 and 0.008, respectively. These small values are found because the large s orbitals overlap significantly with the torus as well as the lobe of the d_{z^2} orbital on the neighboring atom. In VNb, however, the 4s-$4d\sigma$ overlap is 0.036 in magnitude, and the $3d\sigma$-5s overlap is 0.021. These larger values are due to a combination of the differing sizes of the vanadium and niobium orbitals, and the bond length of VNb that is intermediate between those of V_2 and Nb_2. When considering s-d hybridization of the σ orbitals it is important to recall that all ground states are highly correlated, and configurations involving both σ_g orbitals mix strongly with the reference configuration. The DFT orbitals might be a better representation than the (uncorrelated) INDO/S SCF MOs of the s-d hybridization in the σ orbitals, since the functionals used in obtaining the DFT orbitals inherently include some correlation effects.

Configuration Interaction Calculations

One purpose of this work is to design a CI treatment that captures most of the essential correlation of the ground state and isoconfigurational $^1\Sigma^+$ state of each molecule, while minimizing explicit (i.e. not already present in the parameters) consideration of dynamic correlation. It is thus important to include only those excited configurations that make substantial contributions to the two states, since these configurations incorporate the essential correlation. The straightforward way to identify the appropriate configurations would be to perform a full CI calculation in the entire valence space and select all configurations with expansion coefficients above a certain reasonable limit in the ground state wavefunction. Although attractive in its simplicity, calculations of this size are intractable with the Rumer-diagram valence bond structure CI code used in the present implementation of INDO/S, and do not appear to be necessary in any case.

A well-defined procedure for selecting an appropriate active space was developed in chapter four based on orbital localization. In a CI treatment, complete localization of an MO entails equal distributions of electrons in the bonding and antibonding MOs in the ground state. This causes cancellation of bonding character and leaves a proper quantum mechanical average of determinants involving the atomic orbitals. The size of population of the antibonding MO in the CI ground state is therefore a direct measure of the extent of localization, which varies for orbitals of different symmetry since the σ, π, and δ combinations have different overlaps. In the last chapter, for example, a CI calculation including only the dπ orbitals and electrons showed that these orbitals experience very little localization in V_2, and could safely be left out of the active space. Applying the same procedure to the orbitals of VNb and Nb_2 will allow active spaces tailored to correlation effects in each molecule to be established.

Based on these considerations, the strategy employed here has three steps. In the first, small CI calculations are performed using the ns and (n-1)d orbitals of each symmetry separately, and populations of the antibonding MOs are computed in each case. In the second step, restricted active space full CI calculations are carried out using active spaces containing those orbitals found to be significantly localized in the first step. For V_2, for example, the dσ_g, sσ_g, δ_g, δ_u, sσ_u, and dσ_u orbitals are correlated in this step. Finally, since the specific interest is in essential correlation of the ground state, the configurations making significant contributions to the ground states found in the second step are selected, and smaller CI calculations using only these configurations are performed. The ground state spin-orbit splittings computed in steps two and three are then compared to judge the effect of the dynamic correlation that is included in the larger calculations. Results for each step of the process are described in the following three sections.

Selection of active spaces

Orbital populations for each molecule computed from CI wavefunctions obtained using active spaces restricted by orbital symmetry are shown in table 5-2. It should again be emphasized that this represents three CI calculations for each molecule, involving the σ, π, and δ orbitals separately. When selecting active spaces, only those MOs with antibonding orbital populations greater than 0.05 electrons per pair of electrons in the

Table 5-2. Populations of the MOs listed in table 5-1 from full CI calculations using the orbitals of each symmetry as active spaces.

Orbital	Population, V_2	VNb	Nb_2
$d\pi_u$[a]	3.92	3.95	3.96
$d\sigma_g$	1.94	1.92	1.86
$s\sigma_g$	1.87	1.89	1.98
$d\delta_g$	1.62	1.71	1.84
$d\delta_u$	0.39	0.29	0.16
$s\sigma_u$	0.13	0.06	0.04
$d\sigma_u$	0.07	0.13	0.12
$d\pi_g$	0.08	0.05	0.04

[a] The subscripts *g* and *u* are not applicable in the case of VNb, other than to signify the bonding and antibonding combinations.

bonding MO(s) are included in the active space. It is important to note that this is 0.10 electrons for the $d\pi^*$ MOs since there are four electrons in the dπ orbitals in the reference configuration. Complete localization would require a population of two electrons in the antibonding π orbitals, whereas the bonding σ and δ orbitals each would be localized by a population of only one electron in the antibonding orbitals.

In the case of V_2, the δ-symmetry antibonding orbitals and both the 4sσ and 3dσ antibonding orbitals have electron populations larger than the limit set above, but the dπ antibonding orbitals do not (table 5-2). For V_2, then, the active space selected consists of the eight dσ, sσ, and dδ orbitals. Similar results are seen for VNb (table 5-2), with a very small $d\pi_g$ population and more significant populations of the $d\delta_u$, $s\sigma_u$, and $d\sigma_u$ orbitals. The population of the $d\sigma_u$ orbital is larger in VNb than in V_2, while the opposite is true of the sσ_u populations in the two molecules. This is interesting at first sight, but the differences in hybridization of the σ orbitals in the two molecules (see table 5-1) complicates this observation. The total population of the σ_u orbitals is very similar in the two molecules, 0.20 for V_2 and 0.19 for VNb, which is not surprising because the σ overlaps are similar for the two molecules (sσ overlap is 0.696 for V_2 and 0.664 for VNb; dσ overlap is 0.113 for V_2 and 0.114 for VNb). This similarity is caused by a cancellation of smaller overlap due to the increased bond length of VNb and larger overlap due to the larger size of the niobium atomic orbitals. Subsequent calculations on VNb include the eight σ and δ orbitals in the active space.

The total population of the σ_u orbitals is slightly smaller in Nb_2 than in V_2 and VNb. This follows the trend in orbital overlaps, as the sσ overlap is similar in the three molecules, and the dσ overlap in Nb_2 (0.122) is similar to but larger than these overlaps in V_2 and VNb (0.113 and 0.114, respectively). The major difference in the orbital populations of Nb_2 compared to those in the other two molecules is that the sσ_g orbital loses very few electrons, and the sσ_u orbital gains only a very small population. The active space for Nb_2 is limited to the six dσ and dδ orbitals.

The correlation of the sσ orbitals in the three molecules is very interesting. These corrections are clearly not orbital localization corrections because the orbital overlaps are quite large, on the order of 0.70 for each molecule. Nevertheless, substantial occupations of the sσ_u orbitals are found in V_2 and VNb (0.13 and 0.06, respectively). Only in the case of Nb_2 is the population of the antibonding orbital small enough (0.04) to justify excluding the sσ orbitals from the treatment of essential correlation. In the following discussion V_2 and Nb_2 are compared, with the understanding that VNb is intermediary. The large essential correlation of the sσ orbitals is necessary for V_2 because the 4s-4s interaction is very weak, while the 5s-5s interaction in Nb_2, while still weak, is considerably stronger. This is due to the weakly-bound nature of transition metal ns orbitals compared to (n-1)d oritals, and the much larger radial extent of the ns orbitals. Both effects are more pronounced for 3d metals than for 4d metals.

The weakly bound nature of ns orbitals compared to (n-1)d orbitals is demonstrated by bonding and antibonding σ orbitals of a homonuclear diatomic molecule formed using the ns and (n-1)d orbitals. The difference in the energies of the σ_g and σ_u orbitals is a direct measure of the strength of the interaction between the atomic orbitals. Assuming single occupancy, the energy difference $\Delta E = E(\sigma_g{}^0\sigma_u{}^1) - E(\sigma_g{}^1\sigma_u{}^0)$ depends only on one-electron integrals $H_{\mu\nu}$. Invoking the INDO/S approximation for these integrals gives ΔE as

$$\Delta E = -2\beta S \tag{5-28}$$

where S is the overlap and β is the resonance integral. Here βS represents the two-center one electron matrix element described in chapter two,

$$H_{\mu\nu}^{AB} = \frac{1}{2}\left(\beta_\mu^0 + \beta_\nu^0\right)S_{\mu\nu} \tag{5-29}$$

The strength of the interaction of the orbitals is therefore directly related to the size of the one electron parameter β^0, which is much larger for (n-1)d orbitals in the INDO/S parameterization. For vanadium, for example, β_{3d}^0 is –20.0 eV, and β_{4s}^0 is -1.0 eV, a situation that reflects the fact that the 4s orbital is much more diffuse and penetrates into the vicinity of the nucleus much less effectively than the 3d orbitals. This effect is more pronounced for 3d metals, because in general β^0_{5s} is larger than β^0_{4s}, and β^0_{4d} is smaller than β^0_{3d}. With niobium as an example, β^0_{5s} is –2.0 eV and β^0_{4d} is –13.0 eV. When comparing the 4sσ and 3dσ interactions in V_2, the combination of larger overlap and smaller β^0 in the former leads to interactions of similar strength. In Nb_2 the 5sσ interaction is stronger than the 4dσ interaction, however, due to the larger size of β^0_{5s} relative to β^0_{4d}.

This picture is complicated by the large differences in the radial extents of ns and (n-1)d orbitals, table 5-3, discussed in detail in chapter one. When the (n-1)d orbitals are partially filled and thus available for bonding, bond distances approach the optimum range for d-d interactions. This distance is much shorter than the optimum distance for s-s interaction due to the much more compact size of the d orbitals. The expectation value of r for the 4s orbital of vanadium, $\langle r_{4s} \rangle$, is significantly larger than the bond

Table 5-3. Comparison of orbital sizes for vanadium and niobium and bond distances of homonuclear diatomic molecules.

Quantity	V	Nb
$\langle r_{ns} \rangle$ (Å)	1.83	2.09
$\langle r_{(n-1)d} \rangle$ (Å)	0.68	0.97
$\frac{\langle r_{ns} \rangle}{\langle r_{(n-1)d} \rangle}$	2.69	2.15
Bond distance, M_2 (Å)	1.766[a]	2.078[b]

[a] Reference [49].
[b] Reference [107].

distance of V_2, in fact. That being the case, it is not surprising that the 4s orbitals interact weakly in V_2, which can be thought of as behavior that is incipiently Rydberg-like. Here too the effect is more pronounced for 3d metals, since $\left\langle r_{ns} \right\rangle / \left\langle r_{(n-1)d} \right\rangle$ is larger for 3d metals than for 4d metals. This behavior contrasts with what is typically observed for transition metal complexes, in which the bond distances are within the optimum range for interaction of the ns orbitals and the ligand orbitals, and are too long for strong overlap with the (n-1)d orbitals. The success of "d orbital-only" models based on ligand field theory relies on this. The bonding in metal diatomics is richer, however, and requires a more sophisticated approach.

Restricted active space full CI

The active spaces chosen based on the orbital populations listed in table 2 are the sσ, dσ, and dδ orbitals for V_2 and VNb, and the dσ and dδ orbitals for Nb_2. Configurations contributing to the ground states obtained with full CI calculations in these active spaces are listed in tables 5-4 through 5-6. All configurations with coefficients of magnitude greater than or equal to 0.01 are listed. The size of the coefficient of the leading determinant is smaller for V_2 than it is for Nb_2, indicating a higher degree of multireference character for the former. This is expected because localization and near-degeneracy effects are known to be larger in the 3d metals [23,24]. The results for VNb are similar to those obtained for V_2, with a slightly larger leading coefficient and a similar number of excited configurations mixing with the ground state. There are in fact a larger number of configurations contributing to the ground state of VNb, which might arise due to the richer s-d sigma hybridization found for VNb.

Table 5-4. Configurations contributing to the $X^3\Sigma_g^-$ ground state of V_2 from full CI in the σ and δ MOs listed for V_2 in table 5-1. All configurations with coefficients of magnitude greater than 0.01 are listed.

Configuration	$\left\|C_i\right\|^2$
$(d\pi_u)^4(d\sigma_g)^2(s\sigma_g)^2(\delta_g)^2$	0.773
$(d\pi_u)^4(d\sigma_g)^2(s\sigma_g)^2(\delta_u)^2$	0.095
$(d\pi_u)^4(d\sigma_g)^2(\delta_g)^2(s\sigma_u)^2$	0.031
$(d\pi_u)^4(s\sigma_g)^2(\delta_g)^2(d\sigma_u)^2$	0.011
$(d\pi_u)^4(d\sigma_g)^2(s\sigma_u)^2(\delta_u)^2$	0.008
$(d\pi_u)^4(s\sigma_g)^2(\delta_u)^2(d\sigma_u)^2$	0.004
$(d\pi_u)^4(d\sigma_g)^1(s\sigma_g)^2(\delta_g)^1(s\sigma_u)^1(\delta_u)^1$	0.013
$(d\pi_u)^4(d\sigma_g)^1(s\sigma_g)^1(\delta_g)^2(s\sigma_u)^1(d\sigma_u)^1$	0.003
$(d\pi_u)^4(s\sigma_g)^2(\delta_g)^2(\delta_u)^2$	0.006
$(d\pi_u)^4(d\sigma_g)^2(s\sigma_g)^1(\delta_g)^1(s\sigma_u)^1(\delta_u)^1$	0.011
$(d\pi_u)^4(\delta_g)^2(s\sigma_u)^2(d\sigma_u)^2$	0.001
$\Sigma\left\|C_i\right\|^2$	0.965

It is interesting to consider the Σ-symmetry excited states of V_2 and VNb. Two excited states of Σ symmetry have been observed for V_2. The transition $A'^3\Sigma_u^- \leftarrow X^3\Sigma_g^-$ was observed and assigned by Spain et al. [189]. Two spin-orbit components of the upper state were found at 11811 cm^{-1} and 11899 cm^{-1}. The second was originally observed by

Table 5-5. Configurations contributing to the $X^3\Sigma^-$ ground state of VNb from full CI in the σ and δ MOs listed for VNb in table 5-1. All configurations with coefficients of magnitude greater than 0.01 are listed.

Configuration	$\lvert C_i \rvert^2$
$(d\pi)^4(d\sigma)^2(s\sigma)^2(\delta)^2$	0.778
$(d\pi)^4(d\sigma)^2(s\sigma)^2(\delta^*)^2$	0.075
$(d\pi)^4(d\sigma)^2(\delta)^2(s\sigma^*)^2$	0.012
$(d\pi)^4(d\sigma)^2(\delta)^2(d\sigma^*)^2$	0.010
$(d\pi)^4(s\sigma)^2(\delta)^2(d\sigma^*)^2$	0.008
$(d\pi)^4(d\sigma)^1(s\sigma)^2(\delta)^1(s\sigma^*)^1(\delta^*)^1$	0.020
$(d\pi)^4(d\sigma)^2(s\sigma)^1(\delta)^2(s\sigma^*)^1$	0.007
$(d\pi)^4(d\sigma)^1(s\sigma)^2(\delta)^2(s\sigma^*)^1$	0.007
$(d\pi)^4(d\sigma)^2(\delta)^2(s\sigma^*)^1(d\sigma^*)^1$	0.004
$(d\pi)^4(s\sigma)^2(\delta)^2(\delta^*)^2$	0.006
$(d\pi)^4(d\sigma)^1(s\sigma)^1(\delta)^2(s\sigma^*)^2$	0.003
$(d\pi)^4(s\sigma)^2(\delta^*)^2(d\sigma^*)^2$	0.003
$(d\pi)^4(d\sigma)^2(\delta^*)^2(d\sigma^*)^2$	0.002
$(d\pi)^4(d\sigma)^2(s\sigma^*)^2(\delta^*)^2$	0.001
$(d\pi)^4(s\sigma)^2(\delta)^2(s\sigma^*)^2$	0.001
$\Sigma \lvert C_i \rvert^2$	0.936

Table 5-6. Configurations contributing to the $X^3\Sigma_g^-$ ground state of Nb_2 from full CI in the dσ and δ MOs listed for Nb_2 in table 5-1. All configurations with coefficients of magnitude greater than 0.01 are listed.

Configuration	$\left\|C_i\right\|^2$
$(d\pi_u)^4(s\sigma_g)^2(d\sigma_g)^2(\delta_g)^2$	0.864
$(d\pi_u)^4(s\sigma_g)^2(d\sigma_g)^2(\delta_u)^2$	0.059
$(d\pi_u)^4(s\sigma_g)^2(\delta_g)^2(d\sigma_u)^2$	0.040
$(d\pi_u)^4(s\sigma_g)^2(d\sigma_g)^1(\delta_g)^1(\delta_u)^1(ds\sigma_u)^1$	0.019
$(d\pi_u)^4(s\sigma_g)^2(\delta_u)^2(d\sigma_u)^2$	0.005
$(d\pi_u)^4(s\sigma_g)^2(\delta_g)^2(\delta_u)^2$	0.002
$\Sigma\left\|C_i\right\|^2$	0.990

Langridge-Smith et al. [49] close to 15000 cm^{-1}, but was assigned only as an $\Omega' = 1 \leftarrow \Omega'' = 1$ transition. This excited state was later assigned as $B^3\Sigma_u^-$ in chapter four. For VNb, James et al. [197] observed and assigned a $^3\Sigma^- \leftarrow X^3\Sigma^-$ transition with excited state spin-orbit components at 15625 cm^{-1} and 15689 cm^{-1}. Although two states of Σ symmetry were found for V_2, a second excited Σ state was not found for VNb, even though a range of energies between approximately 11100 cm^{-1} and 18350 cm^{-1} was scanned.

The CI calculations that gave the ground states listed in tables 5-4 and 5-5 also give two allowed $^3\Sigma^- \leftarrow X^3\Sigma^-$ transitions for both molecules (table 5-7). For V_2, the

Table 5-7. Energies of ${}^3\Sigma^- \leftarrow X^3\Sigma^-$ transitions of V_2 and VNb. All values in cm^{-1}.

Transition	V_2		VNb	
	Calculated[a]	Experiment	Calculated[a]	Experiment
$A'^3\Sigma^- \leftarrow X^3\Sigma^-$	11982	11811, 11899[b,c]	15537	15625, 15689[c,e]
$B^3\Sigma^- \leftarrow X^3\Sigma^-$	14262	~15000[d]	17081	?

[a] Spin-orbit coupling not included.
[b] Reference [189].
[c] Energies of the $\Omega' = 0$ and $\Omega' = 1$ components of the upper state.
[d] $\Omega' = 1 \leftarrow \Omega'' = 1$ transition, reference [49].
[e] Reference [197].

calculated energies are 11982 cm^{-1} and 14262 cm^{-1}, in good agreement with the experimental results [49,189]. As described in more detail in the last chapter, the intensities of the transitions from the ground state into these ${}^3\Sigma_u^-$ states show a trend that agrees with the experimental trend [49,189]. In the case of VNb, the lower-lying ${}^3\Sigma^-$ state is found at 15537 cm^{-1} by the calculations, again in close agreement with experiment. The second ${}^3\Sigma^-$ state of VNb is predicted by these calculations to have an energy of 17081 cm^{-1}, well within the energy range scanned by James et al. There is thus a discrepancy between theory and experiment regarding this second excited ${}^3\Sigma^-$ state of VNb.

There are two plausible explanations for this discrepancy. First, the energy predicted by the calculations for the upper excited state of VNb, 17081 cm^{-1}, could be in error by 1000 cm^{-1} or more. In the case of V_2 the calculated energy of the higher-lying ${}^3\Sigma_u^-$ state displays error of this magnitude, and is calculated to be too low. If the same is true for VNb, the higher-lying $^3\Sigma^-$ state of VNb could in actuality be at an energy above the range scanned by James et al. A second possibility is that the higher-energy $^3\Sigma^- \leftarrow X^3\Sigma^-$ transition in VNb is too weak to be observed. In the case of V_2, the $A'^3\Sigma_u^- \leftarrow X^3\Sigma_g^-$ transition observed near 11900 cm^{-1} was found to have an oscillator strength on the order of 0.01 [189], but the $B^3\Sigma_u^- \leftarrow X^3\Sigma_g^-$ transition was much less intense [49]. James et al. reported that the $^3\Sigma^- \leftarrow X^3\Sigma^-$ transition they observed for VNb near 15650 cm^{-1} occurred in a portion of the spectrum dominated by much stronger features of Nb_2 and NbO, which were present in the molecular beam along with VNb [197]. If the transition to the higher-lying $^3\Sigma^-$ state is less intense, as is the case with the analogous transition in V_2, it could easily be lost in the noise of the more prominent Nb_2 and NbO features.

The $^3\Sigma^- \leftarrow X^3\Sigma^-$ transitions in both V_2 and VNb are predicted to be $\sigma^* \leftarrow \sigma$ transitions by the INDO/S calculations. The $A'^3\Sigma_u^- \leftarrow X^3\Sigma_g^-$ transition was originally assigned as a $\delta^* \leftarrow \delta$ transition [189] based on Xα calculations [194]. James et al. judged that it was unlikely that the $^3\Sigma^- \leftarrow X^3\Sigma^-$ transition observed for VNb was a $\delta^* \leftarrow \delta$ transition [197], however. Taken together with the theoretical results reported here and in chapter four, this calls for a reassessment of the orbital symmetry of the $^3\Sigma^- \leftarrow X^3\Sigma^-$ transitions in both molecules. Molecular beam spectroscopy aimed at elucidating the higher-lying $^3\Sigma^-$ state of VNb could be helpful in resolving this issue.

Several electronic transitions involving the $X^3\Sigma_g^-$ ground state of Nb_2 have been observed, but symmetries have not been assigned for any of the excited states [107]. Unfortunately INDO/S SOCI calculations do not provide any insight into the identities of the observed transitions, since there is very little resemblance between the calculated and experimental transition energies. This failure can almost certainly be attributed to the parameterization of the 4d metals, which uses theoretical rather than spectroscopic Slater-Condon factors. The 3d metal parameterization, on the other hand, does use spectroscopic parameters. The INDO/S method is known for effectively treating electronic spectroscopy of complexes containing 3d metals [24,93,96], but is not generally useful for this purpose with the 4d metals because of this difference in parameterization. It is interesting to note that the energy of the $^3\Sigma^- \leftarrow X^3\Sigma^-$ transition observed for VNb [197] is reproduced rather well by INDO/S SOCI calculations despite the presence of a niobium atom. An obvious future direction for this work, and the INDO/S model in general, would be fitting spectroscopic Slater-Condon factors for the 4d metals in a fashion similar to that used for the 3d metals [164]. Unfortunately many of the necessary atomic state energies are not known experimentally [159], as discussed in chapter two.

"Essential correlation-only" CI calculations

An important choice that has not been discussed yet is the magnitude of the contribution to the ground state that is required for a particular configuration to be included in the final "essential correlation-only" calculations. There is no precisely defined value of coefficient required for a configuration to be included. Indeed, as magnitude of coefficients becomes small, the line between essential and dynamic correlation becomes indistinct in a CI model. After some consideration, a value of 0.01 was selected as a reasonable choice based on an examination of the coefficients in the ground state of V_2 (table 5-4). In that case, there are eleven configurations with coefficients having absolute values greater than or equal to 0.01, and the sums of the squares of these eleven coefficients is 0.97 (see table 5-4). Since the squares of the coefficients of the remaining configurations that contribute to the state must sum to 0.03,[1] and each coefficient for these configurations is less than 0.01, there must on the order of 300 configurations with coefficients less than 0.01 contributing to the ground state of V_2. These two sets of configurations, eleven representing a total of 97% of the state and 300 (or more) representing 3%, satisfy the definitions of essential and dynamic correlation used here. Adopting 0.01 as the limit amounts to including all configurations listed in tables 5-4 through 5-6 in the final calculations.

CI calculations including only the configurations shown in tables 5-4 through 5-6 yield ground state spin-orbit splittings of V_2 and VNb in very good agreement with experiment, 75 cm^{-1} versus 75 cm^{-1} in the first case and 232 cm^{-1} versus 230 cm^{-1} in the second (table 5-8). Given this success, it is reasonable to assume that the estimate for Nb_2, 419 cm^{-1}, is reliable as well. This is strong corroboration of the tentative assignment [190] of the value of 410 cm^{-1} measured by Li, Van Zee, and Weltner [201] as the splitting of the Nb_2 ground state. Assuming that this matrix value can be translated directly to the gas phase, the $^3\Sigma^-$ ground states of V_2, VNb, and Nb_2 have spin-orbit splittings which increase in the order 75 cm^{-1}, 230 cm^{-1}, and 410 cm^{-1}, respectively.

---

[1] Coefficients taken in the basis of Schmidt-orthogonalized CSFs

The good agreement between experimental and INDO/S values of the ground state splittings suggests that the energies predicted for the isoconfigurational $^1\Sigma^+$ states in each molecule (table 5-8) are also reliable estimates. In the case of V_2, the calculated energy of 1306 cm^{-1} agrees more closely with the value of 1196 cm^{-1} predicted by James et al. [190] than with the value of 1821 cm^{-1} predicted by Spain et al. [189], as discussed in detail in chapter four. The conclusion reached based in the calculations on V_2 described in this chapter is the same: the discrepancy between observed and calculated energies is large enough that it is doubtful that the state observed near 1860 cm^{-1} [47] is the $^1\Sigma_g^+$ state. There is a slight spin contamination of the excited state of roughly 6%.

Table 5-8. Spin-orbit splittings of the ground states (Δ) of V_2, VNb, and Nb_2 and energies of the $^1\Sigma^+$ states isoconfigurational with the $X^3\Sigma^-$ ground states. Values computed with both "essential correlation-only" CI calculations and full CI calculations are included for comparison. See text for details. Experimental results for Δ and the two-state model estimates of James et al. (reference [190]) are shown in parentheses. All values are in cm^{-1}.

	V_2		VNb		Nb_2	
Level of Calculation	Δ	$E\left(^1\Sigma_g^+\right)$	Δ	$E\left(^1\Sigma_g^+\right)$	Δ	$E\left(^1\Sigma_g^+\right)$
"Essential Correlation-Only" CI	75 (75[a])	1306 (1196[b])	232 (230[b])	2014 (1763[b])	419 (410[b])	2705 (2375[b])
Restricted Active Space Full CI	99	1010	354	1442	449	2565

[a] Reference [49].
[b] Reference [190].

For VNb the calculated energy of the $^1\Sigma^+$ state, 2014 cm^{-1}, is in reasonable agreement with the prediction of 1763 cm^{-1} made by James et al. [190]. The spin contamination is here on the order of 11%. Two values were predicted previously for E($^1\Sigma_g^+$) of Nb_2, 2375 cm^{-1} from the two-state matrix model [190] and 2834 cm^{-1} from second order perturbation theory [107]. The value predicted here, 2705 cm^{-1}, falls between these two estimates. As in the other two cases, the transition between the ground state and excited state has zero intensity despite the spin contamination of 16%. A feature observed near 2450 cm^{-1} in matrix with resonance Raman spectroscopy [199] has been assigned as the $^1\Sigma_g^+$ state [190]. In this case the calculated energy is close to the observed energy. It is therefore possible that the state observed near 2450 cm^{-1} is the $^1\Sigma_g^+$ state. If it is not, and the state observed near 1860 cm^{-1} for V_2 is also not the $^1\Sigma_g^+$ state of V_2, the observed states in V_2 and Nb_2 are quite possibly the same state. The INDO/S calculations do not resolve this in either case. Perhaps a more rigorous method such as CASPT2 could shed light on this question.

Analysis of Empirical Two State Models

A trend that is obvious in table 5-8 is that the INDO/S predictions for E($^1\Sigma^+$) are systematically larger than the predictions of the two-state model of James et al. [190]. This disagreement indicated that an analysis of the contributions of the various sources of error in the two-state models would be valuable. The three principle sources of error are neglect of overlap and delocalization effects, the order at which the perturbation theory is evaluated, and the consideration of only one perturbing state. It can be anticipated that the last of these will be the most significant error, given the highly multireference nature of the ground states indicated in tables (5-4) through (5-6). In the first case, delocalization is incorporated by using equation (5-12) for the coupling matrix element V_{12} in place of equation (4-8). Doing so requires estimates of the delta-symmetry overlap integral S and the coefficients weighting the $(d\pi)^4(d\sigma)^2(s\sigma)^2(d\delta)^2$ and $(d\pi)^4(d\sigma)^2(s\sigma)^2(d\delta^*)^2$ configurations for each molecule. These quantities are easily obtained with INDO/S CI calculations limited to these two configurations, and are shown in table 5-9 along with the values of V_{12} obtained from equations (4-8) and (5-12). Spin-orbit radial integrals $\zeta_{(n-1)d}$ were taken from James et al. [190] in computing these matrix elements. The inclusion of overlap is seen to reduce the coupling in each case, which will decrease the prediction of $E(^1\Sigma^+)$ since a smaller energy difference between the states will make up for the weaker coupling to preserve the magnitude of the experimentally-determined splitting. The trend in the other quantities in table (5-9) is as expected, with the overlap increasing from V_2 to VNb to Nb_2 due to the greater extent of

Table 5-9. Matrix elements of the $(d\pi)^4(d\sigma)^2(s\sigma)^2(d\delta)^2$ and $(d\pi)^4(d\sigma)^2(s\sigma)^2(d\delta^*)^2$ configurations over the spin-orbit operator (V_{12}) determined with and without overlap

Molecule	V_{12}, no overlap (cm^{-1})	**S**	$\lvert C_1\rvert^2$	V_{12}, with overlap (cm^{-1})
V_2	290.0	0.0397	0.8073	283.4
VNb	593.8	0.0490	0.8532	574.6
Nb_2	897.6	0.0714	0.9183	848.3

the 4d orbitals, and the multireference nature of the ground state decreasing as the overlap increases.

Table 5-10 displays values of $E(^1\Sigma^+)$ computed at second order (equation (5-16)) and at infinite order (2×2 matrix diagonalization, equation (5-17)) and at second order with overlap for the three molecules. The INDO/S results from table (5-8) are shown for comparison. All empirical predictions are seen to be too small, as expected since the most severe approximation, limitation to two states, has yet to be considered. It is interesting to note that the least exact model, second order perturbation theory with no overlap, gives the best results. This clearly results from cancellation of errors. Incorporation of additional states will make $E(^1\Sigma^+)$ larger, because the two-state models assume that the perturbation of the $\Omega = 0$ component of the ground state that produces the

Table 5-10. Predictions for $E(^1\Sigma^+)$ made with several empirical two-state models. V_{12} is the coupling matrix element without overlap, equation (4-8), and V'_{12} is the matrix element with overlap, equation (5-16). Δ is the spin-orbit splitting observed for the ground state. All energies in wavenumbers.

Model	$E(^1\Sigma^+)$ given by	V_2 ($\Delta = 75$ cm^{-1})	VNb (230 cm^{-1})	Nb_2 (410 cm^{-1})
second order, no overlap	$\dfrac{V_{12}^2 + 2\Delta^2}{\Delta}$	1271 cm^{-1}	1993	2785
second order with overlap	$\dfrac{(V'_{12})^2 + 2\Delta^2}{\Delta}$	1221	1896	2575
infinite order, no overlap	$\dfrac{V_{12}^2 + \Delta^2}{\Delta}$	1196	1763	2375
INDO/S	(table (5-8))	1306 (Δ 75 cm^{-1})	2014 (232 cm^{-1})	2705 (419 cm^{-1})

splitting is entirely caused by interaction with the $^1\Sigma^+$ state. If a part of the perturbation is caused by interaction with other states, however, the size of the interaction with the $^1\Sigma^+$ state is overestimated. Since the energy of the $^1\Sigma^+$ state is inversely proportional to the strength of interaction, limiting the model to two states underestimates E($^1\Sigma^+$). As shown in table 5-10, inclusion of overlap and increasing the order of the perturbation expansion both make E($^1\Sigma^+$) smaller. Therefore the errors incurred by neglecting additional states on one hand, and neglecting overlap and using second order perturbation theory on the other hand, will tend to cancel.

It is also clear from the above analysis that a model (with two or more states) will have to yield values at second order without consideration of overlap that are higher than the INDO/S predictions, so that a "complete" model in the sense of number of states, overlap, and order would yield results comparable to those obtained with the SOCI calculations. It turns out that addition of only two states is enough to accomplish this, as illustrated using the four state model described in the previous section. The pertinent equation is equation (5-26), which is quadratic in the unperturbed energy of the $^1\Sigma^+$ state. Values of V_{12} and Δ_1 are provided in table 5-9 (second column). The unperturbed energy of the $^3\Sigma^-$ state arising from the $(d\pi)^4(d\sigma)^2(d\delta)^2\left(s\sigma^*\right)^2$ configuration, $E_3^{(0)}$ in equation (5-26), is obtained from INDO/S CI calculations limited to the configurations $(d\pi)^4(d\sigma)^2(s\sigma)^2(d\delta)^2$ and $(d\pi)^4(d\sigma)^2(d\delta)^2\left(s\sigma^*\right)^2$. The important quantities and results are shown in table 5-11, where it is seen that the predicted values of E($^1\Sigma^+$) are larger than the INDO/S values for each molecule. Adding overlap and increasing the order of perturbation theory used would lower these empirical predictions below the INDO/S values again, but only one additional singlet state has been added to the model, and based on the configurations listed in tables 5-4 through 5-6 it is clear that many states might contribute. This is demonstrated in the case of Nb_2 in table 5-12, which shows components and expansion coefficients for the $\Omega'' = 0$ level of the $X^3\Sigma_g^-$ ground state of Nb_2 obtained from the INDO/S SOCI calculation. Several other singlet states are seen to contribute to the ground state. Inclusion of these states in an empirical model analogous to the four state model developed here would further increase $E(^1\Sigma^+)$ beyond the values given in table 5-11, which would counterbalance decreases caused by incorporating overlap and going beyond second order.

Table 5-11. Results of empirical four state model developed in the previous section. All results given in wavenumbers

Molecule	$E_3^{(0)}$ [a]	V_{12} [b]	$\lvert\Delta_1\rvert$ [c]	$E_2^{(0)}$ [d]	Δ_2 [e]	$E(^1\Sigma^+)$ [f]
V_2	23115	290.0	75	1176	68	1319
VNb	25344	593.8	230	1625	202	2057
Nb_2	22506	897.6	410	2135	338	2883

[a] From INDO/S calculations, see text for details.
[b] From equation (4-8).
[c] Experimental, reference [49] for V_2, reference [197] for VNb and Nb_2.
[d] Positive root from equation (5-26).
[e] Obtained from equation (5-27).
[f] $E(^1\Sigma^+) = E_2^{(0)} - E_1^{(0)} + \Delta_2 - \Delta_1$

Correlation Effects in the INDO/S Model

Comparison of results of the restricted active space full CI calculations and the smaller, "essential correlation-only" CI calculations (table 5-8) indicates that inclusion of dynamic correlation by means of the CI calculation leads to significantly poorer results. The discrepancy is large for the two cases that were demonstrated above to have significant dynamic correlation effects, V_2 and VNb, and considerably smaller in the case of Nb_2, where dynamic correlation was shown to play only a small role. In fact, the size of the error in the ground state spin-orbit splittings follows the trend in the importance of dynamic correlation as demonstrated by tables 5-4 through 5-6, which is VNb, V_2, Nb_2 in descending order. This suggests that the INDO/S parameters have been optimized to

Table 5-12. Components contributing to the $\Omega'' = 0$ level of the $X\,^3\Sigma_g^-$ state of Nb_2. All components with coefficients of magnitude greater than 0.01 are included.

Configuration	Multiplicity	$\lvert C_i \rvert^2$
$(d\pi_u)^4(s\sigma_g)^2(d\sigma_g)^2(\delta_g)^2$	3	0.729
$(d\pi_u)^4(s\sigma_g)^2(d\sigma_g)^2(\delta_u)^2$	3	0.050
$(d\pi_u)^4(s\sigma_g)^2(\delta_g)^2(d\sigma_u)^2$	3	0.034
$(d\pi_u)^4(s\sigma_g)^2(d\sigma_g)^1(\delta_g)^1(\delta_u)^1(ds\sigma_u)^1$	3	0.013
$(d\pi_u)^4(s\sigma_g)^2(\delta_u)^2(d\sigma_u)^2$	3	0.004
$(d\pi_u)^4(s\sigma_g)^2(d\sigma_g)^2(\delta_g)^2$	1	0.120
$(d\pi_u)^4(s\sigma_g)^2(d\sigma_g)^2(\delta_u)^2$	1	0.020
$(d\pi_u)^4(s\sigma_g)^2(\delta_g)^2(d\sigma_u)^2$	1	0.006
$(d\pi_u)^4(s\sigma_g)^2(d\sigma_g)^1(\delta_g)^1(\delta_u)^1(ds\sigma_u)^1$	1	0.006
$(d\pi_u)^4(s\sigma_g)^2(\delta_u)^2(d\sigma_u)^2$	1	0.002

incorporate dynamic correlation at the independent particle level, but make no provision for essential correlation. Thus they are reliable only when dynamic correlation is not included in a subsequent correlation treatment, but essential correlation is included.

Historically the INDO/S model has been applied largely to problems where there is only a limited degree of essential correlation, which explains the great success [93] of INDO/S for these problems at a level of theory (CIS) that does not correlate the ground state. Metal clusters are not this kind of problem, however, because substantial essential correlation contributions are the norm rather than the exception. A major difficulty in extending INDO/S to metal cluster spectroscopy, then, is the systematic application of electron correlation treatments. The INDO/S parameters incorporate dynamic correlation in an amount that is difficult to quantify, which leads to "overcounting" of this correlation at levels of theory beyond Hartree Fock [104]. The results presented here indicate that the INDO/S model could in principle be extended to metal clusters if an approach to parameterization that is consistent with systematic techniques for electron correlation could be developed. There is hope in this direction, as an understanding of the fundamental relationship between semiempirical and *ab initio* methods continues to be developed [100,101].

Conclusions

Isoconfigurational mixing in the ground states of V_2, VNb, and Nb_2 has been thoroughly investigated with INDO/S configuration interaction calculations including spin-orbit effects. Calculated magnitudes of ground state spin-orbit splittings agree closely with experiment for V_2 and VNb, and the value of 410 cm^{-1} measured by Li, Van Zee, and Weltner is confirmed as the ground state splitting of Nb_2. Previous assignments of experimentally-observed low-lying states as the isoconfigurational ${}^1\Sigma_g^+$ states of V_2 and Nb_2 are questioned based on state energies.

Energies calculated for two Σ excited states previously observed for V_2 and one excited Σ state observed for VNb are in good agreement with experiment. A second excited Σ state that has not been observed was also predicted for VNb. It is suggested that the transition into the second state could lie outside the range of energies that have been studied spectroscopically, or was not observed due to weak intensity.

Comparisons have been made between simple two-state perturbative models and the INDO/S SOCI calculations for predicting the location of the ${}^1\Sigma^+$ states. Consideration of only two states is found to be a potentially serious shortcoming of the two-state model, leading to a systematic underestimation of the energies of the ${}^1\Sigma^+$ states in the three molecules.

Estimations of ground state splittings for the three molecules are much more reliable from CI calculations that exclude the majority of the dynamic correlation of the $X^3\Sigma^-$ and ${}^1\Sigma^+$ states. This demonstrates that the parameters of semiempirical models like INDO/S that are parameterized against experiment must inherently contain some level of dynamic correlation within the valence space. This can lead to an inaccurate representation of the dynamic correlation when there is also explicit inclusion of this effect in calculations beyond the Hartree Fock level.

CHAPTER 6
CONCLUSIONS AND FUTURE PLANS

Conclusions

Three purposes for carrying out this investigation were stated at the end of the first chapter. The first was to demonstrate by example that the INDO/S method can, in principle, successfully treat the electronic spectroscopy of a transition metal diatomic. The second was to contribute to the basic research on the group five diatomics V_2, VNb, and Nb_2 as a complement to the experimental work, and the third was to investigate correlation effects in the INDO/S model. Significant progress in all three areas has been made. In addition, the INDO/S Rumer SOCI code has been improved. Changes include adoption of the Schmidt rather than Löwdin (symmetric) orthogonalization of the basis of configuration state functions to increase execution speed, streamlining of the output format for spin-orbit eigenvectors, and addition of code to determine the spin character of spin-orbit levels.

The strategy used in treating the electronic spectroscopy of divanadium, full CI in a restricted active space, was designed based on the effective valence shell Hamiltonian studies of semiempirical methods [100,101,135], and on the experience gained from ab initio calculations on dichromium [27-33,72,73]. Good agreement between theory and experiment was obtained for energies, symmetries, and spin-orbit splittings of all well-characterized states. Similar calculations on VNb also gave good agreement with experiment for the one transition that has been observed [197]. This success indicates, for these examples at least, that the INDO/S model applied at the restricted active space full CI level is effective for modeling the electronic spectroscopy of transition metal diatomics.

A second important question addressed here regards the role of dynamic electron correlation at the restricted active space full CI level. It is thought that dynamic correlation is incorporated in an ad hoc way in a set of semiempirical parameters, because the values adopted are fit to reproduce experimental results (rather than results calculated ab initio at the same level of theory) for a set of test cases [24,93,100]. Introducing this correlation explicitly (in effect overcounting its contribution) might then have a deleterious effect on results [24,104]. These assumptions were tested by computing ground state spin-orbit splittings (which are second order effects and depend on the energy of the excited perturbing states) with two procedures: restricted active space full CI calculations, and calculations using only those configurations contributing to the essential correlation. The results are much better in every case using the latter approach. This supports the hypotheses provided by the effective valence shell Hamiltonian work, at least for the small number of examples considered here. These results also indicate that resonance integrals fit at the CIS level are not optimum for higher levels of electron correlation.

Much has been accomplished from a basic research standpoint by investigating the spectroscopy of V_2, VNb, and Nb_2. In the case of V_2, the $A^3\Pi_u \leftarrow X^3\Sigma_g^-$ transition [49] has been assigned as a $d\delta_g \leftarrow d\pi_u$ promotion. The previously unassigned transition observed near 15000 cm^{-1} [49] has been assigned as $B^3\Sigma_u^- \leftarrow X^3\Sigma_g^-$. Both that and the observed $A^3\Sigma_u^- \leftarrow X^3\Sigma_g^-$ transition [189] are found to be $\sigma_u \leftarrow \sigma_g$ promotions, contrary to a previous suggestion that the $A'^3\Sigma_u^- \leftarrow X^3\Sigma_g^-$ transition is a $d\delta_u \leftarrow d\delta_g$ promotion [189]. The new assignment is corroborated by DFT predictions [107] and experimental results on V_2^+ [195] and VNb [197]. A $^1\Sigma_u^+$ state isoconfigurational with and spin-contaminated by spin-orbit coupling with the $A'^3\Sigma_u^-$ state is suggested as a candidate for an unassigned transition observed in the range 11250 – 12500 cm^{-1} [189]. A second, higher-energy $^3\Sigma^- \leftarrow X^3\Sigma^-$ transition is predicted for VNb. It is suggested that this transition has not been observed because it is either just above the range of energies scanned by James et al. [197], or is too weak to be observed, falling in a region of the spectrum contaminated by transitions in impurities in the molecular beam.

Previous suggestions [189,190] that second order spin-orbit splittings in the $X^3\Sigma^-$ ground states of V_2, VNb, and Nb_2 are caused by interaction with the isoconfigurational $^1\Sigma^+$ states are supported by the INDO/S results. Tentative assignment [190] of the value of 410 cm^{-1} measured by Weltner et al. as the spin-orbit splitting of the $X^3\Sigma_g^-$ ground state of Nb_2 is supported as well. The theoretical results presented here for the energy of the isoconfigurational $^1\Sigma_g^+$ state in V_2 agree much more closely with the empirical prediction of James et al. [190] than with that of Spain et al. [189], casting doubt on the assignment [190] of a state observed at low energy [47] as the $^1\Sigma_g^+$ state. A similar state observed for Nb_2 [199] cannot be ruled out as the isoconfigurational $^1\Sigma_g^+$ state of Nb_2.

Finally, an analysis of empirical two state models for predicting the energies of the isoconfigurational $^1\Sigma^+$ states in the three molecules reveals that consideration of only two states is a potentially serious shortcoming due to the multiconfigurational nature of the ground states of these diatomics. Second order perturbation theory without consideration of overlap or delocalization is the most reliable two state model due to cancellation of errors.

Future Plans

The work reported in this dissertation could be the first step in an ongoing program of research. In this sense it may be regarded as a feasibility study indicating that a method similar to INDO/S could become a useful tool for the study of transition metal clusters. At the very least the results obtained here indicate that calculations on other diatomics should be carried out with the INDO/S model in present form. Doing so would further test the assertions made here, and, hopefully, determine areas in which the model should be modified or improved. A direct extension of the calculations reported here would be similar work on the cations V_2^+, VNb^+, and Nb_2^+. Spin-orbit splittings have been determined for the ground states of V_2^+ [190,195] and VNb^+ [190], and the ground state bond length of V_2^+ is known as well [195]. Although the electronic spectroscopy of these cations has not been characterized, such experiments could potentially be carried out at the University of Florida. Other test cases similar to the ones used here are Y_2 and Y_2^+, which are known to exhibit second order ground state spin-orbit effects [200,202]. Empirical two-state models have been used to predict locations of the perturbing state in each case.

There is also a number of other diatomics for which electronically excited states have been observed and characterized, by both optical spectroscopy and resonance Raman spectroscopy, in the gas phase and in matrix isolation. Examples among the 3d diatomics include Ti_2 and Zr_2 [45,203,204], Cr_2 [20,50,52,54,194,205-209], Ni_2 [46,48,51], and Cu_2 [53,210-215]. Other important information including ground state symmetries has been obtained in a number of cases using matrix isolated electron spin resonance experiments.

Dimanganese and the cation Mn_2^+ are interesting cases due to significant electronic relaxation in the cation compared to the neutral [42,55,58-60]. Another example is Sc_2 and Sc_2^+ [37,216].

A related area in which there is a growing body of spectroscopic data involves diatomics formed from a transition metal and a main group atom. These molecules could also be useful test cases, as they should not be as difficult to treat as metal diatomics. Examples of interesting cases include CuO [11,217], the nitrides TiN [218], VN [218-223], CrN [218,223], and NbN [224-227]. A large number of other examples are discussed in the recent review article by Harrison [228].

Finally, spectroscopic data on diatomics composed of lanthanide elements is a growing area of research. See for example the recent work of Lombardi and coworkers on Ce_2, Pr_2, and Nd_2 [229]. The INDO/S model has been parameterized for the lanthanides [156,157,185], and has been applied successfully to small molecules [156,157], complexes [185,230-233], and lanthanide impurities in semiconductors [234-

236]. It would be interesting to see how the model performs with lanthanide diatomics. A part of this motivation is that lanthanide diatomics often display similarities to the transition metal diatomics. A good example is Gd_2, which has a ground state analogous to Mn_2 in the 4f shell while at the same time being very similar to Sc_2 in the 5d and 6s shells [237].

The other focus of potential future research drawing on the work of this dissertation is development of the INDO/S model. There is a clear need for implementation of a configuration interaction program designed for large Hamiltonian matrices. Full CI in the entire valence orbital space of transition metal diatomics would be readily tractable with existing algorithms. These calculations could contribute to investigations of the fundamental basis of semiempirical methods, since approaches like the effective valence shell Hamiltonian that purport to model semiempirical methods assume full CI in the valence space [100]. Calculations at that level with a successful semiempirical method like INDO/S could thus play an important role in the elucidation of electron correlation effects in semiempirical methods. This is especially important for potential future application to larger metal clusters, because full CI calculations are not feasible for clusters with more than two atoms. It will therefore be necessary to carefully study various levels of correlation to determine the proper balance between effectiveness and computational cost.

In a more specific extension of the calculations reported here, full CI calculations on the group 5 diatomics might shed light on some of the questions left unanswered by this dissertation, such as the identities of the states observed at low energy in matrix-isolated resonance Raman work for V_2 [47] and Nb_2 [199], and the inversion of the energies found computationally for the $A^3\Pi_u$ and $B^3\Sigma_u^-$ states of V_2 compared to experiment.

Another potential extension of this dissertation involves parameterization. As noted previously, there is a clear need for spectroscopic parameters for the 4d metals. Several other possible improvements involve the resonance integrals, the $\{\beta_\mu^A\}$ of equation (2-101). These parameters could for instance be made to depend on interatomic distance, which might be useful because of the very different radial properties of the ns and (n-1)d orbitals. The resonance integrals are the only parameters fit empirically (as opposed to being obtained from experimentally-measured quantities), which is accomplished by adjusting the parameters until good results for spectral transition energies are obtained for a set of test molecules at a specific level of electron correlation. An important question is whether the values used should depend on the level of correlation. Results from the effective valence shell Hamiltonian work indicate that the resonance integrals are rather insensitive to the level of correlation [103], but again this assumption has not been tested with an actual semiempirical method. It is also true that no systematic parameterization of the resonance integrals has been carried out for the INDO/S model. The transition metal diatomics could be used as a set of test cases for a systematic fitting of the resonance integrals, which could then be used for studying larger clusters.

It is anticipated that the three efforts described above, calculations on additional transition metal diatomics, implementation of a full CI code, and parameterization efforts, would complement each other in an overall effort aimed at furthering understanding of semiempirical methods themselves, thus allowing intelligent design of a method that could be successfully used for practical application to transition metal clusters. If a combination of parameters and level of theory that systematically accounts for electron correlation effects could be developed, the advantages of a semiempirical approach could be brought to bear on highly-correlated problems like larger metal clusters.

REFERENCES

1 M. Jacobs, *Chemical & Engineering News* **78,** 48 (2000).

2 G. L. Miessler and D. A. Tarr, *Inorganic Chemistry* (Prentice-Hall, Inc., Englewood Heights, New Jersey, 1991).

3 L. S. Perkins and A. E. DePristo, *Surf. Sci.* **317,** L1152-L1156 (1994).

4 A. Forni and G. F. Tantardini, *Surf. Sci.* **352-354,** 142-147 (1996).

5 J.-F. Paul and P. Sautet, *Surf. Sci.* **356,** L403-L409 (1996).

6 F. Galan, M. Fouassier, M. Tranquille, J. Mascetti, and I. Pápai, *J. Phys. Chem. A* **101,** 2626-2633 (1997).

7 F. Delbecq, B. Moraweck, and L. Vérité, *Surf. Sci.* **396,** 156-175 (1998).

8 Z. G. Yi, D. A. Micha, and J. Sund, *J. Chem. Phys.* **110,** 10562-10575 (1999).

9 A. W. Castleman, Jr. and K. H. Bowen, Jr., *J. Phys. Chem.* **100,** 12911-12944 (1996).

10 Koutecký, *Chem. Rev.* **86,** 539-587 (1986).

11 H. Wu, S. R. Desai, and L.-S. Wang, *Phys. Rev. Lett.* **77,** 2436 (1996).

12 J. A. Alonso, *Chem. Rev.* **100,** 637-677 (2000).

13 S. C. Richtsmeier, E. K. Parks, K. Liu, L. G. Pobo, and S. J. Riley, *J. Chem. Phys.* **82,** 3659-3665 (1985).

14 P. J. Brucat, C. L. Pettiette, S. Yang, L. S. Zheng, M. J. Craycraft, and R. E. Smalley, *J. Chem. Phys.* **85,** 4747-4748 (1986).

15 H. A. Duarte and D. R. Salahub, *J. Phys. Chem. B* **101,** 7464-7471 (1997).

16 D. L. Freeman and J. D. Doll, in *Annual Review of Physical Chemistry*, Vol. 47, edited by H. L. Strauss, G. T. Babcock, and S. R. Leone (Annual Reviews, Inc., Palo Alto, California, 1996), pp. 43-80.

17 Z. El-Bayyari, *Phys. Stat. Sol. B* **208,** 339 (1998).

18 H. Sun, Y.-H. Luo, J. Zhao, and G. Wang, *Phys. Stat. Sol. B* **215,** 1127 (1999).

19 S. Erkoç and R. Shaltaf, *Phys. Rev. A* **60,** 3053 (1999).

20 M. D. Morse, *Chem. Rev.* **86,** 1049 (1986).

21 W. Weltner, Jr. and R. J. Van Zee, *Annu. Rev. Phys. Chem.* **35,** 291 (1984).

22 T. G. Dietz, M. A. Duncan, D. E. Powers, and R. E. Smalley, *J. Chem. Phys.* **74** (1981).

23 P. E. M. Siegbahn, in *Advances in Chemical Physics*, Vol. 93, edited by I. Prigogine and S. A. Rice (John Wiley & Sons, Inc., New York, 1996).

24 C. H. Martin and M. C. Zerner, in *Inorganic Electronic Sructure and Spectroscopy*, Vol. 1, edited by E. I. Solomon and A. B. P. Lever (John Wiley and Sons, New York, 1999).

25 E. R. Davidson, *Chem. Rev.* **100,** 351-352 (2000).

26 D. R. Salahub, in *Ab Initio Methods in Quantum Chemistry*, Vol. 2, edited by K. P. Lawley (John Wiley Sons, Ltd., New York, 1987), pp. 447-520.

27 C. W. Bauschlicher, Jr. and H. Partridge, *Chem. Phys. Lett.* **231,** 277-282 (1994).

28 B. Roos, *Acc. Chem. Res.* **32,** 137-144 (1999).

29 E. J. Thomas, III, J. S. Murray, C. J. O'Connor, and P. Politzer, *J. Mol. Struct. Theochem* **487,** 177-182 (1999).

30 K. Andersson, B. O. Roos, P.-Å. Malmqvist, and P.-O. Widmark, *Chem. Phys. Lett.* **230,** 391-397 (1994).

31 B. O. Roos and K. Andersson, *Chem. Phys. Lett.* **245,** 215-223 (1995).

32 K. Andersson, *Chem. Phys. Lett.* **237,** 212-221 (1995).

33 H. Dachsel, R. J. Harrison, and D. A. Dixon, *J. Phys. Chem. A* **103,** 152-155 (1999).

34 I. N. Levine, *Quantum Chemistry* (Prentice Hall, Englewood Cliffs, New Jersey, 1991).

35 S. P. Walch and C. W. Bauschlicher, Jr., in *Comparison of Ab Initio Quantum Chemistry with Experiment for Small Molecules*, edited by R. J. Bartlett (Reidel, Dordecht, 1985), pp. 17-51.

36 R. L. DeKock and H. B. Gray, *Chemical Structure and Bonding* (Benjamin/Cummings Publishing Company, Menlo Park, CA, 1980).

37 L. B. Knight, R. J. Van Zee, and W. Weltner, Jr., *Chem. Phys. Lett.* **94,** 296 (1983).

38 Y. Suzuki, S. Asai, K. Kobayashi, T. Noro, F. Sasaki, and H. Tatewaki, *Chem. Phys. Lett.* **268,** 213-217 (1997).

39 C. J. Barden, J. C. Rienstra-Kiracofe, and H. F. Schaefer, III, *J. Chem. Phys.* **113,** 690-700 (2000).

40 H. Purdum, P. A. Montano, G. K. Shenoy, and T. Morrison, *Phys. Rev. B* **25,** 4412 (1982).

41 M. Moskovits and D. P. DiLella, *J. Chem. Phys.* **73,** 4917 (1980).

42 M. Moskovits, D. P. DiLella, and W. J. Limm, *J. Chem. Phys.* **80,** 626 (1984).

43 J. G. Dong, Z. D. Hu, R. Craig, J. R. Lombardi, and D. M. Lindsay, *J. Chem. Phys.* **101,** 9280 (1994).

44 I. Shim and K. A. Gingerich, *J. Chem. Phys.* **78,** 5693 (1983).

45 M. Doverstål, B. Lindgren, U. Sassenberg, A. C. A., and M. D. Morse, *J. Chem. Phys.* **97,** 7087-7092 (1992).

46 J. C. Pinegar, J. D. Langenberg, C. A. Arrington, E. M. Spain, and M. D. Morse, *J. Chem. Phys.* **102,** 666-674 (1995).

47 C. Cossé, M. Fouassier, T. Mejean, M. Tranquille, D. P. DiLella, and M. Moskovits, *J. Chem. Phys.* **73,** 6076-6085 (1980).

48 H. Wang, H. Haouari, R. Craig, J. R. Lombardi, and D. M. Lindsay, *J. Chem. Phys.* **104,** 3420-3422 (1996).

49 P. R. R. Langridge-Smith, M. D. Morse, G. P. Hansen, R. E. Smalley, and A. J. Merer, *J. Chem. Phys.* **80,** 593-600 (1984).

50 V. E. Bondybey and J. H. English, *Chem. Phys. Lett.* **94,** 443 (1983).

51 E. M. Spain and M. D. Morse, *J. Chem. Phys.* **97,** 4641-4660 (1992).

52 S. M. Casey and D. G. Leopold, *J. Phys. Chem.* **97,** 816-830 (1993).

53 R. S. Ram, C. N. Jarman, and P. F. Bernath, *J. Mol. Spectrosc.* **156,** 468 (1992).

54 D. L. Michalopoulos, M. E. Geusic, S. G. Hansen, D. E. Powers, and R. E. Smalley, *J. Phys. Chem.* **86,** 3914 (1982).

55 C. A. Baumann, R. J. Van Zee, S. V. Bhat, and W. Weltner, Jr., *J. Chem. Phys.* **78,** 190-199 (1982).

56 A. D. Kirkwood, K. D. Bier, J. K. Thompson, T. L. Haslett, A. S. Huber, and M. Moskovits, *J. Phys. Chem.* **95,** 2644-2652 (1991).

57 C. W. Bauschlicher, Jr., H. Partridge, S. R. Langoff, and M. Rosi, *J. Chem. Phys.* **95,** 1057 (1991).

58 M. Cheeseman, R. J. Van Zee, H. L. Flanagan, and W. Weltner, *J. Chem. Phys.* **92,** 1553-1559 (1990).

59 R. J. Van Zee and W. Weltner, Jr., *J. Chem. Phys.* **89,** 4444-4446 (1988).

60 C. W. Bauschlicher, *Chem. Phys. Lett.* **156,** 95-99 (1989).

61 S. Yanagisawa, T. Tsuneda, and K. Hirao, *J. Chem. Phys.* **112,** 545-553 (2000).

62 P. O. Löwdin, *Adv. Chem. Phys.* **2,** 207 (1959).

63 J. Simons and J. Nichols, *Quantum Mechanics in Chemistry* (Oxford University Press, New York, 1997).

64 M. R. A. Blomberg, U. B. Brandemark, P. E. M. Seigbahn, K. B. Mathisen, and G. Karlström, *J. Phys. Chem.* **89,** 2171-2180 (1983).

65 C. W. Bauschlicher, Jr., P. S. Bagus, C. J. Nelin, and B. O. Roos, *J. Chem. Phys.* **85,** 354-364 (1986).

66 P. Pyykkö, *Chem. Rev.* **88,** 563-594 (1988).

67 P. A. M. Dirac, *The Principles of Quantum Mechanics*, Fourth ed. (Oxford University Press, London, 1958).

68 P. W. Atkins, *Molecular Quantum Mechanics*, Second ed. (Oxford University Press, New York, 1983).

69 B. Simard, M.-A. LeBault-Dorget, A. Marijnissen, and J. J. ter Meulen, *J. Chem. Phys.* **108,** 9668 (1998).

70 E. A. Rohlfing and J. J. Valentini, *J. Chem. Phys.* **84,** 6560 (1986).

71 M. M. Goodgame and W. A. Goddard, III, *Phys. Rev. Lett.* **54,** 661 (1985).

72 S. P. Walch, C. W. Bauschlicher, B. O. Roos, and C. J. Nelin, *Chem. Phys. Lett.* **103,** 175-179 (1983).

73 B. O. Roos, K. Andersson, M. P. Fülscher, P.-Å. Malmqvist, L. Serrano-Andrés, K. Pierloot, and M. Merchán, in *Advances in Chemical Physics*, Vol. 93, edited by I. Prigogine and S. A. Rice (John Wiley & Sons, Inc., New York, 1996), pp. 219.

74 S. R. Langhoff and C. W. Bauschlicher, Jr., *Ann. Rev. Phys. Chem.* **39,** 81 (1988).

75 B. O. Roos, in *Advances in Chemical Physics: Ab Initio Methods in Quantum Chemistry*, Vol. 2 (John Wiley & Sons, Chichester, United Kingdom, 1987), pp. 399.

76 K. Andersson, P.-Å. Malmqvist, B. O. Roos, A. J. Sadlej, and K. Wolinski, *J. Phys. Chem.* **94,** 5483 (1990).

77 S. Niu and M. B. Hall, *Chem. Rev.* **100,** 353 (2000).

78 M. Castro, C. Jamorski, and D. R. Salahub, *Chem. Phys. Lett.* **271** (1997).

79 H. H. Heinze, A. Görling, and N. Rösch, *J. Chem. Phys.* **113,** 2088-2099 (2000).

80 A. Szabo and N. S. Ostlund, *Modern Quantum Chemistry: Introduction to Advanced Electronic Structure Theory* (McGraw-Hill, New York, 1989).

81 J. A. Pople, D. P. Santry, and G. A. Segal, *J. Chem. Phys.* **43,** S129 (1965).

82 J. A. Pople and G. P. Segal, *J. Chem. Phys.* **43,** S136 (1965).

83 J. A. Pople and G. A. Segal, *J. Chem. Phys.* **44** (1966).

84 J. A. Pople, D. L. Beveridge, and P. A. Dobosh, *J. Chem. Phys.* **47,** 2026 (1967).

85 J. A. Pople and D. L. Beveridge, *Approximate Molecular Orbital Theory* (McGraw-Hill, New York, 1970).

86 W. Thiel, *J. Am. Chem. Soc.* **103,** 1413 (1981).

87 A. Schweig and W. Thiel, *J. Am. Chem. Soc.* **103,** 1425 (1981).

88 W. Thiel, *J. Am. Chem. Soc.* **103,** 1420 (1981).

89 S. Schröder and W. Thiel, *J. Am. Chem. Soc.* **107** (1985).

90 S. Schröder and W. Thiel, *J. Am. Chem. Soc.* **108,** 7985 (1986).

91 J. Ridley and M. C. Zerner, *Theoret. Chim. Acta* **32,** 111-134 (1973).

92 M. C. Zerner, G. H. Loew, R. F. Kirchner, and U. T. Mueller-Westerhoff, *J. Am. Chem. Soc.* **102,** 589-599 (1980).

93 M. C. Zerner, in *Reviews in Computational Chemistry*, Vol. 2, edited by K. B. Lipkowitz and D. B. Boyd (VCH, 1991), pp. 313-363.

94 W. P. Anderson, W. D. Edwards, and M. C. Zerner, *Inorg. Chem.* **25,** 2728-2732 (1986).

95 J. Zeng, J. S. Craw, N. S. Hush, and J. R. Reimers, *J. Phys. Chem.* **98,** 11075-11088 (1994).

96 N. S. Hush and J. R. Reimers, *Chem. Rev.* **100,** 775-786 (2000).

97 G. L. Estiú and M. C. Zerner, *J. Phys. Chem.* **98,** 9972-9978 (1994).

98 G. L. Estiú and M. C. Zerner, *J. Phys. Chem.* **100,** 16874-16880 (1996).

99 G. L. Estiú, M. G. Cory, and M. C. Zerner, *J. Phys. Chem. A* **104,** 233-242 (2000).

100 K. F. Freed, in *Structure and Dynamcs of Atoms and Molecules: Conceptual Trends*, edited by J. L. Calais and E. S. Kryachko (Dordrecht, 1995).

101 P. O. Löwdin, *Int. J. Quantum Chem.* **72,** 379-391 (1999).

102 C. H. Martin, *Chem. Phys. Lett.* **257,** 229-237 (1996).

103 C. H. Martin, *J. Phys. Chem.* **100,** 14310-14315 (1996).

104 C. H. Martin and R. R. Birge, *J. Phys. Chem. A* **102,** 852-860 (1998).

105 P. O. Löwdin, *J. Chem. Phys.* **19,** 1396 (1951).

106 W. T. Borden and E. R. Davidson, *Acc. Chem. Res.* **29,** 67-75 (1995).

107 A. M. James, P. Kowalczyk, R. Fournier, and B. Simard, *J. Chem. Phys.* **99,** 8504-8517 (1993).

108 M. C. Zerner, J. E. Ridley, A. D. Bacon, W. D. Edwards, J. D. Head, J. McKelvey, J. C. Culberson, P. Knappe, M. G. Cory, B. Weiner, J. D. Baker, W. A. Parkinson, D. Kannis, J. Yu, N. Rösch, M. Kotzian, T. Tamm, M. M. Karelson, X. Zheng, G. M. Pearl, A. Broo, K. Albert, J. M. Cullen, C. J. Cramer, D. G. Truhlar, J. Li, G. D. Hawkins, and D. A. Liotard, (University of Florida, Gainesville, FL,).

109 E. Schrödinger, *Ann. Physik* **79,** 361 (1926).

110 M. Born and J. R. Oppenheimer, *Ann. Physik* **84,** 457 (1927).

111 H. Eyring, J. Walter, and G. E. Kimball, *Quantum Chemistry* (John Wiley & Sons, New York, 1944).

112 S.-I. Tomonaga, *The Story of Spin* (The University of Chicago Press, Chicago, 1997).

113 G. Uhlenbeck and S. Goudsmit, *Naturwiss* **13,** 953 (1925).

114 G. Uhlenbeck and S. Goudsmit, *Nature* **117,** 264 (1926).

115 J. C. Slater, *Phys. Rev.* **34,** 1293 (1929).

116 D. Hartree, *Proc. Cambridge Phil. Soc.* **24,** 89 (1928).

117 V. Fock, *Z. Physik* **61,** 126 (1930).

118 J. C. Slater, *Phys. Rev.* **35,** 210 (1930).

119 C. C. J. Roothaan, *Rev. Mod. Phys.* **23,** 69 (1951).

120 G. G. Hall, *Proc. Royal Soc. London Ser. A* **205,** 541 (1951).

121 R. S. Mulliken, *Rev. Mod. Phys.* **2,** 60 (1930).

122 R. S. Mulliken, *J. Chem. Phys.* **3,** 375 (1935).

123 W. D. Edwards and M. C. Zerner, *Theoret. Chim. Acta* **72,** 347-361 (1987).

124 C. C. J. Roothaan, *Rev. Mod. Phys.* **32,** 179 (1960).

125 P. Pulay, *Chem. Phys. Lett.* **73,** 393 (1980).

126 M. C. Zerner, *Int. J. Quantum Chem.* **35,** 567-575 (1989).

127 J. C. Slater, J. B. Mann, T. M. Wilson, and J. H. Wood, *Phys. Rev.* **184,** 672 (1969).

128 S. F. Abdulnur, J. Linderberg, Y. Öhrn, and P. W. Thulstrup, *Phys. Rev. A* **6,** 889 (1972).

129 P. Jørgensen and Y. Öhrn, *Phys. Rev. A* **8,** 112 (1973).

130 K. K. Stavrev and M. C. Zerner, *Int. J. Quantum Chem.* **65,** 877-884 (1997).

131 R. Pauncz, *Spin Eigenfunctions: Construction and Use* (Plenum Press, New York, 1979).

132 L. Brillouin, *Les Champs Self-Consistent de Hartree et de Fock* (Hermann and Cie, Paris, 1934).

133 J. Cizek and J. Paldus, *Physica Scripta* **21,** 251 (1980).

134 R. J. Bartlett and J. F. Stanton, in *Reviews in Computational Chemistry*, Vol. 5, edited by K. B. Lipkowitz and D. B. Boyd (VCH, New York, 1994), pp. 65-169.

135 K. F. Freed, *J. Chem. Phys.* **45,** 4214 (1966).

136 C. H. Martin and K. F. Freed, *J. Chem. Phys.* **101,** 4011-4027 (1994).

137 R. G. Parr and W. Yang, *Density Functional Theory of Atoms and Molecules* (Oxford University Press, New York, 1989).

138 W. Thiel, *Tetrahedron* **44,** 7393-7408 (1988).

139 R. Pariser and R. G. Parr, *J. Chem. Phys.* **21,** 767-776 (1953).

140 R. Pariser and R. G. Parr, *J. Chem. Phys.* **21,** 466-471 (1953).

141 J. A. Pople, *Trans. Faraday Soc.* **49,** 1375 (1953).

142 P. Lykos and R. G. Parr, *J. Chem. Phys.* **24,** 1166 (1956).

143 R. C. Bingham, M. J. S. Dewar, and D. H. Lo, *J. Am. Chem. Soc.* **97,** 1285 (1975).

144 R. C. Bingham, M. J. S. Dewar, and D. H. Lo, *J. Am. Chem. Soc.* **97,** 1307 (1975).

145 M. J. S. Dewar and W. Thiel, *J. Am. Chem. Soc.* **99,** 4899 (1977).

146 M. J. S. Dewar, E. G. Zoebisch, E. F. Healy, and J. J. P. Stewart, *J. Am. Chem. Soc.* **107,** 3902 (1985).

147 J. J. P. Stewart, *J. Comput. Chem.* **10,** 209 (1989).

148 J. J. P. Stewart, *J. Comput. Chem.* **10,** 221 (1989).

149 D. N. Nanda and K. Jug, *Theoret. Chim. Acta* **57,** 95 (1980).

150 K. G. Jug and D. N. Nanda, *Theoret. Chim. Acta* **57,** 131 (1980).

151 J. Del Bene and H. H. Jaffé, *J. Chem. Phys.* **48,** 1807 (1968).

152 J. Del Bene and H. H. Jaffé, *J. Chem. Phys.* **48,** 4050 (1968).

153 A. D. Bacon and M. C. Zerner, *Theoret. Chim. Acta* **53,** 21-54 (1979).

154 W. P. Anderson, T. Cundari, R. S. Drago, and M. C. Zerner, *Inorg. Chem.* **29,** 1 (1990).

155 W. P. Anderson, T. R. Cundari, and M. C. Zerner, *Int. J. Quantum Chem.* **39,** 31-45 (1991).

156 J. C. Culberson, P. Knappe, N. Rösch, and M. C. Zerner, *Theoret. Chim. Acta* **71,** 21-39 (1987).

157 M. Kotzian, N. Rösch, and M. C. Zerner, *Theoret. Chim. Acta* **81,** 201-222 (1992).

158 M. G. Cory, S. Kostlmeier, M. Kotzian, N. Rösch, and M. C. Zerner, *J. Chem. Phys.* **100,** 1353-1365 (1994).

159 C. E. Moore, *Natl. Bur. Stand. (U.S.) Circ.* (1949).

160 R. G. Parr, *Quantum Theory of Molecular Electronic Structure* (W. A. Benjamin, New York, 1963).

161 N. Mataga and K. Nishimoto, *Z. Phys. Chem. (Frankfurt am Main)* **13,** 140 (1957).

162 G. Karlsson and M. C. Zerner, *Int. J. Quantum Chem.* **7,** 35-49 (1973).

163 J. C. Slater, *Quantum Theory of of Atomic Structure* (McGraw-Hill, New York, 1960).

164 T. Anno and H. Teruya, *J. Chem. Phys.* **52,** 2840-2848 (1970).

165 E. Clementi and C. Roetti, *Atomic Dat. Nucl. Data Tables* **14,** 177 (1974).

166 P. Coffey, *Int. J. Quantum Chem.* **8,** 263-266 (1974).

167 M. C. Zerner, *Mol. Phys.* **23,** 963-978 (1972).

168 M. C. Zerner, in *Computational Methods For Large Molecules,* edited by F. Herman, A. S. McLean, and R. K. Nesbet (Plenum Press, New York, London, 1973), pp. 117.

169 P. O. Löwdin, *J. Chem. Phys.* **18,** 365 (1950).

170 M. Wolfsberg and L. Helmholz, *J. Chem. Phys.* **20** (1952).

171 R. S. Mulliken, *J. Phys. Chem.* **56,** 295 (1952).

172 L. L. Lohr and W. N. Lipscomb, *J. Chem. Phys.* **38,** 1607 (1963).

173 M. Kolb and W. Thiel, *J. Comp. Chem.* **14,** 775-789 (1993).

174 J. D. Da Motta-Neto, , University of Florida, Gainesville, FL, 1997.

175 W. Heitler and G. Rumer, *Z. Phys.* **68,** 12 (1931).

176 J. C. Slater, *Phys. Rev.* **38,** 1109 (1931).

177 R. McWeeny, *J. Chem. Phys.* **42,** 1717 (1965).

178 R. Manne and M. C. Zerner, *Int. J. Quantum Chem. Symp.* **19,** 165 (1986).

179 G. Rumer, *Göttinger Nachr.* **3,** 337 (1932).

180 M. Simonetta, E. Gianinetti, and I. Vandoni, *J. Chem. Phys.* **48,** 1579 (1978).

181 L. Lefebvre-Brion and R. W. Field, *Perturbations in the Spectra of Diatomic Molecules* (Academic, Orlando, 1986).

182 G. Rumer, E. Teller, and H. Weyl, *Göttinger Nachr.* **3,** 449 (1932).

183 I. L. Cooper and R. McWeeny, *J. Chem. Phys.* **45** (1966).

184 B. T. Sutcliffe, *J. Chem. Phys.* **45,** 235 (1966).

185 M. Kotzian, N. Rösch, and M. C. Zerner, *Int. J. Quantum Chem. Symp.* **25,** 545-555 (1991).

186 M. Kotzian, N. Rösch, R. M. Pitzer, and M. C. Zerner, *Chem. Phys. Lett.* **160,** 168-174 (1989).

187 D. S. McClure, *J. Chem. Phys.* **17,** 905 (1949).

188 T. M. Dunn, *Trans. Faraday Soc.* **57,** 1441 (1961).

189 E. M. Spain, J. M. Behm, and M. D. Morse, *J. Chem. Phys.* **96,** 2511-2516 (1992).

190 A. M. James, P. Kowalczyk, E. Langlois, M. D. Campbell, A. Ogawa, and B. Simard, *J. Chem. Phys.* **101,** 4485-4495 (1994).

191 H. Grönbeck and A. Rosén, *J. Chem. Phys.* **107,** 10620-10625 (1997).

192 S. E. Weber, B. K. Rao, P. Jena, V. S. Stepanyuk, W. Hergert, K. Wildberger, R. Zeller, and P. H. Dederichs, *J. Phys.-Condens. Mat.* **9,** 10739-10748 (1997).

193 D. R. Salahub and N. A. Baykara, *Surf. Sci.* **156,** 605 (1985).

194 M. P. Andrews and G. A. Ozin, *J. Phys. Chem.* **90,** 2852-2859 (1986).

195 D. S. Yang, A. M. James, D. M. Rayner, and P. A. Hackett, *J. Chem. Phys.* **102,** 3129-3134 (1995).

196 B. Simard, A. M. James, P. Kowalczyk, R. Fournier, and P. A. Hackett, *Proc. SPIE* **2124,** 376 (1994).

197 A. M. James, P. Kowalczyk, and B. Simard, *Chem. Phys. Lett.* **216,** 512-518 (1993).

198 A. M. James, P. Kowalczyk, and B. Simard, *J. Mol. Spectrosc.* **164,** 260-274 (1994).

199 Z. Hu, B. Shen, S. Zhou, S. Deosaran, J. R. Lombardi, and D. M. Lindsay, *SPIE* **1599** (1991).

200 D.-S. Yang, B. Simard, P. A. Hackett, A. Bréces, and M. Z. Zgierski, *Int. J. Mass Spec. and Ion Proc.l* **159,** 65-74 (1996).

201 S. Li, R. J. Van Zee, and W. Weltner, Jr., reported in reference 190.

202 D.-S. Yang and P. A. Hackett, *J. Electron Spectrosc.* **106,** 153-169 (2000).

203 M. Doverstål, L. Karlsson, B. Lindgren, and B. Sassenberg, *Chem. Phys. Lett.* **270,** 273-277 (1997).

204 M. Doverstål, L. Karlsson, B. Lindgren, and S. U., *J. Phys. B* **31,** 795-803 (1998).

205 Y. M. Efremov, A. N. Samoilova, and L. V. Gurvich, *Opt. Spectry.* **36,** 381 (1974).

206 E. P. Kündig, M. Moskovits, and G. A. Ozin, *Nature* **254,** 503 (1975).

207 M. J. Pellin and D. M. Gruen, *J. Chem. Phys.* **79,** 5887 (1983).

208 S. J. Riley, E. K. Parks, L. G. Pobo, and S. Wexler, *J. Chem. Phys.* **79,** 2577 (1983).

209 M. Moskovits, W. Limm, and T. Mejean, *J. Chem. Phys.* **82,** 4875 (1985).

210 V. E. Bondybey, *J. Chem. Phys.* **77,** 3771-3772 (1982).

211 J. L. Gole, J. H. English, and V. E. Bondybey, *J. Phys. Chem.* **86,** 2560-2563 (1982).

212 D. M. Kolb, H. H. Rotermund, W. Schrittenlacher, and W. Schroeder, *J. Chem. Phys.* **80,** 695-700 (1984).

213 J. G. McCaffrey, R. R. Bennett, M. D. Morse, and W. H. Breckenridge, *J. Chem. Phys.* **91,** 92-103 (1989).

214 R. H. Page and C. S. Gudeman, *J. Chem. Phys.* **94,** 39-51 (1991).

215 M. Doverstål, B. Lindgren, U. Sassenberg, and H. Yu, *Chem. Phys. Lett.* **192,** 283-288 (1992).

216 L. B. Knight, Jr., A. J. McKinley, R. M. Babb, and D. W. Hill, *J. Chem. Phys.* **99,** 7376-7383 (1993).

217 H. Xian, Z. X. Cao, X. Xu, X. Lu, and Q. E. Zhang, *Chem. Phys. Lett.* **326,** 485-493 (2000).

218 J. F. Harrison, *J. Phys. Chem.* **100,** 3513-3519 (1996).

219 S. L. Peter and T. M. Dunn, *J. Chem. Phys.* **90,** 5333-5336 (1989).

220 B. Simard, C. Masoni, and P. A. Hackett, *J. Mol. Spectrosc.* **136,** 44-55 (1989).

221 W. J. Balfour, A. J. Merer, H. Niki, B. Simard, and P. A. Hackett, *J. Chem. Phys.* **99,** 3288-3303 (1993).

222 S. M. Mattar and B. J. Doleman, *Chem. Phys. Lett.* **216,** 369-374 (1993).

223 T. C. Steimle, J. S. Robinson, and D. Goodridge, *J. Chem. Phys.* **110,** 881-889 (1999).

224 Y. Azuma, J. A. Barry, M. P. J. Lyne, A. J. Merer, J. O. Schroder, and J. L. Femenias, *J. Chem. Phys.* **91,** 1-12 (1989).

225 S. R. Langhoff and C. W. Bauschlicher, *J. Mol. Spectrosc.* **143,** 169-179 (1990).

226 Y. Azuma, G. Huang, M. P. J. Lyne, A. J. Merer, and V. I. Srdanov, *J. Chem. Phys.* **100,** 4138-4155 (1994).

227 R. S. Ram and P. F. Bernath, *J. Mol. Spectrosc.* **201,** 267-279 (2000).

228 J. F. Harrison, *Chem. Rev.* **100,** 679-716 (2000).

229 X. Shen, L. Fang, X. Chen, and J. R. Lombardi, *J. Chem. Phys.* **113,** 2233-2237 (2000).

230 V. Jahns, S. Kostlmeier, M. Kotzian, N. Rösch, and P. L. Watson, *Int. J. Quantum Chem.* **44,** 853-867 (1992).

231 M. Kotzian and N. Rösch, *J. Phys. Chem.* **96,** 7288-7293 (1992).

232 G. L. Estiú, N. Rösch, and M. C. Zerner, *J. Phys. Chem.* **99,** 13819-13829 (1995).

233 M. Kotzian, T. Fox, and N. Rösch, *J. Phys. Chem.* **99,** 600-605 (1995).

234 T. A O'Brien, P. D. Rack, P. H. Holloway, and M. C. Zerner, *J. Lumin.* **78,** 245-257 (1998).

235 P. D. Rack, T. A O'Brien, M. C. Zerner, and P. H. Holloway, *J. Appl. Phys.* **6,** 2377-2384 (1999).

236 T. A O'Brien, P. D. Rack, P. H. Holloway, and M. C. Zerner, *J. Electrochem. Soc.* **147,** 792-795 (2000).

237 R. J. Van Zee, S. Li, and W. Weltner, Jr., *J. Chem. Phys.* **100,** 4010-4012 (1994).

BIOGRAPHICAL SKETCH

Ted A O'Brien was born to Jim and Barbara O'Brien on February 3, 1972, at St. John's Hospital in Springfield, Missouri, with a letter in lieu of a middle name. The choice of letter was, it seems, the first one that naturally comes to mind. He spent his fourth year in Delaware before returning to southwest Missouri, where he spent the rest of his childhood. At age five he entered kindergarten at Greenwood Laboratory School (not like it sounds) on the campus of Southwest Missouri State University in Springfield, where he drifted uncertainly until coming out of nowhere to win the fifth grade chess championship. After this inspiring event, he began to excel academically and socially. He remained at Greenwood through his high school years. He liked the setting so much, in fact, that after high school he moved into a dormitory across the street from Greenwood and started undergraduate studies at Southwest Missouri State University.

After a brief period as an English major, O'Brien came to his senses and declared a chemistry major. At this time he met his future wife Julie in organic chemistry, an inauspicious beginning to the relationship certainly. In 1993 he worked as a NSF Research Experience for Undergraduates Fellow in the group of Dennis Marynick at the University of Texas at Arlington, applying semiempirical methods to transition metal complexes. This experience led to his choice of Professor Michael C. Zerner of the Quantum Theory Project at the University of Florida as a graduate advisor. In 1994 Ted married Julie, graduated *summa cum laude* with a bachelor of science degree in chemistry and a minor in mathematics, and moved to Florida in quick succession.

O'Brien joined Professor Zerner's research group at QTP as a NSF Graduate Research Fellow in August of 1994. He considers his time working and learning with Professor Zerner to be a very special experience.

I certify that I have read this study and that in my opinion it conforms to acceptable standards of scholarly presentation and is fully adequate, in scope and quality, as a dissertation for the degree of Doctor of Philosophy.

N. Yngve Öhrn, Chairman
Professor of Chemistry

I certify that I have read this study and that in my opinion it conforms to acceptable standards of scholarly presentation and is fully adequate, in scope and quality, as a dissertation for the degree of Doctor of Philosophy.

Rodney J. Bartlett

Rodney J. Bartlett
Graduate Research Professor of Chemistry

I certify that I have read this study and that in my opinion it conforms to acceptable standards of scholarly presentation and is fully adequate, in scope and quality, as a dissertation for the degree of Doctor of Philosophy.

William Weltner, Jr.

William Weltner, Jr.
Professor of Chemistry

I certify that I have read this study and that in my opinion it conforms to acceptable standards of scholarly presentation and is fully adequate, in scope and quality, as a dissertation for the degree of Doctor of Philosophy.

Daniel R. Talham
Professor of Chemistry

I certify that I have read this study and that in my opinion it conforms to acceptable standards of scholarly presentation and is fully adequate, in scope and quality, as a dissertation for the degree of Doctor of Philosophy.

John R. Sabin
Professor of Physics

This dissertation was submitted to the Graduate Faculty of the Department of Chemistry in the College of Liberal Arts and Sciences and to the Graduate School and was accepted as partial fulfillment of the requirements for the degree of Doctor of Philosophy.

December 2000

Dean, Graduate School